The Tectonic Evolution of Khao Khwang Fold-Thrust Belt, Central Thailand: new Insights in the Permian and Triassic Evolution of the Indosinian Orogeny in SE Asia

Francesco Arboit

Department of Earth Sciences

School of Physical Sciences

The University of Adelaide

Table of Contents

Abstract 3

Journal articles 7

Statement of Authorship 8

Declaration 18

Chapter I 19

Project Overview 20

Chapter II 22

Thesis Outline 23

References 26

Chapter III 28

Structural of the Sibumasu-Indochina Collision, Central Thailand: A section through the Khao Khwang Fold and Thrust Belt. 29

Chapter IV 49

Determination of the tectonic evolution from fractures, faults and calcite twins on the south-western margin of the Indochina Block 50

Chapter V 82

Detrital zircon analysis of the southwest Indochina terrane, central Thailand: Unravelling the Indosinian orogeny 83

Chapter VI 111

Geochronological and geochemical study of mafic and intermediate dykes from the Khao Khwang Fold-Thrust Belt: Implications for petrogenesis and tectonic evolution 112

Chapter VII 140

The effect of active margin tectonic on palaeostress magnitudes: Results after calcite twin analysis in central Thailand 141

Conclusions and Perspective 159

Supplementary Data 162

Appendix A 163

Appendix B 181

Appendix C 213

Appendix D 217

Appendix E 219

Abstract

The south-western margin of the Indochina Block and more specifically the Khao Khwang Fold-Thrust Belt (KKFTB) within the Saraburi region in the southern portion of the Loei volcanic belt, holds a pivotal role in the reconstruction of the Permo-Triassic evolution of the Indosinian orogeny in SE Asia. Bound to the east by the Khorat Plateau and to the west by the Nan-Uttardit-Sa Kaeo Suture Zone; the KKFTB offers a breath of information regarding inter-terrane correlations and the Late Palaeozoic –Early Mesozoic tectonic setting on the northern margin of the Palaeo and Meso Tethys. The KKFTB offers a natural and ideal laboratory to work out critical components of the tectonic evolution of SE Asia. However it has not often been deeply considered in the models describing the Palaeozoic and Mesozoic phases of the Indosinian tectonic events. The trend of the regional suture zones between the terranes involved in the Indosinian orogeny, such as the sutures between the Sukhothai and Indochina terranes (*Chiang Rai Tect. Line*, *Nan Suture Zone*), and between the Sukhothai and Sibumasu terranes (*Sa Kaeo Chanthaburi Accretionary complex*), are roughly N-S oriented. Hence, in the last decades it has been widely accepted the interpretation where the Indosinian orogeny developed between strongly linear terranes. However, the effects of the Permian and Triassic tectonic events in Thailand have often been interpreted without considering the detailed tectonic evolution of the portion of the Indochina terrane's margin formed by Khao Khwang Carbonate Platform area of the Saraburi Group, in central Thailand. This area is unusual because: 1) an extensive area representing a thin-skinned fold and thrust belt is well-exposed due to quarrying; and, 2) the fold and thrust belt displays a series of E-W and WNW-ESE striking thrusts and associated folds that are not easily explained in the context of the traditional interpretation where the terranes have been accreted broadly along N-S striking collisional zones. Detailed structural observations in numerous quarries around Highway 21, in a 13 km long dip-direction traverse, revealed that overall the thrust belt is composed of several large thrusts with an approximately northwards transport direction. In the southern part of the area, south-verging structures are present. Although the dominant structural trend is northwards-verging, interference structures, and late strike-slip faults indicate there is more than one phase of structural development present.

Considering the polyphase tectonic history of this zone, we considered that integrating a study of fault and fracture with calcite twin analysis might be useful in order to determine the evolving paleo-stress magnitudes and principle stress directions that developed during the tectonic evolution of this highly deformed, polyphase orogen. The tectonic data from the Permian and Triassic carbonates of the Khao Khad Formation of the Saraburi Group, revealed that five tectonic stages might have developed before, during, and after, the Triassic Indosinian Orogeny. Only the first three stages pre-date the main layer-parallel shortening event. Sone and Metcalfe (2008) modelled a back-arc opening between the Sukhothai volcanic-arc and the Indochina terrane. Hence, we interpreted the first phase of extension as a pre-Indosinian N-S deformation reflecting either pre-Indosinian extension, possibly related to, extension foreland-ward of an evolving contractional orogeny, created due to flexure in the peripheral bulge (Doglioni, 1995; Langhi et al., 2011; Tavani et al., 2015), or Permian supra-subduction zone extension. The second stage yields paleostress tensors of both strike-slip and pure compression, which are consistent with a pre-folding compression. This phase described an event that was largely perpendicular to the fold axes of the main structures, while the third stage is associated with an E-W compressional strike-slip phase. A further two stages took place after, or during, the main folding event and correspond to N-S compression and to an E-W

composite strike-slip/contractional stage, the latter which is interpreted to represent Cenozoic deformation related to the India-Asia collision.

Central Thailand and more specifically the KKFTB has a remarkable record of Palaeozoic and Mesozoic sedimentation preserved in a sequence of well-exposed quarries. These rocks have been traditionally lumped together in several formations forming the Saraburi Group. However, until recently, there has been very little sedimentological data with almost no geochronological study available to investigate the depositional environment and tectonic setting where the sedimentation took place. Until now, very little has been known about the ages of the siliciclastic rocks within the basin on the edge of the Indochina terrane, the provenance of the original sediments and, particularly, the change of provenance through time. Because of this, the existing basin evolution models lack essential constraints and, therefore, the significance of this basin for the tectonic evolution of central Thailand is poorly known. Hence, we performed a coupled U-Pb and Lu-Hf isotopic study on 837 detrital zircons from in-situ sedimentary rocks packages within the KKFTB. These analyses revealed that the detrital age spectra spanning from Upper Triassic to Palaeoarchean. The entire dataset have a common age peak at ca. 450 Ma, and all samples contain zircons with ages between 0.2-0.3, 0.4-0.6, 1.0-1.3, 1.7-1.8, 2.2-2.7 Ga. A few zircons predate 3.0 Ga. Multidimensional-scaling analysis of detrital zircons from throughout SE Asia demonstrate that the detrital zircon age spectra of the siliciclastic units of the Saraburi Group resemble that of Permian-Triassic detritus found elsewhere in the Khorat Plateau and throughout Vietnam and southeast China, implying that these areas share similar sources. These sources may be the, now largely covered, Indochina basement, and/or contiguous continental crust in terranes already amalgamated to Indochina at that time. Detrital zircons as young as 205 ± 6 Ma show that some formations of the Saraburi Group, previously considered being of Middle-Late Permian age, are no older than Late Triassic. Therefore, we propose a depositional model, for the region, of a Permian rift or passive margin setting that evolved into piggy back and foredeep basins during an extended period of folding and thrusting in the Triassic.

The collision between Sukhothai and Indochina is marked by the emplacement of a moderately large igneous and volcanic province on the margin of the Indochina terrane named the Loei volcanic belt. However, the southern portion of the volcanic belt has never been investigated and, here we attempt to bridge this gap of information presenting new geochronological, geochemical and isotopic data. The KKFTB records two different stages of from ca. 250 Ma (Pak Chong granodiorite – east to the KKFTB) to ca. 200 Ma (Khao Yai rhyolite – south of the KKFTB) associated with the collision of the Sukhothai volcanic arc. The mafic dyke swarming in the folded layers of the KKFTB are calc-alkalic in major element compositions, highlighting the possible continental setting. The entire set of mafic dykes can be subdivided in three different volcanic groups; however, all the groups present similar chemical footprints with high LILE and LREE, and low HFSE. This exposes the volcanic arc nature of the Loei volcanic system. Isotopically, the three groups are characterized by subtle differences in εNd(t) values (from 2.94 to 5.16) and initial $^{87}Sr/^{86}Sr$ ratios (from 0.705 ~ 0.706). The high levels of NI, Cr and Mg# along with low levels of SiO_2 suggests high inputs from the mantle during their genesis. However, the volcanism is likely to not represent primary melts, as judged from their MgO (average <6.1%), Mg# (0.29–0.99) and Ni contents (1.5–320 ppm). These characteristics suggest that they most likely underwent a degree of fractional crystallization prior to emplacement. All the rocks from the KKFTB show a distinct trend that straddle from MORB to IAT Ti/V fields. These geochemical features might be representative of a tectonic setting where the arc-affine rocks of the

KKFTB represent the stage of the subduction of the slab (proximal BAB) between Sukhothai and Indochina. During the Late Triassic the volcanic system evolved, possibly after the Indochina-Sukhothai slab break-up, in a more MORB-like magma with higher levels of Ti depletion, represented by the samples within the MORB field.

The complex structural characters, the spread depositional ages of the sedimentary units, the different ages of the deformation and the complex geochemistry of the volcanic rocks within the KKFTB strongly support that this small tectonic domain underwent to a complex and polyphasic tectonic history during the Permian and Triassic stages of the Indosinian orogeny associated with the amalgamation of the actual SE Asia.

“Science, my lad, is made up of mistakes,

but they are mistakes which it is useful to make,

because they lead little by little to the truth.”

-Jules Verne – ***A Journey to the Centre of the Earth***

Journal articles

Arboit, F., Collins, A. S., King, R., Morley, C. K., & Hansberry, R. (2014). Structure of the Sibumasu–Indochina collision, central Thailand: A section through the Khao Khwang Fold and thrust belt. *Journal of Asian Earth Sciences*, *95*, 182-191.

Arboit, F., Amrouch, K., Collins, A. S., King, R., & Morley, C. (2015). Determination of the tectonic evolution from fractures, faults and calcite twins on the south-western margin of the Indochina Block. *Tectonics*. **34**, 1576-1599.

Arboit, F., Collins, A. S., Morley, C., King, R., Amrouch, K. (2016). Detrital zircon analysis of the southwest Indochina terrane, central Thailand: Unravelling the Indosinian orogeny, *GSA Bulletin*. *In press*.

Arboit, F., Collins, A. S., Morley, C., King, R., Amrouch, K. (2016). Geochronological and geochemical study of mafic dykes from the Khao Khwang Fold-Thrust Belt: Implications for petrogenesis and tectonic evolution. *Gondwana Research. Submitted.*

Arboit, F., Amrouch, K., Morley, C., Collins, A. S., & King, R. (2016). The effect of active margin tectonic on palaeostress magnitudes: Results after calcite twin analysis in central Thailand. *Tectonophysics*. *Submitted.*

Statement of Authorship

Title of Paper	Structure of the Sibumasu–Indochina collision, central Thailand: A section through the Khao Khwang Fold and thrust belt
Publication Status	☑ Published ☐ Accepted for Publication ☐ Submitted for Publication ☐ Unpublished and Unsubmitted work written in manuscript style
Publication Details	Arboit, F., Collins, A. S., King, R., Morley, C. K., & Hansberry, R. (2014). Structure of the Sibumasu–Indochina collision, central Thailand: A section through the Khao Khwang Fold and thrust belt. *Journal of Asian Earth Sciences*, *95*, 182-191.

Author Contributions

By signing the statement of Authorship, each author certifies that their stated contribution to the publication is accurate and that permission is granted for the publication to be included in the candidate's thesis

Name of Principal Author (Candidate)	Francesco Arboit		
Contribution to the Paper	Carried out the analyses and interpretation of the data, wrote the manuscript, acted as corresponding author		
Certification:	This paper reports on original research I conducted during the period of my Higher Degree by Research candidature and is not subject to any obligations or contractual agreements with a third party that would constrain its inclusion in this thesis. I am the primary author of this paper.		
Signature		Date	15/01/2016

Name of Co-Author	Prof. Alan Collins		
Contribution to the Paper	Supervised work, help with data interpretation and manuscript revision		
Signature		Date	15/01/2016

Name of Co-Author	Dr Rosalind King

Contribution to the Paper	Supervised work, help with data interpretation and manuscript revision		
Signature		Date	15/01/2016

Name of Co-Author	Prof. Chris Morley		
Contribution to the Paper	Supervised work, help with data interpretation and manuscript revision		
Signature		Date	15/01/2016

Name of Co-Author	Mr. Rowan Hansberry		
Contribution to the Paper	Assistance with data collection		
Signature		Date	15/01/2016

Statement of Authorship

Title of Paper	Determination of the tectonic evolution from fractures, faults and calcite twins on the south-western margin of the Indochina Block
Publication Status	☑ Published ☐ Accepted for Publication ☐ Submitted for Publication ☐ Unpublished and Unsubmitted work written in manuscript style
Publication Details	Arboit, F., Amrouch, K., Collins, A. S., King, R., & Morley, C. (2015). Determination of the tectonic evolution from fractures, faults and calcite twins on the south-western margin of the Indochina Block. Tectonics.

Author Contributions

By signing the statement of Authorship, each author certifies that their stated contribution to the publication is accurate and that permission is granted for the publication to be included in the candidate's thesis

Name of Principal Author (Candidate)	Francesco Arboit		
Contribution to the Paper	Carried out the analyses, prepared samples, and interpreted the data, wrote the manuscript, acted as corresponding author		
Certification:	This paper reports on original research I conducted during the period of my Higher Degree by Research candidature and is not subject to any obligations or contractual agreements with a third party that would constrain its inclusion in this thesis. I am the primary author of this paper.		
Signature		Date	15/01/2016

Name of Co-Author	Dr Khalid Amrouch		
Contribution to the Paper	Supervised work, help with data interpretation and manuscript revision		
Signature		Date	15/01/2016

Name of Co-Author	Prof. Alan Collins

Contribution to the Paper	Supervised work, help with data interpretation and manuscript revision		
Signature		Date	15/01/2016

Name of Co-Author	Prof. Chris Morley		
Contribution to the Paper	Help with data interpretation and manuscript revision		
Signature		Date	15/01/2016

Name of Co-Author	Dr Rosalind King		
Contribution to the Paper	Supervised field-work, manuscript revision		
Signature		Date	15/01/2016

Statement of Authorship

Title of Paper	Detrital zircon analysis of the southwest Indochina terrane, central Thailand: Unravelling the Indosinian orogeny
Publication Status	☐ Published ☑ Accepted for Publication ☐ Submitted for Publication ☐ Unpublished and Unsubmitted work written in manuscript style
Publication Details	Arboit, F., Collins, A. S., Morley, C., King, R., Amrouch, K. (in press). Detrital zircon analysis of the southwest Indochina terrane, central Thailand: Unravelling the Indosinian orogeny, *GSA Bulletin*.

Author Contributions

By signing the statement of Authorship, each author certifies that their stated contribution to the publication is accurate and that permission is granted for the publication to be included in the candidate's thesis

Name of Principal Author (Candidate)	Francesco Arboit		
Contribution to the Paper	Carried out the analyses, prepared samples, and interpreted the data, wrote the manuscript, acted as corresponding author		
Certification:	This paper reports on original research I conducted during the period of my Higher Degree by Research candidature and is not subject to any obligations or contractual agreements with a third party that would constrain its inclusion in this thesis. I am the primary author of this paper.		
Signature		Date	15/01/2016

Name of Co-Author	Prof. Alan Collins		
Contribution to the Paper	Supervised work, help with data interpretation and manuscript revision		
Signature		Date	15/01/2016

Name of Co-Author	Prof. Chris Morley

Contribution to the Paper	Helped with data collection. Help with data interpretation and manuscript revision		
Signature		Date	15/01/2016

Name of Co-Author	Dr Rosalind King		
Contribution to the Paper	Assistance with data collection, manuscript revision and collaboration		
Signature		Date	15/01/2016

Name of Co-Author	Dr Khalid Amrouch		
Contribution to the Paper	Manuscript revision		
Signature		Date	15/01/2016

Statement of Authorship

Title of Paper	Geochronological and geochemical study of mafic dykes from the Khao Khwang Fold-Thrust Belt: Implications for petrogenesis and tectonic evolution
Publication Status	☐ Published ☐ Accepted for Publication ☑ Submitted for Publication ☐ Unpublished and Unsubmitted w ork w ritten in manuscript style
Publication Details	Francesco Arboit, Alan S. Collins, Christopher K. Morley, Fred Jourdan, Rosalind King, John Foden, and Khalid Amrouch, (in press). Geochronological and geochemical study of mafic dykes from the Khao Khwang Fold-Thrust Belt: Implications for petrogenesis and tectonic evolution, *Gondwana Research.*

Author Contributions

By signing the statement of Authorship, each author certifies that their stated contribution to the publication is accurate and that permission is granted for the publication to be included in the candidate's thesis

Name of Principal Author (Candidate)	Francesco Arboit		
Contribution to the Paper	Carried out the analyses, prepared samples, and interpreted the data, wrote the manuscript, acted as corresponding author		
Certification:	This paper reports on original research I conducted during the period of my Higher Degree by Research candidature and is not subject to any obligations or contractual agreements with a third party that would constrain its inclusion in this thesis. I am the primary author of this paper.		
Signature		Date	15/01/2016

Name of Co-Author	Prof. Alan Collins		
Contribution to the Paper	Supervised work, supervised during filed-work and data collection, help with data interpretation and manuscript revision		
Signature		Date	15/01/2016

Name of Co-Author	Prof. Chris Morley

Contribution to the Paper	Helped with data collection, help with data interpretation and manuscript revision		
Signature		Date	15/01/2016

Name of Co-Author	Prof. Fred Jourdan		
Contribution to the Paper	Helped with data interpretation and manuscript revision.		
Signature		Date	15/01/2016

Name of Co-Author	Dr Rosalind King		
Contribution to the Paper	Assistance with data collection.		
Signature		Date	15/01/2016

Name of Co-Author	Prof. John Foden		
Contribution to the Paper	Helped with data interpretation		
Signature		Date	15/01/2016

Name of Co-Author	Dr Khalid Amrouch		
Contribution to the Paper	Manuscript revision		
Signature		Date	15/01/2016

Statement of Authorship

Title of Paper	The effect of active margin tectonic on palaeostress magnitudes: Results after calcite twin analysis in central Thailand
Publication Status	☐ Published ☐ Accepted for Publication ☑ Submitted for Publication ☐ Unpublished and Unsubmitted w ork w ritten in manuscript style
Publication Details	Francesco Arboit, Khalid Amrouch, Christopher K. Morley, Alan S. Collins, and Rosalind King (in review). The effect of active margin tectonic on palaeostress magnitudes: Results after calcite twin analysis in central Thailand, T*ectonophysics.*

Author Contributions

By signing the statement of Authorship, each author certifies that their stated contribution to the publication is accurate and that permission is granted for the publication to be included in the candidate's thesis

Name of Principal Author (Candidate)	Francesco Arboit		
Contribution to the Paper	Carried out the analyses, prepared samples, and interpreted the data, wrote the manuscript, acted as corresponding author		
Certification:	This paper reports on original research I conducted during the period of my Higher Degree by Research candidature and is not subject to any obligations or contractual agreements with a third party that would constrain its inclusion in this thesis. I am the primary author of this paper.		
Signature		Date	15/01/2016

Name of Co-Author	Dr Khalid Amrouch		
Contribution to the Paper	Supervised work, supervised during data collection, help with data interpretation and manuscript revision		
Signature		Date	15/01/2016

Name of Co-Author	Prof. Chris Morley		
Contribution to the Paper	Helped with data collection, help with data interpretation and manuscript revision		
Signature		Date	15/01/2016

Name of Co-Author	Prof. Alan Collins		
Contribution to the Paper	Supervised work		
Signature		Date	15/01/2016

Name of Co-Author	Dr Rosalind King		
Contribution to the Paper	Assistance with data collection.		
Signature		Date	15/01/2016

Declaration

I certify that this work contains no material which has been accepted or offered for the award of any other degree or certificate in my name, in any other university or other tertiary institution and to the best of my knowledge and belief, contains no material that has been previously published or written by other authors, with the only except of the references made in the text. In addition, I certify that no part of this work will, in the future, be used in a submission in my name, for any other degree or diploma in any university or tertiary institution without the prior approval of the University of Adelaide and where applicable, any partner institution responsible for the joint-award of this degree.

I give consent to this copy of my thesis when deposited in the University Library, being made available for loan and photocopying, subject to the provisions of the CopyrightAct 1968.

The author acknowledges that copyright of published works contained within this thesis resides with the copyright holder(s) of those works.

Also give permission for the digital copy of my thesis to be made available on the web, via the University's digital research repository, the Library Search and also through web search engines, unless permission has been granted by the University to restrict access for a certain period of time.

Francesco Arboit

Chapter I

Project Overview

Aesthetically appealing thrust systems and related large-scale anticlines, in both active and fossil foreland fold- thrust belts, and the economic potential associated with them, have captured the interest of structural geologists for many decades. Further, fold-thrust belts are geological archives able to record the most useful information for reconstructing their geodynamic evolution. Here we try to provide a review of the deformation pattern templates from field data within the foreland Khao Khwang Fold-and-Thrust-Belt (KKFTB), with data that aim to show how the KKFTB holds fundamental information necessary to reconstruct the geodynamic evolution on the southwestern margin of the Indochina terrane.

This fold and thrust belt is one of the key area for better understanding the various deformational stages of the Indosinian orogeny in central Thailand. The KKFTB was formed during the early phases of the Indosinian event, on the onset of the collision between the Indochina terrane and the Sukhothai volcanic arc (Sone and Metcalfe, 2008). The KKFTB lies on the south-western margin of the Indochina Block and exposes an area of ± 2900 km^2 of east-west trending, polydeformed and slightly metamorphosed Permian and Triassic rocks. The KKFTB is bounded to the east by the Khorat Plateau and to the west by the Nan Suture Zone. Recent studies revealed the extremely complex tectonic framework of the KKFTB and that the large portions of this deformed belt have experienced different stages of deformation and low-pressure regional metamorphism (Morley et al., 2013).

The Indosinian orogenic belt, within central SE Asia, is characterized by various subduction and collision-related events that span the period from around 260 Ma to 190 Ma (see reviews in Lepvrier et al., 2004; Sone and Metcalfe, 2008 and Barber et al., 2011). In Thailand, the tectonic belts trend predominantly N–S, including the back-arc suture zone (Nan-Uttardit-Sa Kaeo) and the Palaeo-Tethyean sutures (Inthanon Zone). It is commonly accepted that the Nan-Uttardit-Sa Kaeo Suture Zone is related to the closure of the back-arc basin and collision of the volcanic-arc dominated Sukhothai zone with Indochina during the Early to Middle Triassic, and a later collision occurred between the combined Sukhothai-Indochina block with Sibumasu as Palaeo-Tethys closed during the Late Triassic-Early Jurassic, (e.g. Fontaine and Workman, 1978; Hahn, 1984; Sone and Metcalfe, 2008; Booth and Sattayarak, 2011; Barber et al., 2011). However, the position of these suture zones is cryptic in several areas and working out the timing of their closure has previously proved elusive. The key to unravelling the evolution of central Thailand, and the tectonic architecture of the south-western margin of Indochina lies in the exposed sedimentary and volcanic rocks of the Saraburi Group within the KKFTB. Mixed carbonate-siliciclastic Permian to Triassic rocks on the eastern side of the lower Chao Phraya Central Plain from Nakhon Sawan to the Saraburi Province, and on the western margin of the Khorat Plateau from Loei to Chaiyaphum/Phetchabun provinces belong to the Saraburi Group. Bunopas (1981) was the first to propose a separate Indochina Block stratigraphic division (Saraburi Group) for the units in the Saraburi-Pak Chong area. Later Hinthong (1985) and Hinthong et al. (1985) revised the stratigraphy within the KKFTB subdividing the Group in six main formations, namely the: Phu Phe, Khao Khwang, Nong Pong, Pang Asok, Khao Khad, and Sap Bon formations. Originally these formations were thought to constitute a simple upward succession; however, biostratigraphical, structural, and geochronological analyses now show that the extension of the

Saraburi Group is not limited to the Permian but gets to the Late Triassic (Norian-Rhaetian) and few of the formations are synchronous.

Studies of the sedimentology of the Saraburi Group started only in the last decades, and include those by Pendexter (1980), Dawson (1993), Dawson and Racey (1993), Dawson et al. (1993), Charoentitirat (2002), and Udchachon et al. (2007, 2008). The presence of folds and faults within the Saraburi Group was observed for the first time by Dawson and Racey (1993). However, in one of the latest regional geological maps (Ueno and Charoentitirat, 2011) the Phu Phe Formation is the only formation that is shown as being overthrust onto the Khao Khad and Sap Bon formations. Detailed sedimentological and structural analyses of the KKFTB are yet to be established. The known geological architecture shows in the southern portion of the KKFTB more than one carbonate platforms stepping laterally into clastic-dominated depositional environments. Seismic reflection data on the Khorat Plateau show a series of coeval basins, which are E-W striking rift-related Permian basins, controlled by extensional faults, and that carbonates tend to occupy the high, intra-basinal areas, while clastics or mixed clastics and carbonates fill the basins (Booth and Sattayarak, 2011).

Therefore, it is of fundamental importance to take in account the pivotal role of the KKFTB in order to constraining the compressional events affecting the Sukhothai and Indochina terranes and shed light on the tectonic evolution of the Triassic Indosinian Orogeny in central Thailand. Here we report a sequence of structural, geomechanical, geochronological, isotopic, and geochemical analyses on the tectonic structures, and sedimentary and volcanic rocks of the KKFTB. All the newly discovered data provide an overview on the tectonic framework, Phanerozoic evolution, and palaeogeography of SE Asia, focusing on the tectonic, structural, geochronological, isotopic and geochemical aspects of the rocks lying on the south-western margin of the Indochina Block. Particular emphasis has been placed on the geodynamic evolution of the KKFTB and its importance in reconstructing the evolution of the Indosinian Orogeny during the Permian and Triassic in SE Asia.

Chapter II

Thesis Outline

The thesis aims to bring new information on the evolution of the Indosinian orogeny using several methodologies on the rocks and the structures of the KKFTB.

Chapter 3- In the last decades the effects of the Indosinian orogeny in Thailand have often been interpreted without considering a detailed structural analysis of the south-western margin of the Indochina Block and the Loei Volcanic Belt in central Thailand. The lack of structural data from central Thailand prompted some reconstruction models to interpret the south-western margin of the Indochina Block as the highly linear boundary of an accretionary complex associated to the closure of the Permian back-arc basin between the Sukhothai and Indochina terranes. Therefore, detailed field-based structural analyses were performed through a sequence of scan-areas, scan-lines and geological mapping throughout the best exposed sedimentary sequences of the Saraburi Groups. More than 800 structural features were collected within the Sap Bon, Khao Khad and Nong Pong formations. From south to north several litho-tectonic features were recognised:

- Permian to Triassic volcanic and sedimentary rocks lying east to the cryptic Nan-Uttardit-Sa Kaeo Suture Zone;
- the informal unit “alum shale” (Morley et al., 2013) is the only portion within the KKFTB that shows folded volcanic units; which suggests the record of Permian stages of the early deformation;
- the fold and thrust belt formed by forward (north) propagating deformation in the Triassic, consists only of cover strata and has been displaced mainly along weak horizons of incompetent shale within the Khao Khad Formation, transported by numerous in-sequence thrusts;
- The Khao Khwang represents a thin-skinned fold and thrust belt developed on a detachment that lies between 0.7 and 1.5 kilometres depth which is similar to the stratigraphic thickness of the Khao Khad Formation (Dawson and Racey, 1993; Thambunya et al., 2007, Ueno and Charoentitirat, 2011);
- The in-sequence thin-skinned deformation demonstrates that deformation has migrated from S-SSE to N-NNW along a zone as wide as the fold and thrust belt itself, with lateral variations probably attributed to lateral facies variations;
- Evidence of lateral structural variations occur along the strike of the fold and thrust belt in zones of mechanical weakness in the shale levels, these different rates of strain accommodation are probably related to oblique-lateral ramps between thrusts;
- The imbricated thrusts generally cut the forelimbs of folds in the limestone of the Khao Khad Formation, suggesting a model where some imbricates were formed during the folding, whilst folding continued in the surrounding shales with the development of some minor amplitude buckle folding associated with detachment levels.

All these data revealed that the KKFTB represents a significant kink in the collision between Sibumasu and Indochina, which may be due to either the original geometry of the Indochina margin, or due to a poorly recognised ocean strand that split Indochina into two or more. Although the dominant structural trend is northwards-verging, interference structures, and late strike-slip faults indicate there is more than one phase of structural development present, with an estimated amount of shortening that affected the KKFTB of ± 10/15 km.

Chapter 4- The structural analyses on the architecture of the large scale deformation revealed the polyphase evolution of the palaeostress that affected the KKFTB from the Permian to the Cainozoic. This composite structural framework is attributed to the complex continental amalgamation that led to the actual SE Asia during the Permian and Triassic stages of the Indosinian orogeny. Therefore, in order to characterize and compare the stress-strain record prior to, during, and just after folding at the macroscopic and the microscopic scales and to provide insights into stress levels sustained by folded rocks; we investigate the relationship between the stress-strain distribution in folded strata derived from fractures, striated micro-faults, and calcite twins and the development of the KKFTB. We here focused on the description of the internal deformation of folded strata and characterization of the controlling mechanisms at the microscopic scale, and the mechanical response of rocks during folding and the distribution of strain within the folds. We decided to investigate the stress record through the tectonic phases of the Indosinian orogeny at both microscopic and mesoscopic scales, through a study on the striated micro-faults and calcite twins. Widespread mechanical e-twinning occur in the calcite crystals within the carbonate Khao Khad Formation in the southern portion of the KKFTB. One of the advantages of this technique is that the e-twinning requires a low critical resolved shear stress (RSS) (10 ± 4 MPa), which depends on grain size (e.g., Rowe and Rutter, 1990) and internal twinning strain (Turner et al., 1954; Laurent et al., 2000; Lacombe, 2001, 2007), and has only a small sensitivity to temperature, strain rate and confining pressure, therefore considering the possible slight regional metamorphism that have affected central Thailand during the Indosinian orogeny it is possibly the best tool to evaluate the palaeostress history.

The inversion process takes into account both the twinned and the untwinned planes, the latter being those of the potential e-twinning planes that never experienced a RSS of sufficient magnitude to cause twinning. The inverse problem consists in finding the stress tensor that best fits the distribution of twinned and untwinned planes. The basic hypothesis is that the RSS τ_s acting on any twinned e plane is higher than, or at least equal to the critical RSS τ_a.

Thus, for twinned planes: $\tau_s \geq \tau_a$ and for untwinned planes: $\tau_s < \tau_a$. The Etchecopar's CSIT allows simultaneous computation of principal stress orientations and differential stresses. The tensor solution is calculated as a normalized reduced stress tensor such as (σ1 - σ3) is scaled to $[(\sigma1 - \sigma3)^*=1]$. Thus, the value of the RSS τ_s acting on any plane lies between -0.5 and +0.5, that is, $-(\sigma1 - \sigma3)^*/2$ and $+ (\sigma1 - \sigma3)^*/2$ (Jamison and Spang, 1976). Theoretically, all the twinned planes consistent with a given tensor must sustain a τ_s value larger than the one exerted on any untwinned plane. The best tensor solution is searched as to minimize the function f, ideally equal to 0.

The optimal tensor is obtained when (I) the maximum of twinned planes are taken into account; (II) the maximum of untwinned planes are taken into account; and (III) the f value is minimal (in practice, one can authorize a weak percentage, 10%–15%, of untwinned planes receiving a RSS larger than the smallest applied τ_a because of measurement uncertainties and local heterogeneities at the grain scale).

This process drives through the determination of the orientation of the three principal stresses, we hence used the conjoined analysis of fractures, faults and calcite twins to analyse the paleo-stresses (both magnitudes and principle stress directions) that affected the area during the Indosinian orogeny from the Permian onward. This multi-methodological study revealed the five tectonic stages that were interpreted to have developed before, during, and after, the Indosinian Orogeny.

Chapter 5- This chapter focuses on characterizing the provenance of the siliciclastic rocks throughout the KKFTB. The study utilises LA-ICPMS U-Pb zircon geochronology and multicollector LA-ICPMS Lu-Hf isotopes in zircons to better constraints the provenance, with a particular emphasis placed on the potential source rocks in the adjoining blocks in SE Asia during the Permian and Triassic. The relevance of the information that might come from the stratigraphic control of the Permian and Triassic clastic formations in SE Asia was exposed in the last decades (Bodet and Schärer, 2000; Carter and Bristow, 2003; Carter and Clift, 2008; Li et al., 2012; Burrett et al., 2013). The majority of the exposed areas within the KKFTB present rocks of the Permian carbonate and clastic formations of the Saraburi Group, unfortunately no stratigraphic control have ever been applied on the siliciclastic formations such as the Sap Bon, Pang Asok and Nong Pong formations. The clastic formations of the Saraburi Group were used to provide a control on the timing and tectonic setting of the Indosinian orogeny during the Permian and the Triassic. The poor stratigraphic geochronological and provenance constraints left a gap full of uncertainties on the tectonic setting of SE Asia and more specifically on the tectonic framework of Central Thailand during the Triassic. Therefore, a deep geochronological provenance investigation provided a higher level of constrain on the provenance, maximum depositional ages and depositional environment of the south-western margin of the Indochina terrane through the Late Palaeozoic to Early Mesozoic. The analyses revealed detrital age spectra spanning from Upper Triassic to Palaeoarchean. However, there is a loose control on the sedimentary supply and the possible palaeogeography of central Thailand in the Triassic. Therefore, a more robust statistical approach (Multidimensional-scaling) based on the K-S statistic was considered necessary to individuate the possible sedimentary sources (Vermeesh, 2013). This study demonstrates that the KKFTB was not experiencing uniform deposition throughout the entire area, and that the detrital zircon age spectra of the siliciclastic units of the Saraburi Group resemble that of Permian-Triassic detritus found NE from the southwestern margin of the Khorat Plateau to the southern margin of the South China Block. New data on the maximum depositional ages of the clastic formations lying within the KKFTB drastically changed the depositional history of the Saraburi Group, which was previously considered extending till the Middle-Late Permian age, and now are no older than Late Triassic.

Chapter 6- This chapter investigates the significance of the volcanic rocks that intruded the KKFTB through geochemical and isotopic analyses. The geochemistry of the KKFTB volcanic suite has never been investigated; however, a common conception extends the Loei volcanic belt to the southern portion of the KKFTB. This chapter integrates all the newly acquired zircon U–Pb age data, mica $^{40}Ar/^{39}Ar$ ages, and whole rock isotopic and geochemical analyses in order to: (I) characterise the magmatic pulses, and their relevance to the current tectonic models; (II) for better constraining the timing of the Sukhothai-Indochina & Sibumasu-Indochina collisions during the Permo-Triassic stages of the Indosianian orogeny. It is shown that the entire set of mafic dykes can be subdivided in three different volcanic groups on the basis of trace and incompatible element abundances. However, a similar geochemical imprinting is shown with high LILE - LREE, and low in HFSE, highlighting the volcanic arc nature of the system. These geochemical features suggest that the KKFTB mafic dykes and the volcanic rocks in central-northern Thailand were likely crystallized in different times and orogenic settings.

Chapter 7- The concept of stress is of primary importance when dealing with the mechanics of materials. Although the validity of applying concepts of continuum mechanics to natural rock masses that are neither continuous nor purely solid may be questioned, in practice the idealisation of reality by the definition of an equivalent continuum has proved very powerful for many mechanical purposes (Lacombe, 2009). There are several reasons for portraying the distribution of stresses in the crust such as geological hazards, engineering activities and resource exploration, but also from fundamental geological purposes, such as understanding the mechanical behaviour of geological materials and deciphering the various tectonic mechanisms that led to the investigated structure, from those related to plate motions at a large scale to those causing jointing and faulting or even microstructures at a smaller scale. Therefore, in this chapter we tried to integrate geomechanic and microstructural data and hence to deal with the reconstruction of intraplate paleostresses magnitudes.

References

Bodet, F., Schärer, U., 2000. Evolution of the SE-Asian continent from U–Pb and Hf isotopes in single grains of zircon and baddeleyite from large rivers. Geochimica et Cosmochimica Acta 64, 2067–2091

Burrett, C., Zaw, K., Meffre, S., Lai, C. K., Khositanont, S., Chaodumrong, P., Udchachon, M., Ekins, S., Halpin, J., 2013. The configuration of Greater Gondwana—Evidence from LA ICPMS, U–Pb geochronology of detrital zircons from the Palaeozoic and Mesozoic of Southeast Asia and China. Gondwana Research. Vol. 26, pp. 31-51.

Carter, A., & Bristow, C. S., 2003. Linking hinterland evolution and continental basin sedimentation by using detrital zircon thermochronology: a study of the Khorat Plateau Basin, eastern Thailand. Basin Research, 15(2), 271-285.

Carter, A., & Clift, P. D., 2008. Was the Indosinian orogeny a Triassic mountain building or a thermotectonic reactivation event?. Comptes Rendus Geoscience, 340(2), 83-93.

Dawson, O., & Racey, A. 1993. Fusuline—calcareous algal biofacies of the Permian Ratburi Limestone, Saraburi, Central Thailand. *Journal of Southeast Asian Earth Sciences*, *8*(1), 49-65.

Lacombe, O. 2001. Paleostress magnitudes associated with development of mountain belts: Insights from tectonic analyses of calcite twins in the Taiwan Foothills. Tectonics, 20(6), 834-849.

Lacombe, O. 2007. Comparison of paleostress magnitudes from calcite twins with contemporary stress magnitudes and frictional sliding criteria in the continental crust: Mechanical implications. Journal of Structural Geology, 29(1), 86-99.

Lacombe, O., Malandain, J., Vilasi, N., Amrouch, K., & Roure, F. 2009. From paleostresses to paleoburial in fold–thrust belts: Preliminary results from calcite twin analysis in the Outer Albanides. *Tectonophysics*, *475*(1), 128-141.

Laurent, P., Kern, H., & Lacombe, O. 2000. Determination of deviatoric stress tensors based on inversion of calcite twin data from experimentally deformed monophase samples. Part II. Axial and triaxial stress experiments. Tectonophysics, 327(1), 131-148.

Li, X. H., Li, Z. X., He, B., Li, W. X., Li, Q. L., Gao, Y., & Wang, X. C., 2012. The Early Permian active continental margin and crustal growth of the Cathaysia Block: in situ U–Pb, Lu–Hf and O isotope analyses of detrital zircons. Chemical Geology, 328, 195-207.

Morley, C.K., Ampaiwan, P., Thanudamrong, S., Kuenphan, N., Warren, J., 2013. Development of the Khao Khwang Fold and Thrust Belt: Implications for the geodynamic setting of Thailand and Cambodia during the Indosinian Orogeny. Journal of Asian Earth Sciences, 62, 705-719.

Rowe, K. J., & Rutter, E. H. 1990. Palaeostress estimation using calcite twinning: experimental calibration and application to nature. Journal of Structural Geology, 12(1), 1-17.

Thambunya, S., Visut, P.A., Khantaprab C., 2007. Depositional Environments of Permian Rocks of the Khao Khad Formation in Central Thailand. *ScienceAsia* N.33. 371-381

Turner, F. J., T GRIGGS, D. A. V. I. D., & Heard, H. 1954. Experimental deformation of calcite crystals. Geological Society of America Bulletin, 65(9), 883-934.

Ueno, K., Charoentitirat, T., 2011. Carboniferous and Permian. In: Ridd, M.F., Barber,A.J. Crow, M.J. (eds.), The Geology of Thailand, The Geological Society of London, 71–136.

Vermeesch, P., 2013. Multi-sample comparison of detrital age distributions. Chemical Geology, 341, pp. 140-146

Chapter III

Arboit, F., Collins, A. S., King, R., Morley, C. K., & Hansberry, R. (2014). Structure of the Sibumasu–Indochina collision, central Thailand: A section through the Khao Khwang Fold and thrust belt. *Journal of Asian Earth Sciences*, *95*, 182-191.

Structural of the Sibumasu-Indochina Collision, Central Thailand: A section through the Khao Khwang Fold and Thrust Belt.

ABSTRACT

Mainland SE Asia is composed of a number of continental fragments and volcanic arcs, separated by oceanic suture zones, that were accreted to the growing Asian continent during the Triassic Indosinian orogeny. The evolution of this orogeny has always been quite controversial. Indeed, the effects of this orogeny in Thailand have often been interpreted without considering the detailed tectonic evolution of the portion of the Indochina Block's margin formed by Khao Khwang Platform area of the Saraburi group, in central Thailand. This area is unusual because: 1) an extensive area representing a thin-skinned fold and thrust belt is well-exposed due to quarrying and 2) the fold and thrust belt displays a series of E-W and WNW-ESE striking thrusts and associated folds that are not easily explained in the context of the traditional interpretation where the terranes have been accreted broadly along N-S striking collisional zones. Detailed structural observations in numerous quarries around Highway 21 in a 13 km long dip-direction traverse have revealed that overall the thrust belt is composed of several large thrusts with an approximately northwards transport direction. In the southern part of the area south-verging structures are present. Although the dominant structural trend is northwards-verging, interference structures, and late strike-slip faults indicate there is more than one phase of structural development present.

1. Introduction

Fold and thrust belts are widely studied in the geologic record because they are both the most common way the upper crust accommodates shortening and for having a worldwide distribution (Cunningham and Mann, 2007). The interest in this type of structural system goes beyond pure scientific curiosity. The study of fold and thrust belts is essential in developing a complete understanding of the evolution of an orogenic belt. In addition, they commonly trap hydrocarbons, and form major exploration targets (Poblet et al., 2011; Cooper, 1986).

Mainland Southeast Asia is the key area for understanding the Permo-Triassic Indosinian orogeny (Fontaine and Workman, 1978, Metcalfe, 2002, 2005, 2011). An orogeny that, in the present use of term, encompasses Late Palaeozoic to Early Mesozoic orogenesis in places as diverse as Korea (Cluzel et al., 1991; Metcalfe, 2006), central China (Li et al., 2006), and throughout South-East Asia (Metcalfe 2013; Morley et al., 2013). Exposed parts of the orogeny are also key locations to use as analogues to assist in understanding sub-surface tracts of Permian-Triassic fold and thrust belts, the main target for hydrocarbon exploitation in northeast Thailand.

The case study presented here comes from the Khao Khwang Fold-and-Thrust Belt of central Thailand. This fold and thrust belt lies on the southern edge of the Indochina block (Morley, 2013). Between its Devonian separation from Gondwana, and its Triassic collision with Sibumasu, the Indochina Block records deposition/formation of carbonates, clastic sedimentary rocks, chert and basalt of the Late Carboniferous to Permian Saraburi Group (Hinthong, 1985), in both neritic and pelagic environments (Metcalfe, 1999, 2006; Ferrari et al., 2008, Ueno and Charoentitirat, 2011). Among the previously published plate-tectonic models, the Indosinian orogeny had two peaks of activity that have been defined

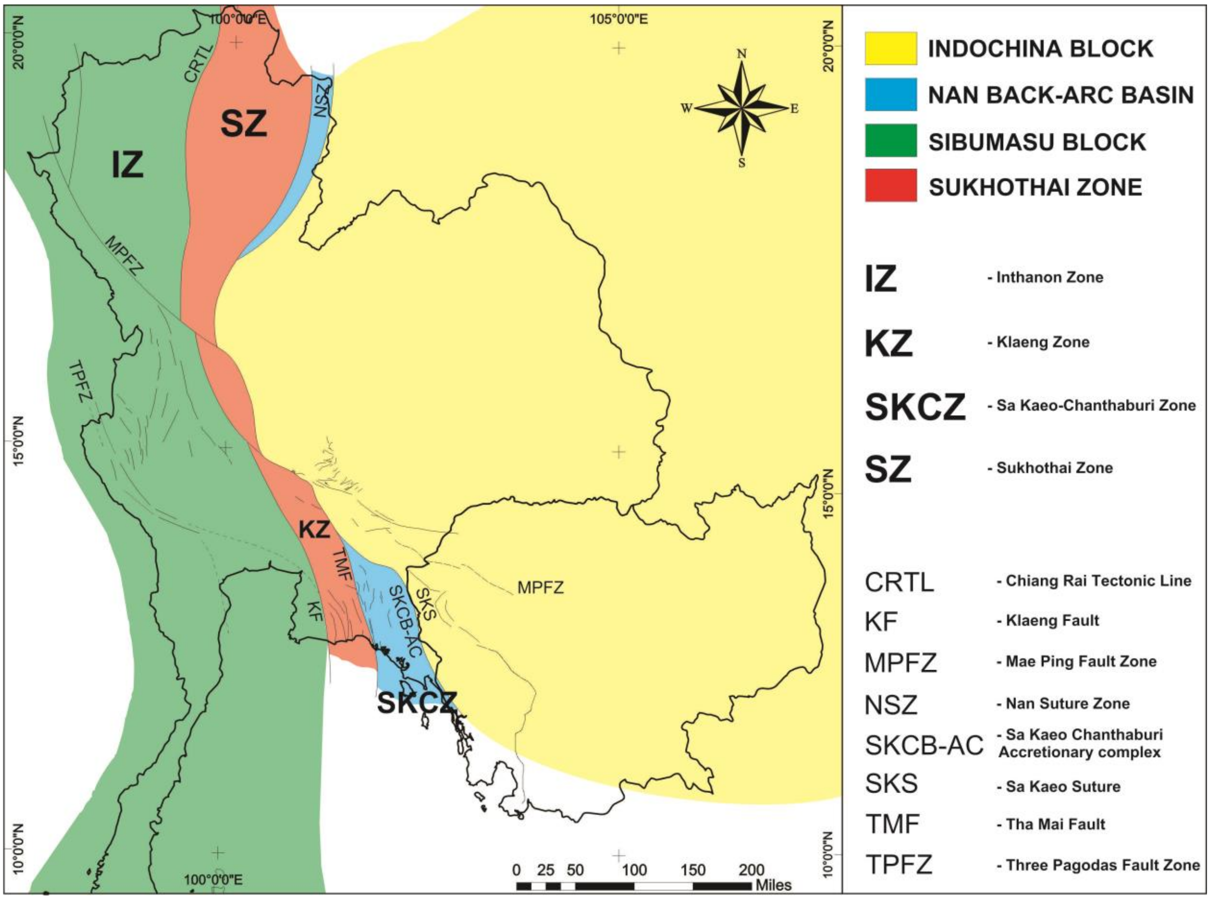

Fig. 1. Geotectonic subdivision of Thailand into main tectonic areas collided during the Indosinian Orogeny (modified from Ueno and Charoentitirat, 2011) and distribution ofthe major lineaments of the study area.

in Thailand as an early stage developed between the Lopingian – Carnian and the late stage during the latest Triassic (Helmcke and Lindenberg, 1983; Sone and Metcalfe, 2008; Morley et al., 2013). The aim of this paper is to analyse and reconstruct the structural framework of the Triassic KKF&T Belt in this southern strand of the Indosinian orogen. This reconstruction is based on the analysis of the contractional structures developed in the carbonate rocks of the Khao Khad Formation (Saraburi Group) and their interpretation in a regional cross section through the Saraburi region. This cross section is a powerful tool that allows us to (1) define more precisely the main architectural elements such as faults, the linkage between low-angle and high-angle reverse faults, propagation mechanisms and associated folding styles and their distribution across the KKF&T Belt, (2) propose a kinematic model for the Triassic geodynamic evolution of the south-western margin of the Indochina Block.

2. Tectonic Framework of Thailand

Bunopas (1981) was the first person to introduce the plate tectonic concept for the geological evolution of Southeast Asia. Later workers have revealed that the region is made up of a composite puzzle of terranes derived from Gondwana during the Palaeozoic (Devonian – Permian) (Metcalfe, 1988, 1990, 1991, 1998, 2002, 2005, 2011; Lepvrier, 1994; Morley et al., 2002, 2013). Numerous models have been proposed to unravel the geotectonic evolution across the countries of SE Asia (Metcalfe, 1988, 1990, 2002, 2011;

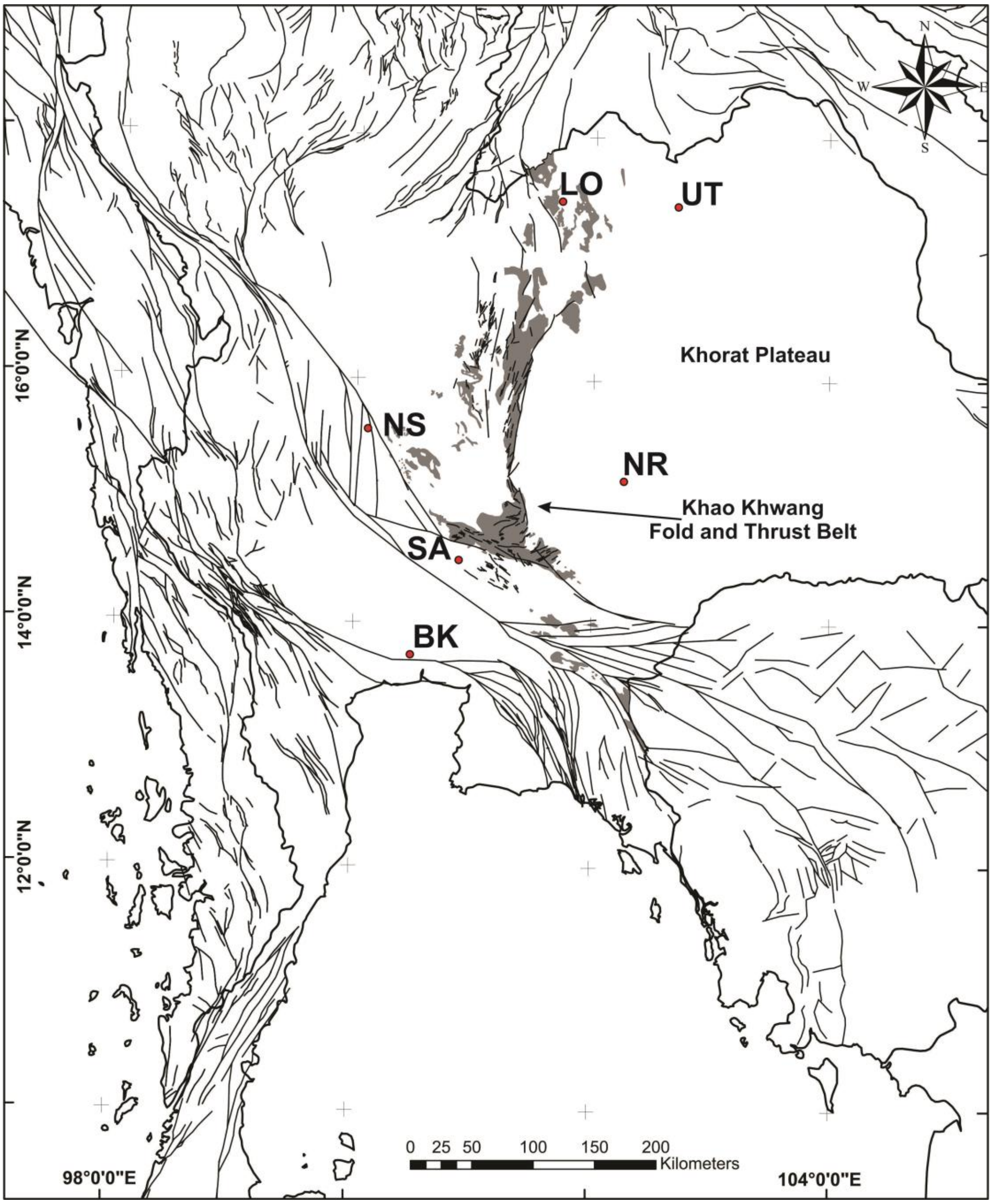

Fig. 2. Map with major lineaments (after Morley et al., 2013) at a regional scale (solid lines), based on Landsat 7 satellite imagery analysis, and distribution of Permian rock in Thailand (grey areas), based on the geological map of Thailand (from DMR, 1999). NR = Nakhon Ratchasima, BK = Bangkok, SA = Saraburi, NS = Nakhon Sawan, PH = Phetchabun, LO = Loei, UT = Udon Thani.

Ueno, 1999, 2002; Charusiri et al., 2002, Sone and Metcalfe, 2008; Ferrari et al., 2008, Ridd et al., 2012, Zaw et al., 2013, Burrett et al., 2013). Thailand and Malaysia, have often been depicted as two major continental masses—Sibumasu and Indochina—that collided during the Triassic. Recent reconstructions have also recognised the Nan Suture Zone (and its southern expression the Sa Kaeo Chantarburi Accretionary Complex) (Metcalfe, 2005; Ueno and Charoentitirat, 2011; Sone and Metcalfe 2008) (Figure 1), which isolates a domain of central Thailand, known as the Sukhothai Arc (Sone and Metcalfe, 2008). The Nan Suture Zone was previously interpreted as the site of closure of

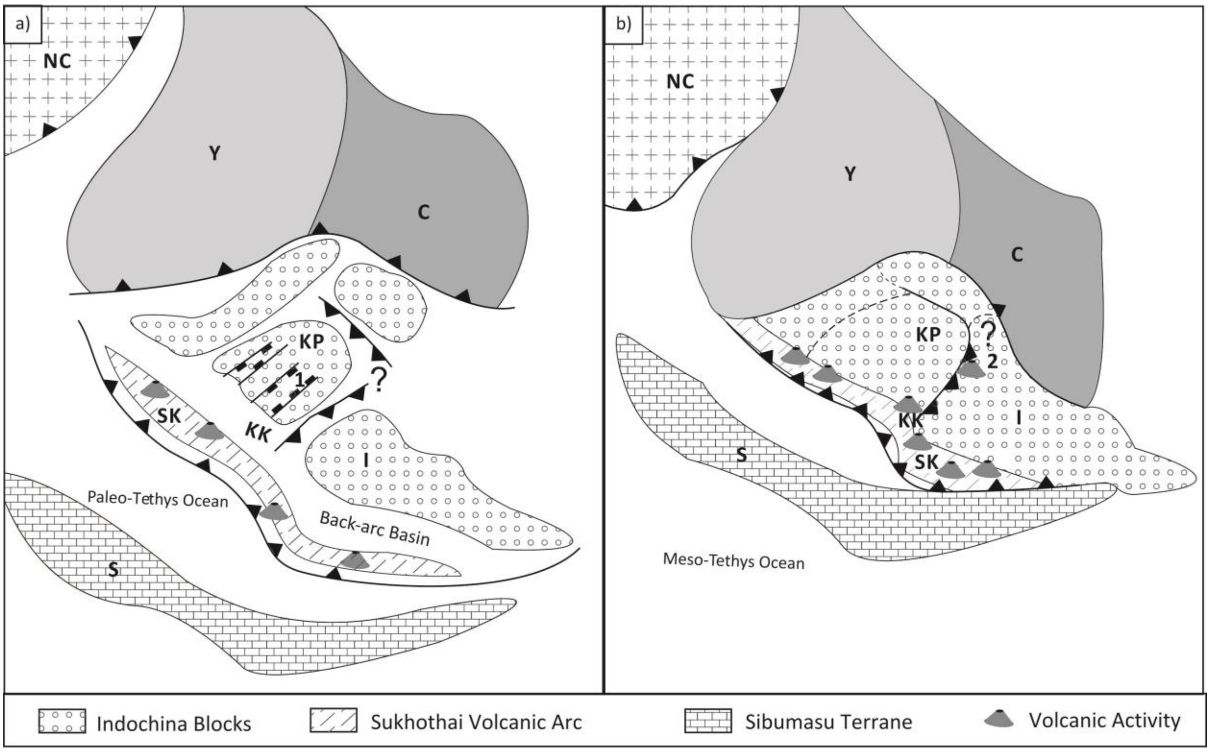

Fig. 3. Map view reconstruction of the plate tectonic evolution of the SE Asia during Early Triassic (A) and Middle Triassic (B). Modified from Morley et al. (2013) and Lepvrier et al. (2004). NC = North China, Y = Yangtze Block, C = Cathaysian Block, I = Indochina Block, KP = Khorat Plateau, KK = Khao Khwang carbonate platform, SK = Sukhothai Terrane, 1 = rift related Permian Basin in the Khorat Plateau, 2 = possible minor suture zone running on edge of the Khorat Plateau.

the Palaeo-Tethys Ocean, which, during the Palaeozoic (Middle Devonian – Early Triassic), spanned the area between the Indochina Block (Cathaysian domain) and the Gondwana-derived Sibumasu Block (Ueno and Hisada, 2001; Ueno et al., 2012, Metcalfe, 2005, 2006, 2011, 2013). Ueno (1999), and successively, Ueno and Hisada (2001) and Sone and Metcalfe (2008), used stratigraphic and biostratigraphic evidence to suggest that this suture zone more likely represents the closure of a Late Devonian Late Permian back-arc basin related to an extensional regime between Indochina to the east and the Permian Sukhothai terrane, to the west (Barr and Macdonald, 1991; Metcalfe, 2006, 2011, 2013; Sone and Metcalfe 2008; Yang et al. 2009; Barber and Charusiri, 2011). Sibumasu lies to the west of the Sukhothai terrane, and is separated from it by the Chiang Rai and Klaeng sutures (Metcalfe, 1999, 2005, 2006; Ueno and Hisada, 1999, 2001; Sone and Metcalfe, 2008) (Figure 1). The Chiang Rai and Klaeng sutures are interpreted as being the site of the closure of a second strand of the Palaeo-Tethyan Ocean (Late Triassic – Early Jurassic) (Ferrari et al., 2008; Sone and Metcalfe, 2008; Barber et al., 2011, Metcalfe, 2011).

Structurally, two sets of major lineaments are seen in north/central Thailand; N-S and NW-SE (Figure 2). The N-S trend corresponds to the overall E-W (present coordinates) collision proposed by most workers for the collision of both Sukhothai/Indochina and Sibumasu/Sukhothai (Metcalfe, 1998, 2000, 2005, 2011; Sone and Metcalfe, 2008; Ridd, 2012), as well as the trends of Cenozoic extensional faults, and some local trends of Cenozoic strike-slip faults. The NW-SE trend is

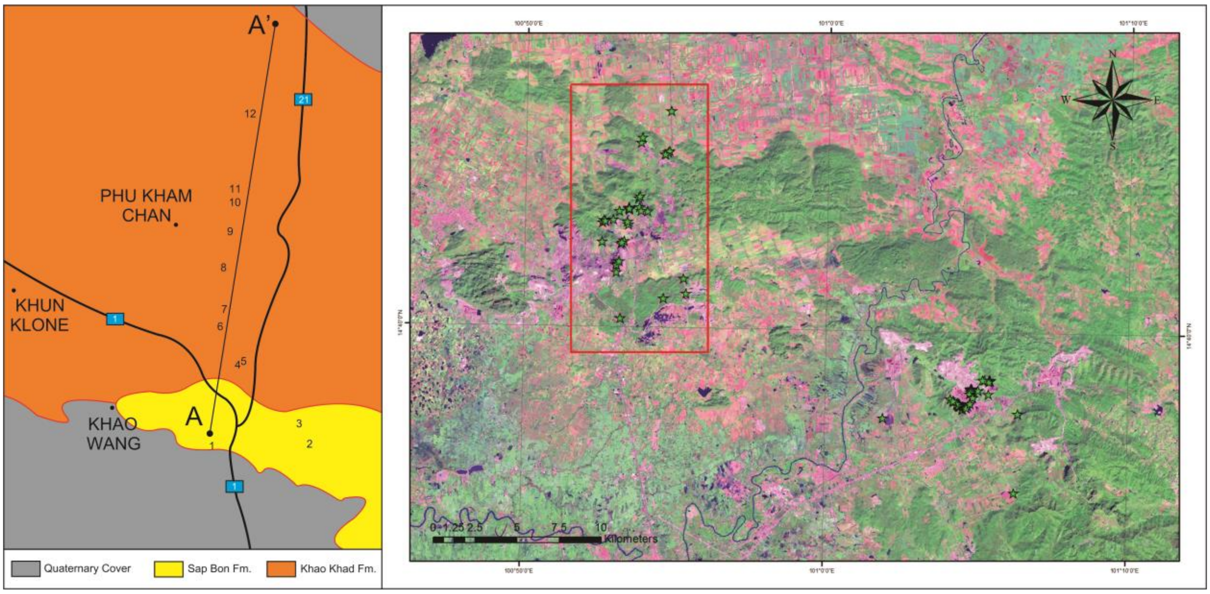

Fig. 4. GPS stops superimposed atop of Landsat 7 satellite images (bands 8-4-2). Geological map of the study area (DMR, 1999); 1-2-3 quarries in the southern portion of the cross-section, 4-5 quarries on ridge one, 6 quarry on ridge two, 7 quarry on ridge three, 8-9-10-11 quarries on ridge 4, 12 quarry on ridge 6. A–A' length of the cross-section. 1-21 national Thai Highways.

seen throughout eastern Myanmar and western Thailand and could correspond to an extensive network of Cenozoic strike-slip faults (Morley et al., 2007), related to Cenozoic continental deformation after the India – Eurasia collision (Tapponnier et al., 1986). The strike-slip faults commonly combine NW-SE, NNW-SSE, ENE-WSW, E-W and N-S trending segments to form horsetailing splays and strike-slip duplexes. One of the major NW-SE striking faults running into Thailand is the Mae Ping (also known as Wang Chao) fault zone (Morley et al., 2007; Lacassin et al., 1997; Leloup et al, 2001; Tapponier, 1986).

3. Permian Stratigraphy in Northern and Central Thailand

The Permian carbonates of the Saraburi area were once considered part of the Ratburi Limestone (Brown et al., 1951; Toriyama et al., 1974; Hinthong et al., 1981, 1985). Subsequently, Bunopas (1985) named all the Permian limestones of the Indochina Block in Thailand as the Saraburi Group. In this article, we use the classification proposed by Ueno and Charoentitirat (2011) (after Hinthong, 1981, 1985), where the Saraburi Group of the southwest Indochina Block (the Khao Khwang Platform) is divided into six formations, namely the: Phu Phue, Pang Asok, Khao Khad, Sap Bon, Khao Khwang and Nong Pong Formations. The sedimentary cover of the carbonate platform does not have a well-defined thickness, because of its complex structural framework, but, it has been estimated to range from c. 1400 up to c. 3500 m (Chutakositkanon et al., 2000; Dawson and Racey, 1993) and spans the Upper Carboniferous to the Lower Triassic. The carbonates of the study area are grouped under the Khao Khad Formation (Bunopas, 1985), which has been described as mainly thin- to very thick-bedded limestone with chert nodules and locally interbedded argillite, dolomitic shale, siltstone, sandstone and conglomerate (Ueno and Charoentitirat, 2011). Previous work on the Khao Khad Formation has concentrated on interpreting the outcrop facies distribution, primarily by

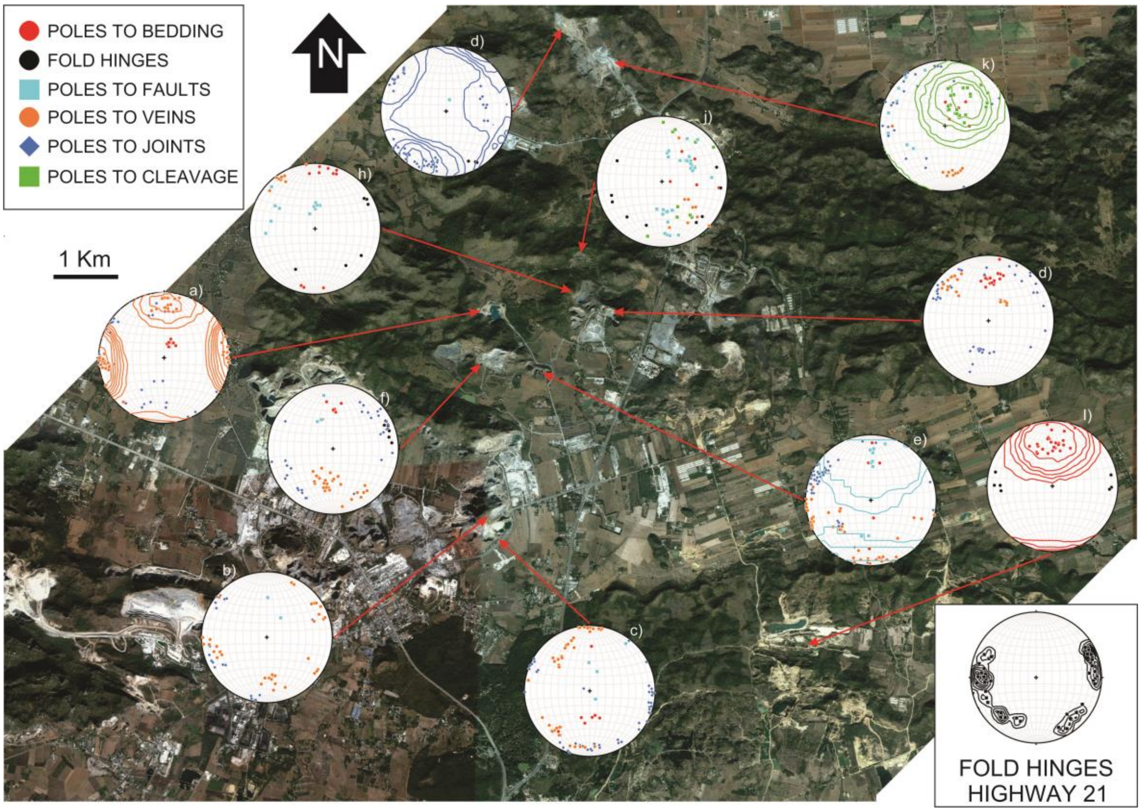

Fig. 5. Satellite photo of the study area and location of the structural stations and relative stereoplot: a–k relative to structural data on Khao Khad Fm., l on Sap Bon Fm.

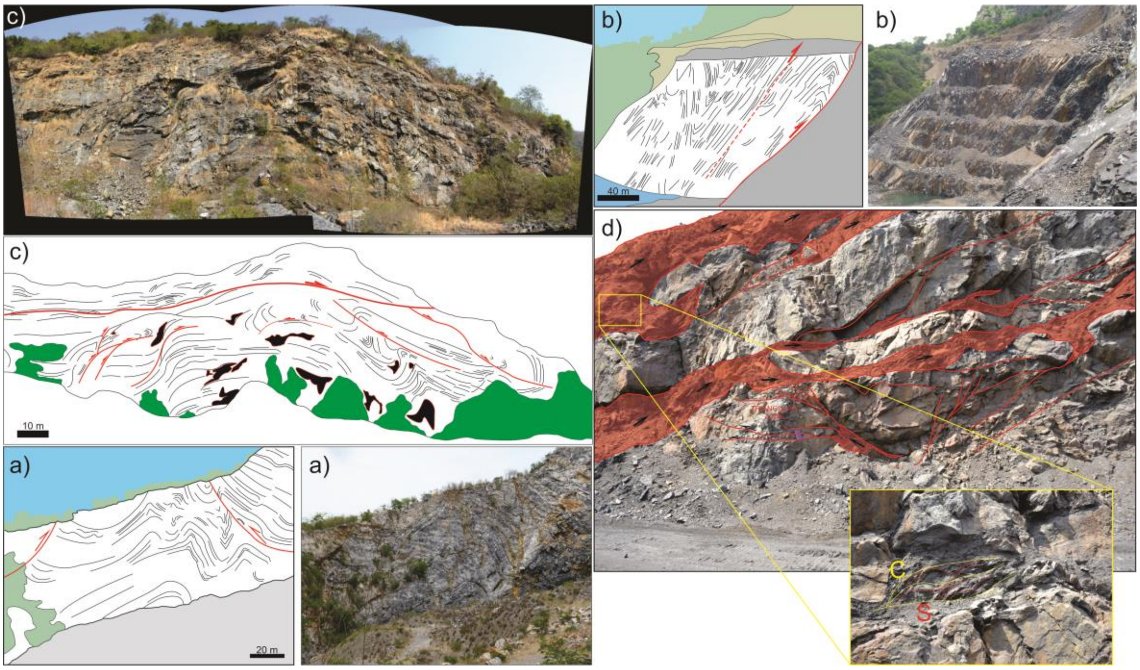

Fig. 6. (a) Photograph and line drawing of the disharmonic folding in Khao Yai Hill on ridge 1. (b) Fault propagation fold and parasitic folding related to the emplacement of two main slip surfaces. (c) Panoramic view of one of the quarries on ridge four and the relative interpretation highlighting the main structural features as faults and bedding. (d) Detachment levels in quarry 12 on ridge 6 and line drawing of the shale (red) with superimposed the C–S fabric. (For interpretation of the references to colour in this figure legend, the reader is referred to the web version of this article.)

lateral and vertical lithological changes due to variability in the lateral and temporal depositional environments (Chutakositkanon et al., 2000; Thambunya et al., 2007). Only Dawson and Racey (1993) introduced the possibility of structural complication along a particularly well-exposed N-S section along the Thai national Highway 21. These authors documented structural thickening through the section and the presence of a possible vertical alternation of facies due to folding and thrusting. The goal of this project is not to redefine the stratigraphy of the area but to provide a reconstruction of the geodynamic evolution across the Saraburi Region. The most deformed zone along Highway 21 is characterised by the presence of well bedded carbonates – wackestones/packestones plus occasional grainstones and boundstones (Dawson and Racey, 1993) – with a notable presence of chert lenses, and dark grey limestones with shaly and volcanic-tuffaceous levels. Limitations in this study include uncertainties in detailed stratigraphic columns for these rocks that have been historically attributed to the Mid-Permian. The lack of deep well control and seismic or other geophysical imaging constrain the cross sections (Figures 7) to non-unique solutions. However, the section represents a consistent interpretation of the data on the base of the modern concepts of fold and thrust belt interpretations (Mitra and Boyer, 1984; Mitra, 2002; Cosgrove, 2000; Poblet and Lisle, 2011; Morley et al. 2011). The cross section therefore has been carried out taking in consideration both the available ages (Dawson and Racey, 1993) and the lithological facies distribution along Highway 21.

4. The Khao Khwang Fold and Thrust Belt

We have constructed one regional cross section across the Saraburi Region, perpendicular to the trend of the KKF&T Belt. The lack of subsurface data through the fold and thrust belt restricts the subsurface interpretation to being solely based on projection from surface data. This limitation is balanced by the excellent exposure of the deformed Permian stratigraphy along the investigated section line. The lack of highly exhumed ‘basement’ thrust sheets, or thrust sheets bearing significantly pre-Permian sequences also constrains us to an interpretation for the thrust belt as a thin-skinned belt, where each thrust fault and related folds are linked to major detachments.

Along Highway 21 (Figure 4) a sequence of 10 quarries and highway 21 road cuts have excavated the Khao Khad and Sap Bon Formations (Hinthong, 1985) to provide the expansive outcrop that has led to a number of publications on the stratigraphy of the area (Dawson and Racey, 1993; Racey et al., 1996; Chitnarin et al., 2008; Fontaine, 2002, Thambunya et al., 2007). However, many of these have underestimated the thrust imbricate nature of the fold-thrust belt, which has often been interpreted as an undeformed sequence of facies (Thambunya et al., 2007, Chutakositkanon et al., 2000). Lithologically, the KKF&T Belt is dominated by thickly-bedded platform carbonates (the Khao Khad Formation and the Phu Phe Formation), intercalated with intrabasinal shale and chert units that have focussed much of the strain, and acted as detachment horizons (Hansberry et al., in review).

5. The Highway 21 section

The westernmost cross section was constructed through the KKF&T Belt along Highway 21. The first 10 kms, from Phu Khae to Chong Sarika, exposes an excellent section through the thrust imbricated Permian Khao Khad Formation (Figure 7), which crops out as WNW-ESE ranges in the Saraburi region. Field investigation occurred across 10 limestone quarries along the western side of Highway 21, where structural characterization has been carried out. This cross section, and the relative fault and fracture analysis, were constructed through methodologies such as geological mapping, scan lines, scan areas and satellite photomosaic in a GIS environment.

The investigated field locations (Figure 4), presented different stages of deformation, including folded regions verging almost entirely north, gently deformed slabs composed of layered carbonate, reverse and thrust faults, back-thrusts, and evidence of strike-slip fault zones. The quarries, where detailed fieldwork (Figure 7) has been undertaken, were selected in order to determine the structural evolution with clear structural and spatial relationships. The study area has been divided into southern and northern areas, the boundary corresponds with the intersection between Highways 1 and 21, and approximately with the stratigraphical boundary proposed by Hinthong (1985) between the Khao Khad and Sap Bon Formations (Figure 4). Here, the deformation style also changes drastically.

Highway 21 stratigraphy

Hinthong (1985) described as conformable the boundary between the Sap Bon and the Khao Khad Formations (Figure 4). Field based observation along Highway 21 revealed the gradational change in the lithology from latitude N 14°42’00’’ (massive carbonates alternated with thin bedded dark carbonates) to latitude N 14°41’00’, where, the presence of cherty carbonates alternates with cm-bedded siltstone and fine sandstone. Khao Yai Hill represents the first topographic high along the cross-section (Figure 7). This portion of the KKF&T Belt consists of a stack of thrusts imbricating a sequence of carbonates, characterised by the absence of chert and clastic rocks. Dawson and Racey (1993) described this part of the Khao Khad Formation as inter-bedded dolomitic algae (stromatolites) and fenestral mudstones/wackestones (peritidal flats facies). However, this interpretation did not take in consideration the structural framework and the consequent stratigraphical implications. The flat area north of Khao Yai Hill (*c.* N 14°42’31.14’’ – E 100°53’15.58’’) shows a sequence of grey, dark grey limestone (mostly mudstone) with chert lenses and nodules, alternating with layers of shale and silt. This part of the KKF&T Belt gets wider on the eastern side of Highway 21 making it possible to infer the presence of a lateral facies change of the carbonates of the Khao Yai Hill. A sequence of six ridges characterised by considerable structural complexity governs the topography of this portion of the KKF&T Belt. The stratigraphy in this area has been described by Dawson and Racey (1993) and Thambunya et al., (2007), either without taking in consideration, or by underestimating, the structural framework and the consequent possible repetitions in the stratigraphy. Lithologies to the north are typically composed of bioclastic rocks in the northernmost portion, with boundstone dominated by *Tubiphytes* and binding algae as *Archaeolithoporella* (Dawson and Racey, 1993), whereas the southern part of this ridge domain largely consists of a platform-derived exoclast in a matrix of mudstone-wackestone (Dawson and Racey, 1993). Dawson and Racey (1993) described the lithology of the northern ridge domain as dominated by silicified mudstone with chert nodules. The upper part of this sequence displays numerous sedimentary structures related to mass transport as turbidites and debris flow deposits. The depositional model of the Khao Khad Formation is, therefore, represented by a shallow carbonate ramp prograding northward (respect to the present orientation), with a protected lagoon and peritidal depositional environment in the extreme south (Dawson and Racey, 1993; Chutakositkanon et al., 2000; Thambunya et al., 2007).

SOUTHERN HIGHWAY 21

The southern part of the cross section (Figure 7) consists of highly deformed layers of orange, purple and brownish thinly-bedded siltstone and mudstone, which vary in thickness from a few cm up to 1 metre. The southernmost part of the section solely consists of siliciclastic material, with no observable carbonate component. While to the north, lithologies consist of an alternation of thin silty sandstone and widespread lenses and layers of recrystallised carbonate rocks. The rocks in this region dip south (with a range of dip directions from 160° to 190°) (Figure 5), with no major folding and with the strain accommodated by a pervasive intra-bed slip and folding at the sub-metric to metric scale. In the north of this region, near Highway 21, the alternation of incompetent mud units and the more competent carbonate units has contributed to the emplacement of weakly to intensively folded and deformed zones. In some of the layers, the shaly units display extremely narrow zones (from 10 cm up to about 1 m) of thinly foliated breccia and fault gouge forming zones of displacement. These damage zones are characterised by the presence of calcite veins. It is therefore possible to interpret these as low temperature thrust faults (Sibson, 1977). The pervasive strain observed in the southern part of this region is interpreted as a region of distributed shear strain forming a parallel shear zone (Mitra, 2002). The interlayered slip in this highly deformed zone is interpreted to be associated with the presence of a major basal detachment running at the base of the clastic unit.

NORTHERN HIGHWAY 21

Ridge 1

Quarries number 4 and 5 (Figure 6), lie within Khao Yai Hill, which lies one kilometre east of the Highway 21 and road 3385 intersection. Hinthong (1985) placed the boundary between the Sap Bon and Khao Khad formations three kms south of Khao Yai Hill. This stratigraphic boundary is based on the lithological transition from the southern incompetent carbonate – clastic alternation of the Sap Bon Formation, to the massive competent carbonate of the Khao Khad Formation (Hinthong, 1985). The structural style at Khao Yai Hill is strongly influenced by the mechanical anisotropy of the stratigraphy. Figure 6 shows a sequence of tight chevron disharmonic folds lying in the foot-wall of a major thrust whilst two major folds (fault propagation fold and fault bend fold) occur in the hanging-wall, above a south verging fault. In the south side of Khao Yai Hill this different deformation style probably occurred because of the different competence of the two deformed slabs of rock. The hanging-wall is a slab composed of competent thick layers of carbonate (packestone – wackestone), overthrusting a slab of alternating dark shales and thin-bedded carbonate (packestone – wackestone).

The major fault is traceable for a couple of kilometres and parallels bedding in the fore-limb of the fold, whilst cutting obliquely through the Khao Khad Formation in the back-limb (Figure 7). Small portions of this ramp are tectonically thickened by a sequence of small duplex structures. The northern part of the hill preserves a major fault with a related detachment fold (Figure 7); the straight bed-parallel geometry of this fault suggests that it may have been present before folding. Poles to bedding are bimodal, which is a clear evidence for almost planar fold limbs (Figure 5). The only cleavage exhibited is observed within the layers of interbedded shale, but in quarry number 4 it is more pervasive near the synclinal hinge. In quarry number 5 (in the northern part of the Khao Yai Hill) cleavage is observed in shale units of the small duplexes. Cleavage is mostly developed at a high angle to bedding (75° - 85°) and dips north into the shale levels of the Khao Khad Formation. This may be related to the increased deformation in the damage zone of the major faults.

Ridge 2

Quarry number 6 is on the second ridge, approximately 500 metres north of Khao Yai Hill. It is a prominent structure, five km in length and 1 km in width. This ridge is formed from a doubly plunging fold, the southern (backlimb) of the anticline dips uniformly S – SSE. The northern (forelimb) is vertical to slightly overturned in places. The shortening strain is accommodated by a sequence of folds within the body of a thrust sheet and is cored by a sequence of imbricated thrusts with steep dip angles, ranging from 80° to about 40° (Figure 7). The folds, related to the southernmost thrust, have a chevron configuration with a box fold geometry at high levels. The box-fold kink-band axial planes merge towards the base of the outcrop, forming chevron folds.

Ridge 3

The third ridge along Highway 21 (Figure 7) contains a well-exposed fault-propagation fold, where the thrust breaks through the Khao Khad Formation with a moderately steep angle of dip (47°). Figure 6 shows that two bright green units of andesite are almost isoclinally folded and follow the bedding, suggesting that they may be two sills or tuffs. In contrast to the Khao Yai folds, this fault-propagation fold is recumbent with a fold axis orientation of 25° → 270°. Both the limbs are planar with an average angle of ~45°. Units of shale are interbedded with dark grey limestone. The bedding within these units is totally overprinted by a pervasive cleavage. The coloured volcanic layers are excellent marker horizons that highlight the complex geometry and deformation in the folds, demonstrating diffuse parasitic folding of second and third order folds (Figure 6). The lowest beds in the northernmost anticline form angular hinges with more rounded hinges in the upper levels. The minor thrusting is restricted to an interbedded unit; therefore strata thickness is expected to be homogeneous without duplications, although, it is possible to observe a slight thickening in the back-limb (*c*. 5-10%). Vein orientation is rather homogeneous throughout the entire quarry. Whereas, intense fracturing is restricted to the most deformed zones close to the thrust. The homogeneity of veins and joints across the folds is associated with a notable amount of interbedded flexural slip, which used the clastic shaly units to accommodate the strain. Sequences of hill-type meshes (Sibson, 1996), with opened tension gashes in competent carbonate layers alternated with shears along shale beds, have been observed and are interpreted to form due to the extreme shale/carbonate competence contrast.

Ridge 4

Rocks of the fourth ridge are well exposed in two large quarries (Figure 4). Here fold styles differ from the more southerly ridges by having larger wavelengths and wider hinges with 1.6 kilometres between the back- and the front-limbs of the anticline (Figure 7). The southern side of the ridge (back-limb) displays a well-bedded carbonate, folded into a wide syncline – anticline (radius ~ 100m) with a north dipping axial plane (32°/185°) and an east plunging hinge 11°→088°. Further north (Figure 7), the lithology passes from well-bedded carbonate to dark grey massive limestone with an increase of the shale

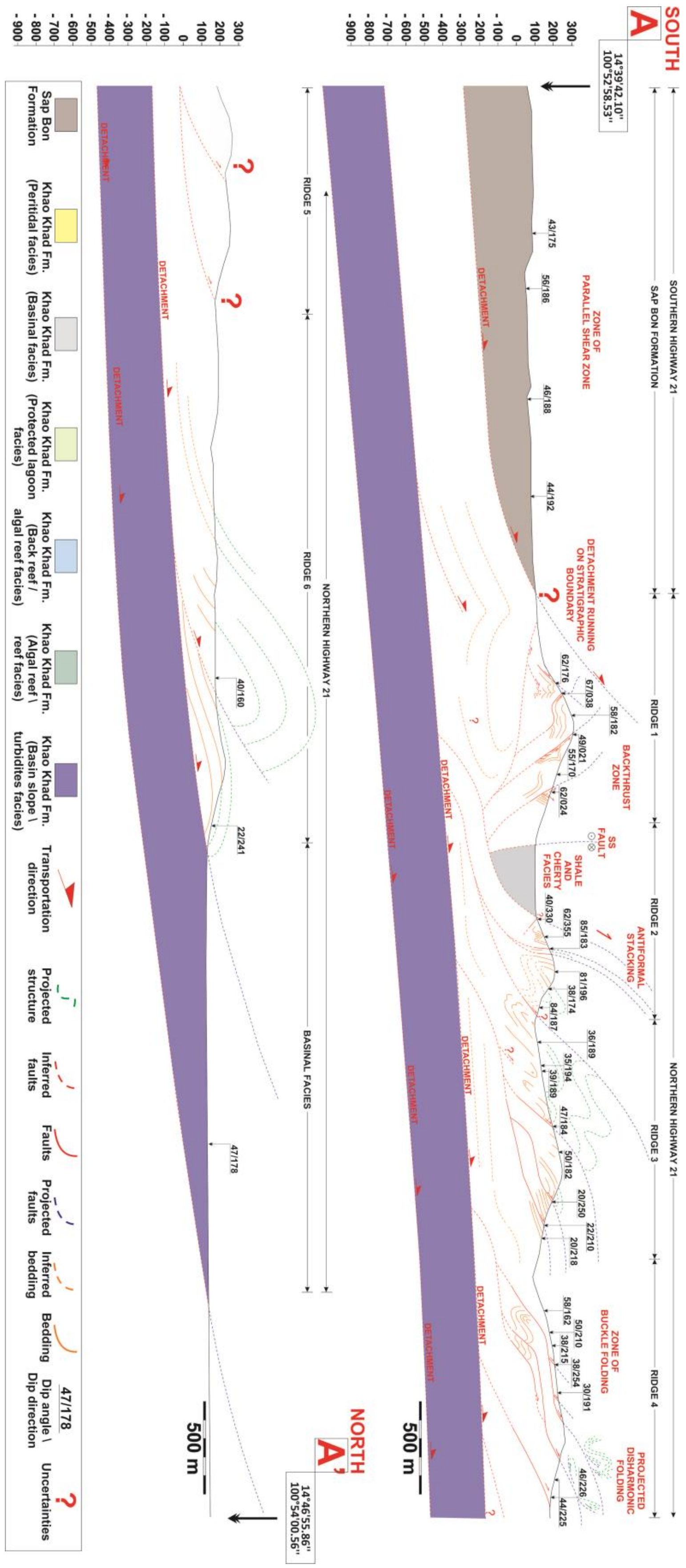

Fig. 7. Regional cross-section A–A0 through the southern portion of the Saraburi Region, the Khao Khwang Fold-and-thrust belt (see Fig. 4 for location).

amount (2-5%). The northern part of the hillside along Highway 21 is characterized by numerous slip planes that tend to follow bed parallel fissility. The shale and carbonate masses are folded with wavelengths ranging from 1 to 10 m. The folds are disharmonic (Figure 6). Chevron to isoclinal folds occur throughout the entire quarry, the deformation is so intense that the shale has been displaced from the cores of folds. Folding was not enough to accommodate the strain and at some stage (syn- or post-folding) high-angle reverse faults formed to accommodate the displacement, on the scale of these two quarries. Folds in this part of the section have a very consistent SW-NE direction. The deviation from the E-W fold hinge trend could be because of later, possible Cenozoic deformation, or due to decoupling deformation at the core of a detachment dying out on a flat level of shale. Macroscopic observations demonstrate that calcite veins are most abundant in the footwall, with a horizontal (en-echelon) pattern consistent with a horizontal maximum principal stress.

Ridge 5

The fifth ridge from the south is poorly exposed, therefore, the interpretation in Figure 7 follows the same structural style of the other ridges, and is not discussed further for lack of knowledge.

Ridge 6

The northernmost ridge preserves two major fold propagation faults associated with two well exposed thrusts running on levels of shale measuring 1-10 meters in thickness. These leading edge anticlines formed at the frontal part of a thrust as a result of thrust propagation. The southern of the two folds (Figure 6) has been partially removed by erosion. Close to the core of the fold, the high content of shale led to disharmonic folding. The southern thrust preserves a steeper dip angle (30°/240°) with respect to the northernmost thrust (22°/241° – 25°/190°). Deformation is localized along the cleavage surfaces or shear bands giving a sigmoidal shape fabric to the shale, with two different well-developed cleavage planes resembling a C-S structure (Figure 6). Calcite veins are common in the shales suggesting considerable fluid migration. Within approximately 50 cm of the thrust surface the shale is characterized by intense cataclasis (mesocataclasite with matrix content around 70-80%).

6. The Khao Khwang Fold-and-Thrust Belt cross section

The cross section presented here was constructed across the KKF&T Belt in central Thailand, using a combination of 1:250000 geological maps (Hintong et al., 1985), satellite image interpretation (SRTM and Landsat-7 imagery) and field data from exposures across the southern part of the belt.

There are no subsurface data (such as seismic sections or well-log data) in the area, thus it is difficult to interpret the geometry of the structures at depth within the KKF&T Belt. A variety of structural models are possible to predict the geometry and distribution of folds and thrusts in the subsurface. The observed geometries of folds and thrusts in outcrops best fit a kink-band fold deformational style. Thus, the application of the fault-bend fold or fault-propagation fold modelling technique is here deemed appropriate, since the majority of the folds have been generated in response to faulting (Suppe, 1985; Mitra, 2002). However, there is a component of pure buckle folding mostly related to incompetent layers of shale. The evolution of the KKF&T Belt has been interpreted with a forward (northward) propagating model of staircase imbricated trajectories with a sequence of three detachment faults, which have been positioned at a depth calculated on the base of the fold geometries, formation thicknesses and their morphological expression (Epard and Groshong, 1993) (Figure 7).

Between the Highway 21-1 intersection and the locality of Phu Kham Chan (Figure 4), the maximum vertical relief of exposures is limited to tens of metres, but the horizontal section is continuous along a sequence of 10 quarries. The overall trend of the imbricated pre-Permian strata of the carbonate Khao Khad Formation, have a predominantly N – NNE vergence (Fig. 5). A different imbricate set, with a S – SSW vergence, has been identified in the Khao Yai Hill (southernmost major topographic expression along Highway 21) and recognising that this the only portion of the belt with south dipping features (Fig. 5), we interprete this as a back-thrust region (Fig. 7).

Along the entire section there are no exposures of crystalline basement, or any Pre-Permian formations, which suggests that, there may be a major detachment possibly coincident with the base of the Khao Khad Formation. Typically, it is difficult to estimate the depth of the detachments or identify the involved stratigraphic level just from the fold geometry (Ramsay, 1974; Escher and Watterson, 1974; Epard and Groshong, 1993; Mitra, 2002). Therefore, the exposed boundary between basin depositional facies has been chosen as a detachment, which has a possible depth of 0.7– 1.5 km according to wavelength and amplitude of major anticlines (Figure 7) (Mitra, 1992; Epard and Groshong, 1993).

Many folding mechanisms have been observed in the study area, these cross the entire possible spectrum between the two end members ranging from buckling to bending (Cosgrove, 2000). This alternation of geometries has been attributed to the lithological heterogeneity of the Khao Khad Formation that is the prominent deformed lithology in this part of the KKF&T Belt. Folds are the most frequent and best exposed structural feature along Highway 21. The illustrated cross-section (Figure 7) shows an interpretation of the strain distribution throughout the fold and thrust belt within the Khao Khad Formation, where several deformation themes have been observed. The (commonly asymmetric) folds have been classified as features related to bending events (forced folds or fault related folds), while buckle folds are more representative for accommodating the strain at the metric (<10 m) scale. Buckle folding is prevalent where the alternation of clastic basinal and carbonate layers is present. The geometry of the folds and the alternation of basinal with shallow marine carbonate sediments imply the presence of more than a single detachment level. Since the Phu Phe Formation is not seen along the analysed cross section, it is possible to exclude a detachment running at the very base of the Saraburi Group. Instead, the basinal facies within the Khao Khad Formation is taken as the main basal detachment. The distance between the main outcropping thrust and the wavelengths between the anticlines do not change, having the same intensity of deformation across the area and revealing that the detachment could lie at approximately the same depth for the entire length of the cross-section.

7. Discussion

The north-directed regional transport represented by the KKF&T Belt has been accommodated within limestone of the Permian Khao Khad Formation. The mesoscopic structures, including major thrusts, backthrusts, and forced and buckle folds, represent the typical set of structures observed in well-known convergent boundaries (Morley et al., 2011). In these structural environments, basal thrusts along weak horizons confine and define thrust belts, and relative structural features. The specific mechanisms of structural development we present here are similar in carbonate deformation with shale detachments (Morley et al., 2011).

Mesoscale analysis revealed both compression and dilatation widespread throughout the KKF&T Belt. Several large contraction faults divide the Khao Khad Formation in a series of thrust sheets. These have listric geometries and most likely merge at depth with a detachment horizon with a high range of dip angles decreasing to the direction of propagation as expected in an imbricate system of a thin-skinned geometry. Minor reverse faults often truncate large regional anticlines and synclines and are refolded throughout the entire cross section. Mesoscopic contraction faults are visible in outcrops and have displacement in the order of several metres. An intense cleavage occurs in shales, mudstones and siltstones. At the outcrop scale, joints at an angle with respect to the bedding are a visible expression of the cleavage structures, and cleavage appears to be absent, or generally refracted into thin layers of limestone beds, due to their higher competence. The idea of forced folds generated by the emplacement of major thrusts throughout the belt is reinforced by the general dip directions of the pervasive cleavage in the layers of shale used for the thrust propagation. Furthermore, the cleavage being parallel to mesoscopic fold axial traces also indicates syn-deformational generation.

Most of the mesoscale fractures and faults show evidence that they have been used as corridors for fluid migration (e.g. Warren et al., 2014). It is possible to observe a relatively high number of bed-parallel stylolites in the footwall and hanging-wall, both which increase towards the thrust surfaces. Often shear surfaces in the thrust have been used as preferential corridors for fluid migration and facilitating solution transfer processes (dissolution and precipitation). Most of the observed veins in the footwall have a sub-vertical dip (70°/85°) and trend E-W trend. They are notably less abundant that in the hanging-wall. This may indicate that fluids were not present in substantial amounts in the hanging-wall, coupled with the hanging-wall experiencing less strain. This is interpreted as being because of stress being guided along the thrust plane and in the adjacent footwall. The N-S extension expressed by the vertical veins with en-echelon pattern in the footwall may result from increased hydraulic pressure, caused by the concentration of water in the footwall, bringing the footwall nearer to tensile failure. Clearly, thrusts and shear zones in general, behave differently for fluid flow, depending on lithology, structural setting and geometry.

The roughly N-S Sibumasu – Indochina Block convergence has been accommodated in the KKF&T Belt by a combination of (present orientation) E-W and NW-SE trending structures. Elsewhere in Thailand, the same collision is represented by approximately E-W shortening on N-S trending faults and folds. The change in fold strike is notable only in the KKF&T Belt and does not involve a larger portion of the Permian-Triassic collisional belt. This leads to the question as to why does the orogeny bend at the Khao Khwang Belt? The answer may lie in the geometry of the terranes involved in the collision (Sone and Metcalfe, 2008; Ridd et al., 2012; Metcalfe, 2013). This pre-collisional geometry may have been as simple as a bend in the original Indochina margin. Or, as suggested by Morley et al. (2013), it may be the result of the

Indochina Block itself being split by an approximately E-W suture stretching from the Khao Khwang Platform in the Saraburi Region of Thailand, along the southern margin of the Khorat Plateau to central Vietnam. This interpretation has circumstantial support in the Permian E-W rift sequence developed in the southern Khorat Plateau (Hutchison, 1975; Morley et al., 2013), suggesting that Permian N-S extension occurred in the area, but it is unknown whether this is related to an oceanic margin to the south.

8. Conclusions

The fold and thrust belt formed by forward (north) propagating deformation in the Triassic, consists only of cover strata and has been displaced mainly along weak horizons of incompetent shale within the Khao Khad Formation, transported by numerous in-sequence thrusts. The KKF&T Belt represents a thin-skinned fold and thrust belt developed on a detachment that lies between 0.7 and 1.5 kilometres depth that is similar to the stratigraphic thickness of the Khao Khad Formation (Dawson and Racey, 1993; Thambunya et al., 2007, Ueno and Charoentitirat, 2011). The in-sequence, thin-skinned, deformation demonstrates that deformation has migrated from S-SSE to N-NNW along a zone as wide as the fold and thrust belt itself, with lateral variations probably attributed to lateral facies variations. Evidence of lateral structural variations occur along the strike of the fold and thrust belt in zones of mechanical weakness in the shale levels, these different rates of strain accommodation are probably related to oblique-lateral ramps between thrusts. The imbricated thrusts generally cut the forelimbs of folds in the limestone of the Khao Khad Formation, suggesting a model where some imbricates were formed during the folding, whilst folding continued in the surrounding shales with the development of some minor amplitude buckle folding associated with detachment levels. The KKF&T Belt represents a significant kink in the collision between Sibumasu and Indochina, which may be due to either the original geometry of the Indochina margin, or due to a poorly recognised ocean strand that split Indochina into two or more late Palaeozoic continents (Fig. 3).

Acknowledgements

This work was funded by Australian Research Council Discovery Award #DP 120101460. ASC is funded by Australian Research Council grant #FT120100340. This is a contribution to IGCP 628 – The Gondwana Map. We gratefully acknowledge all the funding organizations. This publication forms TRaX Record. 299.

References

Barber, A.J. & Crow, M.J., 2009. Structure of Sumatra and its implications for the tectonic assembly of Southeast Asia and the destruction of Paleotethys. Island Arc 18(1), 3-20.

Berberian, M., 1995. Master “blind” thrust faults hidden under the Zagros folds: active basement tectonics and surface morphotectonics. Tectonophysics, 241(3), 193-224.

Barr, S.M., Charusiri, P., 2011. Volcanic Rocks. The Geology of Thailand. Geological Society, London, 415-439.

Barr, S.M., Macdonald, A.S., Ounchanum, P. Hamilton, M.A., 2006. Age, tectonic setting and regional implications of the Chiang Khong volcanic suite, northern Thailand. Journal of the Geological Society, 163(6), 1037-1046.

Brown, G.F., 1951. Geologic reconnaissance of the mineral deposits of Thailand. US Government Printing Office, Vol. 984.

Bunopas, S., 1982. Paleogeographic history of western Thailand and adjacent parts of South-east Asia: A plate tectonics interpretation. Geological Survey Division, Department of Mineral Resources, (No. 5).

Bunopas, S., 1992. Regional stratigraphic correlation in Thailand. In Proceedings of a National Conference on Geologic Resources of Thailand, Thailand: Department of Mineral Resources pp. 189-208.

Bunopas, S., 1994. The regional stratigraphy, paleogeographic and tectonic events of Thailand and continental Southeast Asia. Proceedings of the International Symposium on Stratigraphic Correlation of Southeast Asia. Vol. 306, pp. 2-24.

Burrett, C., Zaw, K., Meffre, S., Lai, C. K., Khositanont, S., Chaodumrong, P., Udchachon, M., Ekins, S., Halpin, J., 2013. The configuration of Greater Gondwana—Evidence from LA ICPMS, U–Pb geochronology of detrital zircons from the Palaeozoic and Mesozoic of Southeast Asia and China. Gondwana Research. Vol. 26, pp. 31-51.Carter, A., Roques, D., Bristow, C., Kinny, P., 2001. Understanding Mesozoic accretion in Southeast Asia: significance of Triassic thermotectonism (Indosinian orogeny) in Vietnam. Geology, 29(3), 211-214.

Charusiri, P., Imsamut, S., Zhuang, Z., Ampaiwan, T. Xu, X., 2006. Paleomagnetism of the earliest Cretaceous to early late Cretaceous sandstones, Khorat Group, Northeast Thailand: implications for tectonic plate movement of the Indochina block. Gondwana Research, 9(3), 310-325.

Chitnarin, A., Crasquin, S., Chonglakmani, C., Broutin, J., Grote, P.J. Thanee, N., 2008. Middle Permian ostracods from Tak Fa Limestone, Phetchabun Province, central Thailand. Geobios, 41(3), pp 341-353.

Chutakositkanon, V., Charusiri, P., Sashida, K., 2000. Lithostratigraphy of Permian marine sequences, Khao Pun Area, central Thailand: Paleoenvironments and tectonic history. Island Arc, 9(2), 173-187.

Cluzel, D., Lee, B.J., Cadet, J.P., 1991. Indosinian dextral ductile fault system and synkinematic plutonism in the southwest of the Ogcheon belt (South Korea). Tectonophysics, 194(1), 131-151.

Cooper, M.A., Trayner, P.M., 1986. Thrust-surface geometry: implications for thrust-belt evolution and section-balancing techniques. Journal of Structural Geology, 8(3), 305-312.

Cosgrove, J.W., 1999. Forced folds and fractures: An introduction. Geological Society, London, Special Publications, 169(1), 1-6.

Cosgrove, J.W., Ameen, M.S., 1999. A comparison of the geometry, spatial organization and fracture patterns associated with forced folds and buckle folds. Geological Society, London, Special Publications, 169(1), 7-21.

Cunningham, W.D., Mann, P., 2007. Tectonics of strike-slip restraining and releasing bends. Geological Society, London, Special Publications, 290(1), 1-12.

Dawson, O., Racey, A., Whittaker, J., 1994. Permian foraminifera from northeast and peninsular Thailand. In: Proceedings of the International Symposium on Stratigraphic Correlation of Southeast Asia, pp. 323-332.

Epard, J.L., Groshong Jr, R.H., 1993. Excess area and depth to detachment. AAPG bulletin, 77(8), 1291-1302.

Escher, A., Watterson, J., 1974. Stretching fabrics, folds and crustal shortening. Tectonophysics, 22(3), 223-231.

Ferrari, O.M., Hochard, C., Stampfli, G.M., 2008. An alternative plate tectonic model for the Palaeozoic–Early Mesozoic Palaeotethyan evolution of southeast Asia (Northern Thailand–Burma). Tectonophysics, 451(1), 346-365.

Fontaine, H., Workman, D.R., 1978. Review of the geology and mineral resources of Kampuchea, Laos and Vietnam. In: Third Regional Conference on Geology and Mineral Resources of Southeast Asia, pp. 541-603.

Fontaine, H., 2002. Permian of Southeast Asia: an overview. Journal of Asian Earth Sciences, 20(6), 567-588.

Helmcke D., Lindenberg H.G., 1983. New data on the Indosinian orogeny from central Thailand. Geologische Rundschau, 72(1), 317-328.

Hinthong C., 1981. Geology and mineral resources of the Changwat Phranakorn Sri Ayutthaya. Department of mineral resources, Geological survey Report N. 4.

Hinthong C., Chuaviroj S., Kaewyana W., Srisukh S., Pholprasit C., Pholachan S., 1985. Geological map of Thailand 1: 250 000 (Changwat Phranakorn Sri Ayutthaya, ND 47–8). Geological Survey Division of the Department of Mineral Resources, Bangkok, Thailand.

Hutchison, C.S., 1975. Ophiolite in southeast Asia. Geological Society of America Bulletin, 86(6), 797-806.

Jackson, J., McKenzie, D., 1988. The relationship between plate motions and seismic moment tensors, and the rates of active deformation in the Mediterranean and Middle East. Geophysical Journal, 93(1), 45-73.

Ji-Shun, R., 1984. The Indosinian orogeny and its significance in the tectonic evolution of China. Acta Geosicientia Sinica, 6(2), 31-42.

Zaw, K., Meffre, S., Lai, C. K., Burrett, C., Santosh, M., Graham, Manaka, T., Salam, A., Kamvong, T., Cromie, P., 2013. Tectonics and metallogeny of mainland Southeast Asia - A review and contribution. Gondwana Research. Vol. 26, pp 5-30.

Lacassin, R., Maluski, H., Leloup, P.H., Tapponnier, P., Hinthong, C., Siribhakdi, K., Charoenravat, A., 1997. Tertiary diachronic extrusion and deformation of western Indochina: structural and 40Ar/39Ar evidence from NW Thailand. Journal of Geophysical Research. 102(B5), 10013-10037.

Leloup, P.H., Arnaud, N., Lacassin, R., Kienast, J.R., Harrison, T.M., Trong, T.T., Tapponnier, P., 2001. New constraints on the structure, thermochronology, and timing of the Ailao Shan-Red River shear zone, SE Asia. Journal of Geophysical Research. 106(B4), 6683-6732.

Lepvrier, C., Maluski, H., Van Tich, V., Leyreloup, A., Truong Thi, P., Van Vuong, N., 2004. The early Triassic Indosinian orogeny in Vietnam (Truong Son Belt and Kontum Massif); implications for the geodynamic evolution of Indochina. Tectonophysics, 393(1), 87-118.

Li, X.H., Li, Z.X., Li, W.X., Wang, Y., 2006. Initiation of the Indosinian Orogeny in South China: evidence for a Permian magmatic arc on Hainan Island. The Journal of Geology, 114(3), 341-353.

Metcalfe, I., 1988. Origin and assembly of south-east Asian continental terranes. Geological Society, London, Special Publications, 37(1), 101-118.

Metcalfe, I., 1990. Stratigraphic and tectonic implications of Triassic conodonts from northwest Peninsular Malaysia. Geological Magazine, 127(06), 567-578.

Metcalfe, I., 1991. Late Palaeozoic and Mesozoic palaeogeography of southeast Asia. Palaeogeography, Palaeoclimatology, Palaeoecology, 87(1), 211-221.

Metcalfe, I., 1998. Palaeozoic and Mesozoic geological evolution of the SE Asian region: multidisciplinary constraints and implications for biogeography. Biogeography and geological evolution of SE Asia, 25-41.

Metcalfe, I., 2002. Permian tectonic framework and palaeogeography of SE Asia. Journal of Asian Earth Sciences, 20(6), 551-566.

Metcalfe, I., 2005. Asia: South-East. In: Selley, R.C., Cocks, L.R.M., Plimer, I.R. (Eds.), Encyclopedia of Geology, Elsevier, Oxford, vol. 1, 169–198.

Metcalfe, I., 2006. Palaeozoic and Mesozoic tectonic evolution and palaeogeography of East Asian crustal fragments: the Korean Peninsula in context. Gondwana Research, 9(1), 24-46.

Metcalfe, I., 2009. Late Palaeozoic and Mesozoic tectonic and palaeogeographical evolution of SE Asia. Geological Society, London, Special Publications, 315(1), 7-23.

Metcalfe, I., 2011. Tectonic framework and Phanerozoic evolution of Sundaland. Gondwana Research, 19(1), 3-21.

Metcalfe, I., 2013. Tectonic evolution of the Malay Peninsula. Journal of Asian Earth Sciences, 76, 195-213.

Mitra, G., Adolph Y.W., 1985. Relationship of spaced cleavage to folds and thrusts in the Idaho-Utah-Wyoming thrust belt. Journal of Structural Geology, 7(3), 361-373.

Mitra, G., Boyer, S.E., 1986. Energy balance and deformation mechanisms of duplexes. Journal of Structural Geology, 8(3), 291-304.

Mitra, S., 2002. Structural models of faulted detachment folds. AAPG bulletin, 86(9), 1673-1694.

Morley, C.K., 2002. A tectonic model for the Tertiary evolution of strike–slip faults and rift basins in SE Asia. Tectonophysics, 347(4), 189-215.

Morley, C.K., 2007. Variations in late Cenozoic–Recent strike-slip and oblique-extensional geometries, within Indochina: The influence of pre-existing fabrics. Journal of Structural Geology, 29(1), 36-58.

Morley, C.K., King, R., Hillis, R., Tingay, M., Backe, G., 2011. Deepwater fold and thrust belt classification, tectonics, structure and hydrocarbon prospectivity: A review. Earth-Science Reviews, 104(1), 41-91.

Morley, C.K., Ampaiwan, P., Thanudamrong, S., Kuenphan, N., Warren, J., 2013. Development of the Khao Khwang Fold and Thrust Belt: Implications for the geodynamic setting of Thailand and Cambodia during the Indosinian Orogeny. Journal of Asian Earth Sciences, 62, 705-719.

Poblet, J., Lisle, R J., 2011. Kinematic evolution and structural styles of fold-and-thrust belts. Geological Society, London, Special Publications, 349(1), 1-24.

Racey, A., Love, M.A., Canham, A.C., Goodall, J.G.S., Polachan, S., Jones, P.D., 1996. Stratigraphy and reservoir potential of the Mesozoic Khorat Group, NE Thailand: Part 1: Stratigraphy and sedimentary evolution. Journal of Petroleum Geology, 19(1), 5-39.

Ramsay, J.G., 1974. Development of chevron folds. Geological Society of America Bulletin, 85(11), 1741-1754.

Ramsay, J. G., 1980. Shear zone geometry: a review. Journal of Structural Geology, 2(1), 83-99.

Ramsay, J.G., Huber, M.I., 1987. The Techniques of Modern Structural Geology, Volume 2: Folds and fractures.

Ridd, M.F., 2012. The role of strike-slip faults in the displacement of the Palaeotethys suture zone in Southeast Thailand. Journal of Asian Earth Sciences, 51, 63-84.

Savage, H.M., Cooke, M.L., 2003. Can flat-ramp-flat fault geometry be inferred from fold shape? A comparison of kinematic and mechanical folds. Journal of Structural Geology, 25(12), 2023-2034.

Savage, H.M., Cooke, M.L., 2004. The effect of non-parallel thrust fault interaction on fold patterns. Journal of Structural Geology, 26(5), 905-917.

Şengör, A.C., 1984. The Cimmeride orogenic system and the tectonics of Eurasia. Geological Society of America Special Papers, 195, 1-74.

Sibson, R.H., 1977. Fault rocks and fault mechanisms. Journal of the Geological Society, 133(3), 191-213.

Sibson, R.H., 1996. Structural permeability of fluid-driven fault-fracture meshes. Journal of Structural Geology, 18(8), 1031-1042.

Sone, M., Metcalfe, I., 2008. Parallel Tethyan sutures in mainland Southeast Asia: new insights for Palaeo-Tethys closure and implications for the Indosinian orogeny. Comptes Rendus Geoscience, 340(2), 166-179.

Suppe, J., 1985. Principles of structural geology. New York: Prentice-Hall, (Vol. 537).

Tapponnier, P., Brace, W.F., 1976. Development of stress-induced microcracks in Westerly granite. In: International Journal of Rock Mechanics and Mining Sciences & Geomechanics Abstracts, Vol. 13, N. 4, pp. 103-112.

Tapponnier, P., Peltzer, G., Armijo, R., 1986. On the mechanics of the collision between India and Asia. Geological Society, London, Special Publications, 19(1), 113-157.

Thambunya, S., Visut, P.A., Khantaprab C., 2007. Depositional Environments of Permian Rocks of the Khao Khad Formation in Central Thailand. *ScienceAsia* N.33. 371-381

Toriyama, R., Kanmera, K., Kaewbaidhoam, S., Hongnusonthi, A.N., 1974. Biostratigraphic zonation of the Ratburi Limestone in the Khao Phlong Phrab area, Saraburi, central Thailand. Geology and Palaeontology of Southeast Asia, N. 14, 25-48.

Ueno, K., 1999. Gondwana/Tethys divide in East Asia: solution from Late Paleozoic foraminiferal paleobiogeography. In: Proceedings of the International Symposium on Shallow Tethys, N. 5, pp. 45-54.

Ueno, K., Hisada, K.I., 2001. The Nan-Uttaradit-Sa Kaeo Suture as a Main Paleo-Tethyan Suture in Thailand: Is it Real? Gondwana Research, 4(4), 804-806.

Ueno, K., Charoentitirat, T., 2011. Carboniferous and Permian. In: Ridd, M.F., Barber,A.J. Crow, M.J. (eds.), The Geology of Thailand, The Geological Society of London, 71–136.

Ueno, K., Miyahigashi, A., Kamata, Y., Kato, M., Charoentitirat, T., Limruk, S., 2012. Geotectonic implications of Permian and Triassic carbonate successions in the Central Plain of Thailand. Journal of Asian Earth Sciences, 61, 33-50.

Warren, J., Morley, C.K., Charoentitirat, T., Cartwright, I., Ampaiwan, P., Khositchaisri, P., Mirzaloo, M., Yingyuen, J., 2014. Structural and fluid evolution of Saraburi Group sedimentary carbonates, central Thailand: A tectonically driven fluid system. Marine and Petroleum Geology, Doi: 10.1016/j.marpetgo.2013.12.019

Wielchowsky, C.C., Young, J.D., 1985. Regional facies variations in Permian rocks of the Phetchabun fold and thrust belt, Thailand. In: Conference on Geology and Mineral Resources Development of the Northeast, Thailand (Proceeding), Khon Kaen University, Khon Kaen, Thailand, pp. 26-29.

Chapter IV

Arboit, F., Amrouch, K., Collins, A. S., King, R., & Morley, C. (2015). Determination of the tectonic evolution from fractures, faults and calcite twins on the south-western margin of the Indochina Block. *Tectonics*. **34**, 1576-1599.

Determination of the tectonic evolution from fractures, faults and calcite twins on the south-western margin of the Indochina Block

ABSTRACT

In polyphase tectonic zones, integrating a study of fault and fracture with calcite twin analysis can determine the evolving paleo-stress magnitudes and principle stress directions that affected the area. This paper presents the results of the analyses of fractures, striated faults and calcite twins collected within the Khao Khwang Fold-Thrust Belt (KKFTB) in central Thailand (SE Asia). Here we attempt to reconstruct the orientation of the principal stresses that developed during the tectonic evolution of this highly deformed, polyphase orogen. Tectonic data were collected in the Permian carbonates of the Khao Khad Formation of the Saraburi Group, and five successive tectonic stages are determined that are interpreted to have developed before, during, and after, the Triassic Indosinian Orogeny. The first three stages pre-date the main deformation event: the first stage is interpreted as a pre-Indosinian N-S extensional stage, the second stage described a N-S strike-slip and compressional regime, largely perpendicular to the fold axes of the main structures, while the third stage is associated with an E-W compressional strike-slip phase. A further two stages took place after, or during, the main folding event and correspond to N-S compression and to an E-W composite strike-slip/contractional stage, the latter which is interpreted to represent Cenozoic deformation related to the India-Asia collision.

1. Introduction

South East Asia is formed from a number of continental fragments and volcanic arcs, separated by oceanic suture zones, which accreted to the growing Asian continent during the latest Paleozoic-early Mesozoic Indosinian Orogeny. In Thailand, this tectonic event, developed mainly during the Triassic (Sone and Metcalfe, 2008; Metcalfe, 2011) and is the result of the collision between the Sibumasu, Sukhothai and Indochina Terranes (Figure 1a, b). Models for the tectonic evolution of Thailand from the Indosinian Orogeny to the present have been defined using biostratigraphical, petrological, structural and geochronological data (Metcalfe and Sone, 2008; Sone and Metcalfe, 2008; Ridd and Morley, 2011; Morley et al., 2013; Arboit et al. 2014; Hansberry et al. 2014) and involve broadly N-S trending tectonic domains converging in E-W directions (with respect to the present-day orientation) (Sone and Metcalfe, 2008; Morley et al., 2013). However, these are based on the present day orientations of the tectonic domains and little constraints on the original orientations or paleo-stress determinations have been previously attempted.

Central Thailand, and more specifically the Khao Khwang Fold-Thrust Belt (KKFTB), provides a natural laboratory to obtain the necessary information, with many well exposed quarries along Highway 21 (Table 1, Figure 1c). The complex structural architecture in the KKFTB evolved from the Permian, mainly with the growth of E-W to ENE-WSW striking reverse faults and associated drag-folds that developed in this thin-skinned fold and thrust belt (Morley et al., 2013; Arboit et al., 2014). Associated with this deformation, there are a number of N-S to E-W trending sets of fractures that developed before, during, and after, the main Layer-Parallel Shortening (LPS) event of the Indosinian Orogeny. In order to develop a permissive model for the dynamic evolution of the region, we took advantage of the rocks of the Khao Khad Formation (Ueno and

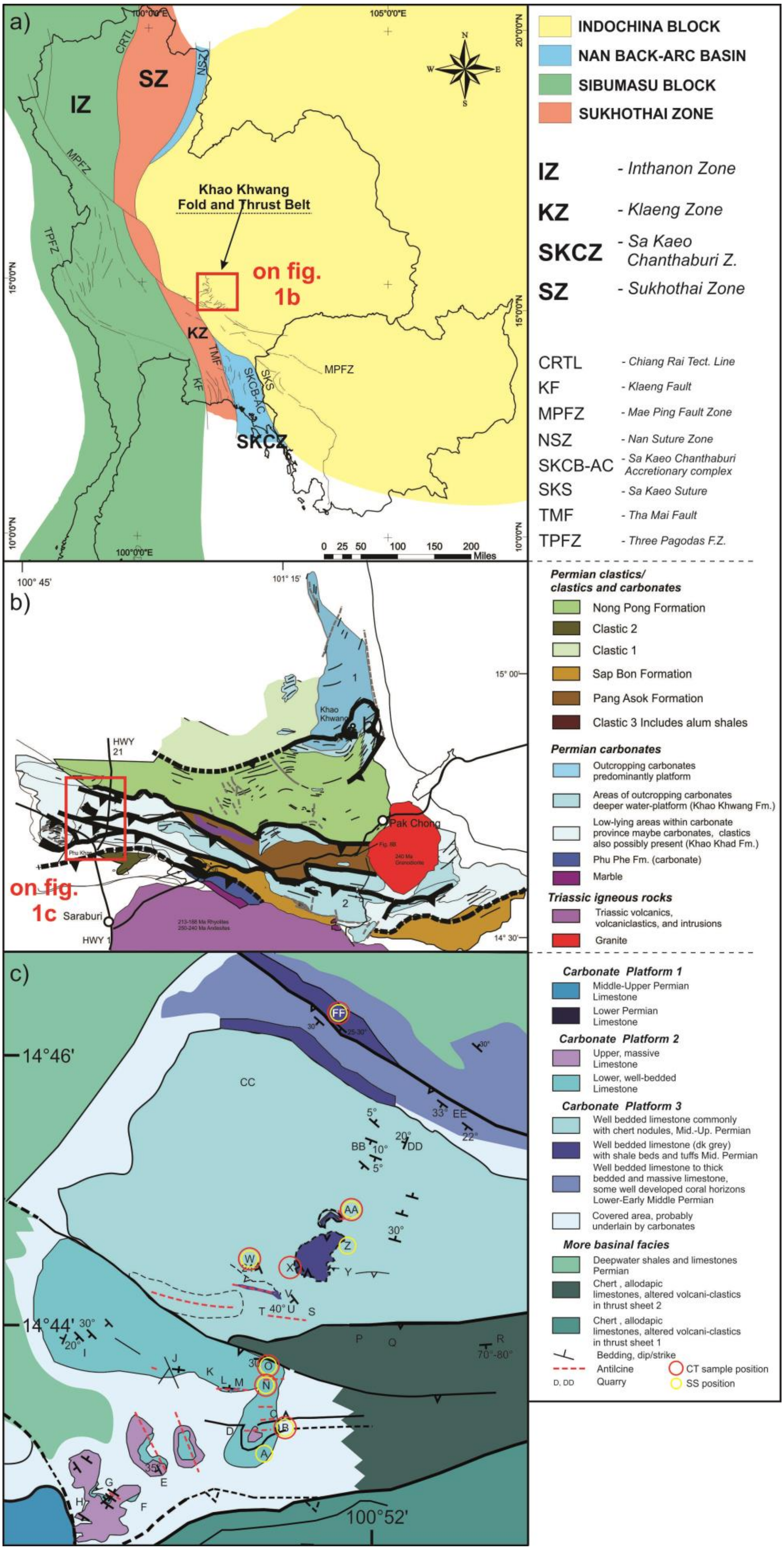
a)
INDOCHINA BLOCK
NAN BACK-ARC BASIN
SIBUMASU BLOCK
SUKHOTHAI ZONE
IZ - Inthanon Zone
KZ - Klaeng Zone
SKCZ - Sa Kaeo Chanthaburi Z.
SZ - Sukhothai Zone
CRTL - Chiang Rai Tect. Line
KF - Klaeng Fault
MPFZ - Mae Ping Fault Zone
NSZ - Nan Suture Zone
SKCB-AC - Sa Kaeo Chanthaburi Accretionary complex
SKS - Sa Kaeo Suture
TMF - Tha Mai Fault
TPFZ - Three Pagodas F.Z.
Khao Khwang Fold and Thrust Belt
on fig. 1b
b)
Permian clastics/ clastics and carbonates
Nong Pong Formation
Clastic 2
Clastic 1
Sap Bon Formation
Pang Asok Formation
Clastic 3 Includes alum shales
Permian carbonates
Outcropping carbonates predominantly platform
Areas of outcropping carbonates deeper water-platform (Khao Khwang Fm.)
Low-lying areas within carbonate province maybe carbonates, clastics also possibly present (Khao Khad Fm.)
Phu Phe Fm. (carbonate)
Marble
Triassic igneous rocks
Triassic volcanics, volcaniclastics, and intrusions
Granite
on fig. 1c
Saraburi
Pak Chong
c)
Carbonate Platform 1
Middle-Upper Permian Limestone
Lower Permian Limestone
Carbonate Platform 2
Upper, massive Limestone
Lower, well-bedded Limestone
Carbonate Platform 3
Well bedded limestone commonly with chert nodules, Mid.-Up. Permian
Well bedded limestone (dk grey) with shale beds and tuffs Mid. Permian
Well bedded limestone to thick bedded and massive limestone, some well developed coral horizons Lower-Early Middle Permian
Covered area, probably underlain by carbonates
More basinal facies
Deepwater shales and limestones Permian
Chert, allodapic limestones, altered volcani-clastics in thrust sheet 2
Chert, allodapic limestones, altered volcani-clastics in thrust sheet 1
Bedding, dip/strike
Antilcine
CT sample position
SS position
D, DD Quarry
14°46'
14°44'
100°52'

Fig 1. (a) Subdivision of Thailand into main tectonic terranes that amalgamated during the Indosinian Orogeny (modified from Ueno and Charoentitirat [2011]) and distribution of the major lineaments of the study area [after Arboit et al., 2014]. (b) Geological map of the Khao Khwang Fold-Thrust belt region [from Morley et al., 2013]. (c) Detailed description of the western portion of the Khao Khwang Fold-Thrust belt [from Warren et al., 2014]. The described lithologies are "informal units" based on the description from Hinthong [1981]. The red circles show the location where the samples have been collected, and the yellow circles where data for structural stations have been taken, coordinates on Table 1.

Charoentitirat, 2012) to compare fracture and fault sets with a paleostress analysis carried out using calcite twins (Lacombe et al., 1992; Lacombe et al., 2007; Amrouch et al., 2010a, b). In combination, these data provide an accurate estimate on the evolving stress orientation and resulting deformation before, during, and after, the Indosinian Orogeny.

Quarry	Latitude	Longitude
A	14° 42' 01.40"N	100°53'20.28"E
B	14° 42' 06.45"N	100°53'08.49"E
AA	14° 44' 12.08"N	100°53'43.33"E
FF	14° 46' 07.13"N	100°53'33.67"E
N	14° 43' 27.09"N	100°52'54.27"E
O	14° 43' 16.51"N	100°53'25.40"E
W	14° 43' 41.22"N	100°53'03.66"E
X	14° 43' 46.02"N	100°53'44.55"E
Z	14° 53' 58.18"N	100°53'48.67"E

Table 1. List of the Quarries With Location Coordinates Quarry

2. Geological setting

The study area has undergone a complex geological history, which mainly developed during the Indosinian tectonic event, this is characterised by different subduction and collision episodes that covered the period from ca. 260 to 200 Ma (Late Permian to Late Triassic) (Sone and Metcalfe, 2008; Morley, 2007; Morley et al., 2013). The resulting tectonic belts and suture zones in Thailand have a dominant N-S trend. The Indosinian orogeny in Thailand has been considered to involve two stages of collision during the Triassic-Early Jurassic between the three main terranes, which, from east to west, are: Indochina, Sukhothai and Sibumasu (Figure 1a) (Sone and Metcalfe, 2008; Metcalfe, 2013). Additionally, beyond Thailand, to the NE, coeval Triassic collision also occurred between both the Indochina/ South China Blocks (Cai and Zhang, 2009; Halpin et al. in press) and the South/North China Cratons (Dong et al. 2015)..

The Sukhothai Terrane is believed to have been a volcanic arc that rifted away from the south-western margin of Indochina in the Early Permian, as consequence of rollback above the subducting Paleo-Tethys, and opening of the back-arc basin between the volcanic arc (Sukhothai) and the Indochina Terrane (Sone and Metcalfe, 2008). The first tectonic event is commonly interpreted as resulting from the Early Triassic collision as the Sukhothai Terrane re-amalgamated with Indochina, with the related closure of the Permian back-arc basin (Metcalfe, 2005; Sone and Metcalfe, 2008; Metcalfe, 2013). Subsequently, in the Late Triassic, during the late stages of the Indosinian collision, the Sibumasu Terrane is thought to have collided with the now combined Indochina/Sukhothai Terrane, causing the complete closure of the Paleo-Tethys in this region. The Indosinian orogeny has usually been thought as resulting from the collisions between these two strongly linear terranes and Indochina. However, despite the common N-S trend of the suture zones (Nan-Sra Kaeo and Changning-Menglian S.Z.) (Figure 1a) between the blocks involved in the collision, in some areas the tectonic trend diverges from simply N-S to NW-SE and E-W trends. The most prominent of these regions is the Saraburi region (Morley et al., 2013; Arboit et al., 2014). One explanation for the different trend is that the belt was rotated from a N-S direction to a more E-W orientation by motion along the NW-SE trending Cenozoic Mae Ping Fault Zone; Tapponier et al. (1986) proposed sinistral displacement of about 150 km on this fault. However, even after restoring this offset, and applying a relative clockwise rotation of about 25°-30° (Charusiri, 2006; Cung and Geissman, 2013; Singsoupho et al. 2014) to the northern side of the fault, the boundary does not restore to a N-S orientation (Anchuelas et al., 2012; Mochales et al., 2012; Morley et al., 2013). Alternatively, the deflection may be due to the original orientation of the continental margins, or possibly due to a poorly documented intra-Indochina suture, that strikes east-west, and lies close to the southern margin of the Khorat Plateau (Hutchinson, 1975; Morley et al. 2013).

The KKFTB lies in the Saraburi Province in central Thailand, and it is tectonically located on the SW margin of the Indochina Block (Bunopas, 1982; Metcalfe, 2011; Morley et al., 2013). It is bounded to the north and to the east by the Khorat Plateau, which trends NW-SE, and to the south by the Cenozoic Mae Ping strike-slip fault (Morley, 2007; Morley et al., 2013). Bunopas (1981) was the first to propose a separate Indochina Block by stratigraphic division (Saraburi Group) of the lithological units in this province. A few years later, Hinthong (1981) and Hinthong et al. (1985) defined the stratigraphy that is still used today and described three main carbonate formations, the Phu Phe, Khao Khad and Khao Khwang formations, that formed Permian carbonate platforms, separated by clastic and mixed clastic and carbonate facies formations (Sap Bon, Pang Asok, and Nong Pong) (Ueno and Charoentitirat, 2011; Morley et al., 2013).

The thickest and most deformed formation exposed within the KKFTB is the Khao Khad Formation, which tectonically underlies the Sap Bon Formation and is thrust over the Nong Pong Formation to the north. In the Saraburi area of the KKFTB, the Khao Khad Formation consists of approximately 1400 m of tectonically thickened Permian carbonate platform facies (Dawson and Racey, 1993; Morley et al., 2013; Warren et al., 2014; Arboit et al., 2014) (Figure 1). The present trend of the belt (from E-W to ENE-WSW) lies at a high angle to the interpreted orientation of the approximately N-S Indosinian suture zones that run throughout SE Asia. The study region represents a natural laboratory to investigate the processes that affected the general kinematic framework on the south-western margin of the Indochina Block; and thus contributing to better illustrate the Permo-Triassic phases of the paleostress evolution during the Indosinian Orogeny.

3. Methodology

3.1. Field and mapping methods

Fractures were measured on, and normal to, bedding surfaces along the length of the folds, mainly in a direction perpendicular to thrust vergence, or in single positions in order to decrease the level of bias due to the orientation of the outcrop. Analyses were carried out with detailed mapping of structural stations at a few, well-exposed, surfaces, of the thickly bedded limestone of the Early – Middle Permian Khao Khad Formation (Ueno and Charoentitirat, 2012), in a number of quarries exposed along highway 21 in the Saraburi region, as well as in oriented thin-sections. As fracture sampling was undertaken unsystematically through the region, due to outcrop availability and access, density distributions and relative clusters have not been filtered to avoid any possible bias to the data. Fracture orientations, lengths and modes of deformation (opening and sliding) were recorded as well as cross-cutting relationships. This information has been collected in order to provide new data on the geometries and chronologies of fracturing that affected the western portion of the KKFTB since the Permian stage of the Indosinian Orogeny. According to the quality of the exposure, from 30 to 80 fractures were measured for each stop, in order to statistically identify the orientation of the main fracture families. Facies variations within the rocks of the KKFTB have not been taken in consideration, although these are certainly present and are likely to affect the mechanical properties of the rocks. Despite this, no large variations in the orientations of the fracture sets have been noticed throughout the western portion of the KKFTB. Here the term "fractures" is used in general to describe either opening-, sliding-, or closing-mode discontinuities, such as pressure-solution seams, joints and veins. Small faults, with negligible offset (less than 10 mm), have here been referred as fractures when kinematic indicators were lacking (Pollard and Aydin, 1988). Structural and geological maps have been constructed using a variety of methods, including scan lines, scan areas with a 1 – 1 m resolution combined with Landsat and SRTM orthorectified photomosaic satellite images and topographic data in ArcGIS® environment.

3.2. Calcite twin analysis

Over the last 50 years many different methods for inferring certain elements of the stress tensor from fault populations have been used (Ramsey, 1962; Angelier and Mechler, 1977; Angelier, 1984). In order to inspect the stress history before and after folding at both meso- and micro-scale, we carried out an analysis of fractures and calcite twins. Several calcite twinning and inversion techniques have been applied to non-metamorphosed to weakly metamorphosed carbonate rocks to obtain regionally meaningful paleostress tensor orientations (Etchecopar, 1984; Tourneret and Laurent, 1990; Lacombe et al., 1992, 2007; Lacombe, 2001). The geometry of calcite twinning has been exhaustively described by Handin and Griggs (1951). Mechanical e-twinning (Figure 2) often occurs in calcite crystals deformed at low temperatures (Burkhard, 1993) (Figure 2). In terms of deformation, an individual *e*-twin can be considered as a zone of perfect simple shear resulting from the slide of the position of the atoms in the crystal lattice along a plane (*e*); which for unmetamorphosed calcite are e_i :$\{01\bar{1}2\}$, and these three *e* planes are geometrically forced around the optic axis *C* (Figure 2). Twin gliding in calcite requires a resolved shear stress (RSS) that exceeds the yield stress value for twinning (τ_s) of 10±4 MPa in order to develop (Turner et al., 1954; Lacombe and Laurent, 1996; Ferrill, 1998; Laurent et al., 2000; Lacombe, 2007, Lacombe 2010). Resolved shear stress is the component of stress that is aligned with the twinning direction. The yield stress value has a very small sensitivity to temperature and confining pressure but depends mainly on grain size and internal twinning strain (Tullis, 1980; Rowe and Rutter, 1990; Lacombe et al., 2007). The inversion process takes into account both the twinned and untwinned planes, the latter of which are those of the potential e-twin planes that never experienced a resolved shear stress of sufficient magnitude to cause twinning (Tourneret and Laurent, 1990). The inverse problem consists in finding the stress tensor that best fits the distribution of twinned and untwinned planes. If more than 30% of the twinned planes in a sample are not explained

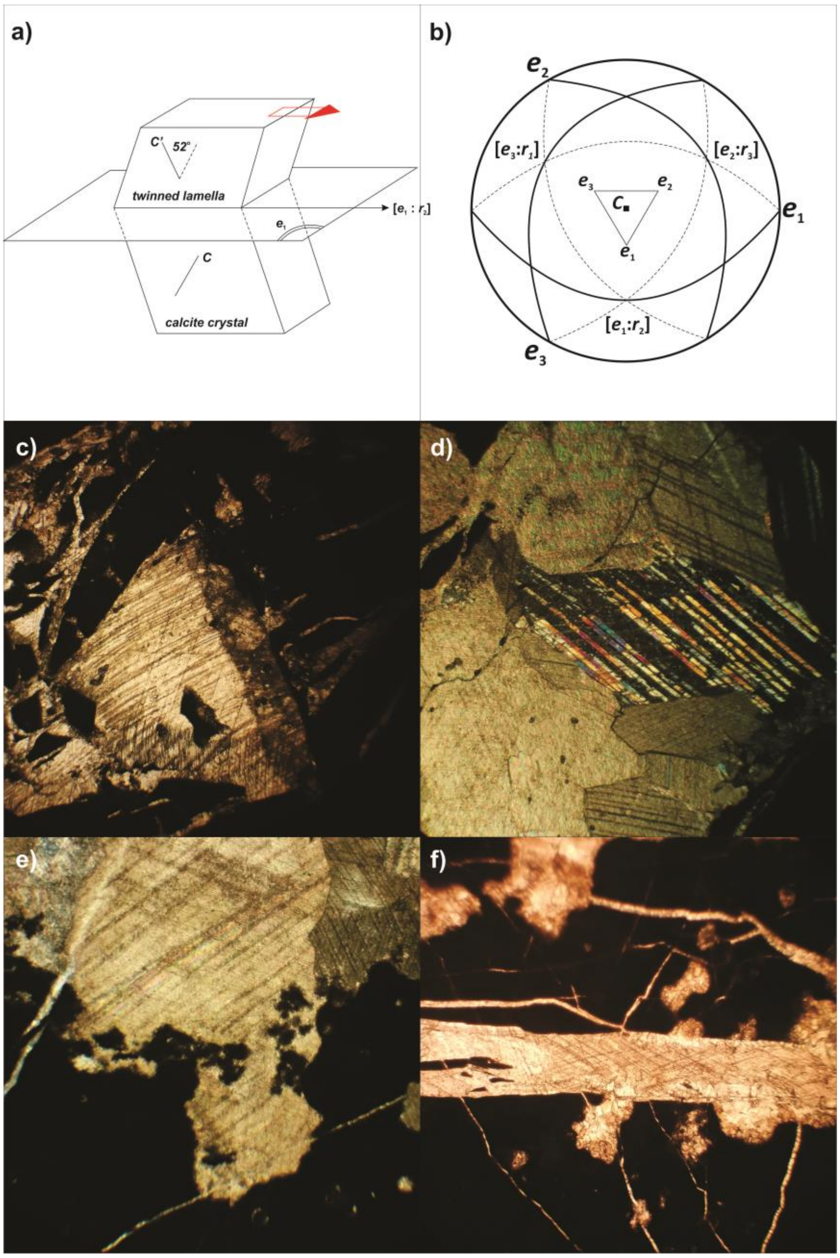

Figure 2. a) Schematic sketch of a twin lamella {01$\bar{1}$2} in a calcite crystal (after Bukhard, 1993). The twinning direction [e_1:r_2] corresponds to the direction of movement of the atoms situated above the twin plane. The sense of shear is indicated by the arrow and is imposed by the crystal geometry. b) Stereographic projection (lower hemisphere, equal area) of the calcite twin planes. The optic axis C, at the centre of the diagram is vertical. The poles to the three sets of twin planes e_1, e_2 and e_3 are at 26.5° to the C axis. The planes of twinning are the three great circles containing the three directions of twinning {01$\bar{1}$2} – [e_i:r_j] (modified from Evans and Groshong, 1994). The lower images describe samples of twinned crystals from veins and matrix of the Khao Khad Fm. All the crystals show type I & II geometry (Burkhard, 1993). Most of the deformation describes a low temperature deformation environment (from <200° C up to 300° C) with deformation varying from low to high degrees. c) Twins deformed by intense shear, d) thick twins (>>1μm), e) thin twins in matrix, f) vein filled with large sparry calcite crystals in the centre and untwinned calcite crystals on the walls.

by a unique tensor, the inversion process is repeated with the uncorrelated twinned planes and the whole set of untwinned planes.

Several methods for determining stress or strain components from calcite twin lamellae have been proposed (Groshong, 1972; Etchecopar, 1984). For this study we used Etchecopar's calcite stress inversion technique

(CSIT) (Etchecopar, 1984) to obtain the stress tensor, while other methods such as the Groshong's calcite strain gauge technique (CSGT) (Groshong, 1972) allow production of a strain ellipsoid. The CSIT applies to small twinning strains that can be approximated by coaxial conditions, so orientation of the twinning strain can be correlated with paleostress orientation (Amrouch et al., 2010a) [see details in works by Lacombe, 2001, 2007].

Etchecopar's CSIT leads directly to the simultaneous computation of principal stress orientations (with: σ_1- maximum principal stress; σ_2- intermediate principal stress; σ_3- minimum principal stress) and differential stresses (Tourneret and Laurent, 1990; Lacombe and Laurent, 1992; Amrouch et al., 2010a), which also yields data on the ellipsoid shape ratio $\Phi=(\sigma_2- \sigma_3)/(\sigma_1-\sigma_3)$, and the peak differential stress ($\sigma_1- \sigma_3$) (with $\sigma_1\geq\sigma_2\geq\sigma_3$ as a compressive stresses, positive in value). The tensor solution is calculated as a normalised reduced stress tensor, such that ($\sigma_1- \sigma_3$), and is scaled to $[(\sigma_1- \sigma_3)^*=1]$.

Thus, the value of the RSS τ_s acting on a plane lies between -0.5 and +0.5, that is $-(\sigma_1- \sigma_3)^*/2$ and $+(\sigma_1- \sigma_3)^*/2$ (Jamison and Spang, 1976). Theoretically, all the twinned planes consistent with a given tensor must sustain a τ_s value larger than the one exerted on any untwinned plane. The best tensor solution is searched in order to minimize the function f, which is ideally equal to 0, and is defined as:

$$f = \sum_{j=1}^{N} (\tau_{sj} - \tau_{a'})$$

Where $\tau_{a'}$ is the smallest RSS applied on the twinned planes compatible with the tensor and τ_{sj} are the RSS applied on the N untwinned planes j such that $\tau_{sj} > \tau_{a'}$ (Etchecopar, 1984; Laurent, 1984). The $\tau_{a'}$ value is deduced from the inversion and corresponds to the critical RSS for the normalised tensor used for the calculation. The best fitting tensor is obtained when (1) the maximum of the twinned planes are taken into account; (2) the maximum of the untwinned planes are taken into account; and (3) the f value is minimal (in practice, one can authorise a weak percentage, 10% - 15%, of untwinned planes receiving a RSS larger than $\tau_{a'}$, because of measurement uncertainties and local heterogeneities at the crystal scale). Therefore, the quality of the calcite twin data has a further control with the penalization function "*f*", this parameter indicates the quality of the arrangement of the whole measured *e* planes (Lacombe and Laurent, 1996). This process leads to the determination of the orientation of the principal stresses σ_1, σ_2 and σ_3 and the stress ellipsoid shape ratio $\Phi=(\sigma_2 - \sigma_3)/(\sigma_1 - \sigma_3)$ being between 0 and 1 (Etchecopar, 1984; Laurent, 1984). If polyphase deformation has occurred, this provides an efficient way of separating superimposed twinning and therefore deformation events (Etchecopar, 1984; Lacombe et al., 2007).

4. Overview of fracture-deformation framework

Interpretation on the structural framework development within the KKFTB is here based on the statistical analysis of fracture orientations and their relative ages. The analysis of these fractures was carried out both with a field based study at the meso-scale, and at the micro-scale in 27 thin sections. Fracture populations in the field have been sampled along Highway 21 (Figure 1b), along a N-S oriented section within the KKFTB where the Khao Khad Formation crops out. The Permian carbonate of the Khao Khad Formation contains a great variety of fractures, many filled with calcite, which developed during the Indosinian Orogeny (Warren et al., 2014). The term "fractures" is

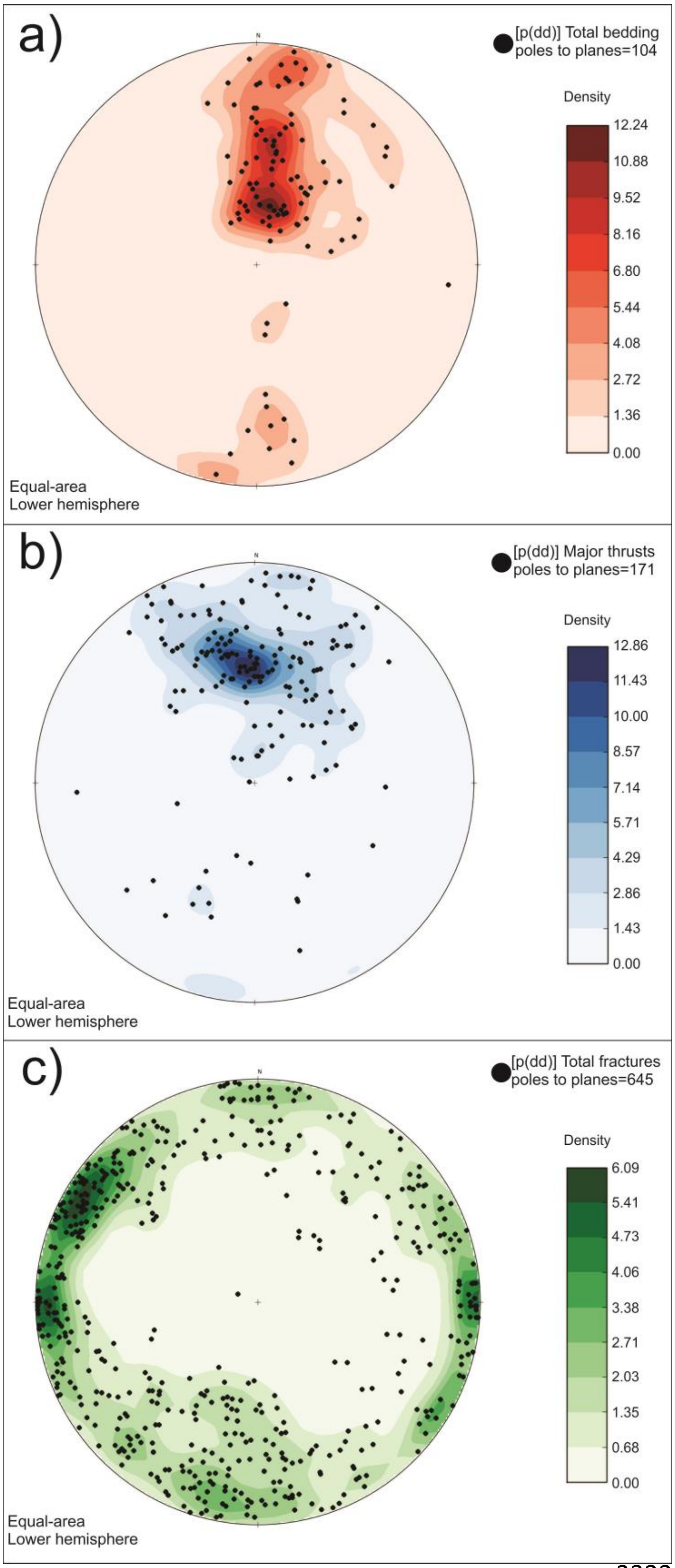

Fig 3. Stereographic plot (equal-area, lower hemisphere projection) showing the attitude of the (a) bedding, (b) major faults, and (c) fractures. Cluster analysis shows main E-W strike of both bedding and thrusts indicating a principal northerly vergence in the western part of the Khao Khwang Fold-Thrust belt. Contouring operations performed with the aid of Openstereo software [Grohmann and Campanha, 2010].

here used in a general sense to refer to either (Type I) opening-, (Type II & III) sliding-, or closing-mode displacement discontinuities along surfaces; such as planar surfaces, pressure-solution seams, joints, and veins (Pollard and Aydin, 1988). Tectonic pressure-solution surfaces (Figure 5e) or stylolites comprises bed-perpendicular surfaces with an average direction of 100°, these are the less frequent structural features, and are not present in many of the investigated quarries. It is well known that analysis of the distribution of such structural features has the potential to increase the constraints on the fold kinematic (Gutierrez-Alonso and Gross, 1999; Tavani et al., 2006, 2015), and therefore on the geodynamic evolution of the KKFTB. But here, considering their statistically irrelevant numbers (6/675), they have been excluded from the analysis. However, the stylolite 'teeth' are aligned normal to the pitted solution surface, implying the σ_1 during stylolite development was parallel to the pole of the stylolite surface (Choukroune, 1969; Eyal and Reches, 1983). Major features, such as bedding and faults, show a preferential E-W trend, while fractures display a wide range of strike orientations from E-W to N-S (Figure 3) with the highest frequency corresponding to fractures almost perpendicular in strike to the direction of major structures. We differentiate five major regionally systematic phases of deformation, composed of 12 fracture sets. The fracture sets form at both low and high angles to bedding (NE-SW and NW-SE) (Figure 3c) and occur in all the sites over the quarries within the Khao Khad Formation. When plotted (Figure 4), the data reveal two main arrays, one with a high-angle to the average dip direction of bedding, and a second array, oblique to the average dip direction of bedding. When close to inter-layered shale, it is difficult to identify clear patterns in the fracture orientations throughout the KKFTB, or, at a smaller scale, to follow them over the same layer, because of intensive dissolution (burial pressure-solution), which significantly affected the thickness of the bedding. In some areas, the relationship to local and regional structures is uncertain as a result of these conditions. Field evidence also shows that the carbonate layers of the Khao Khad Formation are often interlayered with thin shale layers. In these cases, veins and joints developed within a single bed and joint/vein spacing increases with the increasing bed thickness. We observe two systematic fracture sets trending 015° to 050° (Figure 4) throughout the entire area, both before and after unfolding.

4.1. Fracture data processing

Regional fracture sets were identified based on common ranges of strike and dip angle from 7 processed and interpreted quarries. Fracture data were isolated to time and space clusters to reveal natural fracture trends that were not easily identified in a single stereonet (Figure 3c) with all fracture data. A large number of natural fractures appeared to converge to the same direction after isolating data by quarry; however, in each stereonet bedding dip angle was removed by stereographic rotation to align fracture planes with a specific fracture set geometry. The members of a fracture set share a similar strike and dip relative to the bedding, each group has been estimated using a normalised kernel (Long and Billaux, 1987).

4.2. Sequence of fracture development

Here we illustrate the analyses of the fracture data, the raw data along with their description in terms of statistically defined mean sets.

The first deformational phase is composed of Set-AI (65°/150°) and Set-AII (65°/175°) (Figure 4d). These two fracture sets have a more restricted occurrence than other sets, they trend 160° are at a high angle to bedding, and are mostly joints that are partially to totally (veins) filled with coarse calcite. Evidence of fracturing or shearing are both present in thin sections, probably indicative of a Type I opening mode later reactivated with shearing. The relatively narrow strike distribution for fracture Set-AI and AII implies a uniform distribution of minimum stress and a constant position through time of σ_1.

The second phase of deformation is the most prevalent high-angle array, occurring on most of the ridges on the analysed portion of the KKFTB. Phase 2 consists of two fracture sets: Set-AIII (80°/050°) and Set-AIV (90°/080°) (Figure 4c, e, f). These fracture sets commonly consist of fractures that are several meters long and have high angles of dip. In the field, their deformation mode is quiet difficult to determine, as different fractures show characteristics of either joint and shear band morphology. In some cases, the fractures are open, with or without mineral fillings, and in other cases they stand up from the outcrop with small positive relief. This latter attribute may be related either to cementing (for the case of joints or dilational bands) or tighter packing of calcite grains within the fracture during the shear (for the case of deformation bands). As for fracture sets of the Phase 1, the deformation mode remains uncertain, but in thin section, they appear to have initiated either as simple shear-related deformation bands, or as extensional joints with simple

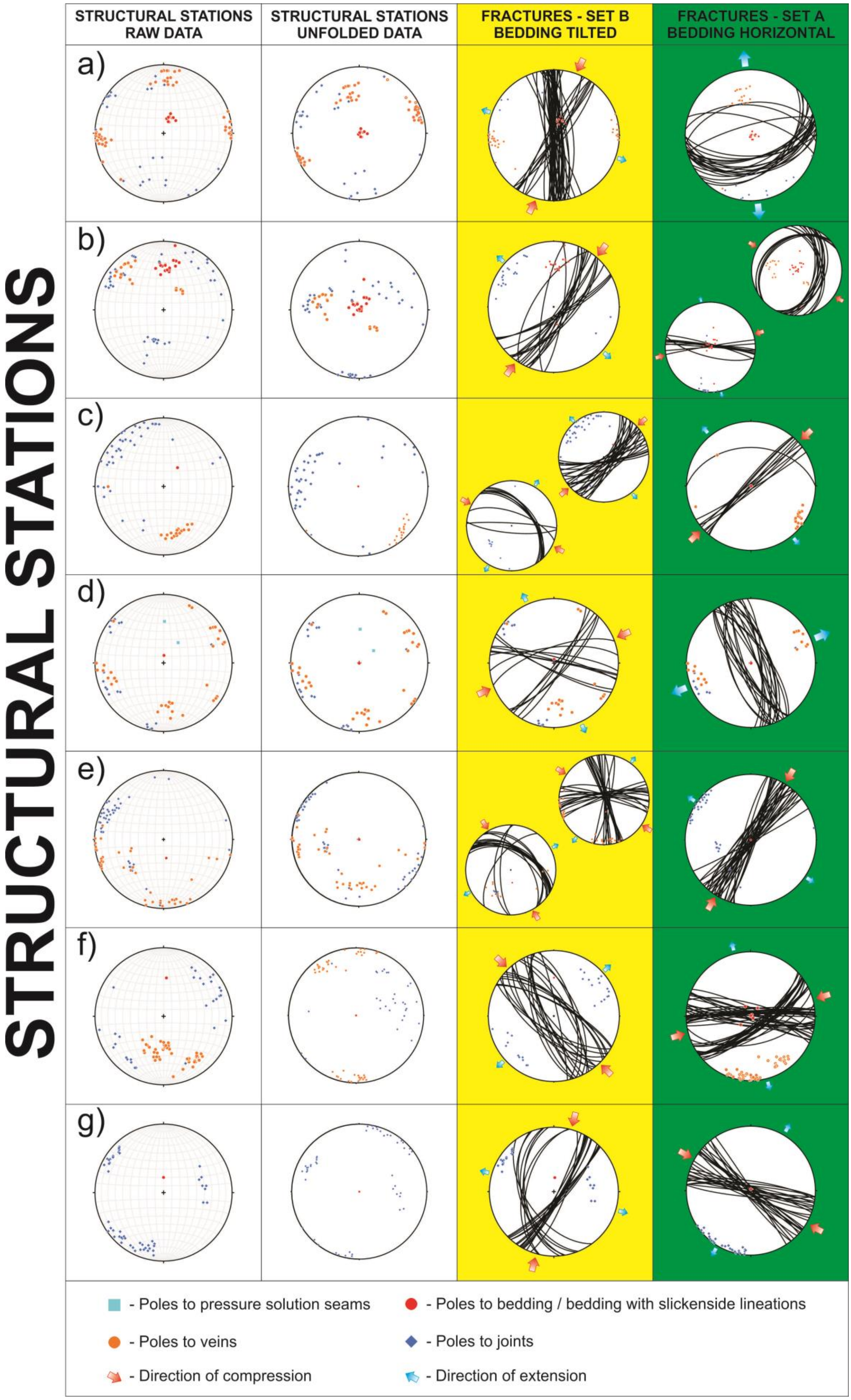

STRUCTURAL STATIONS
STRUCTURAL STATIONS RAW DATA
STRUCTURAL STATIONS UNFOLDED DATA
FRACTURES - SET B BEDDING TILTED
FRACTURES - SET A BEDDING HORIZONTAL
a)
b)
c)
d)
e)
f)
g)
- Poles to pressure solution seams
- Poles to bedding / bedding with slickenside lineations
- Poles to veins
- Poles to joints
- Direction of compression
- Direction of extension

2414

Fig 4. Stereonets (performed with Stereonet software [Allmendinger, 2005]) describing the position of the most relevant structural stations collected in the western portion of the KKFTB (see Figure 1c for location). Each stereonet has been unfolded for the bedding where the structural station was located. Those unfolding operation revealed clusters of data with high (green column) and low angle (low angle) with respect to the average bedding. The analyses of the poles to the main fractures detected within the Khao Khad Fm. show the horizontal and tilted emplacement of the main sets (from NE-SW to NW-SE). The red thick arrows indicate directions of compression (parallel to σ1), while the blue thick arrows indicate direction of extension (parallel to σ3) (a) Quarry W-Bedding 188°/21°, two clear sets: N025° (postfolding SS regime) and N352° (prefolding extensional regime). (b) Quarry X-Bedding 53°/192°, two sets: N055° (oblique postfolding SS regime) and N325° (prefolding thrust regime). (c) Quarry FF-Bedding 24°/227°, two sets both prefolding and postfolding N058° SS regime. (d) Quarry A-Bedding 10°/181°, two clear sets: N051° (postfolding SS regime) and N053° (prefolding extensional regime). (e) Quarry Z-Bedding 22°/351°, N331° (postfolding SS regime) and N028° (prefolding SS regime). (f) Quarry N-Bedding 49°/185°, N339° (postfolding SS regime) and N078° (prefolding SS regime). (g) Quarry FF-Bedding 20°/179°, N019° (postfolding SS regime) and N318° (prefolding SS regime).

shear superimposed. Fracture Set-AIII and AIV cross cuts Set-AI and AII in thin section in both sliding- (Figure 6a) and opening–mode. Fracture sets of both Phase 1 and 2 range from being perpendicular to slightly oblique to the axial trend of the major folds. The observed partial overlay between joints and veins (Figure 4b, d) also implies that these fractures may have initiated as open fractures, later filled and reactivated as sheared veins (Figure 6).

The third phase of deformation is not as pervasive as Phases 1 and 2. The fractures related to this phase are fracture Set-AV (40°/050°) and AVI (25°/130°) (Figure 4b, g). Fracture sets AV and AVI are often associated with tail cracks (Figure 5d) and Riedel arrays (R and R'). Those fractures resemble both joints and deformation bands.

Fracture sets associated with the fourth phase of deformation are Set-BVII (90°/355°) and Set-BVIII (85°/030°) (Figure 4a, b, c, d, g). These fracture sets have similar geometries to fracture Set-AI and AII, with several meters long fractures closely spaced and cutting though several layers of the thick bedded Khao Khad Formation. Fracture Set-BVII and BVIII present a steeper dip angle (~85°), are located mostly in highly deformed zones with linear fracture traces, and they lack tail cracks and Riedel fractures or other shearing-related secondary structures (Pollard and Aydin, 1988). In most of the back-limbs their deformation mode is difficult to determine in the field. They look like joints in some sites, yet in other sites resemble deformational bands. Several additional sets of veins, mainly bed parallel (flexural slip, reactivation of bed-parallel stylolites) or veins associated with enhanced deformation in fold cores (Figure 5a, a'), are associated with folding. The link between high rates of deformation on the hinges, shear and slip along bed-parallel surfaces and compression in non-horizontal layers during folding could be associated with Set-BVIIa striking 250°, dipping 50°, and Set-BVIIIa striking 080° and dipping 60° (Figure 4a). Fractures associated with those two sets are mostly located on the hinges of the folds developed in the KKFTB.

Deformation Phase 5 is associated with two fractures sets; Set-BIX trending 330° and dipping 85°, and Set-BX trending 290° and dipping 80° (Figure 4e, f). These fracture sets are commonly associated with the steeply-dipping layers, which are interpreted as the forelimbs of fault-propagation folds (Morley et al., 2013; Arboit et al., 2014). These fracture sets are present in low abundance in the sub-horizontal southern-limbs of the north verging drag folds, with the longest wavelengths, where the bedding curvature or fold amplitude are at a minimum (Figure 7 in Arboit et al., 2014). While the forelimbs preserve the highest frequency of fractures,

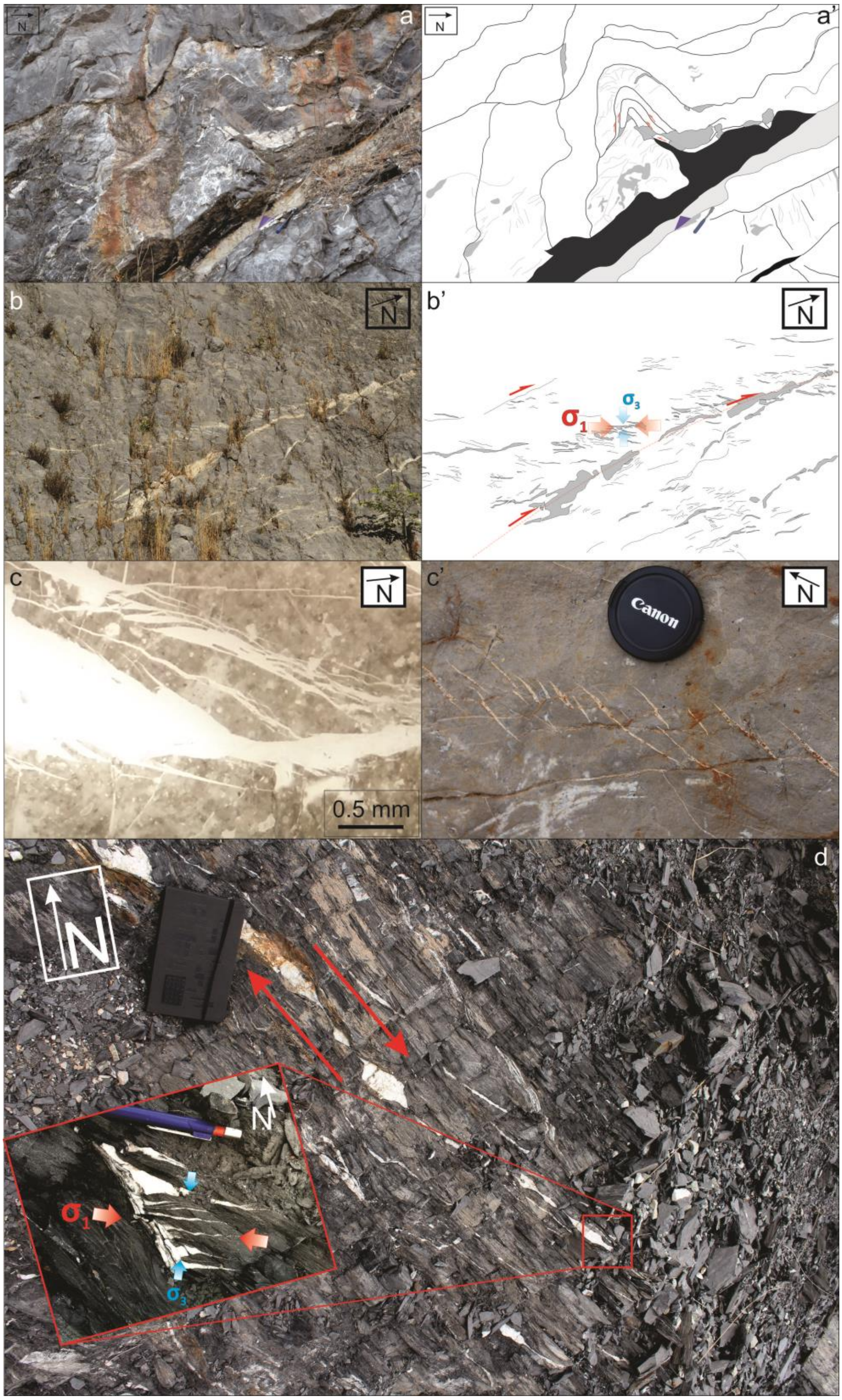

Fig 5. (a) Example of mesoscale chevron fold with veins relative to fold tightening, (a') detail of the deformation: geometries here agree with a progressive evolution of deformation affected a multilayered (fixed-hinge) fold, where tangential-longitudinal strain accumulates in the fixed hinge region and only in the thickest and more competent mechanical layer, while thinnest layers show an higher level of flexural-slip in the libs of the fold. (b) Subhorizontal en-echelon veins possibly occurred during late stage of propagation of the resulted thrust, probably reactivated (188°/47°) during phases of fold tightening (Stage 4); (b') detail of the veins pattern with a subhorizontal σ1. (c and c') Two examples of shearing at the microscale and macroscale, with respectively sinistral movement lined up on a N-S direction showing crosscutting relationships with NW-SE oriented veins attributable to the fourth deformation phase and a left-stepping tensional gashes showing a dextral movement developed during the fifth deformation phase. (d) Linkage of a sequence of en-echelon veins into a shear zone crosscutting N-S oriented veins with NW-SE oriented wing-cracks.

inferring that the fracture sets are induced or at least initiated by folding (Price and Cosgrove, 1990) (Figure 5c, d). Where possible to observe, fractures associated with the fifth phase of deformation are represented by right (higher frequency) and left stepping en-echelon tension gashes (forming a conjugate pattern).

Fractures that met the geometric criteria (dip angle range/strike) of a given pervasive fracture set before and after stereographic rotation (Figure 4), are often used to relate the fractures to a pre- and post- tilting origin

(Hancock, 1985; Bellahsen et al., 2006). The derived sequence of fracturing relies upon abutment and crosscutting relationships both at the meso- and micro-scale, starting from those that apparently initiated before the early stages (Figure 4, horizontal bedding-related), and those that developed during and after the Indosinian Orogeny (Figure 4, tilted bedding-related). We identify six sets of fractures that formed when bedding was horizontal, Set-AI/AII preceding Set-AIII/AIV and AV/AVI, which clearly abut on, and hence post-date, sets AI and AII. We also identify Set-BVII/BVIII as formed during the various stages of folding and Set-BVIIa/BVIIIa during late stage of folding. These sets are present throughout the entire length of the folds but have the highest frequency in the forelimbs and in the hinges. Some of the BVII/BVIII fractures were later reactivated as strike-slip faults. Set-BIX/BX are sub-vertical in their present orientation (folded) and cut across all the previous sets except BVIIa/BVIIIa (where a relationship isn't seen). Hence, sets BIX/BX are treated as the youngest set cutting the carbonates of the Khao Khad Formation (Figure 6). Fractures associated with shear displacements in the field, or thin section (Figure 5c, c', d) demonstrate a bimodal distribution (Figure 4), suggesting that the fracture sets in the western portion of the KKFTB are conjugate arrays (Figure 4).

5. Analysis of fault slip data

The kinematics of the fault population (140 faults) is described using the calcite and rock striations and steps observed on the slip planes in several locations across the study area at various scale (10 cm to 100 m). Their distribution throughout the western part of the KKFTB is heterogeneous both in terms of size and frequency and therefore, to avoid local heterogeneities, all the slip events have been grouped in a single stereonet in order to identify their significance in relation to regional-scale stress regimes. As we are attempting fault slip inversion a few assumptions are required. Firstly, the analysed rocks hosting the fractures are considered physically homogeneous and isotropic; i.e., the rock behaves as a rheologically linear material (Twiss and Unruh, 1998). Secondly, displacements on fault planes are assumed to be small with respect to the fault length and there is no ductile deformation of the material and thus no rotation of the fault planes. Thirdly, each tectonic event is assumed to be characterised by a single stress tensor. Finally, the orientation of slip occurs in the sense of the maximum resolved shear stress in order to explain the presence of oblique slip faults, which are incompatible with Anderson's theory. After measuring fault data in the field, this raw assemblage of data (or *pattern* following the terminology proposed by Angelier, 1994), was divided into sub-sets and used as a starting point for stress inversion. Each sub-set is here defined as a group of faults that moved or have been generated during the same tectonic event. Following Angelier (1994), sub-sets are formed by more than two families of data and each family has been considered a group of brittle data of the same type and with similar geometric characteristics. These preconditions have been necessary in order to find the best solution fitting the observed slip directions and the possible stress tensors that induced these faults. Considering all these preconditions, we carried out a quantitative inversion of all the fault slip data collected within the Khao Khad Formation (Angelier and Mechler, 1977, Lacombe, 2012; Celerier et al., 2012) using the Win-Tensor Software (Delvaux and Sperner, 2003). This inversion has been done in order to obtain data on the stress model (three principal stress axes σ_1 σ_2 σ_3 and on the stress ratio 'R'), which minimizes the differences between the observed and the

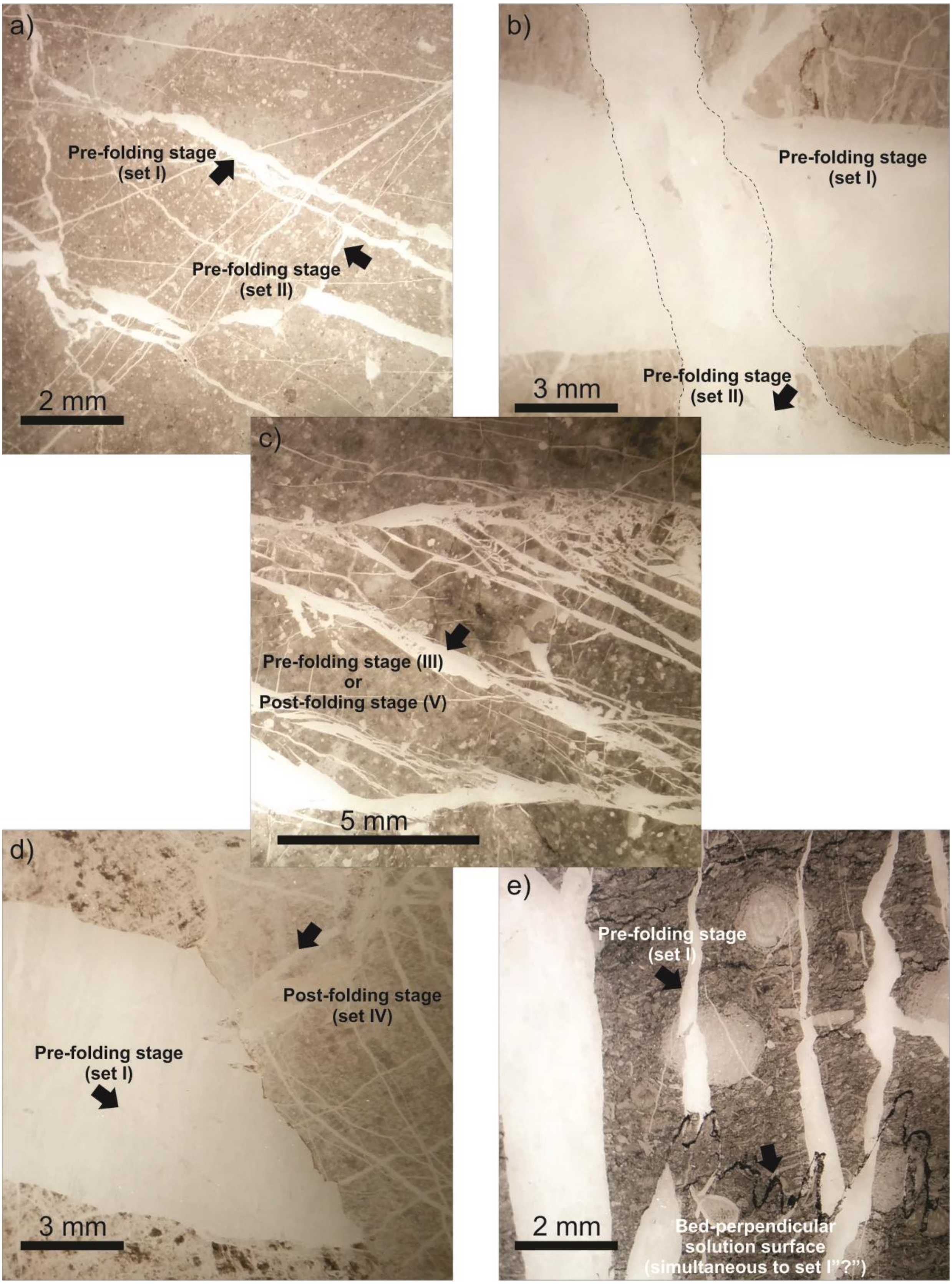

Fig 6. Photomicrographs illustrate the main sets of veins lying within the Khao Khad Formation. It is possible to observe that set I, set III, and dissolution surfaces form crosscutting relationships, their relative ages to be determined. The deformation mode of these fractures remains uncertain, but in thin sections it is possible to observe that they initiated either as simple shear deformation bands (sets II and III) or as extensional joints (set I) later reactivated by shear.

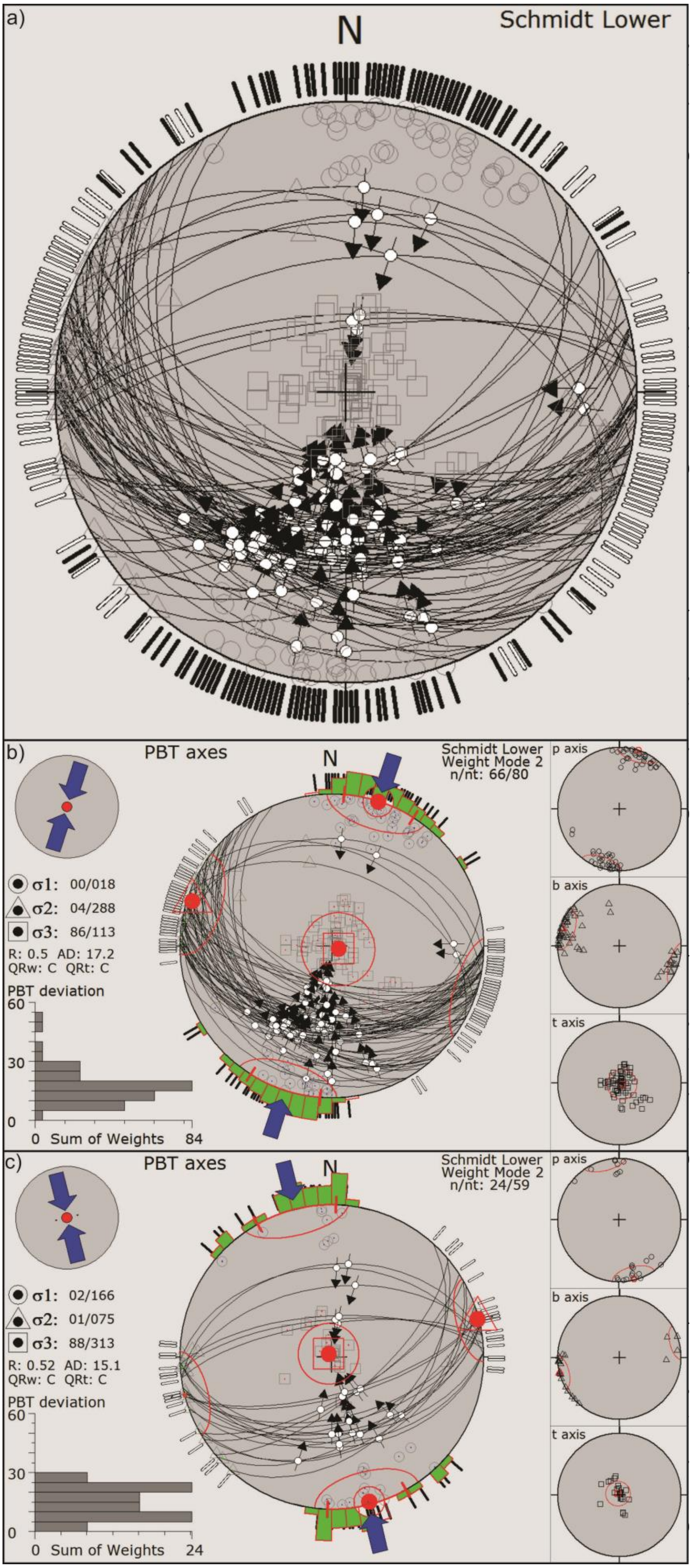

Fig 7. Stereonet (lower hemisphere, equal area projection) (a) illustrating the structural and kinematic data of faults detected in the most significant structural stations in the western portion of the Khao Khwang Fold-Thrust belt. Cluster analysis of the stress axis shows very similar angular deviations and also the presence of two major sets of conjugate compressive faults (both with major compressional and minor strike-slip fault stress regimes) with (b) WNW-ESE and (c) ENE-WSW orientations

predicted slip directions on a set of fault planes. The best fitting models and therefore the quality of the calculated tensors have been chosen based on the minimum difference between the computed shear stress and the observed kinematic indicators on the fault planes. The deformation in the study area has been accommodated by a large number of slip events (140), which have been grouped into different fault populations. The dataset for each fault includes the strike, dip and dip direction of the fault plane; the plunge the azimuth and the sense of shear of the slip lines.

The overwhelming majority of faults (98.8 %), presented here, infer a compressive regime and are observable throughout the entire KKFTB. Fault striae, where observed, indicate a dominant dip-slip sense of movement with reverse offset. Faults cluster into two distinct populations based on orientation and kinematic attitude, striking from WNW-ESE to ENE-WSW (mean 096°, range from 053° to 165°), each with dip angles ranging from quite shallow to steep (30° - 80°). Inversion of the 140 fault slip planes presented here (Figure 7a) yields two reliable stress tensors (a) σ_1=00/018 – σ_2=04/288 – σ_3=86/113, R=0.5 and a "C" quality ranking with an angular deviation of 17.2° ± 8.6° (Figure 7b); (b) σ_1=02/166 – σ_2=01/075 – σ_3=88/313, R=0.52, and a "C" quality ranking with an angular deviation of 15.1° ± 7.5° (Figure 7c) (Delvaux and Sperner, 2003).

6. Calcite twin data processing

Microstructural analysis has been performed on nine oriented samples collected in the Khao Khad Formation. Following the Etchecopar (1984) method, five of these samples, collected in the Khao Khad Formation, have been used to carry out calcite twin analysis. In only two samples is the cement coarse enough to observe deformation-twinning in the matrix. In the rest of the samples, data were obtained exclusively from the vein systems cutting the host limestone. For each sample, approximately 100 to 250 calcite grains were studied with the aid of the universal stage microscope. In all the observed twins, the internal twinning deformation occurred in a thin-twin regime (Figure 2), suggesting that temperature remained lower than ca. 150-200 °C, and that internal strain did not exceed 3-4% (Burkhard, 1993). In each of the three perpendicular thin sections per specimen, twinned calcite grains were measured along random traverses of unit length. When more than 30% twinned planes in a sample are not explained by a unique stress tensor, the inversion process is repeated ("b" samples in Table 2) with the uncorrelated twinned planes and the whole set of untwinned planes. This procedure provides an efficient way to separate superimposed twinning events and to calculate related stress tensors where polyphase deformation has occurred (Amrouch et al., 2010a).

Stress Stage	Sample Number	Bedding Dip Dir. - Dip	Vein Dip Dir. - Dip	Trend of the Principal Stress Axes σ_1	σ_2	σ_3	Ratio Between Differential Stress Φ	Number of T/UT Data	Number of Data Consistent with the Tensor T/UT	Quality Estimator function " f "	Pre/Post Folding Setting	Orientation Stress Regime
I	T_14_020	174/14	068/88	321/58 302/69*	115/29 121/21*	211/12 210/01*	0.6	211/065	100/016	0.37	PRE-FOLDING	
	T_14_029	352/39	235/80	181/53 285/84*	316/28 321/-01*	058/22 050/03*	0.3	365/106	182/092	0.76		
	T_14_019b	160/40	251/72	283/55 219/56*	139/29 142/-09*	039/17 103/00*	0.4	186/081	052/073	0.50		
II	T_14_029b	352/39	358/82	023/16 023/-18*	290/13 292/-07*	163/69 002/72*	0.4	183/106	069/084	1.80		
	T_14_083b	175/59	HOST	272/33 239/22*	037/41 113/55*	159/31 160/-26*	0.9	166/087	056/080	0.30		
	T_14_018v	160/40	138/25	244/27 228/17	006/47 070/73	136/32 140/-05*	0.8	152/068	057/059	0.67		
III	T_14_011b	178/60	HOST	110/33 127/00*	353/36 212/83*	230/38 217/-06*	0.5	249/086	094/075	0.65		
	T_14_019	160/40	322/71	133/49 142/12*	037/05 047/25*	303/41 255/63*	0.2	273/081	087/069	0.96		
	T_14_018v	160/40	322/71	112/33 121/03*	004/24 025/58*	246/47 213/32*	0.5	223/068	071/057	0.91		
	T_14_011	178/60	HOST	107/34 126/02*	355/29 289/87*	234/42 216-02*	0.5	259/086	103/072	0.85		
IV	T_14_081	175/59	140/78	035/20	275/54	136/29	0.3	306/084	128/068	1.03	POST-FOLDING	
	T_14_082	175/59	217/75	028/08	293/30	131/59	0.1	294/078	117/066	0.81		
	T_14_080b	175/59	255/52	282/36	047/38	165/31	0.8	188/084	072/073	0.53		
V	T_14_081b	175/59	281/42	140/15	024/58	238/28	0.4	178/084	089/076	0.92		
	T_14_082b	175/59	261/49	126/09	351/77	217/09	0.3	177/078	081/072	0.47		
	T_14_083	175/59	045/87	160/15	064/20	284/64	0.6	276/087	110/071	0.95		
	T_14_080	175/59	337/85	154/26	057/13	303/61	0.7	303/084	115/073	1.14		

Table 2. Result of Stress Tensor Determination Based on Calcite Twin Data

6.1. Stress tensors from calcite twin data

The rocks are effectively unmetamorphosed and were deformed within five km of the surface (Morley et al., 2013, Arboit et al., 2014). Therefore a principal stress is required to be vertical (Anderson, 1905). To satisfy these criteria, we examined all calculated tensors in a) their present orientation, and, b) after bedding was rotated to horizontal. In cases where unfolding resulted in a principal stress becoming vertical we assigned the RST as being active before tilting. In cases where unfolding resulted in no vertical principal stress we assigned the RST as being active after folding. These bed-unfolding calculations lead us to resolve five different stress tensors (Table 2); three in a horizontal bedding-related position and two in the present position.

6.2. Horizontal-bedding related stress tensors

The first calculated tensor (Figure 8T1) found in samples: T_14_020 / 029 / 019b is related to an extensional event. All the samples present a vertical σ_1, the minimum (σ_3) and intermediate (σ_2) principal stress axes are approximately bedding parallel, respectively trending NE-SW and NW-SE. This stress regime was reconstructed from twinned calcite collected within bed-perpendicular veins striking 150° (Set-AI), 170° and 335° (Set-AII) coming from quarries A and N (Figure 1c).

The second RST (Figure 8T2) has been recorded in samples (T_14_029b / 083b / 018v) collected in quarries B, X, Y in (Figure 1c). This stress tensor corresponds to a strike-slip and compressive regime, both with a horizontal σ_1 axis oriented NE-SW that trends ~30° to the mean fold hinge orientation. The stress tensor corresponding to the third tectonic event has been recorded by twinned calcite in bed-perpendicular veins striking 050°, 065° (Set-AIII) and 110° (Set-AIV). Sample T_14_029b is the only sample presenting a pure compressive stress regime and has the lowest value of differential stress (Φ = 0.368).

The last of the bedding-related stress regimes (Figure 8T3) was reconstructed in samples coming from quarries AA and FF (Figure 1c). This RST has been reconstructed including both strike-slip and compressional regimes, it shows a consistently horizontal σ_1 oriented approximately 300°, a horizontal σ_3 in samples T_14_011b / 011 / 018v oriented 215°, and a horizontal σ_2 in sample T_14_029 trending 255°. This stress tensor has been recorded in both the matrix of the Khao Khad carbonates and from veins striking 050° (Set-AV) and 145° (Set-AVI). The stress ellipsoid shape ratio (Φ) in sample T_14_019 is close to 0, this indicates similar magnitudes for σ_2 and σ_3, hence stress permutations are likely, swapping between compressional and strike-slip regimes

6.3. Tilted bedding related stress tensors

The fourth twinning event (Figure 8T4) is related to both a compressional and a strike-slip regime with a low-angle σ_1 axis trending NE-SW. This RST was found in bed-perpendicular veins striking 355° (samples T_14_082 / 080b, Set-BVII) and 045° (sample T_14_081, Set-BVIII). The ellipsoid shape ratio in sample T_14_082 has a value close to zero (Φ=0.135), which indicates that σ_2 and σ_3 are similar magnitudes. Therefore little stress permutations are required to switch between strike-slip and compressional regimes. The σ_1 axis in the fourth tensor is oriented NE-SW (similarly to the second stress regime), which

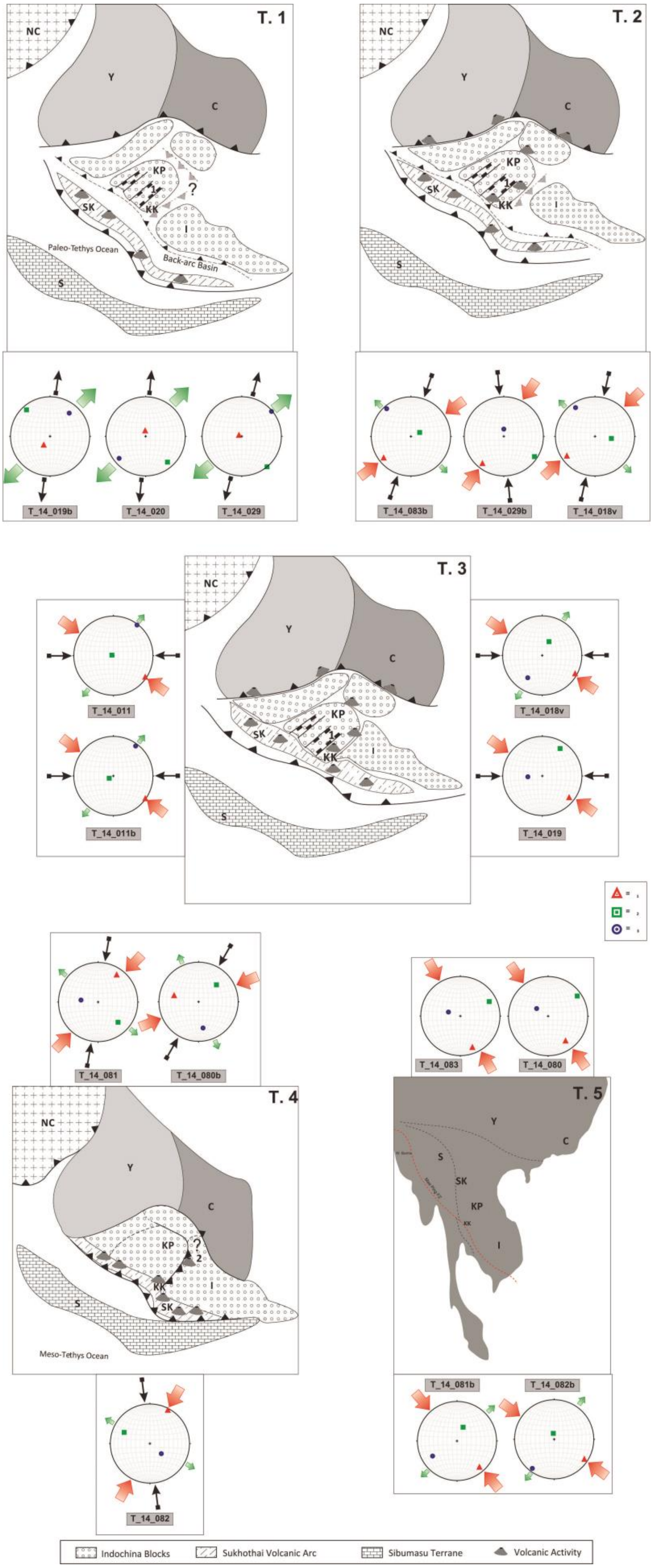

Fig 8. Paleostress orientations related to the Indosinian Orogeny derived from calcite twins. Image illustrates the five different stages of deformation inferred from the twins, The thick arrows reveal the actual calculated stress orientation, and the thin (black/white) arrows display the data corrected to an interpreted original orientation prior to the Late CretaceousPaleocene rotation. Stress data are superimposed on the reconstruction of the plate tectonic evolution of the SE Asia during Late Permian-Early Triassic (T1, T2, and T3) and Mid-Late Triassic (T4), and Late Mesozoic-Early Cenozoic (T5). Modified from Arboit et al. [2014] and Morley et al. [2013]; NC = North China, Y = Yangtze Block, C = Cathaysian Block, I = Indochina Block, KP = Khorat Plateau, KK = Khao Khwang carbonate platform, SK = Sukhothai Terrane, 1 = rift related Permian Basin in the Khorat Plateau, 2 = possible minor suture zone running on edge of the Khorat Plateau.

is almost perpendicular to the fold axes of the major folds. The samples that yield this tensor occur where macroscopic deformation is most intense, such as between closely spaced thrusts and on the steep forelimbs of tight fault-propagation folds or buckled chevron folds (Arboit et al., 2014).

The last of the tilting-related stress tensors (Figure 8T5) has yielded both strike-slip and compressional stress regimes, with a horizontal σ_1 oriented ~145°. The compressional regime was reconstructed in veins striking 330° (samples T_14_081b / 082b, Set-BIX). The strike-slip regime was found in bed-perpendicular veins

7. Discussion

7.1. Comparison of macroscopic and microscopic paleostress analysis

The inversion, and the efficiency of the inversion, of fault slip data have been extensively debated by several authors (e.g. Angelier, 1984, 1990; Lacombe, 2012). In order to make a comparison between the stress tensor calculations from fault-slip inversion and calcite twin analysis, it is needed to estimate the possible margin of error in both paleostress determination techniques. The major source of uncertainties for striated faults lies in the data acquisition, it is important that the number of faults per station is large enough (15-200), and fault orientations are sufficiently variable to be statistically valid. Conversely, for calcite twin analysis, Lacombe et al. (1990) demonstrated that 90 twins per sample is required to remove the possibility of any inversion error and that the main source of error of this technique lies in the preparation of the thin-section and U-stage measurements. We therefore assert that, considering the quantity and quality (*"f"* function ranging between 0.3 and 1.8 in Table 2) of the data presented here, the calculated paleostress tensors from the calcite twin analysis are likely to be reliable (Table 2). Following the previous works of Lacombe et al. (1992; 2007) and Amrouch et al. (2010), calcite twins and mesoscale kinematic features, such as faults, veins, joints and cleavage surfaces, are expected to show regionally consistent results in term of paleostress-orientation. To test this assertion, we calculated the misfit angles between the best-fitting shear stress direction and the measured lineation for each of the considered fault planes, the ratio between the number of data used to generate the tensor versus the number of inputted data—"n/nt" (0.90 in Figure 7b) (0.41 in Figure 7c), the dispersion of planes— "Plen" (0.91 in Figure 7b) (0.83 in Figure 7c), and the dispersion of slip-lines—"Slen" (0.9 in Figure 7b) (0.84 in Figure 7c) for each identified stress state. To calculate the RSTs using the calcite twin inversion method, we considered different parameters in order to evaluate the reliability for each RST. In particular, we used the ratio of the number of twinned and untwinned planes consistent with the stress state of interest compared to the total number of twinned and untwinned collected for each sample. If this ratio gets large (Jaya and Nishikawa; 2013), then the proposed RST is viable. Twinned planes (up to 51%) and untwinned (up to 92%) are compatible with the proposed stress state, while 40-83% of the total number of faults are suitably oriented for motion under the identified stress state. The high number of untwinned planes consistent with the tensor in sample T_14_029b (Table 2) is most likely the reason behind the high value of the quality factor.

Taking into account the uncertainties inherent in paleostress orientation determination (5-10°) (Lacombe et al., 1992), the deviation in order of ~5°-15° between the meso- and micro-scale paleostress inversion presented in this study is considered acceptable and may be justified in terms of local stress perturbations or inhomogeneities in the rocks. Figure 9 illustrates that, despite the complexity of the tectonic framework within the KKFTB, all the paleostress indicators, from fault striae, fractures, and calcite twin analysis, yield very similar σ_1 orientations supporting the validity of the approach.

7.2. Reconstruction of pre-deformation tensor orientation

The paleostress tensors determined here are reconstructed in their present-day orientation. However, in this tectonically active region, rotations of the analysed terranes are likely to have occurred since formation of the rock. Recent results on the geodynamic evolution in SE Asia, demonstrates that the block north of the Mae Ping Fault (including the KKFTB) underwent approximately 150 km sinistral translation after Late Cretaceous times; an amount consistent with paleomagnetic results obtained from the Khorat Plateau that demonstrate a clockwise rotation of about 25° – 30° (Charusiri, 2006; Cung and Geissman 2013; Morley et al., 2013; Singsoupho et al. 2014). To account for this, the subsequent discussion, on the fractures, faults and calcite twins derived RSTs (including Figures 8 and 9) will take this 25° – 30° rotation into account.

7.3. Correlating palaeostress determinations with tectonic environment

Based on the results of previous studies on regional tectonics and paleogeographic reconstructions of SE Asia (Helmke and Lindenberg, 1983; Helmke, 1985; Mitchell, 1989; Metcalfe, 1990; Metcalfe, 1991, Metcalfe, 2000; Metcalfe and Sone, 2008; Metcalfe, 2011; Morley, 2002; Morley, 2004; Morley et al., 2007, Morley et al., 2013), the Permian-Recent history of Thailand began with Early-Mid Permian subduction of Paleo-Tethys underneath the south-western margin of Indochina. This initiated upper-plate extension and subsequent contraction as a back-arc basin first opened, then closed as the arc (represented by the Sukhothai terrane) collided with Indochina. This contractional event was followed by the Late Permian – Early Triassic collision between Sibumasu and the Indochina Block, which during the Mid-Late Triassic itself collided with South China (Cathaysia) to form a large

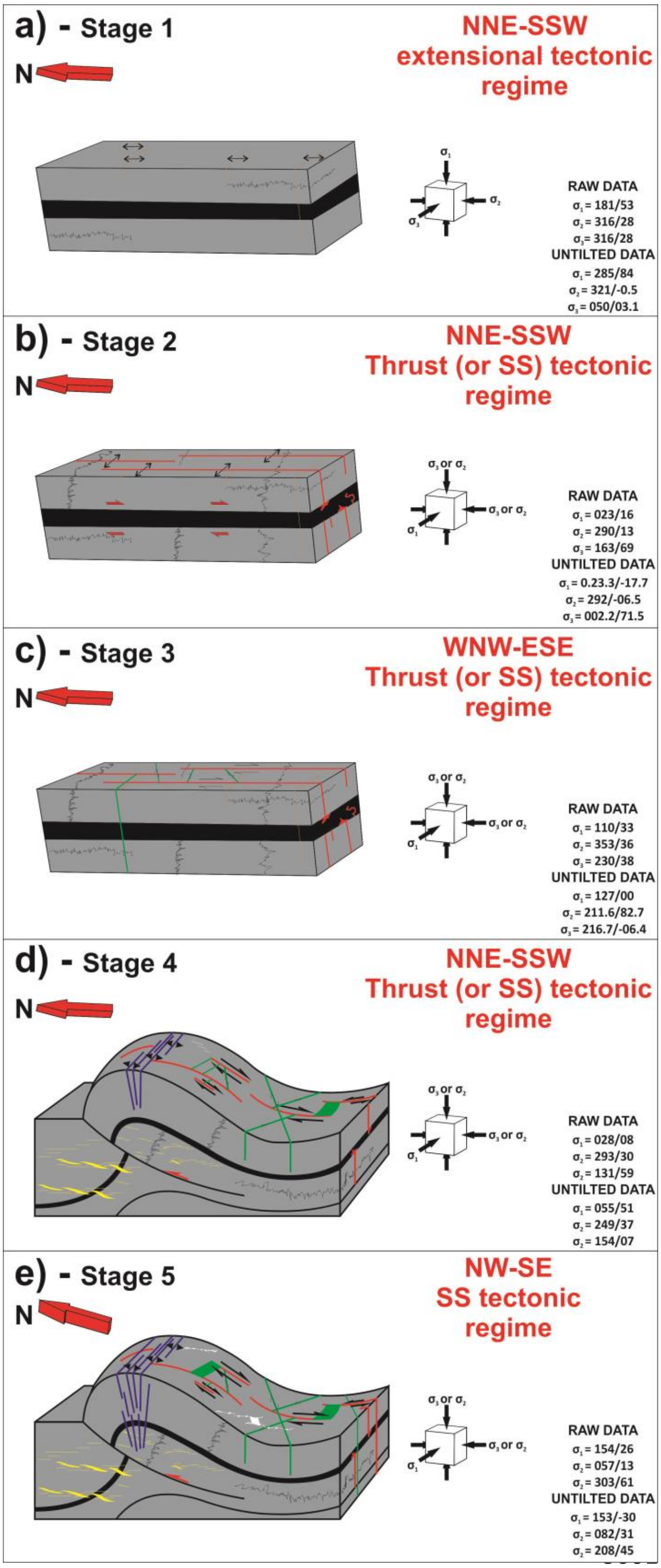

Figure 9. Conceptual models of deformation stages and fracture formation within the Khao Khad Formation compared with the orientation and regimes of the calculated stress tensor for each stage of deformation, involving prefolding and postfolding structural element development

amalgamated continent. The next major deformation to affect the region after the Indosinian occurred in the Cenozoic, where extensive S-type Cretaceous-Paleocene granites in Myanmar and Thailand (Morley, 2004) are associated with upper-crustal deformation (Mae-Ping and Three Pagodas fault zones). The KKFTB lies close to the trace of the Mae-Ping Fault, so we expect to see deformation, in the form of meso-scale faults and calcite twins, in the KKFTB limestones.

The stress states determined here are characterised by an initial NE-SW oriented σ_3 with a vertical σ_1, followed by four later stress tensors that share a horizontal σ_1 direction (oriented variously NE – SW to WNW – ESE) and vertical to moderately plunging σ_2 and σ_3 with variable stress ratios. These stress states are consistent with an early extensional event followed by contractional (thrust or strike-slip) tectonic regimes. Between these five different tectonic regimes; four are interpreted to belong to the Indosinian Orogeny, while the fifth has been attributed to Cenozoic deformation that affected SE Asia during the India-Asia collision. These five tectonic systems have been recorded by structures both at the macro- and micro-scale, which are respectively represented as major anticlines and calcite twins. We present conceptual block models to illustrate the fracture evolution within the KKFTB (Figure 9). These models are composed of three layers, idealized from the stratigraphy of the Khao Khad Formation (Figure 1), including a black layer representing the shale between two gray layers representing limestone, which, being relatively stiffer (higher Young's modulus), can support greater amounts of stress than softer layers when subject to same effective stress. The limestone layer of the Khao Khad Formation responded to the stress by fracturing (Figure 6a, b and e) and shearing (Figure 6a, c and d), while the black layers acted in a more ductile manner, dominantly by plastic flow (detachments), resulting in a less fractured framework (Nelson and Hillis, 2005). The bedding parallel slip at the interfaces between the ductile and brittle layers played an important role for the stress distribution (Cooke and Underwood., 2001; Sanz et al., 2008). The stress tensors that resulted in the deformation observed are:

1- Fracture Set-AI/AII (Figure 4d Set-A) along with RST obtained from samples T_14_020/029/019b are consistent with a pre-folding extensional stage (Figure 9a) with a vertical σ_1 and an almost N-S oriented σ_3. The minimum principal stress lies in the plane of the bedding and is oriented ~N-S, sub-perpendicular to the trend of the KKFTB (T1 in Figure 8). These fracture sets pre-date all the other detected fracture sets as suggested by few macroscopic and microscopic observations along with calcite twin analysis. We suggest that this deformation reflects either pre-Indosinian extension, possibly related to, extension foreland-ward of an evolving contractional orogeny, created due to flexure in the peripheral bulge (Doglioni, 1995; Langhi et al., 2011; Tavani et al., 2015), or Permian supra-subduction zone extension. The KKFTB lies close to the Nan Suture (Figure 1a), which is a narrow zone of Permian ophiolites and melange, and is associated with the back-arc basin between the Sukhothai and Indochina terranes. A K/Ar actinolite age of 269 ± 12 Ma (i.e., Middle/Late Permian) (Barr and Macdonald, 1987) was obtained from mafic schists in the Pha Nom Complex, within the Nam Suture (Barr et al., 1985; Singharajwarapan and

Berry, 1993, 2000; Sone and Metcalfe, 2008). This infers that the back-arc basin related extension predated ca. 269 Ma.

2- Fracture Set-AIII/AIV (Figure 4c, e, f Set-A) along with some calcite twin results, yielding paleostress tensors of both strike-slip and pure compression, from the samples T_14_029b/083b/018v are consistent with a pre-folding compression (Figure 9b). These yield N-S oriented σ_1 that is perpendicular to the fold-axis and is interpreted as related to the first phase of the Indosinian collisional event (Indosinian I) between the Sukhothai and Indochina terranes. This tectonic phase is interpreted to represent the main layer-parallel shortening event, and therefore to be the stress state responsible for the emplacement of the KKFTB. The range of orientations of fracture of Set II is in very good agreement with both the fault-slip and calcite derived stress state. These suggest a range of shortening direction from 020° to 340° with a mean shortening direction of 005°, which is quite consistent with the general trend of the major folds in the western portion of the KKFTB. Andesite intrusions in the Saraburi – Khao Yai area post-date major KKFTB deformation and have recently been dated as crystallising between 250 and 240 Ma (Morley et al., 2013). This constrains the timing of this stress tensor to occurring in the Late Permian-Early Triassic. This collision is thought to have affected the entire Indochina Block. In the sub-surface of NE Thailand there is a major regional unconformity, which was clearly established by the uplift and the consequent erosion associated with major compressional deformation of the Saraburi Group (Booth and Sattayarak, 2011) at around the Permian – Triassic boundary. The RST is here presented by three tensors, two of them with σ_2 close to vertical, indicating a strike-slip fault stress regime. The apparent interchange between the vertical stress being σ_2 or σ_3 is likely due to the similarity in magnitude of these stresses during the Indosinian I event. Similar results were found in the calcite twin analysis study of the Sheep Mountain Anticline (Wyoming, U.S.A.; Amrouch et al., 2010a).

3- Fracture Set–AV/AVI is represented by veins and joints that formed in both pure compressional and strike slip regimes (Figure 4b, g Set-A). These represent an E-W oriented compressional (Figure 9c), strike-slip fault stress regime, which could represent either a pre- or syn-folding event. The σ_1 direction is almost parallel to the main fold axes of the KKFTB. This regime may reflect stress evolution during the early Indosinian Orogeny. However, Lepvrier et al. (2004) and Morley et al. (2013) suggested the possibility that the Indochina Block was actually more than one continental terrane before the “Indosinian I” Orogeny. They suggested that an intra-Indochina ocean may have closed during the main phase of the “Indosinian I”. The tensor described here would be in a favourable orientation to result from the closure of this proposed ocean. Clearly a wider, more regional, view is needed before this RST is attributed to a specific tectonic event. The Ailao Shan region lies 800 km NE of the KKFTB. Here, outcrops of mafic and ultramafic rocks have led various authors to interpret this as a suture zone (Tapponier et al., 1990) associated with the collision between Indochina and South China (Cai et al., 2009). This collision is thought to have started as a south-directed oceanic subduction beneath Indochina, which has been interpreted to have been active at ca. 236 Ma, based on $^{40}Ar/^{39}Ar$ dating (Maluski et al., 2001). Syn- to post-tectonic granites have been U-Pb zircon dated to ca. 252-245 Ma dating the major compression in the region (Halpin et al. in press). This is consistent with the orientation and timing of the third RST.

4- The Indosinian event also probably marked the emplacement of fracture Set-BVII/BVIII. These fractures, ranging in orientation between 355° and 030°, are similar in orientation to Sets-AI/AII. However, these fractures are clearly shear fractures (Type 3). The similarity between these fracture sets suggests that many of the fractures belonging to Set-AIV are reactivated fractures emplaced during the early stages of the Indosinian orogeny. In such a case, sets of the fourth deformation phase in those parts of the KKFTB with near horizontal bedding could not always be distinguishable from fractures active during the second phase of the Indosinian orogeny. In most cases, though, Set-BVII/BVIII fractures consistently abut fractures of the second deformational phase. This later stage of the Indosinian Orogeny is further represented by fracture Set-BVIIa/BVIIIa (Figure 4a Set-A); indeed, these fractures reflect the increasing intensity of folding. Fracture sets developed during the fourth stage of deformation are interpreted to be associated to the syn-folding bending of the layers. This is because they strike almost parallel to the fold axes and are most abundant in the hinge zones of the tight chevron folds in the core of north-verging fault-propagation folds. There is no clear calcite twin regime detected with this orientation but permutations of σ_1 and σ_2 axes in some of the samples provide an extensional stress regime with a horizontal σ_3 axis oriented at high angle to the major fold hinges (samples T_14_083b/018b). We interpret this resumption of ~N-S compression to correspond to the latest Indosinian Orogeny (Indosinian II). Macro deformation associated with this phase is responsible for the tightening of pre-existing fault-propagation folds and partial reactivation of the fractures developed during the earlier event (i.e. SeAII/AIII fractures). During the latest Triassic, the half-graben basins in the Khorat Plateau (NE Thailand) containing the Kuchinarai Group (Late Triassic) ceased to subside and were structurally inverted. The degree of deformation associated with this event is very much less than that which took place during the earlier Indosinian I event. The conceptual model in Figure 11d shows most of the structural events that occurred in the latest stages of fold growth. Indeed as the dip of the fold limbs increased, flexural-slip processes are interpreted to decrease until fold curvature could not accommodate more shortening. When limb dips increase to a maximum for flexural slip amplification (almost 60° as in Figure 5a and a'), further stress and shortening driven by slip on underlying thrust faults (Figure 5b and b') is accommodated by deformation structures cross-cutting the layers.

5- The last fracture Sets BIX/BX are interpreted as the only fracture sets not related to the Indosinian event. Both fractures and calcite twins recorded a consistent post-folding relationship for the RST. The vertical stress vector was σ_2 and σ_1 was oriented NW-SE, consistent with the rupture of post-folding E-W oriented strike-slip faults (Figure 9e). These strike-slip faults were detected in the field (Figures 5d; 6c), and calcite twins from ~150° striking veins, (samples T_14_081b/082b/08/080) yielded results consistent with this stress state. We consider that these fracture sets represent the last event because of the strike slip faults deforming the region, which have similar orientation to Sets-BIX/BX, and cross-cut previous structures emplaced during the main Indosinian Orogeny. These age constraints limit these sets and their relative stress field to being post-Indosinian (i.e. post Triassic). However, the modern stress tensor has a similar orientation to the fifth RST detected by calcite twin analysis, with the modern maximum horizontal stress ranging from N-S to NW-SE (Tingay et al., 2010). The modern stress field has been responsible for the nearby continental-scale NW-SE to NNW-SSE oriented Mae Ping Fault. We therefore assert that this stress tensor might represent Cenozoic deformation related to the India-Asia collision.

7.4. Variations in the ellipsoid stress ratios 'Φ'

There are a variety of phenomena which may be invoked in order to account for variability of the ellipsoid stress ratio. Stress permutations (between σ_1 and σ_2, or σ_2 and σ_3) are common in brittle tectonics at local and regional scales (Angelier et al, 1984; Angelier, 1994; Hu and Angelier, 2004; Amrouch et al., 2010a; Tavani et al., 2015). The results shown in Table 2 illustrate such interchangeable position between σ_2/σ_3 ($\Phi < 0.3$) and between σ_1/σ_2 ($\Phi < 0.7$). Such permutations may induce apparent complexity with several paleostress patterns for a single tectonic event. The origin of these permutations may result from a variety of causes, which can be classified into two groups. The first group involves actual modifications in the stress field induced by far-field changes; e.g., plate motion changes, or local conditions that affect the vertical stress (erosion, burial, elastic rebound, Garcia et al., 2002) and stress relaxation (Du and Aydin, 1996). The second group involves little change in tectonic environmental conditions and is mainly controlled by ongoing brittle deformation inducing stress changes; e.g., stress drop, which may depend on the rheological properties of the affected rock masses (Hu and Angelier, 2004) or an abundance of meso-scale reverse faults versus strike slip faults, pressure solution cleavages and veins (Tavani et al., 2006, 2015), dike injections, and accommodation around tilted blocks. Another possible interpretation is an evolution of the same stress tensor, with the conversion from σ_3 and σ_2 as an effect of transpressive stress partitioning related to the opening of the veins with an orientation of about 50° (80°-90°) with respect to the orientation of σ_1

(Evans and Dunnet, 1991; Jones and Tanner, 1995).

7.5. Local stress perturbation and regional stress orientations

As discussed above all the analysed structural features (fractures, faults and calcite twins) provide related information on the stress evolution history of the western portion of the KKFTB, revealing predominant pre-folding compressional stress regimes and post-folding strike-slip regime. The ellipsoid shape ratio of the two stress tensors reconstructed from fault-slips are near homogeneous; however, some of the samples used for the calcite twin analysis show stress permutations, this suggests that these RST calculated with calcite twins, using different samples, for the same event might have recorded different stress regimes (permutation σ_1-σ_2; σ_2-σ_3). Consideration should be paid to the change in scale, indeed the volume of rock examined using fault-slip analyses is much higher (10^3 to 10^6 m^3) than the volume of rock used for reconstructing paleostress using calcite twins (10^{-3} m^3) (Lacombe et al., 1992). Barquins et al., (1989a) and Petit and Barquins (1990) demonstrated that the shape ratio may vary near to pre-existing defects. Hence, stress perturbation and the methodological uncertainties discussed above, may justify the differences in the values of ratio (Φ) obtained from fault slips and calcite twin analyses, in a given site for a specific tectonic event in a complex structural setting. Fortunately, this variability does not reduce the efficiency of paleostress indicators in terms of orientation, because it has almost no influence on the orientations of the reconstructed RSTs (Lacombe et al., 1992). Thus the regional stress history reconstructed and obtained from calcite twins and fault-slips can be considered reliable.

8. Conclusions

In this study, we have performed qualitative and quantitative tectonic analysis of the brittle deformation at meso- and micro-scales in order to unravel the distribution of the stress in space and time before and after the main folding event in the KKFTB. This has been possible due to the strain acquisition in the folded strata and the stress build-up in the carbonate layers of the Khao Khad Formation. The analyses yielded reliable paleostress states similar and consistent with those from fault-slip and fracture data collected throughout the western margin of the KKFTB. At the meso-scale, the observed fracture population are gathered into six different sets formed during five main events that are interpreted to be developed during the Indosinian I & II tectonic events and subsequent Cenozoic deformation. At the scale of the western margin of the KKFTB, the comparison of major structures, such as major folds, fracture patterns, and the RSTs derived from the calcite twin inversion for each of the detected events demonstrate a consistent record of the tectonic stresses at the scale of the entire KKFTB. Dominant and common stress states throughout the whole study area are characterised by a N-S trending σ_1 and vertical, to ENE-WSW plunging, σ_3 with variable values of stress ratio Φ; which made it possible to link different RSTs obtained with stress tensors coming from distinct samples through σ_1-σ_2 and σ_2-σ_3 permutations.

Unfortunately, there are no syn-deformational sedimentary rocks preserved in the region, restricting the resolution of more precise age constraints on the age of the various deformations. Notwithstanding this, the characteristics of the paleostress regimes, from the calcite twins, and the very good correlation with the distribution of the overall deformation, allowed us to provide a relative chronology of the tectonic events. Calcite twins revealed significant variations of paleostress orientation and regime across the KKFTB, providing a reliable picture of paleostress distribution on the edge of the southern Indochina Block. Beyond regional implications, this study enhance the potential of an analysis based on fault and calcite twin observations which has the potential to lead to a more exhaustive understanding of regional and local stress and stress patterns.

Acknowledgements

This work was funded by Australian Research Council Discovery Project #DP 120101460. ASC is funded by Australian Research Council grant #FT120100340. This is a contribution to IGCP 628 – The Gondwana Map. We gratefully acknowledge all the funding organizations. This publication forms TRaX Record #299. The authors thank Richard Allmendinger for 'Stereonet 8.8.8'; Damien Delvaux for 'Win-Tensor' and Carlos H. Grohmann and Ginaldo A.C. Campanh for 'OpenStereo 0.1.2'. The Editor Nathan A. Niemi, the anonymous associated editor and reviewer are thanked for the constructive reviews that improved the manuscript. Supplementary data for this paper are available by contacting the corresponding author "francesco.arboit@adelaide.edu.au".

References

Allmendinger, R. W. (2005). Stereonet. Program for stereographic projection.

Amrouch, K., Lacombe, O., Bellahsen, N., Daniel, J. M., & Callot, J. P. 2010a. Stress and strain patterns, kinematics and deformation mechanisms in a basement-cored anticline: Sheep Mountain Anticline, Wyoming. Tectonics, 29(1).

Amrouch, K., Robion, P., Callot, J. P., Lacombe, O., Daniel, J. M., Bellahsen, N., & Faure, J. L. 2010b. Constraints on deformation mechanisms during folding provided by rock physical properties: a case study at Sheep Mountain anticline (Wyoming, USA). Geophysical Journal International, 182(3), 1105-1123.

Amrouch, K., Beaudoin, N., Lacombe, O., Bellahsen, N., & Daniel, J. M. 2011. Paleostress magnitudes in folded sedimentary rocks. Geophysical Research Letters, 38(17).

Anderson, E. M. 1905. The dynamics of faulting. Transactions of the Edinburgh Geological Society, 8(3), 387-402.

Angelier J., Mechler P., 1977. Sur une method graphique de recherche des contraintes principals egalement utilisable en tectonique et en seismologie: la method des diedres droits, Bull. Succ. Geol., XIX, N°6, p 1309-1318.

Angelier, J. 1984. Tectonic analysis of fault slip data sets. Journal of Geophysical Research: Solid Earth (1978–2012), 89(B7), 5835-5848.

Angelier, J. 1990, Inversion of field data in fault tectonics to obtain the regional stress. III: A new rapid direct inversion method by analytical means, Geophys. J. Int., 103, 363 – 376.

Angelier, J., 1994. Fault slip analysis and paleostress reconstruction, in Continental Deformation, edited by P. Hancock, pp. 53-100, Pergamon, New York.

Anchuela, Ó. P., Imaz, A. G., & Juan, A. P. 2012. Factors affecting the record of strain fabrics at the anisotropy of magnetic susceptibility: West-Central South-Pyrenean cleavage domain (Southern Pyrenees; NE Spain). Tectonophysics, 554, 1-17.

Arboit, F., Collins, A. S., King, R., Morley, C. K., & Hansberry, R.. 2014. Structure of the Sibumasu–Indochina collision, central Thailand: A section through the Khao Khwang Fold-Thrust belt.Journal of Asian Earth Sciences, 95, 182-191.

Bai, T., & Pollard, D. D. 2000. Fracture spacing in layered rocks: a new explanation based on the stress transition. Journal of Structural Geology, 22(1), 43-57.

Barquins, M., Ghalayini, K., & Petit, J. P. 1989. Branchement des fissures sous compression uniaxiale. Comptes rendus de l'Académie des sciences. Série 2, Mécanique, Physique, Chimie, Sciences de l'univers, Sciences de la Terre, 308(10), 899-905.

Barr S.M., Macdonald A.S. 1987. Nan River suture zone, northern Thailand, Geology, 15 907–910.

Barr S.M., Macdonald A.S., Yaowanoiyothin W., PanjasawatwongY. 1985. Occurrence of blueschist in the Nan River maficultramafic belt, northern Thailand, Warta Geol. 11 47–50.

Bellahsen, N., Fiore, P., Pollard, D.D., 2006. Growth of basement fault-cored anticlines: the example of Sheep Mountain Anticline, Wyoming. Geophysical Research Letter 33.

Booth, J., & Sattarayak, N. 2011. Cretaceous geology of NE Thailand. The Geology of Thailand, 185.

Bunopas, S., 1981. Paleogeographic History of Western Thailand and Adjacent Parts of South-east Asia. PhD Thesis, Victoria University of Wellington, Wellington. (Reprinted in 1982 as Geological Survey Division, Department of Mineral Resources, Geological Survey Paper No. 5, Special Issue.).

Bunopas, S., 1982. Paleogeographic history of western Thailand and adjacent parts of South-east Asia: A plate tectonics interpretation. Geological Survey Division, Department of Mineral Resources, (No. 5).

Burkhard, M. 1993. Calcite twins, their geometry, appearance and significance as stress-strain markers and indicators of tectonic regime: a review. Journal of Structural Geology, 15(3), 351-368.

Cai, J. X., & Zhang, K. J. 2009. A new model for the Indochina and South China collision during the Late Permian to the Middle Triassic. Tectonophysics, 467(1), 35-43.

Célérier, B., Etchecopar, A., Bergerat, F., Vergely, P., Arthaud, F., & Laurent, P. 2012. Inferring stress from faulting: from early concepts to inverse methods. Tectonophysics, 581, 206-219.

Charusiri, P., Imsamut, S., Zhuang, Z., Ampaiwan, T., & Xu, X. 2006. Paleomagnetism of the earliest Cretaceous to early late Cretaceous sandstones, Khorat Group, Northeast Thailand: implications for tectonic plate movement of the Indochina block. Gondwana Research, 9(3), 310-325.

Choukroune, P. 1969. Un exemple d'analyse microtectonique d'une série calcaire affectée de plis isopaques (“concentriques”). Tectonophysics, *7*(1), 57-70.

Cooke, M. L., & Underwood, C. A. 2001. Fracture termination and step-over at bedding interfaces due to frictional slip and interface opening. Journal of Structural Geology, 23(2), 223-238.

Cung, T. C., & Geissman, J. W. 2013. A review of the paleomagnetic data from Cretaceous to lower Tertiary rocks from Vietnam, Indochina and South China, and their implications for Cenozoic tectonism in Vietnam and adjacent areas. J. Geodyn, 69(5).

Dawson, O., Racey, A., Whittaker, J., 1994. Permian foraminifera from northeast and peninsular Thailand. In: Proceedings of the International Symposium on Stratigraphic Correlation of Southeast Asia, pp. 323-332.

Delvaux, D. and Sperner, B. 2003. Stress tensor inversion from fault kinematic indicators and focal mechanism data: the TENSOR program. In: New Insights into Structural Interpretation and Modelling (D. Nieuwland Ed.). Geological Society, London, Special Publications, 212: 75-100.

Dong, Y., Zhang, X., Liu, X., Li, W. Chen, Q., Zhang, G., Zhang, H., Yang, Z., Sun, S., Zhang, F. 2015. Propagation tectonics and multiple accretionary processes of the Qinling Orogen. Journal of Asian Earth Sciences, 104, 84-98.

Doglioni, C. 1995. Geological remarks on the relationships between extension and convergent geodynamic settings. Tectonophysics, 252(1), 253-267.

Du, Y., & Aydin, A. 1996. Elastic stress relaxation: a mechanism for opposite sense of secondary faulting with respect to a major fault. Tectonophysics,257(2), 175-188.

Etchecopar, A. 1984. Etude des e tats de contraintes en tectonique cassante et simulation de de formation plastique (approche mathe matique), the se doctorates-sciences, 270 pp., Univ. Sci. et Tech. du Langue-doc, Montpellier, France.

Evans, M. A., & Dunne, W. M. 1991. Strain factorization and partitioning in the North Mountain thrust sheet, central Appalachians, USA. Journal of Structural Geology, 13(1), 21-35.

Eyal, Y., & Reches, Z. E. (1983). Tectonic analysis of the Dead Sea Rift Region since the Late-Cretaceous based on mesostructures. Tectonics, 2(2), 167-185.

Ferrill, D. A. 1998. Critical re-evaluation of differential stress estimates from calcite twins in coarse-grained limestone. Tectonophysics, 285 (1), 77-86.

Garcia, S., Angelier, J., Bergerat, F., & Homberg, C. 2002. Tectonic analysis of an oceanic transform fault zone based on fault-slip data and earthquake focal mechanisms: the Húsavík–Flatey Fault zone, Iceland. Tectonophysics, 344(3), 157-174.

Grohmann, C.H., Campanha, G.A.C. and Soares Junior, A.V., 2011. OpenStereo: um programa Livre e multiplataforma para análise de dados estruturais. In: XIII Simpósio Nacional de Estudos Tectônicos.

Groshong, R. H. 1972. Strain calculated from twinning in calcite. Geological Society of America Bulletin, 83(7), 2025-2038.

Gutiérrez-Alonso, G., & Gross, M. R. 1999. Structures and mechanisms associated with development of a fold in the Cantabrian Zone thrust belt, NW Spain. Journal of Structural Geology, 21(6), 653-670.

Halpin, J.A., Tran, H.T., Lai, C.-K., Meffre, S., Crawford, A.J., Zaw, K. in press. U–Pb zircon geochronology and geochemistry from NE Vietnam: A ‘tectonically disputed’ territory between the Indochina and South China blocks. Gondwana Research. http://dx.doi.org/10.1016/j.gr.2015.04.005

Hancock, P. L., 1985. Brittle microtectonics; principles and practice. Journal of Structural Geology 7, 437-457.

Handin, J. W., & Griggs, D. 1951. Deformation of Yule marble: Part II—predicted fabric changes. Geological Society of America Bulletin, 62(8), 863-886.

Hansberry, R. L., King, R., Collins, A. S., & Morley, C. K. 2014. Complex structure of an upper-level shale detachment zone: Khao Khwang Fold-Thrust belt, Central Thailand. Journal of Structural Geology,67, 140-153.

Helmke, D. & Lindenberg, H. G. 1983. New data on the 'Indosinian' orogeny from central Thailand. Geologische Rundschau 72, 317-28.

Helmke, D. 1985. The Permo-Triassic ' Palaeotethys' in mainland Southeast-Asia and adjacent parts of China. Geologische Rundschau 74, 215-28.

Hinthong C., 1981. Geology and mineral resources of the Changwat Phranakorn Sri Ayutthaya. Department of mineral resources, Geological survey Report N. 4.

Hinthong C., Chuaviroj S., Kaewyana W., Srisukh S., Pholprasit C., Pholachan S., 1985. Geological map of Thailand 1: 250 000 (Changwat Phranakorn Sri Ayutthaya, ND 47–8). Geological Survey Division of the Department of Mineral Resources, Bangkok, Thailand.

Hu, J. C., & Angelier, J. 2004. Stress permutations: Three-dimensional distinct element analysis accounts for a common phenomenon in brittle tectonics. Journal of Geophysical Research: Solid Earth (1978–2012), 109(B9).

Hutchison, C.S., 1975. Ophiolite in southeast Asia. Geological Society of America Bulletin, 86(6), 797-806.

Jamison, W. R., & Spang, J. H. 1976. Use of calcite twin lamellae to infer differential stress. Geological Society of America Bulletin, 87(6), 868-872.

Jaya, A., & Nishikawa, O. 2013. Paleostress reconstruction from calcite twin and fault–slip data using the multiple inverse method in the East Walanae fault zone: Implications for the Neogene contraction in South Sulawesi, Indonesia. Journal of Structural Geology, 55, 34-49.

Jones, R. R., & Tanner, P. G. 1995. Strain partitioning in transpression zones. Journal of Structural Geology, 17(6), 793-802.

Lacombe, O., Angelier, J., Laurent, P., Bergerat, F., & Tourneret, C. 1990. Joint analyses of calcite twins and fault slips as a key for deciphering polyphase tectonics: Burgundy as a case study. Tectonophysics, 182(3), 279-300.

Lacombe, O., Angelier, J., & Laurent, P. 1992. Determining paleostress orientations from faults and calcite twins: a case study near the Sainte-Victoire Range (southern France). Tectonophysics, 201(1), 141-156.

Lacombe, O., & Laurent, P. (1996). Determination of deviatoric stress tensors based on inversion of calcite twin data from experimentally deformed monophase samples: preliminary results. Tectonophysics, 255(3), 189-202.

Lacombe, O. 2001. Paleostress magnitudes associated with development of mountain belts: Insights from tectonic analyses of calcite twins in the Taiwan Foothills. Tectonics, 20(6), 834-849.

Lacombe, O. 2007. Comparison of paleostress magnitudes from calcite twins with contemporary stress magnitudes and frictional sliding criteria in the continental crust: Mechanical implications. Journal of Structural Geology, 29(1), 86-99.

Lacombe, O., Amrouch, K., Mouthereau, F., & Dissez, L. 2007. Calcite twinning constraints on late Neogene stress patterns and deformation mechanisms in the active Zagros collision belt. Geology, 35(3), 263-266.

Lacombe, O. 2010. Calcite twins, a tool for tectonic studies in thrust belts and stable orogenic forelands. Oil & Gas Science and Technology–Revue d'IFP Energies nouvelles, 65(6), 809-838.

Lacombe, O. 2012. Do fault slip data inversions actually yield “paleostresses” that can be compared with contemporary stresses? A critical discussion.Comptes Rendus Geoscience, 344(3), 159-173.

Langhi, L., Ciftci, N. B., & Borel, G. D. 2011. Impact of lithospheric flexure on the evolution of shallow faults in the Timor foreland system. Marine Geology, 284(1), 40-54.

Laurent, P. 1984. Les macles de la calcite en tectonique: Nouvelles me thodes dynamiques et premieres applications, these doctorat-es-sciences, 324 pp., Univ. Sci. et Tech. du Languedoc, Montpellier, France.

Laurent, P., Kern, H., & Lacombe, O. 2000. Determination of deviatoric stress tensors based on inversion of calcite twin data from experimentally deformed monophase samples. Part II. Axial and triaxial stress experiments. Tectonophysics, 327(1), 131-148.

Lepvrier, C., Maluski, H., Van Tich, V., Leyreloup, A., Thi, P. T., & Van Vuong, N. 2004. The early Triassic Indosinian orogeny in Vietnam (Truong Son Belt and Kontum Massif); implications for the geodynamic evolution of Indochina. Tectonophysics, 393(1), 87-118.

Long, J., Billaux, D.M., 1987. From field data to fracture network modelling, an example incorporating spatial structure. Water Resources Research, 23 (7), 1201-1216.

Maluski, H., Lepvrier, C., Jolivet, L., Carter, A., Roques, D., Beyssac, O. & Avigad, D. 2001. Ar–Ar and fission-track ages in the Song Chay Massif: Early Triassic and Cenozoic tectonics in northern Vietnam. Journal of Asian Earth Sciences, 19(1), 233-248.

Metcalfe, I. 1990. Stratigraphic and tectonic implications of Triassic conodonts from northwest Peninsular Malaysia. Geological Magazine, 127(06), 567-578.

Metcalfe, I. 1991. Late Palaeozoic and Mesozoic palaeogeography of southeast Asia. Palaeogeography, Palaeoclimatology, Palaeoecology, 87(1), 211-221.

Metcalfe, I. 2000. The Bentong–Raub suture zone. Journal of Asian Earth Sciences, 18(6), 691-712. Metcalfe, I., 2005. Asia: South-East. In: Selley, R.C., Cocks, L.R.M., Plimer, I.R. (Eds.), Encyclopedia of Geology, Elsevier, Oxford, vol. 1, 169–198.

Metcalfe, I., 2011. Tectonic framework and Phanerozoic evolution of Sundaland. Gondwana Research, 19(1), 3-21.

Metcalfe, I., 2013. Tectonic evolution of the Malay Peninsula. Journal of Asian Earth Sciences, 76, 195-213.

Metcalfe, I., and M. Sone, 2008. Biostratigraphy and palaeobiogeography of Lower Permian (lower Kungurian) conodonts from the Tak Fa Formation (Saraburi Limestone), Thailand. Palaeogeography, Palaeoclimatology, Palaeoecology 257.1, 139-151.

Mitchell, A. H. G. 1989. The Shan Plateau and Western Burma: Mesozoic-Cenozoic plate boundaries and correlations with Tibet. In Tectonic evolution of the Tethyan region (ed. Sengor, A. M. C). 567-583, Amsterdam, Kluwer Academic Publishers.

Mochales, T., Casas, A. M., Pueyo, E. L., & Barnolas, A. 2012. Rotational velocity for oblique structures (Boltaña anticline, Southern Pyrenees). Journal of Structural Geology, 35, 2-16.

Morley, C. K. 2002. A tectonic model for the Tertiary evolution of strike–slip faults and rift basins in SE Asia. Tectonophysics, 347(4), 189-215.

Morley, C. K. 2004. Nested strike-slip duplexes, and other evidence for Late

Cretaceous–Palaeogene transpressional tectonics before and during India–Eurasia collision, in Thailand, Myanmar and Malaysia. Journal of the Geological Society, 161(5), 799-812.

Morley, C.K., 2007. Variations in late Cenozoic–Recent strike-slip and oblique-extensional geometries, within Indochina: The influence of pre-existing fabrics. Journal of Structural Geology, 29(1), 36-58.

Morley, C.K., Ampaiwan, P., Thanudamrong, S., Kuenphan, N., Warren, J., 2013. Development of the Khao Khwang Fold-Thrust Belt: Implications for the geodynamic setting of Thailand and Cambodia during the Indosinian Orogeny. Journal of Asian Earth Sciences, 62, 705-719.

Nelson, E. J., & Hillis, R. R. 2005. In situ stresses of the West Tuna area, Gippsland Basin. Australian Journal of Earth Sciences, 52(2), 299-313.

Petit, J. P., & Barquins, M. 1990. Fault propagation in Mode II conditions: Comparison between experimental and mathematical models, applications to natural features. In Mechanics of Jointed and Faulted Rock. Balkema Rotterdam. 213-220.

Pollard, D. D., & Aydin, A. 1988. Progress in understanding jointing over the past century. Geological Society of America Bulletin, 100(8), 1181-1204.

Price, N. J., & Cosgrove, J. W. 1990.Analysis of geological structures. Cambridge University Press.

Ramsay, J. G. 1962. The geometry of conjugate fold systems. Geological Magazine, 99(06), 516-526.

Ridd, M. F., & Morley, C. K., 2011. The Khao Yai Fault on the southern margin of the Khorat Plateau, and the pattern of faulting in Southeast Thailand. Proceedings of the Geologists' Association,122(1), 143-156.

Rowe, K. J., & Rutter, E. H. 1990. Palaeostress estimation using calcite twinning: experimental calibration and application to nature. Journal of Structural Geology, 12(1), 1-17.

Sanz, P. F., Pollard, D. D., Allwardt, P. F., & Borja, R. I. 2008. Mechanical models of fracture reactivation and slip on bedding surfaces during folding of the asymmetric anticline at Sheep Mountain, Wyoming. Journal of Structural Geology, 30(9), 1177-1191.

Singharajwarapan S., Berry R.F. 1993. Structural analysis of the accretionary complex in Sirikit Dam area, Uttaradit, northern Thailand, J. Southeast Asian Earth Sci. 8, 233–245.

Singharajwarapan S., Berry R.F. 2000. Tectonic implications of the Nan Suture Zone and its relationship to the Sukhothai Fold Belt, northern Thailand, J. Asian Earth Sci. 18, 663–673.

Singsoupho, S., Bhongsuwan, T., & Elming, S. Å. 2014. Tectonic evaluation of the Indochina Block during Jurassic-Cretaceous from palaeomagnetic results of Mesozoic redbeds in central and southern Lao PDR. Journal of Asian Earth Sciences, 92, 18-35.

Sone, M., Metcalfe, I., 2008. Parallel Tethyan sutures in mainland Southeast Asia: new insights for Palaeo-Tethys closure and implications for the Indosinian orogeny. Comptes Rendus Geoscience, 340(2), 166-179.

Tapponnier, P., Peltzer, G., & Armijo, R. 1986. On the mechanics of the collision between India and Asia. Geological Society, London, Special Publications, 19(1), 113-157.

Tapponnier, P., Lacassin, R., Leloup, P. H., Schärer, U., Dalai, Z., Haiwei, W. & Jiayou, Z. 1990. The Ailao Shan/Red River metamorphic belt: tertiary left-lateral shear between Indochina and South China. Nature, 343 (6257), 431-437.

Tavani, S., Storti, F., Fernández, O., Muñoz, J.A., Salvini, F., 2006. 3-D deformation pattern analysis and evolution of the Anisclo anticline, southern Pyrenees. Journal of Structural Geology, 28 (4), 695-712.

Tavani, S., Storti, F., Lacombe, O., Corradetti, A., Muñoz, J. A., & Mazzoli, S. 2015. A review of deformation pattern templates in foreland basin systems and fold-and-thrust belts: Implications for the state of stress in the frontal regions of thrust wedges. Earth-Science Reviews, 141, 82-104.

Tingay, M., Morley, C., King, R., Hillis, R., Coblentz, D., & Hall, R. 2010. Present-day stress field of Southeast Asia. Tectonophysics, 482(1), 92-104.

Tourneret, C., & Laurent, P. 1990. Paleo-stress orientations from calcite twins in the North Pyrenean foreland, determined by the Etchecopar inverse method. Tectonophysics, 180(2), 287-302.

Tullis, T. E. 1980. The use of mechanical twinning in minerals as a measure of shear stress magnitudes. Journal of Geophysical Research: Solid Earth (1978–2012), 85(B11), 6263-6268.

Turner, F. J., T GRIGGS, D. A. V. I. D., & Heard, H. 1954. Experimental deformation of calcite crystals. Geological Society of America Bulletin, 65(9), 883-934.

Ueno, K., Charoentitirat, T., 2011. Carboniferous and Permian. In: Ridd, M.F., Barber,A.J. Crow, M.J. (eds.), The Geology of Thailand, The Geological Society of London, 71–136.

Warren, J., Morley, C.K., Charoentitirat, T., Cartwright, I., Ampaiwan, P., Khositchaisri, P., Mirzaloo, M., Yingyuen, J., 2014. Structural and fluid evolution of Saraburi Group sedimentary carbonates, central Thailand: A tectonically driven fluid system. Marine and Petroleum Geology, Doi: 10.1016/j.marpetgo.2013.12.019.

Chapter V

Arboit, F., Collins, A. S., Morley, C., King, R., Amrouch, K. (2015). Detrital zircon analysis of the southwest Indochina terrane, central Thailand: Unravelling the Indosinian orogeny, *GSA Bulletin*.

Detrital zircon analysis of the southwest Indochina terrane, central Thailand: Unravelling the Indosinian orogeny

ABSTRACT

The Khao Khwang Fold-Thrust Belt (KKFTB), central Thailand, developed within a basin that formed on the southwestern margin of the Indochina block. Because of limited geochronological and provenance constraints the time of deposition, sediment source location, and tectonic significance of the basin have been uncertain. Here, we present 837 U-Pb detrital zircon ages and 271 Hf isotope in-situ analyses from Permian-Triassic clastic units within the KKFTB in order to constrain the provenance, maximum depositional ages, and depositional environment of the southwestern margin of the Indochina terrane through the Late Palaeozoic to Early Mesozoic. The key lithological units, the Sap Bon, Pang Asok, and Nong Pong formations, are part of the Saraburi Group and have detrital age spectra spanning from Upper Triassic to Palaeoarchean. The entire dataset has a common age peak at ca. 450 Ma, and all samples contain grains with ages of 0.2-0.3, 0.4-0.6, 1.0-1.3, 1.7-1.8, 2.2-2.7 Ga. A few grains predate 3.0 Ga. Multidimensional-scaling analysis of detrital zircon ages from throughout SE Asia demonstrate that the age spectra of the siliciclastic units of the Saraburi Group resemble those of Permian-Triassic detritus found elsewhere in the Khorat Plateau and throughout Vietnam and southeast China, implying that these areas share similar sources. These sources may be the, now largely covered, Indochina basement, and/or contiguous continental crust in terranes already amalgamated to Indochina at that time. Detrital zircons as young as 205 ± 6 Ma show that some formations of the Saraburi Group, previously considered to be of Middle-Late Permian age, are no older than Late Triassic. We propose a depositional model, for the region, of a Permian rift or passive margin setting that evolved into piggyback and foredeep basins during an extended period of folding and thrusting in the Triassic

1. Introduction

The amalgamation of much of east Asia occurred in the Permian-Triassic along a series of arc-continent and continent-continent collisions that are collectively known as the 'Indosinian orogeny' (Carter & Clift 2008). New work in the region is teasing out the timing and nature of plate interactions through this period and demonstrating that the times were particularly dynamic along the west proto-Pacific from Australia to Korea (Cho et al. 2013; Shaanan et al. 2014; Halpin et al. 2014; Dong et al. 2015). Southeast Asia forms part of this end Palaeozoic, earliest Mesozoic tectonic collage. It is a composite region of continental crustal segments (Figure 1) that originated along the northern (with respect to present-day Australia) Gondwana margin (Cocks and Torsvik, 2013; Metcalfe, 2011). These continental fragments rifted off Gondwana in the Palaeozoic and were accreted to the growing Asian continent from the Mid Permian to the Late Triassic (Metcalfe, 2013; Morley et al., 2013). The terranes that make up mainland SE Asia, east of Myanmar, include Indochina, Sukhothai, Sibumasu, and South China. In previous studies, early Palaeozoic reconstructions of these terranes were primarily based on magnetic data, palaeo-biogeography, and stratigraphic correlations (Burrett et al., 1990; Metcalfe and Sone, 2008; Sone and Metcalfe, 2008). The different approaches have resulted in significant ambiguity in the tectonic geography of the region throughout this time. For example, the position of Indochina during the Early Palaeozoic differs widely between reconstructions. Torsvik and Cocks (2009) came to the conclusion that both Indochina and South China were not part of the Palaeozoic Gondwana margin and already existed as isolated terranes during the Cambrian, whereas Burrett et al. (1990), Metcalfe (2006, 2011a, 2011b) and Usuki et al. (2013) adhered to an interpretation where Indochina remained a part of Gondwana until rifting off in the Palaeozoic. This uncertainty in the origin of the SE Asian terranes is mirrored by controversy as to the timing and nature of the ‘Indosinian orogeny’, the pan-East Asian orogeny that evolved during the Late Palaeozoic and Early Mesozoic and led to the formation of much of East Asia (Lepvrier et al., 2004; Morley et al., 2013). These issues arise from the paucity of constraints on the palaeo-position of the SE Asia terranes, the lack of detailed structural studies regarding thrust transport direction and timing, and uncertainties regarding the dating, location, tectonic significance and even existence of suture zones (Metcalfe, 2013; Morley et al., 2013; Gardiner et al., 2015).

The integrated analysis of U-Pb ages and Hf composition of detrital zircons collected from clastic sedimentary rock derived from plutonic, volcanic, metamorphic, or pre-existing sedimentary rocks, can be used as a palaeogeographic tool by depositionally linking a basin to a source region that contains rocks (or at least minerals) of correlatable ages and chemistries (Pettijohn et al., 1987; Collins et al., 2015). This approach, in the SE Asian region, has been successfully used for tracing sediment pathways (van Hattum, 2005; van Hattum et al., 2006, Hall et al., 2008; Sevastjanova et al., 2011, Burrett et al., 2014) with the aim of revealing the geological evolution of the sediment source areas and constraining the tectonic setting of the depositional basins. In addition, this approach provides maximum depositional ages of the sedimentary rocks in question, constraining the stratigraphy of the region. The margin of Indochina contains extensively deformed Permian-Triassic carbonates and associated siliciclastic and volcanic horizons (Ueno and Charoentitirat 2011) that were deposited on the passive margin of Indochina as it was inverted and buried by syn-contractional basins (Arboit et al., 2015). Here, we examine the detrital zircon record preserved within siliciclastic units from the fold-and-thrust belt and from directly north of this region, on the southern margin of the Khorat Plateau (Figure 1), to achieve a better understanding of the tectonic geography of this region through its evolving provenance record.

The Saraburi Group comprises a number of formations that are either dominated by carbonate platform deposits (Khao Khad and Khao Khwang formations), or deeper water deposits comprising a mixture of interbedded shale, sandstone, chert, and limestone (Sap Bon, Pang Asok, and Nong Pong formations (Figure 2a). The Permian limestone has been the subject of extensive palaeontological investigations and is well dated (e.g. Toriyama et al., 1974; Toriyama, 1975; Toriyama and Kanmera, 1979; Udchanon et al., 2007; Ueno and Charoentitirat, 2011). However, there has been less success in dating the clastic-dominated formations, and their provenance has not been investigated in detail, although the continuation of the Permian units to the north (Nam Duk Formation) was investigated by Malila et al. (2008). Indeed, until now, very little has been known about the provenance and ages of detrital zircons and the change of provenance through time of the basinal formations of the Saraburi Group. In this paper, we discuss U-Pb and Hf-isotope data in detrital zircons from 6 samples collected in the Sap Bon, Pang Asok and Nong Pong formations. We seek to provide a better constraint on the tectonostratigraphic

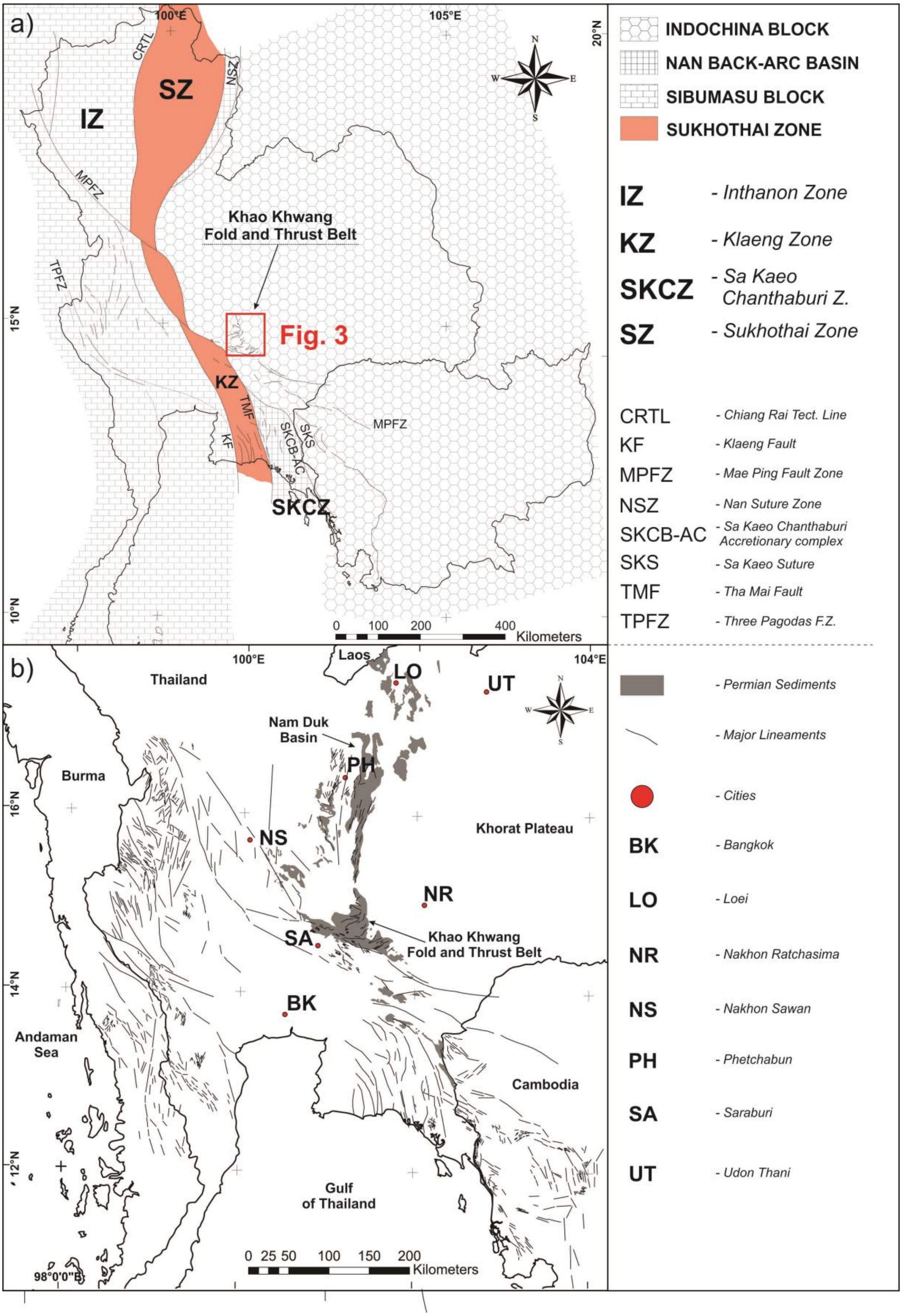

Figure 1. a) Subdivision of Thailand into main tectonic terranes, that amalgamated during the Indosinian Orogeny (modified from Ueno and Charoentitirat, 2011), b) distribution of the major lineaments of the study area (after Arboit et al. 2014).

evolution of the basin that lay in a marginal position on the Indochina terrane. We go on to discuss the implications of these finding on the tectonic and paleogeographic reconstructions for Thailand in the context of the overall SE Asia amalgamation.

2. Geological and stratigraphical setting of Northern and Central Thailand

Ueno (1999) and Ueno et al. (2002) proposed four geotectonic units for northern Thailand (from west to east): the Sibumasu, Inthanon, Sukhothai, and Indochina terranes, separated by the Mae Yuan Fault, Chiang Rai Tectonic Line, and Nan Suture, respectively (Figure 1a). Sone and Metcalfe (2008) suggested a similar tectonic scheme. The Sibumasu Terrane is characterized by an upper Palaeozoic stratigraphy similar to that seen in much of Gondwana, including a Lower Carboniferous hiatus, Upper Carboniferous to Lower Permian glaciogenic diamictites with Gondwanan fauna and flora, and Middle–Upper Permian platform carbonates (Ueno et al., 2010). The Inthanon Zone, originally proposed by Barr and Macdonald (1991), is characterized by Palaeo-Tethyan oceanic rocks, pre-Devonian basement rocks, and Late Triassic and Early Jurassic granitoids, often deformed into gneiss. The Palaeo-Tethyan rocks consist of pelagic Carboniferous–Permian carbonate rocks (the Doi Chiang Dao Limestone) associated with basaltic rocks (the basalts and carbonates have been interpreted as forming on seamounts) and Middle Devonian–Middle Triassic radiolarian chert (Ueno, 1999; Ueno and Hisada, 2001; Ueno et al., 2010). The pre-Devonian basement rocks consist of metamorphic rocks (Dunning et al., 1996), Cambrian sandstone, and Ordovician limestone, corresponding to component rocks of the Sibumasu Terrane. The Cambrian sandstone and Ordovician limestone indicate that sediments of the Sibumasu Terrane are imbricated with Palaeo-Tethyan rocks within the Inthanon Terrane. The Sukhothai Terrane, which largely corresponds to the Sukhothai Zone of Barr and Macdonald (1991) and the Sukhothai Fold-Thrust Belt of Bunopas (1982), is dominated by deformed Palaeozoic to Mesozoic sedimentary rocks, volcanic rocks, and Early-to-Late Permian granitoids. The Sukhothai Terrane has been interpreted to represent a volcanic arc developed along the margin of the Indochina Terrane, related to subduction of the Palaeo-Tethys (Metcalfe, 2005; 2006; Sone and Metcalfe, 2008). The Indochina Terrane has remained within the palaeo-equatorial region since its probable Early to Mid-Palaeozoic breakaway from Gondwana. In eastern Thailand, Upper Palaeozoic shallow-marine carbonate rocks, are widely distributed along the margin of the Indochina Terrane. The Nan Suture Zone, besides being considered the closure of the back-arc basin dividing the Sukhothai and the Indochina terranes, hosts the majority of the Permian clastic sedimentary rocks in Thailand, which within the KKFTB are part of the Saraburi Group (Hinthong et al., 1985; Ueno, 1999; Ueno and Hisada, 2001; Ueno and Charoentitirat, 2011).

The basic depositional setting of the Saraburi Group is interpreted as a suite of Permian rift basins on the southern margin of the Indochina Terrane controlled by extensional faults (Booth and Sattayarak, 2011; Morley et al., 2013). These basins have been viewed as simple, large basins and platforms based on outcrop data (Wielchowsky and Young, 1985), but seismic reflection data from the Khorat Plateau area suggests that the stratigraphy is more complex, with rift basins filled with clastics and mixed clastic and carbonate sediments, and small carbonate platforms developed on the intra-rift basin highs (Booth and Sattayarak, 2011). Hinthong et al. (1985) subdivided the rocks, based on stratigraphic relationships, fossils and structures, into six formations, from older to younger, as the Phu Phe, Khao Khwang, Nong Pong, Pang Asok, Khao Khad, and Sap Bon formations, covering the entire southern limit of the Phetchabun–Saraburi trend (Figure 2a, b).

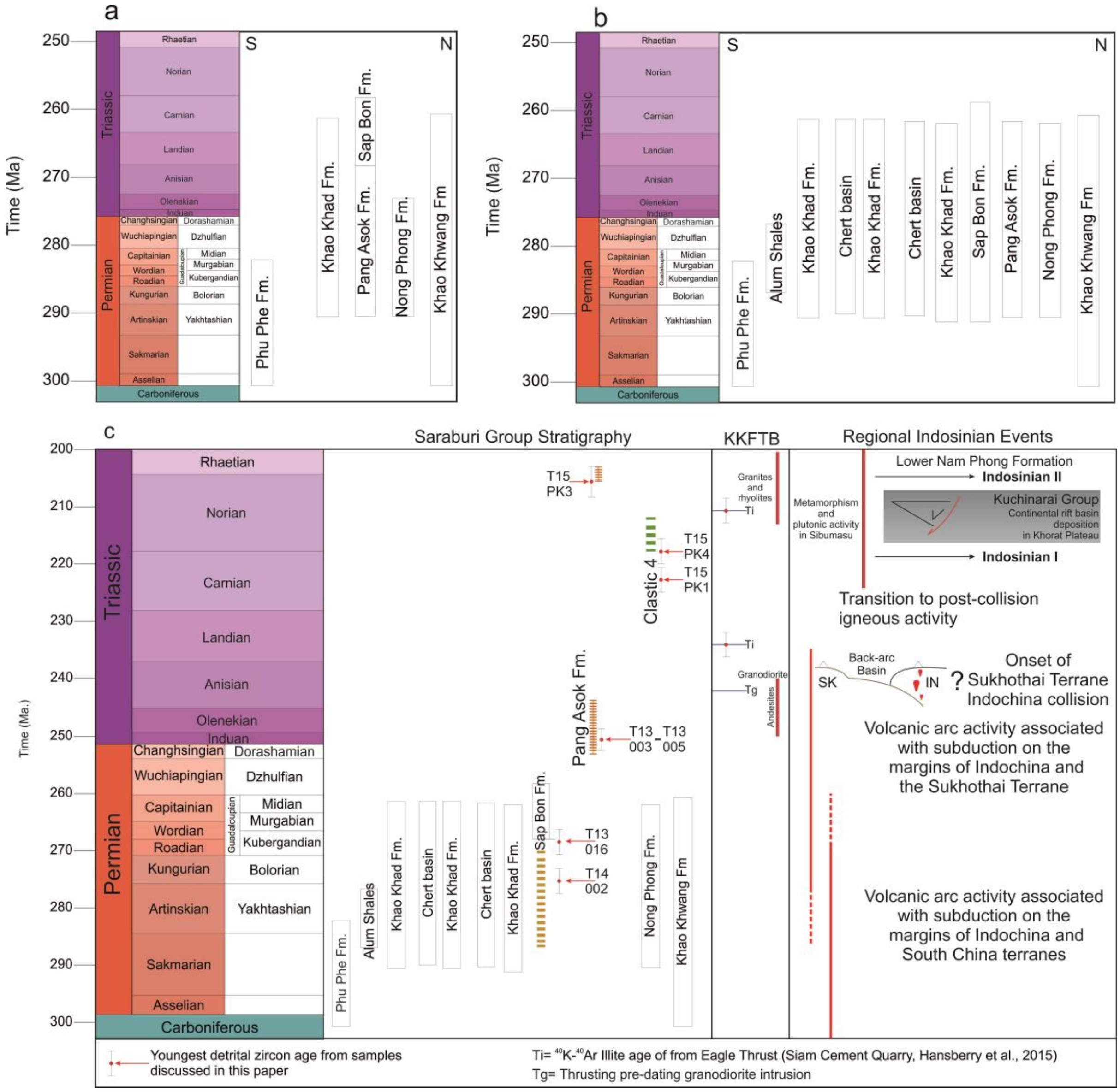

Figure 2. History of the Saraburi Group stratigraphy. a) Stratigraphy based on Ueno and Charoentitrat (2011), b) Working stratigraphic model based on fieldwork. c) Modified working stratigraphic model based on the detrital zircon data discussed in this paper.

Field mapping (Figure 3) shows that the carbonate platforms pass laterally into the mixed clastic and carbonate basinal areas, but also in places the platforms overthrust the basinal sequences, and in other places the basinal sequences overthrust the platforms (Morley et al., 2013, Warren et al., 2014; Arboit et al., 2014). Permian fusulinid-rich carbonates were also re-deposited as debris flow deposits within the deep-water basins. These relationships indicate that the basinal areas and carbonates are of approximately the same age, and were stacked up by thrusting. The stratigraphic relationships are clearly more complex than is shown in the published stratigraphy (Figure 2a, b), but determining the nature of those relationships has been problematic due to issues with

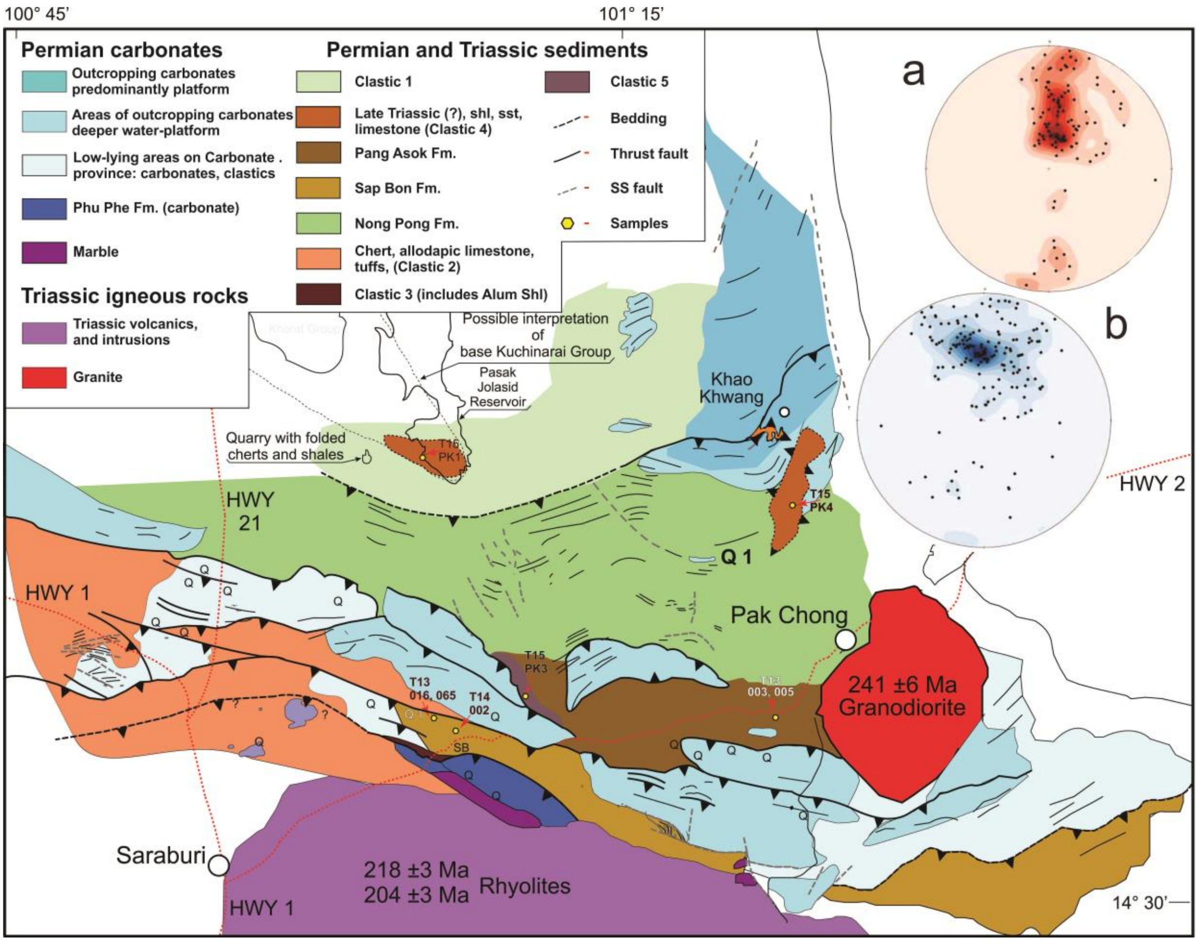

Figure 3. Geological map of the Khao Khwang Fold and Thrust Belt. It has been modified from Warren et al., (2014) to show possible interpretations of the stratigraphy as a consequence of this study. (a) Stereonet of poles to bedding for the region, (b) Stereonet of poles to main thrusts along Highway 21.

dating the clastic sequences. There are two distinct kinds of basinal sequence, one is dominated by chert, with allodapic limestone, tuff levels and, as described above, it is clearly contemporaneous with the Permian carbonate platforms. The other mixed sequences in the area comprise shale, sandstone, and in places carbonate rocks and chert and are not well dated (the Pang Asok, Sap Bon, and Nong Pong formations). The sandstone in these sequences was sampled for the provenance analysis described here.

3. Methodology

3.1. U-Pb laser-ablation inductively coupled plasma mass spectrometry (LA-ICPMS)

Zircons grains were separated from six-kg rock samples using standard separation techniques, such as specific-gravity liquid (ρ≥3.2) and a Frantz magnetic separator. Hand-picked zircons were then mounted on 2.5 cm-diameter circular epoxy mounts and then polished to expose a section at their inner core. Prior to their analysis the grains were imaged using a Gatan cathodoluminescence analyser attached to a Phillips XL20 scanning electron microscope. Zircon U-Pb isotope analysis was performed using LA-ICP-MS at The University of Adelaide following the method of Payne et al. (2010). Zircons were ablated with a New-Wave Research UP-213 laser using a spot-size of 30 µm, a frequency of 5 Hz and intensity of 8-10 J/cm^2 . Isotopic data were acquired with the

Agilent 7500 series Inductively Coupled Plasma Mass Spectrometer on eight masses: ^{206}Pb/^{238}U; ^{207}Pb/^{235}U; ^{207}Pb/^{206}Pb; ^{208}Pb/^{232}U. Mass discrimination of the mass spectrometer and elemental fractionation during laser ablation were corrected by calibration against the GEMOC GJ-1 zircon with thermal ion mass spectrometry (TIMS) normalising ages of ^{207}Pb/^{206}Pb = 607.7 ± 4.3 Ma, ^{206}Pb/^{238}U = 600.7 ± 1.1 Ma and ^{207}Pb/^{235}U = 602.0 ± 1.0 Ma (Jackson et al. 2004). The Plešovice zircon internal standard (ID TIMS ^{206}Pb/^{238}U age = 337.13 ± 0.37 Ma, Sláma et al., 2008), was used to assess accuracy before and during the analysis of the unknowns. Over the course of the laser session, a total of 110 Plešovice internal standards analyses were carried out, and gave a weighted average ^{207}Pb/^{206}Pb = 338 ± 18 Ma (MSWD = 0.93), and a weighted average ^{206}Pb/^{238}U age = 338 ± 2.7 Ma (MSWD = 0.95). Data were collected, corrected and filtered in the GLITTER version 3.0 (Van Achterbergh et al., 2001) software package. Concordia diagrams and weighted averages were calculated using ISOPLOT 4.11 for Excel (Ludwig, 2009), while probability density and kernel distributions were created using DensityPlotter 2.4 (Vermeesch, 2012).

3.2. Lu/Hf isotopes by laser ablation multicollector inductively coupled plasma mass spectrometry (LA-MC-ICPMS)

Lu and Hf isotopic ratios were determined for many of the dated zircon grains using the laser-ablation multicollector (MC)-ICP-MS technique at the Waite (CSIRO) Campus, South Australia. The laser-ablation system and procedure for Hf analysis were carried out only on grains with U-Pb LA-ICP-MS analysis greater than 90% concordance. Zircons were ablated within the same CL zone as the U-Pb data were collected, with a New Wave UP-193 Excimer laser (103 nm) using a spot size of 50 µm, a frequency of 5 Hz, a 4 ns pulse length and an intensity of 8-10 J/cm^2. Zircons were ablated in a helium atmosphere, which was then mixed with argon upstream of the ablation cell. The attached Thermo-Scientific Neptune Multi-Collector ICP-MS measured ^{171}Yb, ^{173}Yb, ^{175}Lu, ^{176}Hf, ^{177}Hf, ^{178}Hf, ^{179}Hf and ^{180}Hf on Faraday detectors with 1011 Ω amplifiers. A 0.232 s integration time was used with a total analysis time of 1-3 minutes. Hf mass bias was corrected using an exponential fractionation law with a stable ^{179}Hf/^{177}Hf ratio of 0.7325. Yb and Lu isobaric interference on ^{176}Hf were corrected by using the methods of Woodhead et al. (2004). ^{176}Yb interference on ^{176}Hf was corrected for direct measurements of the Yb fractionation using measured ^{171}Yb/^{173}Yb with the Yb isotopic value of Segal et al. (2003). The applicability of these values were verified by analysing JMC 475 Hf solution doped with varying levels of Yb with interferences up to ^{176}Yb/^{177}Hf = 0.5. Lu isobaric interference on ^{176}Hf was corrected using a ^{176}Lu/^{177}Lu ratio of 0.02655 (Veevort et al., 2004) assuming the same mass bias behaviour of Yb (Payne et al., 2010). Zircon standards (Mudtank/ Plešovice) were routinely analysed during the analytical session of the unknowns, in order to monitor the accuracy, stability and repeatability of the instruments throughout the session. To calculate model ages (t_{DM}) based on a depleted-mantle source, we have adopted a model with ^{176}Hf/^{177}Hf= 0.282785 ± 11 and ^{176}Lu/^{177}Hf= 0.0336 ± 1; this produces a present-day value of ^{176}Hf/^{177}Hf (0.283251). The measured ^{176}Lu/^{177}Hf of the zircon are used to calculate the “t_{DM}” ages. These can only give a minimum age for the source material of the magma from which the zircon crystallised. Therefore, we have also calculated, for each zircon, a “crustal” model age (t_{DM}^{C} in Supplementary Data 2), which assumes that its parental magma was produced from an average continental crust that was derived from a depleted mantle. For the calculation of εHf values, we have adopted the chondritic values of Bouvier et al. (2008).

3.3. Multi-dimensional scaling test (MDS) for comparison of the detrital ages

All the samples have been compared with compatible published databases (Carter and Bristow, 2003; Li et al., 2012; Hara et al., 2013; Burrett et al., 2014) of detrital zircons from different terranes surrounding the KKFTB from all over SE Asia, using the Multidimensional Scaling (MDS) test (Vermeesch, 2013). Only compatible samples of Permian-Triassic age measured with the same, or similar, techniques (e.g. SHRIMP, LA-ICP-MS) have been chosen, in order to reduce analytical uncertainties. The MDS is based on the Kolmogorov-Smirnov (KS) test, which calculates the maximum probability dissimilarity between two or more cumulative distribution functions (Barbeau et al., 2009; Vermeesch, 2013). Often detrital zircon analyses are represented by age spectra of hundreds of zircons, and when numerous samples are plotted together, the level of information to process can become unwieldy. One of the main advantages of the MDS tool is to provide an objective and straightforward representation of the degree of dissimilarities between samples. This comparison is assessed on a qualitative basis by plotting together their respective age spectra. The MDS maps group samples with similar age distributions, and scatter samples with different ages based on the matrix of KS dissimilarities, while solid and dotted lines are just a useful graphical representation to highlight the least dissimilar and second least dissimilar samples (Vermeesch, 2013). The KS statistic can be considered less sensitive at the extreme ends of the distributions (Sircombe and Hazelton, 2004), and it can be biased by near-unimodal distributions. However, Vermeesch (2013) argued that it is more reliable in distinguishing provenance similarities than other dissimilarity statistics. Lower KS values suggest relatively low distribution dissimilarities and may be used as support for common source regions. This statistical technique provides quantitive support for visual curve matching. But, we caution using the technique in isolation as the MDS technique is relative to the distributions being compared; i.e. one pair of distributions will always have the lowest dissimilarity. Also, the technique weights the gaps in the data as significantly as the peaks. This would be fine if the process of sedimentation and of sample collection, preparation and analysis were random (Vermeesch 2013). We suggest that truly random data are intrinsically unobtainable, meaning that the MDA technique, and other similar techniques, be used only in combination with visual analysis and as a broad comparison tool. In this study, we have combined data collected from the KKFTB to samples from other studies (Carter and Bristow, 2003; Li et al., 2012; Hara et al., 2013; Burrett et al., 2014). In order to limit bias only data with similar maximum depositional ages (Permian-Triassic), and that are not likely to be from terrane boundaries, have been chosen from each specific database.

4. Analytical geochronological and isotopic analyses

4.1. U-Pb analyses

Samples used in this study were collected throughout the KKFTB. Eight hundred and thirty seven U-Pb zircon ages were analysed from six samples collected in the arenaceous formations of the Saraburi Group (Table 1; Supplementary data – Appendix B). The results of the U-Pb dating in this study are shown on concordia diagrams (Figure 4) and relative age probability spectra (Figure 5), U-Pb and Hf data are summarised in the supplementary data that accompanies this paper. The analytical errors are presented at the 2σ level and only data within 10% of concordance were plotted on the density plots. Data quality is generally good, with a few grains displaying evidence of Pb loss. Zircons are generally small (< 80-100 μm) reflecting the fine-grained nature of the clastic formations in the Saraburi Group. Grains are predominantly translucent and colourless, but have a wide range of morphologies.

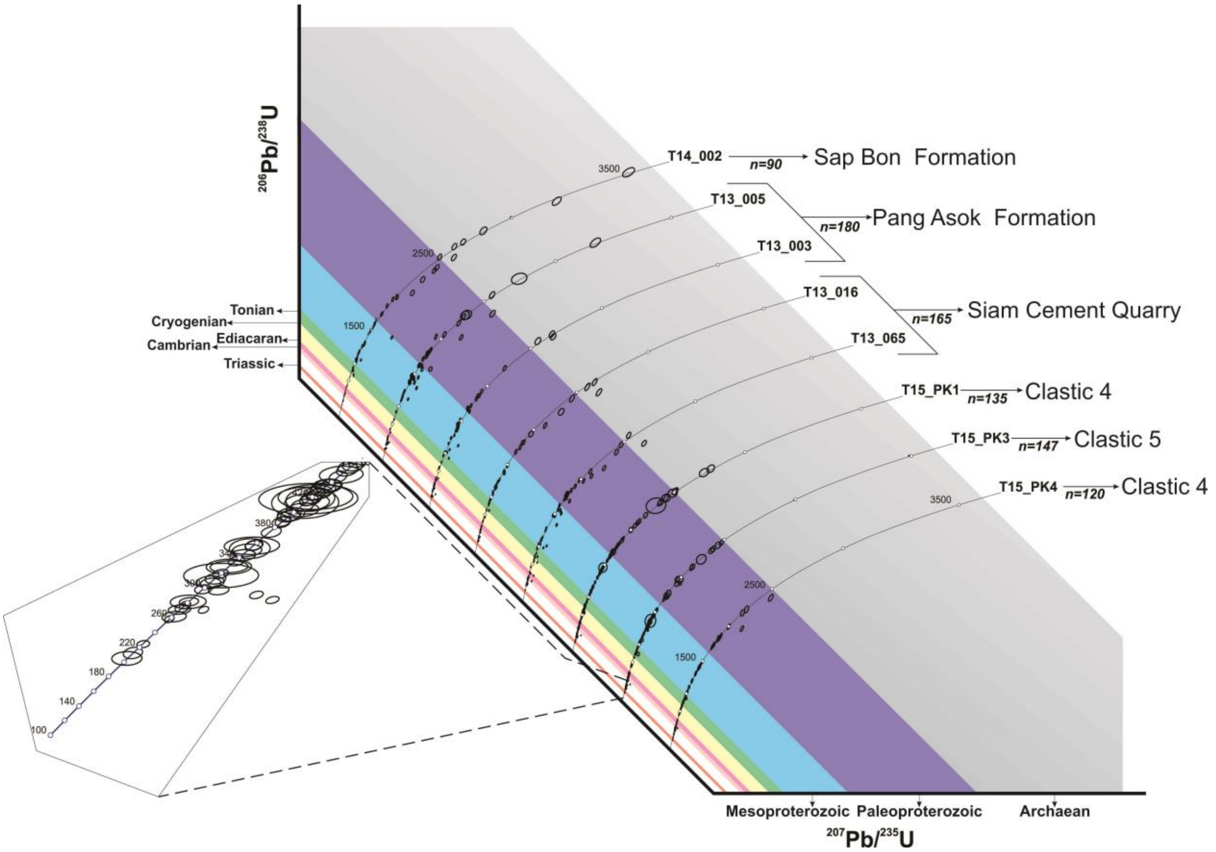

Figure 4. U-Pb concordia diagram of ages (in Ma) obtained from zircon grains in each sample by U/Pb detrital zircon laser-ablation–inductively coupled plasma–mass spectrometry (LA-ICP-MS). Inset showing MDA with 2σ error of sample T15_PK3 from 100 to 450 Ma.

4.1.1. Southern part of the Khao Khwang Fold-Thrust Belt

One hundred and eighty zircon grains were analysed for U-Pb from two samples (T13_003, T13_005) taken from the sandstones that are interbedded with slates of the Pang Asok Formation. One hundred and twenty of these grains yielded results that were within 10% of concordance (Table 1 and Figure 4) with a $^{207}Pb/^{206}Pb$ age maxima at ca. 3211 Ma, while the youngest $^{206}Pb/^{238}U$ ages retrieved from T13_003 and T13_005 are 251 ± 3 Ma and 262 ± 4, respectively (Table 1). These represent the maximum depositional ages of these samples. Age distribution maxima from those two samples are ca. 250, 450, 750, 1200, 1425 and 1725 Ma.

The fine sandstone/siltstone-dominated Sap Bon Formation is thrust over the carbonate Khao Khad Formation in the south of the KKFTB, but elsewhere is overlain by the same Khao Khad Formation (Thambunya et al., 2007; Warren et al., 2014). It is characterised by interbedded sandstone and shale, with a sharp increase of carbonate beds occurring towards the north, where it laterally grades up into the Khao Khad Formation. Ninety zircons from the sample collected in the Sap Bon Formation (T14_002), define distinctive concordant age groups (Figure 5), with broad populations between 2480 and 2830 Ma, 1580 and 1380 Ma, 1270 and 1080 Ma, 980 and 910 Ma, 630 and 430 Ma, and 380 and 270 Ma. The oldest near concordant $^{207}Pb/^{206}Pb$ age was 3508 ± 19 Ma, whereas the youngest ≤ 10% discordant analysis yielded a $^{206}Pb/^{238}U$ age of 275 ± 4 Ma (Table 1), which is interpreted as the maximum depositional age for this sample.

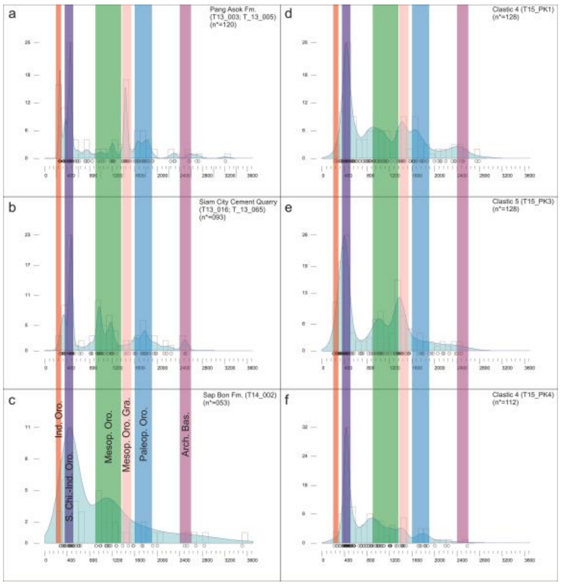

Figure 5. Kernel density estimation (KDE) plots of detrital zircon ages from each clastic unit. Light-cyan shading represents detrital grains between 90% and 110% concordant. Open circles below the KDE represent single analyses. Ind. Oro.: Indosinian Orogeny; S. Chi.-Ind. Oro.: S China – Indochina Orogeny; Mesop. Oro.: Mesoproterozoic Orogens; Mesop. Oro. Gra.: Mesoproterozoic Orogens Granites; Palep. Oro.: Paleoproterozoic Orogens; Arch. Bas.: Archean Basement.

Recent papers on the Saraburi Province (Hansberry et al., 2014, 2015) have described an upper-level detachment zone within the KKFTB. This is well exposed in the Siam City Cement Quarry, where the northernmost of two large, northward-verging thrusts that crop out in the quarry forms a thrust contact between a sandy silty unit (possibly the Sap Bon Formation, Hansberry et al., 2014) and the carbonate Khao Khad Formation. Two samples were collected within this deformed shale-sandstone clastic unit (T13_016, T13_065). Sample T13_016 from the basal (southern) and less deformed part of the section, while T13_065 from the uppermost (northern) part of the section, close to the north-verging shale detachment. Zircon grains in the samples from this clastic unit are mostly stubby with few elongate grains. Zircon size varied considerably, with an average length of ca. 50 µm. Forty-six of the 90 analysed grains from sample T13_016 yielded ≤ 10% discordant data, whereas 49 of the 75 analysed grains from sample T13_065 were ≤ 10% discordant (Table 1). As a result of this similar discordance (T13_016-65%, T13_065-51%) both samples are plotted together (Figure 5). The oldest analysis in this combined dataset yielded a $^{207}Pb/^{206}Pb$ age of 2522 ± 20 Ma (T13_065) and the youngest $^{206}Pb/^{238}U$ age (taken to be the maximum depositional age) was 268 ± 4 Ma (T13_016).

4.1.2. Northern part of the Khao Khwang Fold-Thrust Belt

Generally little information is available on the sandstone in the central and northern section of the KKFTB. The paucity of the sandstone exposure has limited work in this key area directly to the foreland of the highly deformed zone of the KKFTB. Sample T15_PK1 was collected close to the Pasak Jolasid Dam and was exposed during excavation to create the foundations of the dam. This is the northernmost exposure of the mapped Nong Pong Formation. The age of the Nong Pong Formation is uncertain, but is usually assigned to the Permian. One-hundred and thirty-five zircons were selected for U-Pb analysis, and of these 128 grains yielded age data ≤ 10% discordant (Figure 3). The $^{207}Pb/^{206}Pb$ ages of these data date back to 2790± 30 Ma, with the youngest $^{206}Pb/^{238}U$ age of 224 ± 4 Ma interpreted as indicating a Triassic maximum depositional age. The most prominent age peak is at ca. 430 Ma with a distinct secondary peak at ca. 1400 Ma and two less prominent peaks at ca. 900 and ca. 1650 Ma.

Sample T15_PK3 was collected close to the town of Muak Lek (Figure 3). A ca. 500 m long olistolith of Middle Permian Khao Khad Formation fossiliferous limestone occurs in the quarry from where this sample was taken. This is slumped into deeper water clastic sedimentary rocks that are considered to be part of the Pang Asok, or Nong Pong formations. One-hundred and forty-seven analyses were carried out, with 136 zircons yielding data within 10% of concordance. The oldest $^{207}Pb/^{206}Pb$ age is 2478 ± 21 Ma and the youngest $^{206}Pb/^{238}U$ age is 205 ± 6 Ma, again implying a Triassic maximum depositional age. The $^{206}Pb/^{238}U$ ages of these zircons range nearly continuously between ca. 205 and ca. 565 Ma with a few ages around ca. 700 and ca. 900 Ma. For the older zircons, Most of the $^{207}Pb/^{206}Pb$ ages range from 1000 to 1550 Ma with a few dates extending to around 2450 Ma. A distinct peak occurs at ca. 1400 Ma (Figure 5).

Sample T15_PK4 is a sample of sandstone from the Nong Pong Formation. The deep-water siliciclastic deposits of the Nong Pong Formation probably correlate with the Nam Duk Formation, found further north in the Khorat Plateau, forming a N-S oriented depositional basin (Ueno and Charoentitirat, 2011). Sandstones are rare in the Nong Pong Formation. Sample T15_PK4 has evident sole-marks at its base, and is interpreted as a turbidite. In one small excavated pit (14°53’17.17” N, 101° 22’ 21.17” E), north of the sample location, Khao Khwang Formation carbonates are thrust over Nong Pong Formation shale. One hundred and twenty grains were analysed for U/Pb, 112 of which yielded age data ≤ 10% discordant (Figure 3). The oldest $^{207}Pb/^{206}Pb$ age obtained is 2578 ± 21 Ma, while the youngest $^{206}Pb/^{238}U$ age is 217 ± 4 Ma, which is interpreted as the maximum depositional age of this sample. The most prominent peak in the age profile occurs at ~430 Ma with a second major peak at ~900 Ma; while older age, less prominent, peaks occur at ~1220 Ma and ~1450 Ma.

4.2. Hf isotope analyses

The results are listed in Supplementary Table 2. The data show that the $^{176}Lu/^{177}Hf$ ratios are less than 0.002 (only 4.4% of the data have higher values), indicating the absence of any major enrichment of radiogenic Hf after the formation of the zircons. Thus, the initial $^{176}Hf/^{177}Hf$ ratios can be used as a robust reference to evaluate the source characteristics of these zircons (Wu et al., 2007). A total of 271 zircon grains were analysed, and the results show εHf (t) values in the range of −31.34 to +35.31 and Hf crustal model ages in the range of 0.63 Ga to 3.98 Ga.

4.2.1. *Southern part of the Khao Khwang Fold-Thrust Belt*

One hundred and ten <10% concordant zircons were analysed for in situ Lu–Hf isotopic composition (Figure 6a), and the results show $(^{176}Hf/^{177}Hf)_i$ (initial ratio) values ranging from 0.28053826 to 0.282853625 (Supplementary Table 2) and a large range in εHf (t) values varying from −29.52 to +35.31 (although all but 5 analyses yield values >-15), inferring complex sources. The Hf (t_{DM}^{C}) of zircons ranges from 0.63 Ga to 3.91 Ga (Supplementary Table 2).

The eight youngest Permian zircons (ca. 299-252 Ma) are dominated by negative εHf (t) values (−12.15 to +0.20) with ($^{176}Hf/^{177}Hf$) ranging from 0.282278213 to 0.282622441 and Hf crustal model ages from 1.26 to 2.03

Ga, implying a magma source that involved components of Mesoproterozoic or older crust.

The highest number of concordant zircons recovered within the southern portion of the KKFTB range in age from ca. 500-400 Ma, many of these analyses yield positive εHf (Figure 6A) and a lower (^{176}Hf/^{177}Hf) average value (0.282586, which is similar to the value for depleted mantle at that time), and yield crustal model ages (t_{DM}^{C}) ranging from 0.57 to 1.97 Ga, implying that significant mantle-derived melt was involved in the parental magma from which these zircons grew. Zircons that yielded ages between ca. 850 Ma and 600 Ma have noticeably evolved εHf(t) values, indicating a lack of juvenile magmatism in the source region at this time. Zircons that crystallised between ca. 2200 and 850 Ma contrast with the younger Neoproterozoic grains in that their εHf(t) values include significantly positive values (<+12), in addition to the more evolved values, although no values go lower than -12; again, in contrast to the succeeding later Neoproterozoic zircons. In fact, 2050-1800 Ma (Orosirian) zircons appear to mark a change in the nature of the source-region magmatism from pre-existing εHf(t) values close to zero, to a much wider range in values, especially towards values close to those of the contemporary depleted mantle (Figure 6a). Small exceptions to this are the two analyses of ~2500 Ma zircons with highly juvenile values.

4.2.2. Northern part of the Khao Khwang Fold-Thrust Belt

One hundred and sixty-one <10% concordant zircons were analysed for in-situ Lu–Hf isotopic composition (Figure 6a), and the results show ^{176}Hf/^{177}Hf values ranging from 0.280644017 to 0.282842605 (Supplementary Table 2) and a large range in εHf (t) values varying from −31.34 to +23.07, suggesting complex sources. The Hf (t_{DM}^{C}) of zircons ranges from 0.68 Ga to 3.98 Ga (Supplementary Table 2).

The majority of the youngest Triassic zircons are too small for Hf-isotope analysis; only six Triassic zircons could be analysed. These analysed zircons show similar ^{176}Hf/^{177}Hf values (0.28241456 to 0.28273563) (Supplementary Table 2), largely negative εHf (t) values (-8.59 to +2.67, average -2.53), and with Hf (t_{DM}^{C}) ranging from 1.05 Ga to 1.76 Ga, indicating that the parent magmas for these young grains contained Mesoproterozoic or older crustal material.

The Palaeozoic zircons show a similar range of εHf(t) values to those from the southern KKFTB, with values stretching up toward the contemporaneous depleted mantle (and close to those for the contemporaneous ‘new crust’ curve of Dhuime et al., 2012), to values <-14 (Figure 6a). The data spread implies that two populations may be present, one with εHf(t) values of -8 to -14, and a second, larger population, with εHf(t) values between +12 and -5. Data collected from the south KKFTB do not show this bimodal distribution, εHf(t) values also range to considerably more evolved values.

Neoproterozoic zircons do not record the distinct dearth of juvenile εHf(t) values seen in the southern KKFTB, but rather appear to have similar values (approximately between -18 to +13) to those seen in ca. 2200-850 Ma zircons in both the north and south KKFTB (Figures 6a, b). A notable feature of the northern KKFTB detritus, is that between ca. 1500 and 550 Ma there are a number of highly negative εHf(t) zircons (values between -24 to -32) that indicate the presence of Palaeoarchaean, Eoarchaean, or even Hadaean crust in the source magmas. Only one zircon from the southern KKFTB yielded εHf(t) such extreme negative values.

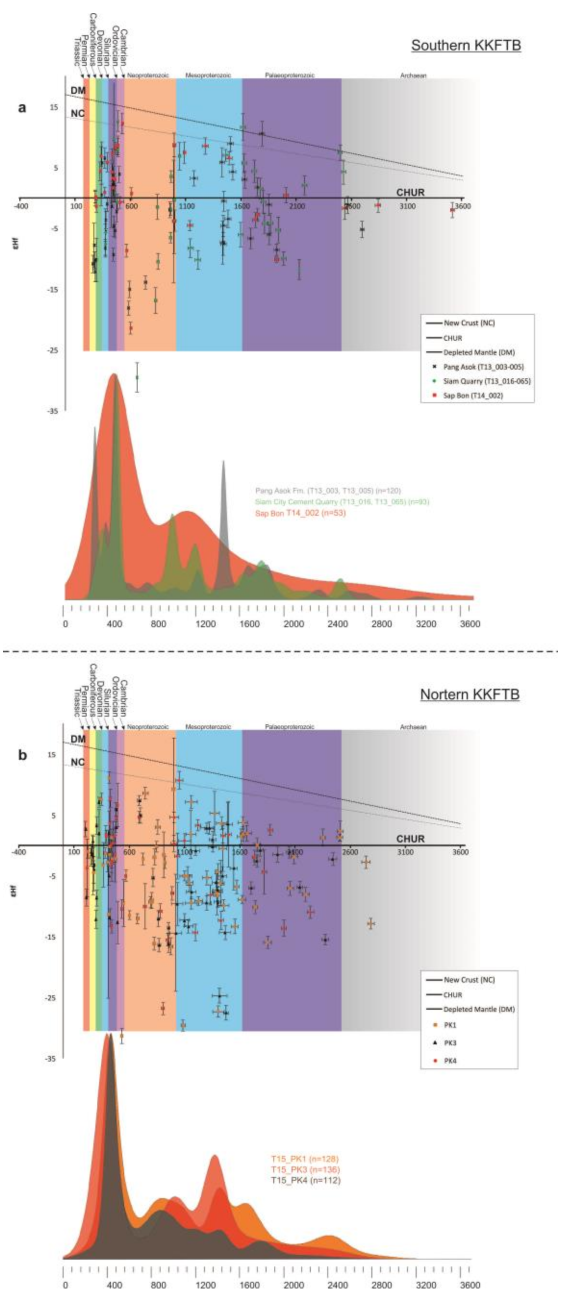

Figure 6. U/Pb age versus εHf(t) plots of detrital zircon data from 8 samples throughout the KKFTB stratigraphy. a) southern portion of the KKFTB, b) northern portion of the KKFTB. The kernel density estimate distribution for the samples are plotted below the U/Pb age versus epsilon Hf plots to provide a measure of the importance of each clastic unit.

Zircons that crystallised between ca. 2700 and 1600 have distinctly evolved εHf(t) values varying from -16 to +3 (Figure 6b), indicating a lack of juvenile magmatism in contrast to 1800-1600 Ma (Statherian) zircons from the southern portion of the KKFTB that show a much wider range in values (+2 to +14) especially close to the earliest Neoproterozoic.

5. Discussion

5.1. Saraburi Group Stratigraphy

The present knowledge of the Saraburi Group stratigraphy was recently reviewed and summarised by Ueno and Charoentitirat (2011). In their stratigraphic scheme the Khao Khwang, Phu Phe, Khao Khad, and Tak Fa formations are all part of one carbonate platform; the Pang Asok and Nong Pong formations are clastic-dominated lateral equivalents of the platform of Lower to Middle Permian age, whereas the Sap Bon Formation is Midian to Dzhulfian (Mid-Capitainian to Wuchiapingian in the International Commission of Stratigraphy chronology; Cohen et al., 2015) in age (Figure 2c), and was thought laterally equivalent to, and younger than, the youngest part of the Khao Khwang Formation. Figures 2a and 2b are simplified versions of the stratigraphic scheme in Ueno and Charoentitirat (2011). While dating of the Permian carbonate platforms in the Saraburi Group has been well established in the last decade using the abundant fusulinid foraminifera, the clastic sediments of the Pang Asok, Nong Pong, and the Sap Bon formations are poor in fossils and correspondingly poorly dated (e.g. Dawson, 1993; Dawson and Racey, 1993; Charoentitirat, 2002; and Udchachon et al., 2014). The problem with this stratigraphic scheme is that the area of exposure of the Saraburi Group is strongly deformed by folding and thrusting, making it difficult to identify coherent stratigraphic packages (e.g. Morley et al., 2013, Hansberry et al., 2014, Arboit et al., 2014; 2015). Morley et al. (2014), and Arboit et al. (2014) constructed structural sections through the Khao Khwang Fold and Thrust Belt and used these to recognise that the Saraburi Group represented multiple carbonate platforms separated by a series of deeper water basins (Warren et al., 2014). These deeper water basins (perhaps reflecting differences in water depth of hundreds of metres), contain either shale and sand (Sap Bon Formation), black shale (Alum Shale), or chert, shale, sand, and allodapic limestone (Nam Phong Formation). Not all these deposits are easily linked to existing formations, and in the absence of a rigorous understanding of the stratigraphy, Morley et al. (2013) used informal nomenclature (Clastic 1, Clastic 2, Clastic 3) to indicate where revisions to the stratigraphic scheme were needed (Figure 3). Figure 7 shows a conceptual modification of the depositional system and the relative stratigraphic scheme that reflects the changing view of the Saraburi Group stratigraphy.

5.2. Impact of detrital zircon ages on interpretations of structure and stratigraphy

The analysed zircons in this study were collected from sedimentary rocks in the KKFTB, previously mapped as being of Mid-Late Permian age. The new detrital zircon data require modification of these ages as the rocks cannot be older than the youngest detrital zircon. We have used only zircons with ages within 10% of concordance to provide a maximum depositional age (MDA) for each specific formation (Table 1).

The maximum depositional ages impact the stratigraphy by shifting the age of the Saraburi Group to the latest Triassic (Figure 2c). The new MDA for the Sap Bon Formation (275 ± 4 Ma) is close to the published depositional age (Hinthong et al., 1985), suggesting erosion and deposition of newly formed source region (McGee et al., 2012); consistent with volcanic source regions such as the Loei volcanic belt and the Sukhothai volcanic arc. However, the Pang Asok Formation is traditionally placed below the Sap Bon Formation (Figure 2a), but now must be younger and, at the most, Early Triassic age (Figure 2c). This is possible as no mapped relationship between these units is known. The Pang Asok Formation is cross-cut by a small granodiorite pluton (Figure 3, Figure 7b), which has been dated at 241 ± 6 Ma (U-Pb on zircon dating by S. Meffre reported in Morley et al., 2013). This leaves a window between 251 ± 3 Ma and ca. 240 Ma during which time the Pang Asok Formation was deposited, and deformed by folding and thrusting (Figure 7c). Sample T15_PK3 is from an area thought to be in continuity with the Pang Asok Formation, and was assumed to be from the Pang Asok Formation prior to the detrital zircon dating. The sample came from a quarry, which lies adjacent to an area about 500 m wide, where fossiliferous shallow water Permian carbonates are present that include algal boundstones, as well as slope conglomerates and crinoidal rudstones. A contact is exposed in the quarry, where the limestone passes abruptly into folded shale that contains small limestone blocks. It is very clear from the relationships that the limestone slid, probably as a coherent rigid block, into deep water environment represented by shale and thin sandstone. Initially it was inferred that the limestone slide was contemporaneous with Permian carbonate platform development, and that the clastic deposits are Permian in age. However, the minimum zircon age from T15_PK3 of 205 ± 6 Ma implies a different scenario (Figure 2c). The implication is that late thrusting caused a lithified block of Permian carbonate to slide into, either on top of a moving single thrust sheet (piggyback basin), or a foredeep basin (Figure 7d), which

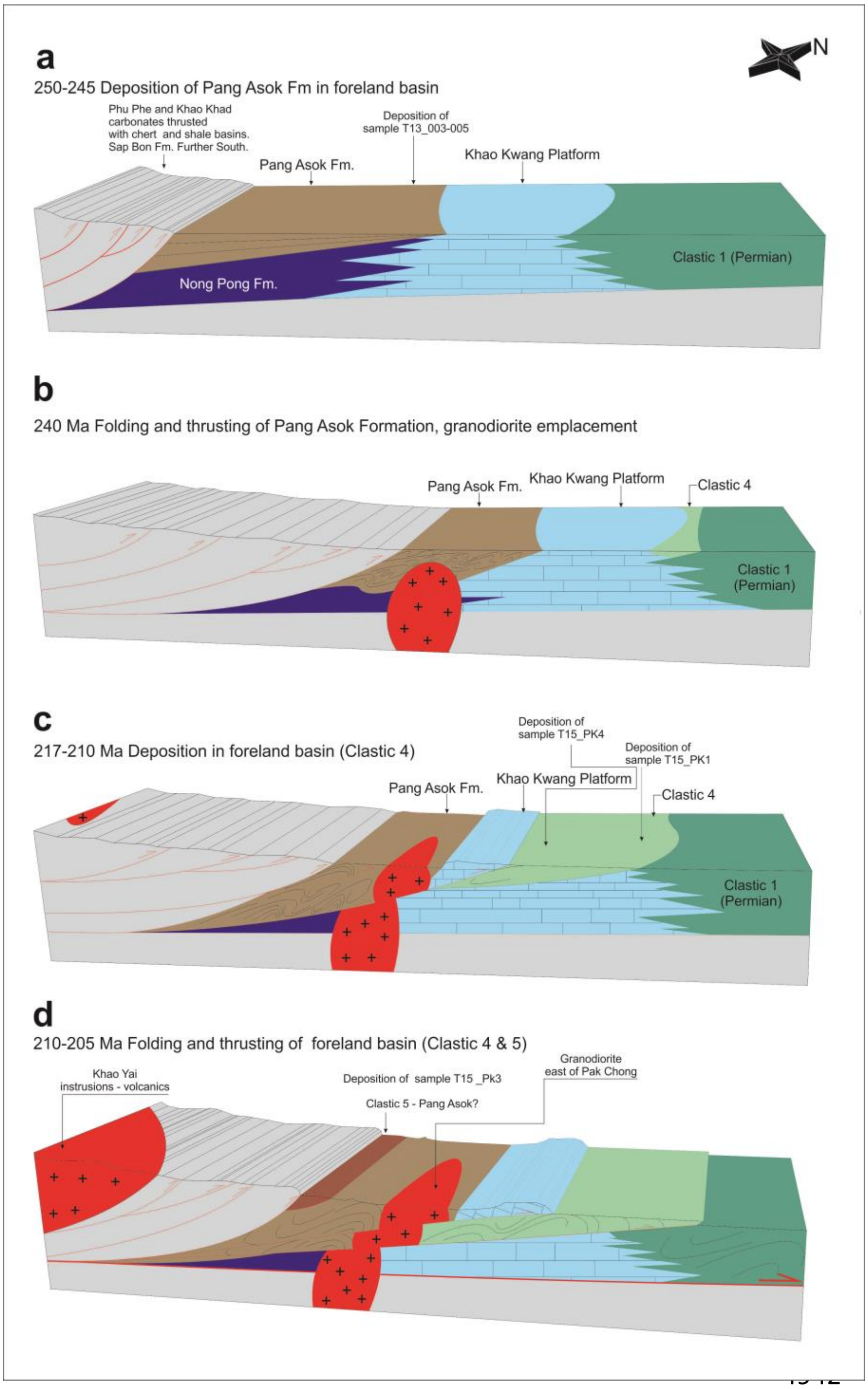

formed during a late phase of thrusting. This requires a separate basin to be developed some 35 My later than deposition of the Pang Asok Formation (referred to informally as Clastic 5). Possibly deposition was in a freshwater environment, since, at this time, regional continental rift basins have been established (Booth and Sattayarak, 2011). Some of the rift basins are inverted both during the late stage of the Indosinian deformation, and during the Paleogene (Booth and Sattayarak, 2011). Consequently despite the Late Triassic age, deformation of the basin could have occurred.

Figure 7. Schematic sequential evolution of the depositional model within the KKFTB from Early to Late Triassic, based on the modified stratigraphy shown in Figure 2c and Figure 3.

The samples from the northernmost portion of the KKFTB are represented by T15_PK1 and T15_PK4. Sample T15_PK4 was taken from an area that was mapped as Nong Pong Formation (based on the map in Ueno and Charoentitirat, 2011) (Figure 3). This sample is an extensively burrowed sandstone with flute marks, and appears to be a marine sandstone. Typically, the Nong Pong Formation comprises shale, chert and deepwater limestones. Some of the deepwater limestones are fusulinid grainstone debris flows (i.e. at location Q1, Figure 3), which demonstrates they are Permian in age, and were deposited in deeper water basins adjacent to the platforms. Sandstone is not normally present. Hence the sandstone sampled represents an unusual occurrence. The youngest age from the sample of 217 ± 4 Ma is Late Triassic indicating the formation sampled is not actually Nong Pong Formation, but a new, undescribed formation (referred to informally as Clastic 4). This raises the question of whether the Clastic 4 unit depositionally overlies the Nam Pong Formation and is preserved in a syncline, or is overthrust by the Permian sequences and exposed in a tectonic window (Figure 7c). The thrust window interpretation is preferred because to the north of the sample location is a small pit where shales that are below a sub-horizontal thrust and overlain by Khao Khwang carbonates. The minimum implied amount of overthrusting, assuming NNW thrust transport, is 9 km (Figure 3).

Sample T15_PK1 is a sandstone that does not occur in natural outcrops, but was dug from the foundations of the Pasak Jolasid Dam (Figure 3), and hence it was not possible to obtain data on the relative depositional environment. The nearest outcrops to the dam are 5 km away in an extensively quarried section that comprises mostly cherts and shales, and no sandstone. This unit was originally referred to as Clastic 1 (Morley et al., 2013). However, the minimum zircon age for the sandstone is 224 ± 4 Ma, and on both a lithology and age basis, sample T15_PK1 is now considered to represent a different unit from Clastic 1. The similar MDA of samples PK1 and PK4 opens to a possible affinity between the two clastic units where the samples were collected, and on Figure 3 they are both mapped as the same unit (Clastic 4). However, given the proximity of the Khorat Group to the Pasak Jolasid Reservoir the sandstones could also be part of the Kuchinarai Group (Figure 3, Figure 2c).

5.3. Evolution of the basin

The early stages of the Indosinian orogeny are poorly dated, and the timing of the continental collision remains uncertain. Ophiolitic sequences along the Nan Suture Zone extend back to ca. 270 Ma (Barr and Macdonald, 1987). However, the onset of collision between the Sukhothai Terrane and Indochina, which triggered N-S thrusting and folding (Arboit et al., 2014; 2015) in the KKFTB, is poorly established (Sone and Metcalfe, 2008; Booth and Sattayarak, 2011; Barber et al., 2011; Morley et al., 2013). The Permian represents pre-collision deposition on the Indochina margin that was possibly undergoing extensive rifting and post-rift subsidence (Booth and Sattayarak, 2011). The width of the basin is uncertain because of: 1) the considerable shortening exhibited within the exposed basins; 2) the unknown amount of eroded material; 3) the uncertain extent of the basins to the south, where exposures are very poor. The minimum width is in the order of 10s of kilometres, but widths in excess of 100 km are possible. The basin comprises a number of highs, on which relatively small, isolated, carbonate platforms were developed, surrounded by deeper water basins dominated by chert deposition with allodapic carbonates. Probably to the north, and possibly to the west, of the chert-dominated basin, the more shale and sandstone-dominated sequence of the Sap Bon Formation is present. South of the chert basin-Khao Khad Formation depositional area lies the region of the Phu Phe Formation, which includes a black (alum) shale clastic unit.

During the latest Permian to Early Triassic the convergence of the Sukhothai Terrane with Indochina would have led to the development of a foredeep basin on the old passive margin. Possibly, the Sap Bon Formation marks the initiation of foredeep basin deposition after ca. 268 Ma. This basin, or a succession of basins, was characterised by propagation towards the north (Morley et al., 2013; Arboit et al., 2015). The Pang Asok Formation may mark a shift in foredeep basin location in front of the thrusted Phu Phe and Khao Khad carbonate platforms and intervening basins around 250 Ma. This basin was deformed and incorporated into the fold and thrust belt by 240 Ma (Figure 7). Direct evidence of mid-Triassic deformation is also preserved in ca. 235 Ma K-Ar ages of syn-shearing illite preserved in shale detachment faults in the Siam City Cement Quarry (Hansberry et al., 2015). No record of any sedimentation after the Early Triassic has been recovered from the samples collected throughout the southern portion of the KKFTB. Further north, the advancing thrust front of the orogen is interpreted to be still active at this time. The Middle-Late Triassic foreland basin (Clastic 4, Figure 7) was feasibly tectonically segmented into satellite basins, such as piggyback or thrust top basins (Ori and Friend, 1984). Based on the new data presented here, it is possible to assume that the sedimentation in the northern portion of the basin might have lasted till the latest Triassic-Early Jurassic (after 205 ± 6 Ma). These data are consistent with Hirsch et al. (2006) who suggested a Sibumasu-East Malaysia collision at the same time, and with the hiatus associated with the Indosinian II event. This unconformity surface underlies the lowermost portion of the Rhaetian (~208-201 Ma) Nam Phong Formation further north in the subsurface of the Khorat Plateau. Having such a short lapse of time between the youngest MDA and the documented Lower Nam Phong Formation, the Late Triassic zircons must be close to the real depositional age of the sandstones in the northern portion of the KKFTB, hence, it is possible to assume that there were some significant igneous activities nearby during the latest Triassic that were not recorded by the southern part of the KKFTB, but may have come from the colliding Sukhothai Arc.

The topography during the Rhaetian is hence interpreted to be the result of the end of the Indosinian contractional event and it is well represented by the overlying Nam Phong Formation, which represents depositional environments, such as fluvial channels (braided and meandering) interbedded with lacustrine or floodplain sequences (Racey and Goodall, 2009).

5.4. Regional correlations and possible tectonic implications

All the samples looked at in this study have appreciable numbers of detrital zircons that yield late Triassic to Palaeoarchean ages (Figure 4, Figure 5). When combined, the data set includes 642 ≤ 10% discordant zircons, with ages that range between ca. 201 Ma and 3508 Ma. U-Pb data presented here reveal two distinct episodes of magmatism at ca. 250-200 Ma and ca. 450 Ma. Palaeozoic magmatism that may be the origin of the ca. 450 Ma zircons, is found in the Kon-tum Massif of central Vietnam, coeval Late Ordovician-Silurian metamorphic activity also occurs along the Phuoc Son-Tam Ky Suture Zone of northern Vietnam (Tran et al., 2014). Late Carboniferous to Permian detrital zircons found in the modern Mekong River and Red River (Bodet and Shärer, 2000) (Figure 8) that drain Indochina and the margin of South China (Figure 10) preserve similar U-Pb and Hf isotopic ratios to those from the KKFTB, with εHf(t) values close to the CHUR. Similar εHf(t) values are also found in coeval detrital zircons preserved in Permian sedimentary rocks in South China (Li et al., 2011; Figure 8). We suggest that these may be all sourced from granites and granodiorites emplaced across Myanmar and NE Vietnam in a syn- to post-collisional setting during the latest stages of the Indochina-South China collision (Gardiner et al., 2015; Halpin et al., 2015). Zircons that date from the 200-250 Ma magmatic phase also show similar εHf(t) values to modern river systems and South China (Figure 8).

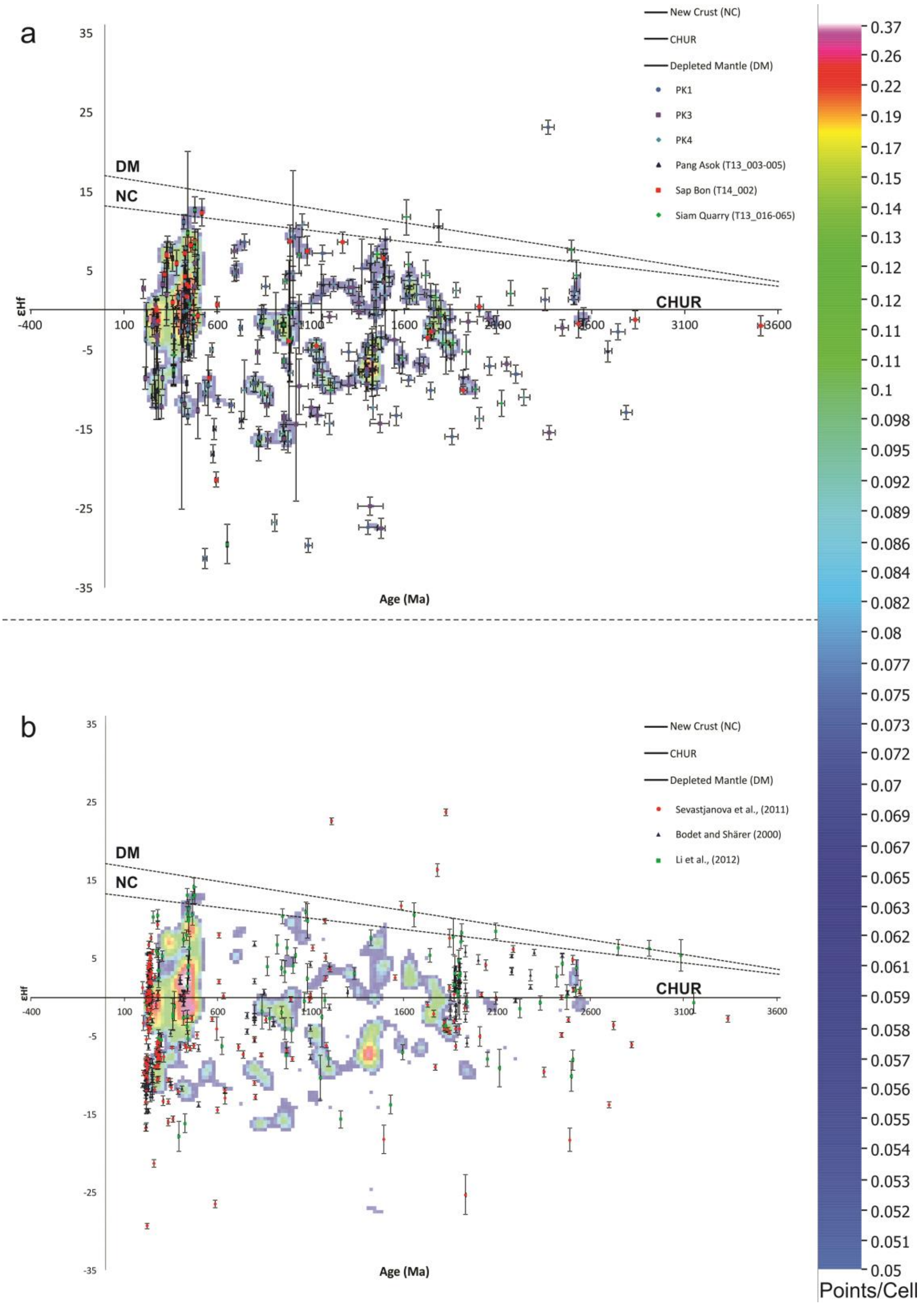

Figure 8. a) U/Pb age versus epsilon Hf plot of all the data from the KKFTB and relative density contour. b) U/Pb age versus epsilon Hf plot of published hafnium isotopic data from zircons from the Mekong River and Red River (replotted from Bodet and Shärer, 2000), from Permian sediments in southeast China (replotted from Li et al., 2012), and the Malaya Peninsula river systems (replotted from Sevastjanova et al., 2011); compared with density contour of all the Hf isotopic data collected within the KKFTB.

Pre-Carboniferous detritus of these river systems, from the Permian of South China (Li et al. 2012) and from the Indochina part of the Malay Peninsula (Sevastjanova et al., 2011) share several similarities with zircons from the KKFTB (Figure 8). In particular, the wide range of εHf(t) values of the latest Mesoproterozoic-Neoproterozoic zircon, and the Neoarchaean juvenile values (Figure 8). This not only implies that pre-Carboniferous rocks occur in the sources to the sedimentary rocks of the KKFTB, S China and Malay Peninsula, but that at least by the Permian, regions as far-flung as South China, central Thailand and Malaya shared similar sedimentary sources. Significant differences do occur, particularly at ca. 1.8-1.9 Ga in South China (Li et al., 2011) and in the dearth of early Mesoproterozoic zircons from the modern rivers and the Permian of South China (Bodet and Shärer, 2000; Sevastjanova et al., 2011). In the latter case, this difference may be attributed to KKFTB Triassic rocks being, at least partially, sourced from the western Sibumasu Terrane, which preserves distinct populations of ca. 1.3-1.4 Ga detrital zircons with negative εHf(t) values (average -6.83) (Figure 8, Supplementary Table 2) (Burrett et al., 2014). This would support a Middle-Late Triassic age for the collision (Booth and Sattayarak, 2011).

5.4.1. Multidimensional scaling analysis

After MDS statistic calculations performed in MATLAB, all the databases used in this study clustered in three different groups of terranes, each cluster contains the samples with the lowest dissimilarity values (Table 2; Supplementary data – Appendix B). Figure 9 is only the visual representation of this clustering based on the values of the dissimilarity matrix. Figure 10 depicts the geographical position of each sample and relative cluster category, throughout the terrane of SE Asia. All the samples collected within the KKFTB have very low dissimilarity values with an average of 0.14416 (Table 2). Similar values occur between the KKFTB and the samples representing sedimentary rocks from the Khorat Plateau (0.2383), Truong Son (0.2233), NE Vietnam (0.1921), and partially with South China (0.3129). The quality of the numerical approximation of the MDS fit is evaluated by the stress parameter “S” that appear to be fairly good (0.1002) (Kruskal, 1964, Vermeesch, 2013). It is hence possible to assume that these values do not indicate statistically significant differences among the above terranes, and they suggest that the zircons were derived from a common underlying population.

All the zircons from western SE Asia are much less similar to those samples from the KKFTB. The significant mismatch with the terranes in the west, such as Sibumasu, Phuket, and Inthanon, is demonstrated by KS values ranging from 0.4239 to 0.4932. This shows that the detrital age spectra are distinctly different, and implies that these terranes were not sourced from similar-aged areas during the Late Palaeozoic.

The KS results for central Vietnam, Loei, Indochina (samples from Cambodia), E Malaysia, and Sukhothai, show little or no links with other data in this study, having disparity of values ranging between 1.0 and 0.5545 (Table 2). The Sukhothai, Loei, and Indochina terranes are interpreted as being separated by a back-arc basin (Sone and Metcalfe, 2008). The low KS dissimilarity (0.1974) (Table 2; Figure 9) between the Permian samples of these terranes appears to confirm the possibility that they shared sediment source regions in the latest Palaeozoic before the opening of the back-arc basin in the Early Permian. Further, the KS dissimilarity value (0.3957) highlights the mismatch within Indochina between the Khorat Plateau in the north and Cambodia in the south. It has been previously suggested by several authors that the Indochina Terrane itself may not have been one single terrane but might have had a more complicated geometry (Lepvrier et al., 2004; Morley et al., 2013). No fewer than 20 belts of mafic-ultramafic assemblages have been named "ophiolite" in the complex SE Asia region of Sundaland, but fewer than half of these can be confidently classified as “ophiolite” (Hutchison, 1975). However, a few previous authors (Fromaget, 1941; Fromaget et al., 1971; Hutchison, 1975) highlighted the presence of the Siem Reap-Stung Treng Line, which consists of gabbro, peridotite and dolerite bodies, trending roughly E-W, south of the Khorat Plateau, and occurring in a large elongate mass in Permian to Triassic sedimentary rocks. The rocks within this line shows similarities with the rocks of the coeval Uttaradit-Luang Prabang-Pak Lay Line (Fromaget, 1941; Baum et al., 1970; Hutchison, 1975) that consists of serpentinized pyroxenite, gabbro, diorite and dolerite and is associated with the suturing of the Sukhothai and Indochina terranes. Given our findings, the two terranes displaying different age spectra, and combining those with observations of Hutchison (1975), we support the idea of an intra-Indochina suture along the Siem Reap-Stung Treng Line (Figure 10).

Several factors associated with detrital U-Pb analysis could alter the statistics, and thus, our interpretation. Firstly, we took into consideration the number of zircons sampled. It has been argued that > 100 analyses are needed to be 95% confident that no fraction >5% of the population is missed (Vermeesch, 2004), although previous authors suggested that at least 40-60 randomly selected grains are sufficient to reduce the probability of missing this component to 5% (Dodson et al,. 1988; Stock and Montgomery, 1996; Ruhl and Hodges, 2005). The nonmetric MDS is not affected by the considerable disparity in the number of analyses between the considered samples, the MDS is only sensitive of the empirical cumulative distribution functions. The goal of nonmetric MDS is not to approximate the dissimilarities themselves, but rather their relative ranks (Vermeesch, 2013). Hence, it is possible to infer that the outcome of the MDS would probably not change with additional data. Therefore, the KS dissimilarity matrix (Table 2) and MDS visual comparison (Figure 9) do indicate that all the samples within the KKFTB share significant similarities only with terranes NE of the Permian-Triassic south-western margin of Indochina, particularly from the Khorat Plateau, South China, Truong Son and NE Vietnam regions (Figure 10).

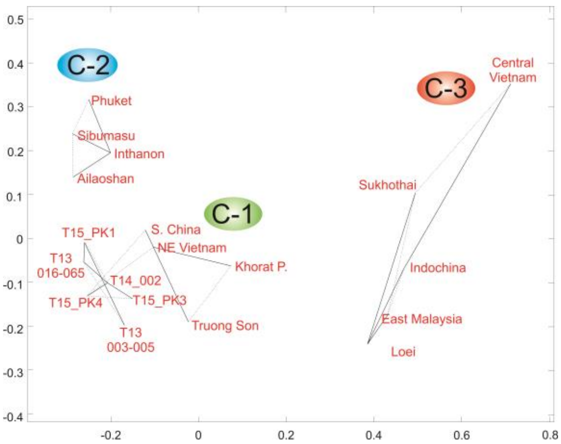

Figure 9. Metric MDS plot of the Asian database (Carter and Bristow, 2003; Li et al., 2012; Hara et al., 2013; Burrett et al., 2014) using the KS effect size as a dissimilarity measure. Solid lines mark the closest neighbours and dashed lines the second closest neighbours (see Vermeesch 2013). The samples with the lowest dissimilarity values are plotted close to each other forming three different clusters C1,2,3. These clusters are only the visual representation of the samples with the lowest dissimilarity values.

6. Conclusions

This study reports a new dataset of zircon U-Pb ages and Hf isotopes of detrital zircons from arenaceous formations of the Saraburi

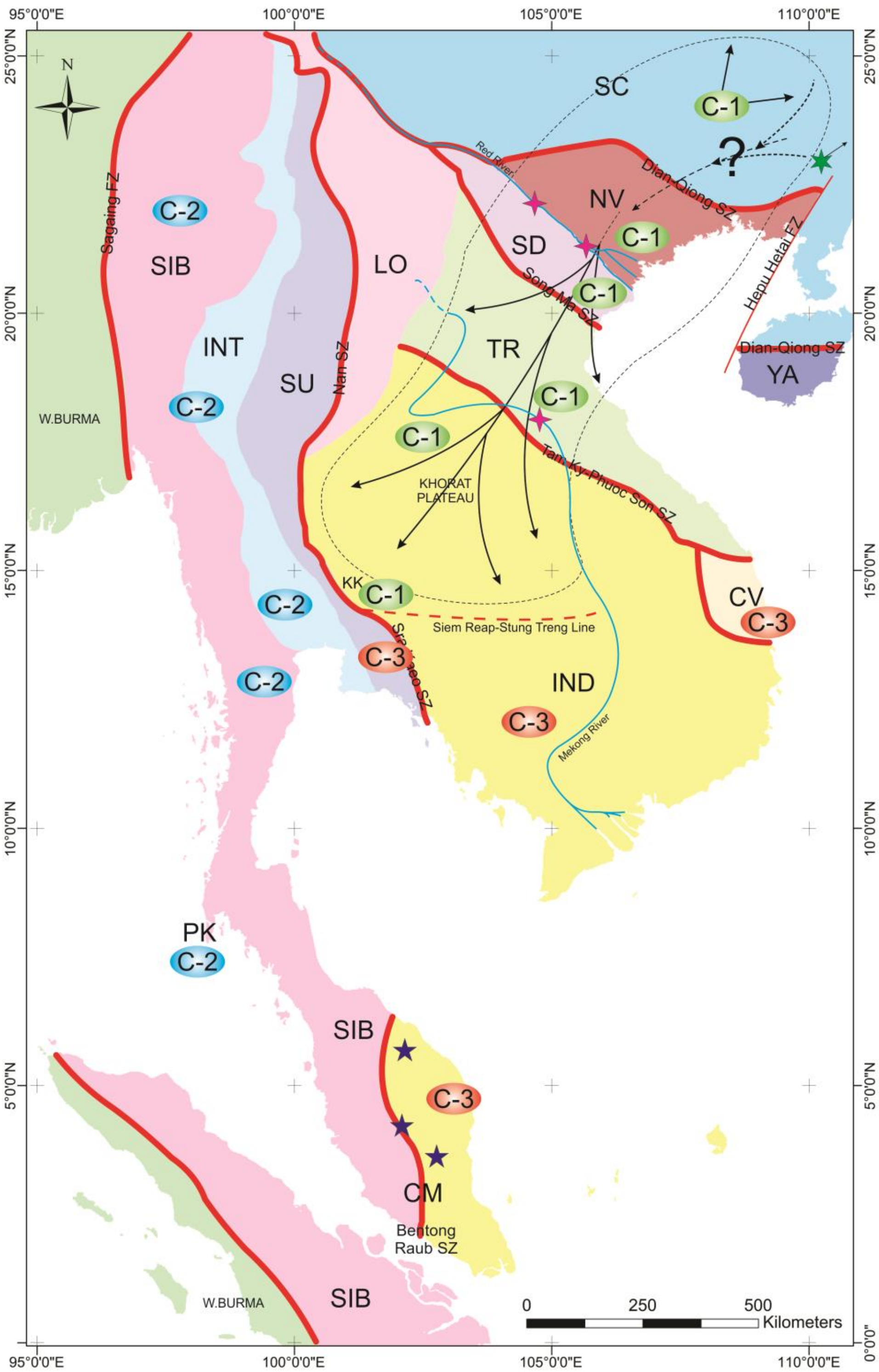

Figure 10. Schematic tectonic map of SE Asia (modified from Metcalfe, 2013; Burrett et al., 2014) representing a tentative reconstruction of the statistically most probable provenance sources and sedimentary pathways (black arrows) during Permian-Triassic ages. C-1,2,3 represent the provenance clusters obtained with MDS analysis. The C1,2,3 logs are placed in the map on the locations where the analysed samples were collected. Five-pointed stars: data from Sevastjanova et al., (2011); four-pointed stars: data from Bodet and Shärer (2000); six-pointed stars: data from Li et al., (2012). CM: Central Malaysia, CV: Central Vietnam, IND: Indochina, INT: Inthanon, LO: Loei, NV: Northeast Vietnam, SIB: Sibumasu, SC: South China, SD: Song Da, SU: Sukhothai, TR: Truong Son; SZ: Suture Zone, FZ: Fault Zone.

Group deposited during latest Palaeozoic-Early Mesozoic on the south-western margin of the Indochina Terrane. Although only maximum possible ages are indicated by the detrital zircons they have important implications for the stratigraphy of the Saraburi Group.

1- A substantial revision to the stratigraphy of the Saraburi Group is indicated, with the Pang Asok Formation changed from the Permian to the Early Triassic. Instead of the Nong Pong and Khao Kwang formations exclusively occupying the northern half of the area a new Upper Triassic marine formation is identified, informally referred to as the Clastic 4 unit.

2- The Triassic basins are re-interpreted as syn-tectonic foredeep or piggyback basins. It is suggested that the Pang Asok Formation records between ca. 250 Ma and 240 Ma a change from deposition in a foredeep basin to being folded, thrusted, and intruded by a ca. 240 Ma granodiorite. Deformation slowly propagated northward with time, or experienced a hiatus. Deposition of the Clastic 4 unit during 230-209 Ma (Norian) implies a possible gap >15 Ma between the end of known thrusting in the southern half of the area, and deformation in the northern area. The different ages probably reflect Early Triassic Sukhothai Terrane-Indochina collision, followed in the Late Triassic by the amalgamated Sukhothai Terrane/Indochina block- Sibumasu collision.

3- U-Pb detrital zircon ages revealed that deposition within the south-western margin of the Indochina terrane lasted until at least 205 ± 6 Ma. It is uncertain whether deposition was in a marine or lacustrine basin.

4- The age distributions yield dominant Ordovician to Devonian (~450-350 Ma) peaks with Neoproterozoic and Mesoproterozoic (~950, ~1200, ~1400 Ma) age groups, and individual zircons dating back to the Palaeoarchean. Hf-isotope data identify different magma sources before and during the subduction of the palaeo-Tethys ocean.

5- Multidimensional scaling analysis on detrital zircon ages from throughout SE Asia collected in the last decades is interpreted to indicate a NE source of sediment feeding the western margin of the Indochina terrane during the Permian and the Triassic.

6- Further, the KS statistical analysis highlights the mismatch within Indochina, between the sediments from the Khorat Plateau in the north, and Cambodia in the south; strengthening the idea already advocated by Lepvrier et al., (2004), and Morley et al., (2013) of a more complicated geometry of the Indochina block. It is possible to speculate about the presence of a possible minor intra-continent ocean that acted as provenance separation (Siem Reap-Stung Treng Line).

7- Upper Triassic detritus from the KKFTB also preserved middle Mesoproterozoic and Triassic detritus that is interpreted as sourced from the newly accreted Sibumasu Terrane.

8- The data indicate that the stratigraphy of the Saraburi Group needs more intensive study, particularly to understand the distribution of Triassic versus Permian sedimentary rocks.

Acknowledgements

The authors would like to thank the editor, the associated editor, and the reviewers for their helpful review and interesting comments on this manuscript. This work was funded by Australian Research Council Discovery Project #DP 120101460. ASC is funded by Australian Research Council grant #FT120100340. This is a contribution to IGCP projects #589 (Development of the Asian Tethyan Realm) and #628 (The Gondwana Map) and we gratefully acknowledge all the funding organizations. This publication forms TRaX Record #xxx.

References

Arboit, F., Collins, A. S., King, R., Morley, C. K., & Hansberry, R., 2014. Structure of the Sibumasu–Indochina collision, central Thailand: A section through the Khao Khwang Fold-Thrust belt. Journal of Asian Earth Sciences, 95, 182-191.

Arboit, F., Amrouch, K., Collins, A. S., King, R., & Morley, C., 2015. Determination of the tectonic evolution from fractures, faults and calcite twins on the south-western margin of the Indochina Block. Tectonics. doi: 10.1002/2015TC003876

Barber, A.J., Ridd, M.F. Crow, M.J., 2011. The origin, movement and assembly of the pre-Tertiary tectonic units of Thailand. The Geology of Thailand, Geological Society, London, 507-537.

Barr, S. M., & Macdonald, A. S., 1987. Nan River suture zone, northern Thailand. Geology, 15(10), 907-910.

Barr, S. M., & Macdonald, A. S., 1991. Toward a late Paleozoic-early Mesozoic tectonic model for Thailand. Journal of Thai Geosciences, 1(1), 11-22.

Baum, F., Braun, E. von, Hahn, L., Hess, A., Koch, K-E., Kruse, G., Quarch, H., and Siebenhuner, M., 1970, On the geology of northern Thailand: Geol. Jahrb. Beihefte, v. 102, p. 1-24, map.

Bodet, F., Schärer, U., 2000. Evolution of the SE-Asian continent from U–Pb and Hf isotopes in single grains of zircon and baddeleyite from large rivers. Geochimica et Cosmochimica Acta 64, 2067–2091

Booth, J.E., Sattayarak, N., 2011. Subsurface Carboniferous – Cretaceous geology of Northeast Thailand. In: Ridd, M.F., Barber, A.J., Crow, M.J. (Eds.), The Geology of Thailand. Geological Society, London, pp. 184–222.

Bouvier, A., Vervoort, J. D., & Patchett, P. J., 2008. The Lu–Hf and Sm–Nd isotopic composition of CHUR: constraints from unequilibrated chondrites and implications for the bulk composition of terrestrial planets. Earth and Planetary Science Letters, 273(1), 48-57.

Bunopas, S., 1982. Paleogeographic history of western Thailand and adjacent parts of South-east Asia: A plate tectonics interpretation. Geological Survey Division, Department of Mineral Resources, (No. 5).

Burrett, C., Long, J., Stait, B., 1990. Early-Middle Palaeozoic biogeography of Asian terranes derived from Gondwana. Geological Society Memoir, 12 (1), pp. 163-174.

Burrett, C., Zaw, K., Meffre, S., Lai, C. K., Khositanont, S., Chaodumrong, P., Udchachon, M., Ekins, S., Halpin, J., 2013. The configuration of Greater Gondwana—Evidence from LA ICPMS, U–Pb geochronology of detrital zircons from the Palaeozoic and

Mesozoic of Southeast Asia and China. Gondwana Research. Vol. 26, pp. 31-51.

Carter, A., & Bristow, C. S., 2003. Linking hinterland evolution and continental basin sedimentation by using detrital zircon thermochronology: a study of the Khorat Plateau Basin, eastern Thailand. Basin Research, 15(2), 271-285.

Carter, A., & Clift, P. D., 2008. Was the Indosinian orogeny a Triassic mountain building or a thermotectonic reactivation event?. Comptes Rendus Geoscience, 340(2), 83-93.

Charoentitirat, T., 2002. Permian Fusulinoidean Biostratigraphy and Carbonate Development in the Indochina Block of Thailand with Their Paleogeographic Implication. PhD Thesis, University of Tsukuba, Tsukuba.

Cho, M., Cheong, W., Ernst, W.G., Yi, K., Kim, J., 2013. SHRIMP U-Pb ages of detrital zircons in metasedimentary rocks of the central Ogcheon fold-thrust belt, Korea: Evidence for tectonic assembly of Paleozoic sedimentary protoliths. Journal of Asian Earth Sciences, 63, pp. 234-249.

Cocks, L. R. M., & Torsvik, T. H., (2013). The dynamic evolution of the Palaeozoic geography of eastern Asia. Earth-Science Reviews, 117, 40-79.

Collins, A.S., et al. 2015. Detrital mineral age, radiogenic isotopic stratigraphy and tectonic significance of the Cuddapah Basin, India, Gondwana Research (2014), http://dx.doi.org/10.1016/j.gr.2014.10.013.

Dawson, O., 1993. Fusiline foraminifera biostratigraphy and carbonate facies of the Permian Ratburi Limestone, Saraburi, central Thailand. Journal of Micropalaeontology, 12 (1), pp. 9-33.

Dawson, O., Racey, A., Whittaker, J., 1994. Permian foraminifera from northeast and peninsular Thailand. In: Proceedings of the International Symposium on Stratigraphic Correlation of Southeast Asia, pp. 323-332.

Dodson, M. H., Compston, W., Williams, I. S., & Wilson, J. F., 1988. A search for ancient detrital zircons in Zimbabwean sediments. Journal of the Geological Society, 145(6), 977-983.

Dong, S.W., Zhang, Y.Q., Gao, R., Su, J.B., Liu, M., Li, J.H., 2015. A possible buried Paleoproterozoic collisional orogen beneath central South China: Evidence from seismic-reflection profiling. Precambrian Research, 264, pp. 1-10.

Dunning, G. R., Macdonald, A. S., & Barr, S. M., 1996. Zircon and monazite U–Pb dating of the Doi Inthanon core complex, northern Thailand: implications for extension within the Indosinian Orogen. Tectonophysics, 251(1), 197-213.

Fromaget, J., 1941, L'Indochine française: Sa structure géologique, ses roches, ses mines, et leurs relations possible avec la tectonique: Hanoi, Service Géol. de l'Indochine, 140 p.

Fromaget, J., Saurin, E., and Fontaine, H., 1971, Geological map of Vietnam, Cambodia, Laos: Dalat, National Geographic Directorate of Vietnam, scale 1:2,000,000.

Gardiner, N. J., Searle, M. P., Morley, C. K., Whitehouse, M. P., Spencer, C. J., & Robb, L. J., 2015. The closure of Palaeo-Tethys in Eastern Myanmar and Northern Thailand: New insights from zircon U–Pb and Hf isotope data, Gondwana Research, http://dx.doi.org/10.1016/j.gr.2015.03.001

Hall, R., van Hattum, M. W., & Spakman, W., 2008. Impact of India–Asia collision on SE

Asia: the record in Borneo. Tectonophysics, 451(1), 366-389.

Halpin, J.A., Jensen, T., McGoldrick, P., Meffre, S., Berry, R.F., Everard, J.L., Calver, C.R., Thompson, J., Goemann, K., Whittaker, J.M. 2014. Authigenic monazite and detrital zircon dating from the Proterozoic Rocky Cape Group, Tasmania: Links to the Belt-Purcell Supergroup, North America. Precambrian Research, 250, pp. 50-67.

Halpin, J.A., et al., 2015, U–Pb zircon geochronology and geochemistry from NE Vietnam: A ‘tectonically disputed’ territory between the Indochina and South China blocks, Gondwana Research. http://dx.doi.org/10.1016/j.gr.2015.04.005.

Hansberry, R. L., King, R., Collins, A. S., & Morley, C. K., 2014. Complex structure of an upper-level shale detachment zone: Khao Khwang Fold-Thrust belt, Central Thailand. Journal of Structural Geology,67, 140-153.

Hansberry, R.L., Alan S. C., Rosalind C. K., Christopher K. M., Andy P. G., Warren J., Stefan C. L., Hall P.A., 2015. Syn-deformation temperature and fossil fluid pathways along an exhumed detachment zone, khao khwang fold-thrust belt, Thailand, Tectonophysics, http://dx.doi.org/10.1016/j.tecto.2015.05.012

Hara, H., Kon, Y., Usuki, T., Lan, C. Y., Kamata, Y., Hisada, K. I., ... & Charusiri, P., (2013). U–Pb ages of detrital zircons within the Inthanon Zone of the Paleo-Tethyan subduction zone, northern Thailand: New constraints on accretionary age and arc activity. Journal of Asian Earth Sciences, 74, 50-61.

Hinthong C., Chuaviroj S., Kaewyana W., Srisukh S., Pholprasit C., Pholachan S., 1985. Geological map of Thailand 1: 250 000 (Changwat Phranakorn Sri Ayutthaya, ND 47–8). Geological Survey Division of the Department of Mineral Resources, Bangkok, Thailand.

Hirsch, F., Ishida, K., Kozai, T., Meesook, A., 2006. The welding of Shan-Thai. Geosciences Journal, 10 (3), pp. 195-204. Hutchison, C.S., 1975. Ophiolite in Southeast Asia. Geological Society of America Bulletin 86, 797–806.

Jackson, S.E., Pearson, N.J., Griffin, W.L., Belousova, E.A., 2004. The application of laser ablation-inductively coupled plasma-mass spectrometry to in-situ U/Pb zircon geochronology. Chemical Geology 211, 47–69.

Kruskal, J., 1964. Multidimensional scaling by optimizing goodness of fit to a nonmetric hypothesis. Psychometrika 29 (1), 1–27.

Lepvrier, C., Maluski, H., Van Tich, V., Leyreloup, A., Thi, P. T., & Van Vuong, N., 2004. The early Triassic Indosinian orogeny in Vietnam (Truong Son Belt and Kontum Massif); implications for the geodynamic evolution of Indochina. Tectonophysics, 393(1), 87-118.

Li, X. H., Li, Z. X., He, B., Li, W. X., Li, Q. L., Gao, Y., & Wang, X. C., (2012). The Early Permian active continental margin and crustal growth of the Cathaysia Block: in situ U–Pb, Lu–Hf and O isotope analyses of detrital zircons. Chemical Geology, 328, 195-207.

McGee, B., Collins, A.S., and Trindade, R.I.F., 2012. G’day Gondwana—The final accretion of a supercontinent: U-Pb ages from the post-orogenic São Vicente Granite, northern Paraguay Belt, Brazil: Gondwana Research, v. 21, no. 2–3, p. 316–322.

Malila, K., Chonglakmani, C., Qinglai, F., Helmcke, D., 2008. Provenance and Tectonic Setting of the Permian Nam Duk Formation, North-Central Thailand: Implications for Geodynamic Evolution. ScienceAsia, 34, 7-22.

Metcalfe, I., 1998. Palaeozoic and Mesozoic geological evolution of the SE Asian region: multidisciplinary constraints and implications for biogeography. Pp. 25-41 in: Hall, R. and Holloway, J.D. (eds) Biogeography and Geological Evolution of SE Asia, Backhuys Publishers, Amsterdam, The Netherlands.

Metcalfe, I., 2005. Asia: South-East. In: Selley, R.C., Cocks, L.R.M., Plimer, I.R. (Eds.), Encyclopedia of Geology, Elsevier, Oxford, vol. 1, 169–198.

Metcalfe, I., 2006. Palaeozoic and Mesozoic tectonic evolution and palaeogeography of East Asian crustal fragments: the Korean Peninsula in context. Gondwana Research, 9(1), 24-46.

Metcalfe, I., 2008. Late Palaeozoic and Mesozoic tectonic and palaeogeographical evolution of SE Asia. Geological Society, London, Special Publications, 315(1), 7-23.

Metcalfe, I., 2011. Tectonic framework and Phanerozoic evolution of Sundaland. Gondwana Research, 19(1), 3-21.

Metcalfe, I., 2013. Tectonic evolution of the Malay Peninsula. Journal of Asian Earth Sciences, 76, 195-213.

Metcalfe, I., and M. Sone, 2008. Biostratigraphy and palaeobiogeography of Lower Permian (lower Kungurian) conodonts from the Tak Fa Formation (Saraburi Limestone), Thailand. Palaeogeography, Palaeoclimatology, Palaeoecology 257.1, 139-151.

Morley, C.K., Ampaiwan, P., Thanudamrong, S., Kuenphan, N., Warren, J., 2013. Development of the Khao Khwang Fold and Thrust Belt: Implications for the geodynamic setting of Thailand and Cambodia during the Indosinian Orogeny. Journal of Asian Earth Sciences, 62, 705-719.

Morley, C.K., Warren, J., Tingay, M., Boonyasaknanon, P., Julapour, A., 2014. Comparison of modern fluid distribution, pressure and flow in sediments associated with anticlines growing in deepwater (Brunei) and continental environments (Iran). Marine and Petroleum Geology, 51, pp. 210-229.

Ori, G. G., & Friend, P. F., 1984. Sedimentary basins formed and carried piggyback on active thrust sheets. Geology, 12(8), 475-478.

Payne, J.L., Ferris, G.M., Barovich, K.M., Hand, M., 2010. Pitfalls of classifying ancient magmatic suites using tectonic discrimination diagrams: an example from the Paleoproterozoic Tunkillia Suite, Gawler Craton, Australia. Precambrian Research 177, 227–240.

Pettijohn, E.J., Potter, P.E., Siever, R., 1987. Sand and Sandstone, third ed. Springer, New York.

Racey, A., Goodall, J.G.S., 2009. Palynology and stratigraphy of the Mesozoic Khorat Group red bed sequences from Thailand. In: Buffetaut, E., Cuny, G., Le Loeuff, J., Suteethorn, V. (Eds.), Late Paleozoic and Mesozoic Continental Ecosystems in SE Asia, Geological Society of London Special Publications. The Geological Society, London, pp. 69–83

Ruhl, K. W., & Hodges, K. V., 2005. The use of detrital mineral cooling ages to evaluate steady state assumptions in active orogens: An example from the central Nepalese Himalaya. Tectonics, 24(4).

Segal, I., Halicz, L., and Platzner, I.T., 2003, Accurate isotope ratio measurements of ytterbium by multiple collection inductively coupled plasma mass spectrometry applying erbium and hafnium in an improved double external normalization procedure: Journal of

Analytical Atomic Spectrometry, v. 18, no. 10, p. 1217–1223, doi: 10 .1039 /b307016f .

Sevastjanova, I., Clements, B., Hall, R., Belousova, E.A., Griffin, W.L., Pearson, N., 2011. Granitic magmatism, basement ages, and provenance indicators in the Malay Peninsula: Insights from detrital zircon U-Pb and Hf-isotope data, Gondwana Research, 19 (4), 1024-1039.

Shaanan, U., Rosenbaum, G., Li, P., & Vasconcelos, P. 2014. Structural evolution of the early Permian Nambucca Block (New England Orogen, eastern Australia) and implications for oroclinal bending. Tectonics, 33(7), 1425-1443.

Sircombe, K.N., Hazelton, M.L., 2004. Comparison of detrital zircon age distributions by kernel functional estimation. Sedimentary Geology, 171 (1-4), pp. 91-111.

Sláma, J., Kosler, J., Condon, D.J., Crowley, J.L., Gerdes, A., Hanchar, J.M., Horstwood,M.S.A., Morris, G.A., Nasdala, L., Norberg, N., Schaltegger, U., Schoene, B., Tubrett, M.N., Whitehouse, M.J., 2008. Plesovice zircon — a new natural reference material for U–Pb and Hf isotopic microanalysis. Chemical Geology, 249, 1–35.

Sone, M., Metcalfe, I., 2008. Parallel Tethyan sutures in mainland Southeast Asia: new insights for Palaeo-Tethys closure and implications for the Indosinian orogeny. Comptes Rendus Geoscience, 340(2), 166-179.

Stock, J. D., & Montgomery, D. R., 1996. Estimating palaeorelief from detrital mineral age ranges. Basin Research, 8(3), 317-327.

Thambunya, S., Visut, P.A., Khantaprab C., 2007. Depositional Environments of Permian Rocks of the Khao Khad Formation in Central Thailand. *ScienceAsia* N.33. 371-381

Toriyama, R., Kanmera, K., Kaewbaidhoon, S. and Hongnusonthl, A., 1974. Biostratigraphic zonation of the Rat Buri Limestone in the Khao Phlong Phrab area, Sara Buri, Central Thailand. In: Kobayashi, T. & Toriyama, R. (eds.), Geology and Palaeontology of Southeast Asia, v. 15, University of Tokyo Press, Tokyo, 39-79.

Toriyama, R., 1975. Fusuline fosslis from Thailand, Part IX. Permian fusulines from the Rat Buri Limestone in the Khao Phlong Phrab area, Sara Buri, Central Thailand. Memoirs of the Faculty of Science, Kyushu University, Series D, Geology, 23, 1-116.

Toriyama, R. and Kanmera, K., 1979. Fusuline fossils from Thailand, Part XII. Permian fusulines from the Ratburi Limestone in the Khao Khao area, Sara Buri, Central Thailand. In: Kobayashi, T., Toriyama, R. and Hasimoto, W. (eds), Geology and Palaeontology of southeast Asia, v. 20, University of Tokyo Press, Tokyo, 23-93.

Udchachon, M., Burrett, C., Thassanapak, H., Chonglakmani, C., Campbell, H., & Feng, Q., 2014. Depositional setting and paleoenvironment of an alatoconchid-bearing Middle Permian carbonate ramp sequence in the Indochina Terrane. Journal of Asian Earth Sciences, 87, 37-55.

Ueno, K., 1999. Gondwana/Tethys divide in East Asia: solution from Late Paleozoic foraminiferal paleobiogeography. In: Proceedings of the International Symposium on Shallow Tethys, N. 5, pp. 45-54.

Ueno, K., Mizuno, Y., Wang, X.D., Mei, S.L., 2002. Artinskian conodonts from the Dingjiazhai Formation of the Baoshan Block, West Yunnan, Southwest China. J. Paleontol. 76, 741–750.

Ueno, K., Miyahigashi, A., Charoentitirat, T., 2010. The Lopingian (Late Permian) of mid-oceanic carbonates in the Eastern Palaeotethys: Stratigraphical outline and foraminiferal faunal succession. Geol. J. 45, 285–307.

Ueno, K., Hisada, K.I., 2001. The Nan-Uttaradit-Sa Kaeo Suture as a Main Paleo-Tethyan Suture in Thailand: Is it Real?. Gondwana Research, 4(4), 804-806.

Ueno, K., Charoentitirat, T., 2011. Carboniferous and Permian. In: Ridd, M.F., Barber,A.J. Crow, M.J. (eds.), The Geology of Thailand, The Geological Society of London, 71–136.

Usuki, T., Lan, C.-Y., Wang, K.-L., Chiu, H.-Y., 2013. Linking the Indochina block and Gondwana during the Early Paleozoic: evidence from U–Pb ages and Hf isotopes of detrital zircons. Tectonophysics 586, 145–159

Van Achterbergh, E., Ryan, C.G., Jackson, S.E., Griffin, W.L., 2001. Data reduction software for LA-ICP-MS. In: Sylvester, P.J. (Ed.), Laser-ablation-ICPMS in the Earth Sciences; Principles and Applications. Mineralogical Association of Canada, Short Course Handbook, Ottawa, pp. 239–243.

van Hattum, M.W.A., 2005. Provenance of Cenozoic sedimentary rocks of northern Borneo. PhD Thesis, Royal Holloway University of London, p. 467.

van Hattum, M.W.A., Hall, R., Pickard, A.L., Nichols, G.J., 2006. Southeast Asian sediments not from Asia: provenance and geochronology of north Borneo sandstones. Geology 34, 589–592.

Vervoort, J.D., Patchett, P.J., Soderlund, U., Baker, M., 2004. Isotopic composition of Yb and

the determination of Lu concentrations and Lu/Hf ratios by isotope dilution using MC-ICPMS. Geochemistry, Geophysics, Geosystems 5.

Vermeesch, P., 2012. On the visualisation of detrital age distributions. Chemical Geology 312–313, 190–194.

Vermeesch, P., 2013. Multi-sample comparison of detrital age distributions. Chemical Geology, 341, pp. 140-146.

Warren, J., Morley, C.K., Charoentitirat, T., Cartwright, I., Ampaiwan, P., Khositchaisri, P., Mirzaloo, M., Yingyuen, J., 2014. Structural and fluid evolution of Saraburi Group sedimentary carbonates, central Thailand: A tectonically driven fluid system. Marine and Petroleum Geology, Doi: 10.1016/j.marpetgo.2013.12.019

Wielchowsky, C.C., Young, J.D., 1985. Regional facies variations in Permian rocks of the Phetchabun fold and thrust belt, Thailand. In: Conference on Geology and Mineral Resources Development of the Northeast, Thailand (Proceeding), Khon Kaen University, Khon Kaen, Thailand, pp. 26-29.

Woodhead, J., Hergt, J., Shelley, M., Eggins, S., Kemp, R., 2004. Zircon Hf-isotope analysis with an excimer laser, depth profiling, ablation of complex geometries, and concomitant age estimation. Chem. Geol. 209, 121–135.

Wu, F.-Y., Yang, J.-H., Wilde, S.A., Liu, X.-M., Guo, J.-H., Zhai, M.-G., 2007, Detrital zircon U-Pb and Hf isotopic constraints on the crustal evolution of North Korea, Precambrian Research, 159 (3-4), pp. 155-177.

Chapter VI

Arboit, F., Collins, A. S., Morley, C., King, R., Amrouch, K. (2016). Geochronological and geochemical study of mafic dykes from the Khao Khwang Fold-Thrust Belt: Implications for petrogenesis and tectonic evolution. *Gondwana Research.*

Geochronological and geochemical study of mafic and intermediate dykes from the Khao Khwang Fold-Thrust Belt: Implications for petrogenesis and tectonic evolution

ABSTRACT

Zircon U–Pb, mica $^{40}Ar/^{39}Ar$ ages and geochemistry of the Permo-Triassic mafic to intermediate dyke swarms at the south-western margin of the Indochina Block, central Thailand, are reported here and used to decipher the timing of the Sukhothai-Indochina & Sibumasu-Indochina collisions during the Permo-Triassic stages of the Indosinian Orogeny. The mafic dyke swarms in the folded layers of the Khao Khwang Fold-Thrust Belt (KKFTB) were emplaced between the Late Permian and the Late Triassic. The volcanic rocks ranges from slightly tholeiitic to mostly calc-alkalic, but can be subdivided into three different volcanic groups on the basis of trace and incompatible element abundances such as Ni, Cr, P, Co, and Th. However, all the groups present similar chemical footprints and are enriched in large ion lithophile elements (LILE) (Rb, Ba, Sr, Pb) and light rare earth elements (LREE), and depleted in HFSE such as Nb, and Ti highlighting the volcanic arc nature of the system. Isotopically, the three groups are characterized by subtle differences in εNd(t) values (from +3.2 to +5.2) and initial $^{87}Sr/^{86}Sr$ ratios (from 0.7056 to 0.7067). The KKFTB mafic dykes share a few geochemical characteristics of the mafic dykes from the Chiang Khong volcanic suite in the Sukhothai terrane, and from the Loei volcanic belt in northern Indochina. These geochemical features suggest that the KKFTB mafic dykes, and the volcanic rocks in central-northern Thailand, were likely crystallized in a similar orogenic setting. The rocks of Group III are interpreted to have intruded from the Early Triassic (255 ± 6 Ma) to the Late Triassic (207 ± 2 Ma), and were probably sourced from a more crustally contaminated magma.

1. Introduction

The 'Indosinian Orogeny' broadly includes all the Late Palaeozoic to Early Mesozoic tectonic events related to closure of the eastern Paleo-Tethys Ocean (Cho et al., 2008). These events comprise collision of a succession of Gondwana-derived continental fragments, and volcanic arcs (Sone and Metcalfe, 2008; Metcalfe 2013). In Thailand, the orogeny mainly developed during the Triassic and earliest Jurassic (Sone and Metcalfe, 2008; Metcalfe, 2011) and is the result of the collision between the Sibumasu, Sukhothai and Indochina Terranes (Figure 1a, b). Models for the tectonic evolution of Thailand from the Indosinian Orogeny to the present have been defined using biostratigraphical, petrological, structural and geochronological data (Metcalfe and Sone, 2008; Sone and Metcalfe, 2008; Ridd and Morley, 2011; Morley et al., 2013; Arboit et al., 2014; Hansberry et al., 2014). However, a consensus on the location of the terrane boundaries, and nature and position of the relative suture zones has not been reached (Barr and Macdonald, 1991; Charusiri et al., 1994, 1997; Metcalfe, 2000). Volcanic rocks are an important tool able to provide fundamental information on the tectonic history of an area. Unfortunately, most of the volcanic and igneous rocks emplaced within central Thailand lack detailed petrochemical data and precise ages. This paper attempts to interrogate the volcanic rocks and mafic dykes in the Saraburi area of central Thailand in order to understand the nature of the magma sources and the tectonic setting of their emplacement.

The igneous rocks studied are intruded within the Khao Khwang fold-thrust belt (KKFTB) and form a large igneous trend south of the KKFTB. This fold-thrust belt occupies an

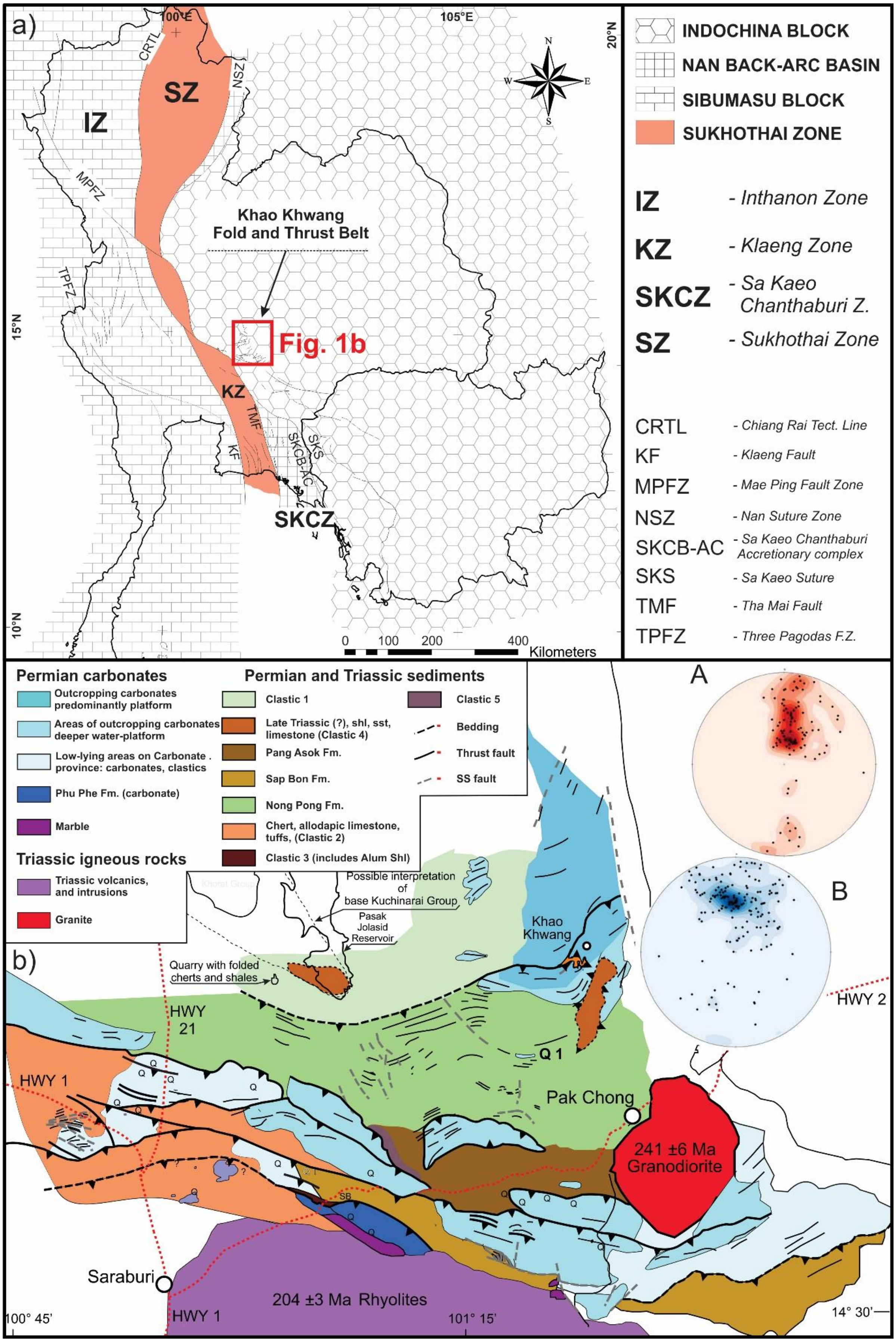

a)
100°E
105°E
20°N
15°N
10°N
CRTL
NSZ
SZ
IZ
MPFZ
TPFZ
Khao Khwang
Fold and Thrust Belt
Fig. 1b
KZ
TMF
KF
SKCB-AC
SKS
SKCZ
N
S
W
E
0 100 200 400
Kilometers
INDOCHINA BLOCK
NAN BACK-ARC BASIN
SIBUMASU BLOCK
SUKHOTHAI ZONE
IZ - Inthanon Zone
KZ - Klaeng Zone
SKCZ - Sa Kaeo Chanthaburi Z.
SZ - Sukhothai Zone
CRTL - Chiang Rai Tect. Line
KF - Klaeng Fault
MPFZ - Mae Ping Fault Zone
NSZ - Nan Suture Zone
SKCB-AC - Sa Kaeo Chanthaburi Accretionary complex
SKS - Sa Kaeo Suture
TMF - Tha Mai Fault
TPFZ - Three Pagodas F.Z.
Permian carbonates
Outcropping carbonates predominantly platform
Areas of outcropping carbonates deeper water-platform
Low-lying areas on Carbonate . province: carbonates, clastics
Phu Phe Fm. (carbonate)
Marble
Triassic igneous rocks
Triassic volcanics, and intrusions
Granite
Permian and Triassic sediments
Clastic 1
Late Triassic (?), shl, sst, limestone (Clastic 4)
Pang Asok Fm.
Sap Bon Fm.
Nong Pong Fm.
Chert, allodapic limestone, tuffs, (Clastic 2)
Clastic 3 (includes Alum Shl)
Clastic 5
Bedding
Thrust fault
SS fault
A
B
b)
Possible interpretation of base Kuchinarai Group
Pasak Jolasid Reservoir
Khao Khwang
Quarry with folded cherts and shales
HWY 21
HWY 1
HWY 2
Q 1
Pak Chong
241 ±6 Ma Granodiorite
SB
Saraburi
204 ±3 Ma Rhyolites
100° 45'
101° 15'
14° 30'

5965

Figure 1. a) Subdivision of Thailand into main tectonic terranes, that amalgamated during the Indosinian Orogeny (modified from Ueno and Charoentitirat, 2011), B) geological map of the Khao Khwang Fold and Thrust Belt. It has been modified from Warren et al., (2014) to show possible interpretations of the stratigraphy as a consequence of this study (A: poles to bedding within the KKFTB; B: poles to major thrusts and strike-slip faults in the southern portion of the KKFTB).

important position on the edge of the Nan-Sa Kaeo suture zone between Indochina and the Sukhothai volcanic arc, and are thought to correlate to the well documented volcanic bodies along the margin of these two terranes (Nakchaiya et al., 2008; Boongsoong et al., 2011) and in northern Thailand (Barr and Macdonald, 2000, 2006).

In this paper, we report new petrological data, $^{40}Ar/^{39}Ar$ mica and U–Pb zircon ages, along with both whole rock elemental and Sr–Nd isotopic data for the most representative dykes in the KKFTB with the aims to (1) establish the average crystallization age for the dykes, (2) unravel the origin and petrogenesis of the dykes, and, (3) constraining the compressional events affecting the Sukhothai and Indochina terranes and shed light on the tectonic evolution of the Triassic Indosinian Orogeny in central Thailand.

2. Regional setting

Ueno (1999) and Ueno et al., (2002) proposed four geotectonic units for northern Thailand (from west to east): the Sibumasu, Inthanon, Sukhothai, and Indochina terranes, separated by the Changning–Menglian–Inthanon, and Jinghong, Nan and Sra Kaeo sutures respectively (Figure 1a). However, the nature and the precise position of some the suture zones running through Thailand have been historically hampered by the lack of information from areas such as the western margin of the Indochina Terrane (Figure 1a). In Thailand, the Nan (or Nan–Uttaradit) suture has been regarded by many workers as a major boundary between the Gondwanan Sibumasu terrane to the west and the Indochina terrane to the east, hence representing the site of the Palaeo-Tethys Ocean during the Late Palaeozoic–Triassic (Hutchison 1975; Bunopas 1981; Barr & Macdonald 1987; Yang et al. 1994; Okamura et al. 1997). However, the Nan suture has more recently been correlated with each of the Jinshajiang–Ailaoshan suture, the Lancangjiang suture, and the Changning–Menglian suture in Yunnan (Barr et al., 2006, see review in Gardiner et al., 2015). Most authors (Ricou, 1994; Ueno et al., 1999, 2001; Sone and Metcalfe, 2008; Metcalfe, 2013; Gardiner et al., 2015) prefer an alternative site for the true Palaeo-Tethys subduction zone in the N-S trending Inthanon Zone-Chiang Rai line to the west where pelagic cherts of Devonian–Triassic ages and Permo-Triassic seamount carbonates are distributed. This zone lies is roughly parallel to the Loei Volcanic belt. Sone and Metcalfe (2008) regarded the Nan and Sra Kaeo sutures as a back-arc suture zone between the Sukothai volcanic arc and the Indochina Terrane (Figure 1a).

The KKFTB is located in the southern portion of the Loei–Phetchabun–Nakhon Nayok Volcanic Belt. This belt is composed of acidic to basic lavas, and compositionally-related. In the Loei area, these volcanic rocks may be further separated into eastern, central, and western sub-belts. The volcanic rocks of the eastern sub-belt are mainly rhyolitic, whereas those of western sub-belt are largely andesitic (Jungyusuk & Khositanont 1992; Della-Pasqua & Khin 2002, Boonsoong et al., 2011). Both have been interpreted to be the products of Permo-Triassic arc volcanism (e.g. Bunopas & Vella 1983). The arc-related rhyolitic samples of the eastern sub-belt, however, yielded U–Pb zircon ages of 425 ± 7 and 433 ± 4 Ma

(Early Silurian-beginning of Palaeo-Tethys subduction) (Khositanont et al., 2008). The central sub-belt is composed mainly of pillow lava, hyaloclastite, and pillow breccia, (Boonsoong et al., 2011) interpreted as forming in a mid-oceanic ridge environment (Intasopa & Dunn 1994). Additionally, Panjasawatwong et al. (2006) reported that the mid-ocean ridge basalt (MORB) exists along with oceanic island-arc mafic lava in the central sub-belt. The arc lavas were probably built on oceanic basement in a major ocean basin or in a mature back-arc basin. The volcanic rocks of the western sub-belt in the Phetchabun area have a mica $^{40}Ar/^{39}Ar$ plateau age of 238 ± 4 Ma (Middle Triassic) and geochemistry indicated formation along an active continental margin (Kamvong et al. 2006; Marhotorn et al. 2008; Tangwattananukul et al. 2008). The volcanic rocks within the KKFTB have not been so thoroughly investigated. The geological map proposed by Morley et al. (2013) highlights a Triassic andesitic-rhyolitic volcanic body south of the KKFTB and a Permian granodioritic intrusion east of the KKFTB. Most of the exposed intrusions of the KKFTB lie within the carbonates of the Khao Khad Formation. Dykes and sills are common features in the KKFTB, in most cases they cross-cut folds and cross-cut or follow thrusts, indicating they were intruded after the main Indosinian deformation. However, in some cases dykes are offset by thrusts or are folded. Hence magmatic activity began before or during deformation, but continued and increased in activity after deformation ceased (Figure 2). Therefore, these dykes have the potential to provide new insights in the understanding of the Sukhothai-Indochina collision that developed during the early stages of the Indosinian orogeny.

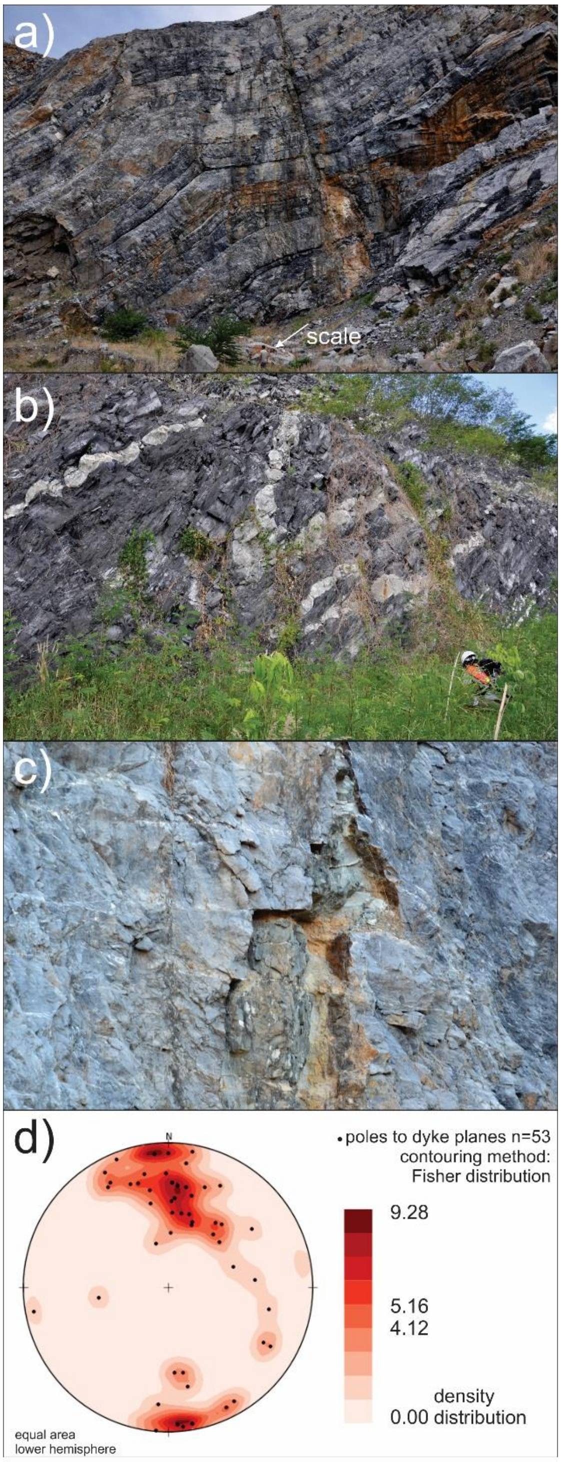

Figure 2. a) photographs of dykes intruding the folded carbonate of the Khao Khad Formation after the main deformation; b) dyke folded within the Alum Shale clastic unit (Morley et al., 2013); c) undeformed dyke within the Khao Khad Formation showing some clear offsetting by flexural slip of bedding ; d) stereogram with the poles of the dyke planes throughout the southern KKFTB showing a clear E-W trend.

3. Analytical methods

We undertook a range of geochemical and geochronological techniques to unravel the age and origin of the basaltic-andesite dyke complex and investigate the relative tectonic setting. These methods are detailed below.

3.1. U/Pb laser-ablation inductively coupled plasma mass spectrometry (LA-ICPMS)

Zircons grains were separated using standard separation techniques such as specific-gravity liquid (ρ≥3.2) and a Frantz magnetic separator. Hand-picked zircons were then mounted on a 2.5 cm-diameter circular epoxy mounts and then polished to expose a section at their inner core. Prior to their analysis the grains were imaged using a Gatan cathodoluminescence analyser attached to a Phillips XL20 scanning electron microscope. Zircon U/Pb isotope analysis was performed using LA-ICP-MS at The University of Adelaide following the method of Payne et al. (2010). Zircons were ablated with a New Wave Research UP-213 laser using a spot-size of 30 μm, a frequency of 5 Hz and intensity at 100%. Isotopic data were acquired with the Agilent 7500 series Inductively Coupled Plasma Mass Spectrometer on eight masses: $^{206}Pb/^{238}U$; $^{207}Pb/^{235}U$; $^{207}Pb/^{206}Pb$; $^{208}Pb/^{232}U$. Mass discrimination of the mass spectrometer and elemental fractionation during laser ablation were corrected by calibration against the GEMOC GJ-1 zircon with thermal ion mass spectrometry (TIMS) normalising ages of $^{207}Pb/^{206}Pb$ = 607.7 ± 4.3 Ma, $^{206}Pb/^{238}U$ = 600.7 ± 1.1 Ma and $^{207}Pb/^{235}U$ = 602.0 ± 1.0 Ma (Jackson et al. 2004). The Plešovice zircon internal standard (ID TIMS $^{206}Pb/^{238}U$ age = 337.13 ± 0.37 Ma, Sláma et al., 2008), was used to assess accuracy before and during the analysis of the unknowns. Over the course of the laser session, a total of 110 Plešovice internal standards analyses were carried out, and gave a weighted average $^{207}Pb/^{206}Pb$ = 334 ± 29 Ma (MSWD = 0.53), and a weighted average $^{206}Pb/^{238}U$ age = 366 ± 4.4 Ma (MSWD = 0.95). Data were collected, corrected and filtered in the GLITTER version 3.0 (Van Achterbergh et al., 2001) software package. Concordia diagrams and weighted averages were calculated using ISOPLOT 4.11 for Excel (Ludwig, 2009).

3.2. Major and trace elements analyses

Thirty-nine samples were prepared for whole-rock analysis by splitting into conveniently sized fragments, and then crushing into small chips, using a Rocklabs hydraulic crusher/breaker. The crushed fragments were cleaned with an air hose; 30–50 g aliquots of the rock chips displaying no sign of weathered surfaces, or veins were pulverised for 2–3 min in a tungsten–carbide Rocklabs ring mill. All the procedures described above were carried out in the Department of Earth Science at the University of Adelaide. Major oxides were determined on 34 samples by wavelength-dispersive X-ray fluorescence spectrometry (XRF) using a Axios featuring a 4.0 kilowatt Rh SST-mAX[50] X-ray tube from Panalytical. The spectrometer is controlled by Super-Q software at the Geology, Geophysics and Geochemistry laboratories in the University of Tasmania. XRF analyses were performed with a Sc-Mo 3kW side window X-ray using standard techniques (Robinson 2003). Corrections for mass absorption are calculated using Philips X40 software with De Jongh's calibration model and Philips (or CSIRO) alpha coefficients. Calibrations are on pure element oxide mixes in pure silica. The trace elements were determined for 39 samples at AcmeLabs (presently Bureau Veritas Minerals) in Vancouver, Canada. The solutions were analysed using a Spectro Ciros Vision emission spectrometer ICP-ES/MS (AQ200 detection level) and a Perkin Elmer

Elan 6000/9000 inductively coupled plasma mass spectrometer (ICP-MS) for 45 elements (Ba, Be, Co, Cs, Ga, Hf, Nb, Rb, Sn, Sr, Ta, Th, U, V, Cr, W, Zr, Y, La, Ce, Pr, Nd, Sm, Eu, Gd, Tb, Dy, Ho, Er, Tm, Yb, Lu, Mo, Cu, Pb, Zn, Ni, As, Cd, Sb, Bi, Ag, Au, Hg, Tl, and Se).

3.3. Whole-rock Sr, and Nd isotopes analyses

Samples of 0.5 g of rock powder from three significative samples were dissolved together with (^{147}Sm and ^{150}Nd) mixed spike, in a solution of 2mL 7M HNO_3 and 4mL 48%HF and left overnight at 140°C, then evaporated to dryness. The procedure was repeated in the same solution, and then evaporated to dryness after a digestion of 48 hours. The dissolution procedure also involves digestion of the solution in 6mL 6M HCl for conversion to chlorides. The solutions were separated for Sr, Nd and Sm by ion chromatography. Two ml of the solution were passed twice through AGW X8 200-400 mesh resin in Polyprep columns and then 1 ml of the final solution was passed once through eichrom Ln resin SPS for the isotopes separation. The analyses were carried out in the University of Adelaide using a Finnigan MAT262 thermal ionization mass spectrometer (TIMS), in double collector dynamic measurement mode. Measurements were done with at least 10 blocks of 10 scans (8 second each) for a minimum of 100 measurements, the results for strontium were then normalized to a fixed ^{88}Sr/^{86}Sr = 8.375209, and for neodymium to a fixed ^{146}Nd/^{144}Nd = 0.721903. Both the isotopes concentrations have been corrected using the outcome of 200 pg blank solution. For an optimal result the Sm concentrations were corrected for 150 pg of blank solution.

3.4. Mica ^{40}Ar/^{39}Ar geochronology

We selected two andesitic dykes with an average of 59.6% in SiO_2 from Group III for ^{40}Ar/^{39}Ar dating and extracted several unaltered biotite and muscovite crystals of 315-500 µm in diameter. These minerals were carefully handpicked under a binocular microscope after magnetic separation from the crushed materials and washed in an ultrasonic bath using ultrapure water. Samples were loaded into a small well of one 1.9 cm diameter and 0.3 cm depth aluminium disc. This well was bracketed by small wells that included Fish Canyon sanidine (FCs) used as a neutron fluence monitor for which an age of 28.294 ± 0.036 Ma (1σ error) was adopted (Renne et al., 2011) and an excellent grain-to-grain reproducibility was demonstrated (Jourdan and Renne, 2007). The discs were Cd-shielded (to minimize undesirable nuclear interference reactions) and irradiated for 40 h in the Oregon TRIGA research reactor in a central position. The mean J-value computed from standard grains within the small pits is 0.01058900 ± 0.00000635, which is determined as the average and standard deviation of J-values of the small wells. Mass discrimination was monitored using an automated air pipette and provided a mean value of 1.005014 (±0.06%) per dalton (atomic mass unit) relative to an air ratio of 298.56 ± 0.31 (Lee et al., 2006). The correction factors for interfering isotopes were (^{39}Ar/^{37}Ar)Ca = 7.60×10^{-4} (±1.2%), (^{36}Ar/^{37}Ar)Ca = 2.70×10^{-4} (±0.74%) and (^{40}Ar/^{39}Ar)K = 7.30×10^{-4} (±12.4%). The ^{40}Ar/^{39}Ar analyses were performed at the Western Australian Argon Isotope Facility at Curtin University. The crystals were step-heated using a 110 W Spectron Laser Systems, with a continuous Nd-YAG (IR; 1064 nm) laser rastered over the sample during 1 min to ensure that all the gas has been extracted from the sample. The gas was purified in a stainless steel extraction line using two SAES AP10 getters and a GP50 getter. Ar isotopes were measured in static mode using aMAP 215-50 mass spectrometer (resolution of ~450; sensitivity of 4×10^{-14}

mol/V) with a Balzers SEV 217 electron multiplier using 9 to 10 cycles of peak-hopping. The data acquisition was performed with the Argus program written by M.O. McWilliams and was run under a LabView environment. The raw data were processed using the ArArCALC software (Koppers, 2002) and the ages were calculated using the decay constants recommended by Renne et al. (2011). Blanks were monitored every 3 to 4 steps and typical ^{40}Ar blanks range from 1 × 10^{-16} to 2 × 10^{-16} mol.

4. Sample description and petrography

The dykes occur within the E-W to NW-SE trending hills of the KKFTB (Supplementary Data-1). For this study, the freshest samples were selected for both geochemical and petrographical analyses. There are no previous studies on the igneous rocks that intruded the KKFTB, and the only geochronological constraints for this area were reported on the Late Permian early Triassic granodiorite east to the KKFTB in Morley et al. (2013). However, the ages of the igneous rocks have here been assumed on the basis of geometrical relationships with the associated sedimentary rocks, and from provenance criteria. Most of the outcrops examined during this study consist of green to dark grey basaltic and andesitic dykes and sills with rare flows or welded tuffs. The mafic dykes in the KKFTB have mostly basaltic and andesitic compositions (Table 1 – Appendix C) and intrude carbonates of the Khao Khad Formation and the Alum Shale unit in the southern portion of the Siam Cement quarry (Figure 1). These two compositions of dykes do not present any type of cross-cutting relationship making it impossible to define a relative age. However, an andesitic dyke cross-cuts the gabbroic intrusion southeast of the KKFTB, revealing their relative late timing of emplacement. There is field evidence for both the basaltic and andesitic dykes to have intruded the KKFTB before and after the main folding event (Figure 2a, b, c). Evidence for pre-deformation emplacement is relatively infrequent and includes folding of intrusions, and offsetting of intrusions by flexural slip of bedding and thrusts. The majority of the dykes cross-cut folds, exhibit an E-W strike and steep dips (Figure 2d). The strike direction is sub-parallel to the orientation of the major fold hinges in the area (Arboit et al., 2014), which also suggests post-tectonic emplacement. Dykes are tensile fractures, which develop in orientations parallel to the maximum horizontal stress, hence emplacement sub-parallel to fold hinges is incompatible with the stress orientation required for fold development. The dykes are commonly free of noticeable metamorphism; although, the presence of rare crypto-crystals of cummingtonite, actinolite, and chlorite in coexistence with crystals of hornblende highlights possible low-grade regional metamorphism. The average thickness of the dykes ranges from 1 m up to 10-15 m. In this study, the representative fresh basaltic and andesitic dykes from quarries were sampled. The basaltic andesite and andesite intrusions are fine grained, dark to green in colour, with porphyritic to aphanitic texture and mainly containing plagioclase crystals set in an interlocking matrix of quartz and alkali feldspar. The plagioclase crystals are usually affected by intense sericitic alteration that has obliterated the primary structure; or they are pseudomorphed by chlorite and calcite. Pyroxenes are mostly euhedral and sometimes are altered to amphiboles (20–35%), clinopyroxene shows disequilibrium features such as rounded/corroded edges. The plagioclase and alkali feldspar are both euhedral. The groundmass presents a scattered presence (40–60%) of biotite and muscovite (2-5%) and accessory cryptocrysts of olivine and magnetite. Most samples lack olivine, others have minor amounts and only a few have quantifiable amounts. The gabbro/gabbroic basalt samples have aphanitic to ophitic textures. Microgabbro samples show porphyritic textures with clinopyroxene and orthopyroxene characterized by inequigranular distributions. The pyroxenes are partially pseudomorphed by epidote, actinolite and calcite microphenocrysts, with subordinate plagioclase, hornblende, and rare accessory magnetite partially altered to hematite. These evidences of greenshist facies conditions might be related to events of high fluid circulations that led to the formation of marbles in the southern portion of the KKFTB (Warren et al., 2014). The metamorphic imprinting represents possible very-low to low grade regional metamorphism, consistent with the maximum temperatures of 160–210 °C reported in the eastern KKFTB by Arboit et al. (2015). The basaltic dykes are extremely fine grained and contain only sporadic euhedral lath-shaped plagioclase phenocrysts (1-5%) (Table 1 – Appendix C). Matrix minerals are mainly plagioclase and crypto-crystals of olivine. The presence of olivine might be a sign of incomplete reaction on account of rapid rise and quick cooling of the magma. Trace amount of magnetite, hematite, hornblende and brownish biotite make up the accessory minerals.

5. Results

5.1. U/Pb dating

Rhyolitic sample T14_004 was selected for U/Pb dating. The sample consists of scattered plagioclase and feldspar phenocrysts and rare felsic and mafic clasts in a fine-grained quartzo-feldspathic groundmass. Sample T14_004 yielded zircons, which vary from fine- to coarse-grained, water-clear, colourless to pale pink or pale yellow, stubby euhedral grains. A few grains are large shard-like fragments, short or equant prisms with slightly irregular crystal faces. Thirty zircon spots were analysed, of which 10 analyses yielded values within 5% of concordance (Supplementary data-2). Of these, three were inherited, one showed evidences of lead loss, and six analyses yielded a weighted $^{206}Pb/^{238}U$ mean age of 207.1 ± 2.4 Ma (MSWD = 0.18), which is interpreted as the age of crystallisation (Figure 3).

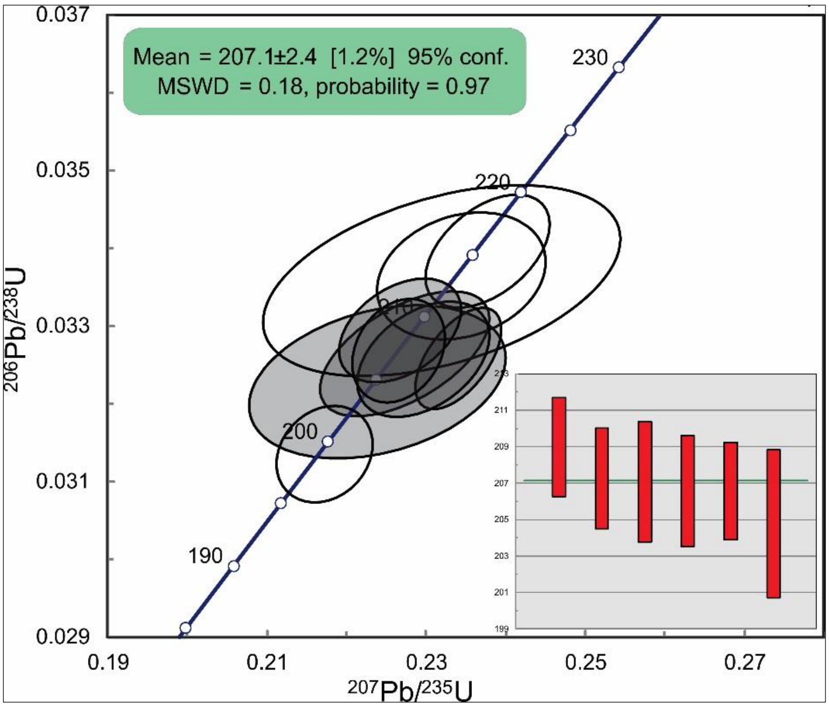

Figure 3. Concordia plot for zircon U-Pb isotopic rats of the Khao Yai rhyolite south to the KKFTB. Black shaded ellipses show the six ages within the 5% of concordance that were used to calculate the weighted mean age.

5.2. Major oxides and trace elements

Major and trace elements were selected for whole-rock chemical analysis from rocks that intruded the KKFTB before, during and after the Indosinian orogeny. Volcanic rocks are susceptible to alteration, and accordingly their chemical compositions are unlikely to be primary. To avoid this we only selected samples with minor traces of alteration. Petrographic evidences, as well as elevated LOI (loss on ignition) values (Figure 4) show that samples in the area have been subjected to very low- to low metamorphism (Table 2 – Appendix C).

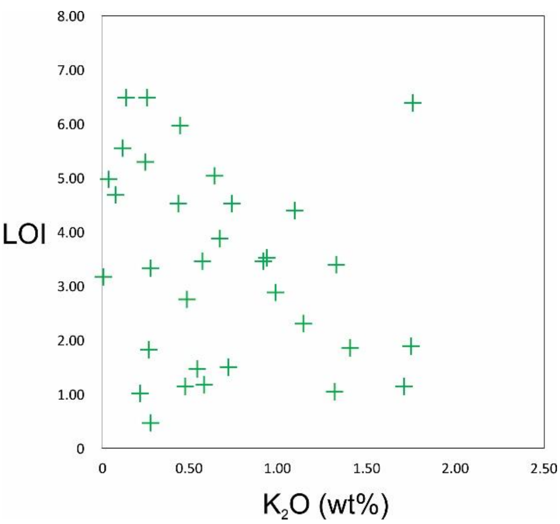

Figure 4. K2O (in wt%) versus the Loss Of Ignition (LOI) showing the level of alteration of the igneous and volcanic suite of the KKFTB.

These secondary processes may have led to alteration of the mobile elements, accordingly only relatively immobile elements have been used herein. Elements such as Cr, Ni, Ti, Nb, Hf, Zr, P, V, and REE (Pearce and Cann, 1976; Pearce, 1996), and the relatively immobile FeO_T/MgO ratio and Mg number (Mg#) (Miyashiro et al., 1975) are taken in consideration. The data are plotted in several diagrams in order to provide their compositional array and help comparison with data from the Chon Daen-Wang Pong area in the western Loei volcanic sub-belt, and from the Pak Chom area within the central Loei volcanic belt (Boonsoong et al., 2011; Panjasawatwong et al., 2006). The majority of the samples analysed are basaltic to andesitic, and with a SiO_2 content between 40 % and 62 % (average 47%) (Table 2 – Appendix C). Most of the major elements, such as FeO_T, Al_2O_3, P_2O_5, present a linear trend with increasing abundances of both SiO_2 and Zr/TiO_2 (Figure 5), while as expected from the observed alteration, the more mobile elements such as the alkali group have a more scattered behaviour. Because of the possible alteration/weathering effects on the samples, it is useful to have immobile element proxy diagrams to replace conventional diagrams for rock classification. At present, the Zr/TiO_2 vs Nb/Y plot (Figure 6) is an efficient replacement for the total alkali-silica (TAS) plot (Winchester and Floyd, 1977). The samples tend to plot in the subalkalic field, with a narrow Nb/Y ratio (0.05 – 0.50) and to have a slightly tholeiitic to calc-alkalic affinity based on the Co/Th ratio (Hastie et al., 2007). They straddle the border between basalts and andesites on the basis of the Zr/Ti ratio (0.05 – 0.76). The entire set of rocks do not show any particular variation of TiO_2 and FeO_T as the fractionation parameter increases; although bivariate plots show an increase of Cr, and Ni contents with increasing Mg# and FeO_T/MgO ratio (Figure 7).

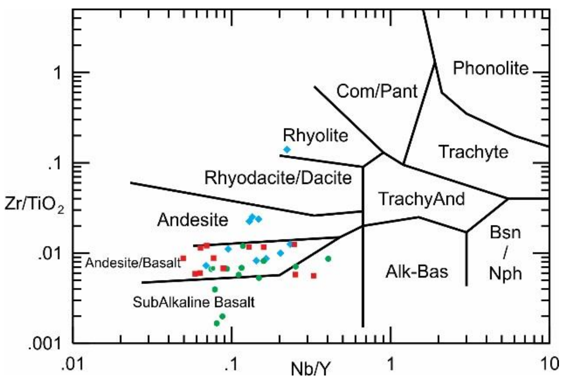

Figure 6. Plot of Nb/Y vs Zr/TiO_2 discimination diagram (Winchester and Floyd, 1977) for the KKFTB igneous and volcanic rocks. For symbology refer to Figure 4.

Therefore, considering this wide compositional range in terms of relatively immobile elements and their ratio; the volcanic rocks separated into three different volcanic groups on the basis of immobile and incompatible elements. Group I (GI, red squares in the bivariate plots) is mostly represented by basalts, these rocks have the highest average Zr/Nb ratio (50.07), with the lowest FeO_T/MgO (average 0.86) ratio along with the highest Cr (average 688 ppm), and Ni (average 222 ppm). Group II (GII, green circles in the bivariate plots) presents intermediate average values of Cr, Ni, and variable values of SiO_2 (38.9-62.2%), with a wide modal distribution. Group III (GIII, cyan diamonds in the bivariate plots) appears to be formed of calc-alkaline basalts and andesites. Group III presents a narrow range of SiO_2 values (41.9-51.7%) and the lowest value for the Zr/Nb ratio (average 29.83) along with Zr/V (0.3647), and also the highest P_2O_5 abundances and the lowest Cr and Ni at similar values of Mg#. Group III shows very low Ni (average 5.5 ppm) and Cr (average 33.7 ppm) abundances. All the rocks of Group III have a fairly consistent average FeO_T/MgO ratio of 2.58, and a very consistent high value of P_2O_5 (average 0.45 %).

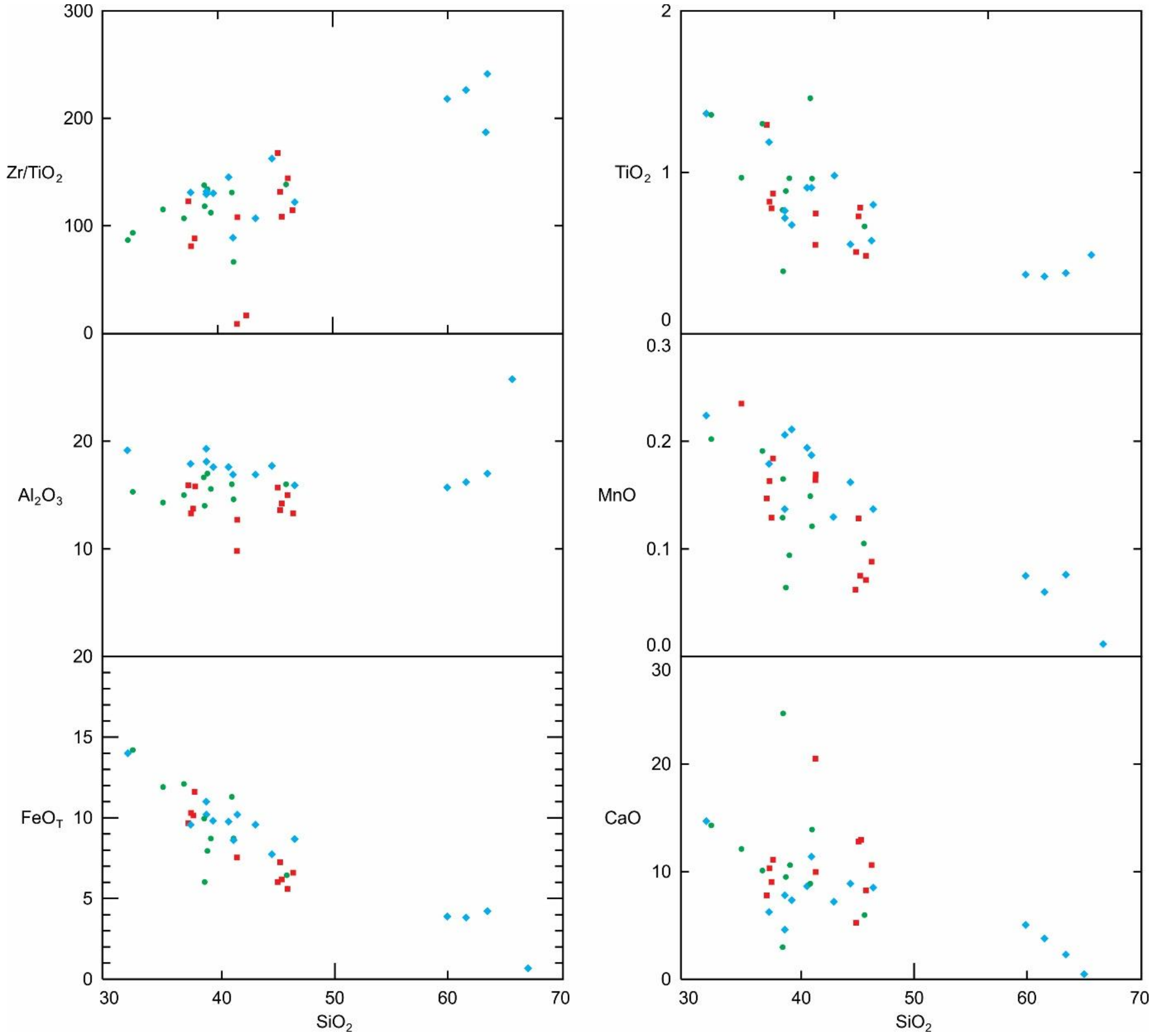

Figure 5. Major elements plotted as function of SiO_2 (all in wt%) for the KKFTB sills, tuffs and dykes. Symbols representing the different groups, Group I= red squares, Group II= green circles, Group III= blue diamonds

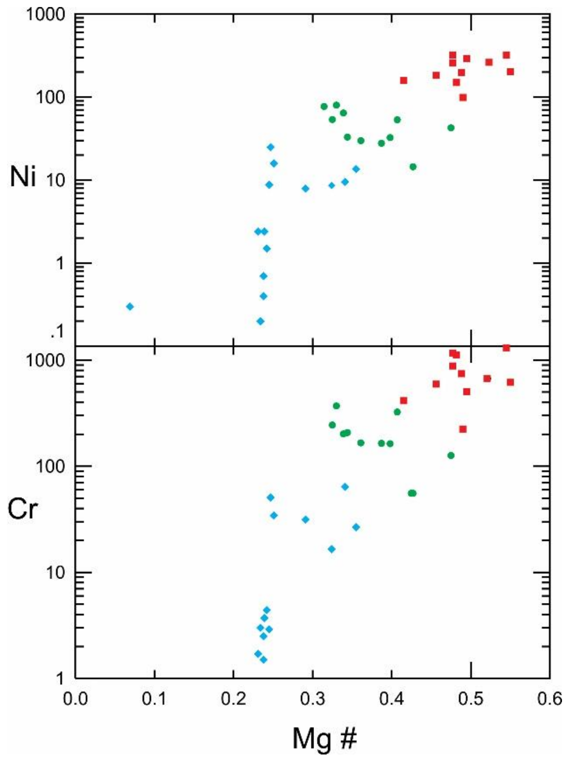

Figure 7. Trace elements Ni and Cr plotted vs the Mg-number. These elements are selected to show the differences between the most mafic of Group I to the more evolved of Group III. For symbology refer to Figure 4.

5.3. Incompatible elements and REEs

The high field strength elements (HFSE) are considered to be relatively immobile during hydrothermal alteration (Winchester and Floyd, 1977; MacLean and Barrett, 1993; Rollinson, 1993). In terms of discrimination of the tectonic setting, the entire KKFTB volcanic suite presents consistent results. The discriminant diagrams such as Nb-Zr-Y (Meschede, 1986), and Th/Yb vs Nb/Yb (Pearce, 2008) suggest a source consistent with a volcanic arc basalt source (Figure 8).

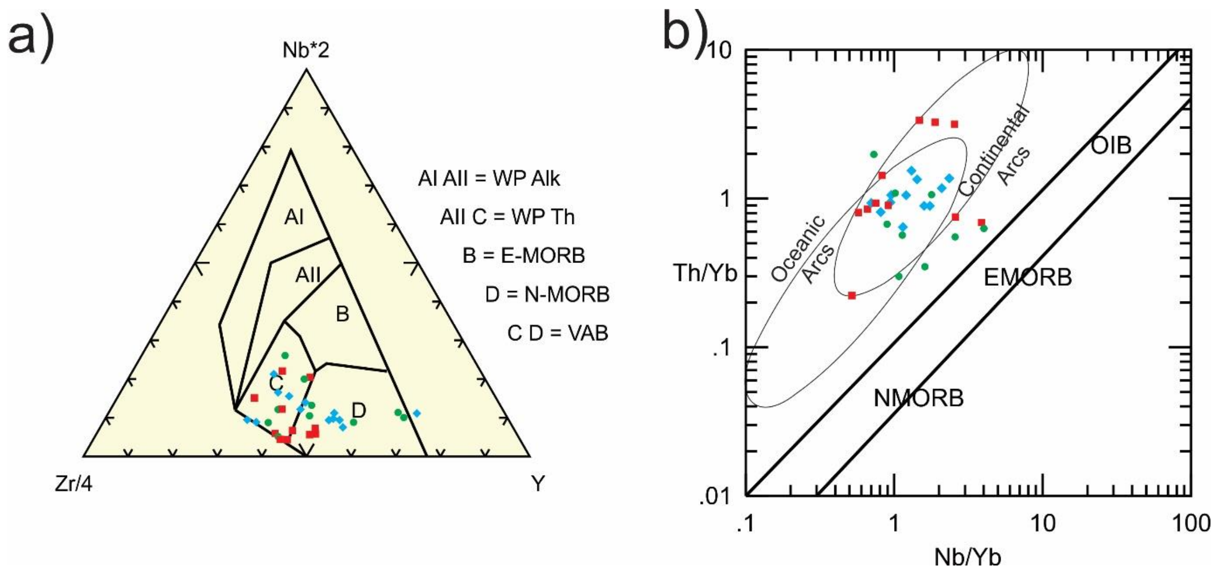

Figure 8. Plots discriminating the tectonic setting of the KKFTB; a) Zr/4-Nb*2-Y (Meschede, 1986); b) Nb/Yb vs Th/Yb (Pearce, 2008). Symbols are as in Figure 4.

Looking to the Zr/(Zr/Y) ratio it is possible to further discriminate the tectonic setting, which might have developed along an active continental margin, with the involvement of continental crust. The rare earth element (REE) data from all the samples show a similar chemical imprinting for the entire KKFTB volcanic suite. As shown by chondrite normalised REE plots (Figure 9a, b, c) each of the volcanic group are characterised by a relatively similar flat pattern of the HREE. The ratios between incompatible trace elements such as Ce/La and Cr/Ni show fairly consistent trends, with the Ce/La ratio being almost constant for all the groups (mean: 2.13, σ: 0.2). This is a little less than the primordial

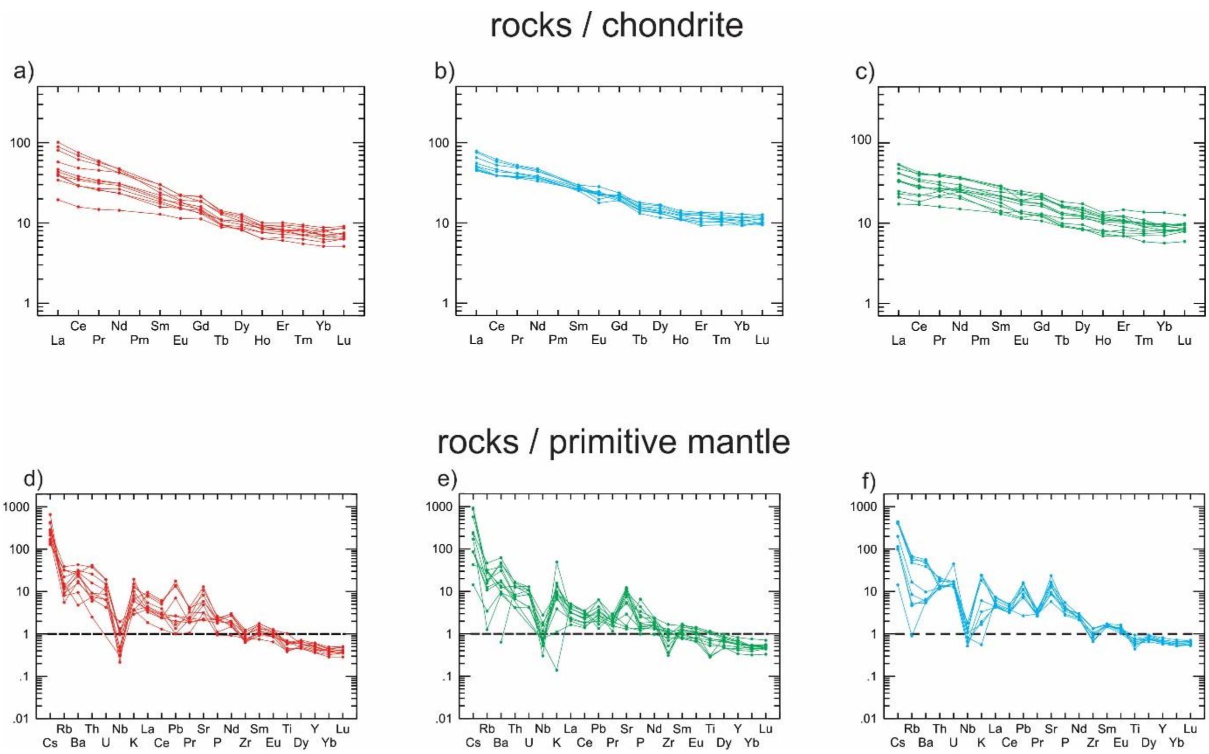

Figure 9. a-b-c) Chondrite normalized REE data from the KKFTB volcanic and igneous suite. Chondrite-normalizing values are from Sun & McDonough (1989). d-e-f) Multi-element variation diagram, with data from the KKFTB volcanic belts normalized to normal mid-ocean ridge basalt (N-MORB) from Sun & McDonough (1989). A-d) Group I; b-e) Group II; c-f) Group III.

mantle value of 2.6, suggested by Wood (1979), and the chondrite value of 2.64, reported by Nakamura (1974). The Cr/Ni ratio in the three volcanic groups is almost the same in the three groups, with values ranging from 0.33 up to 14.99 (mean = 3.5, σ = 0.5). Therefore, the differences between the groups might have originated through several processes, and considering the similar values among each group, was probably due to either crystal fractionation, crustal contamination or to the magma arising from slightly different sources and depth of melting, or a combination of both. The trend of the trace element patterns is best represented by the MREE/HREE fractionation system (Figure 10). The MREE/HREE ratio (e.g. (Sm Yb)$_n$) of all the groups presents systematically similar values (Figure 10a), the low and linear trend of the Sm/Yb ratio of all the groups excludes the presence of garnet in their source which would fractionate the MREE/HREE ratio and rather suggest the melting of a shallow spinel-bearing source. Little distinctions also occur between the LREE/HREE ratio in the volcanic groups of the KKFTB (Figure 10b) showing similar melting conditions. The N-MORB normalized trace elements distributions are analogous to the surrounding volcanic belts (Barr et al., 2000, 2006; Panjasawatwon et al., 2006; Boonsoong et al., 2011), with trace elements patterns strongly depleted in HFSE. Groups II and III have minimal Eu anomalies probably corresponding to the andesites and metamorphic hornblende-bearing microgabbros, whereas basalts of Group I do not show any particular anomaly. The N-MORB multi-element variation diagrams

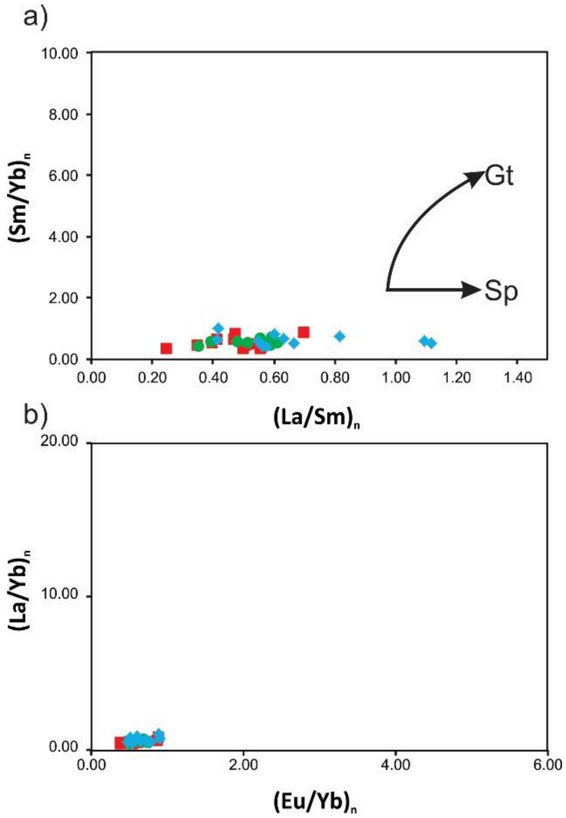

Figure 10. a) $(Sm/Yb)_n$ vs $(La/Sm)_n$ and $(La/Yb)_n$ vs $(Eu/Yb)_n$ for the KKFTB. Values are chondrite-normalized after Boynton (1984). Black curves: estimation of the melting curves of garnet-bearing lherzolite mantle sources.

(Figure 9d, e, f) for each of the volcanic groups reveal the enrichment of LREE and depletion in HFSE compared to the MORB composition. In detail, samples with higher levels of Cr, Ni (Groups I and II), and Mg are slightly lower in their incompatible element abundances in comparison to dykes of Group III. Further, Group III shows a stronger depletion in HREE (higher La_N/Yb_N average ratio). The variation diagrams show a distinct anomaly in Nd relative to highly incompatible large ion lithophile elements (LILE) as well as light rare earth elements such as Th, K, Ce, La. This trend is probably intrinsic to the mantle source composition, as discriminated by using the HFSE (Kelemen et al., 1993; Pearce, 1996) (Figure 8). However, the anomaly in Nd might be evidence for a partial imprinting of crustal contamination. The Ce/Pb ratio is relatively low in the more intermediate andesites of Group III (<15), this ratio compared to the high and uniform in MORB (25 ± 5; Hofmann et al., 1986) strengthens the involvement of partial crustal contamination. Further, most of the samples show similarities with data from the Chiang Khong volcanic suite within the Sukhothai volcanic arc (Barr et al., 2006), with a very distinctive positive anomaly of Sr and Pb probably related to crustal contamination. However, only few of the rocks in GII show slightly higher abundances of Ti and lower degrees of enrichment of middle rare earth elements such as Eu and Dy relatively to Ti.

5.4. Sr and Nd isotopic data

Major elements data can be ambiguous when trying to discriminate between source compositions and crustal contamination as causes of chemical diversification. Three samples, from each of the three different volcanic groups were analysed for initial Sr-Nd isotopic composition, which are commonly used as tracers for magma sources (e.g. Jourdan et al., 2007). The samples have similar chemical imprinting; however they represent three different tectonic stages as follows: 1) Sample T13_027 (Group I) cross-cuts without any evident deformation one of the best exposed fault-bend folds in the Khao Yai hill, and demonstrate post –tectonic emplacement. 2) Sample T13_062 (Group II) has been cut off and displaced several hundred meters by a major thrust supporting the timing of emplacement before or during the main tectonic event, and 3) Sample T13_070 (Group III) is represented by a tuff layer syn-depositional to the Khao Khad Formation. These field relationships in addition to the new $^{40}Ar/^{39}Ar$ and U-Pb analytical results, and to the U-Pb ages from the granodiorite intrusion east of the KKFTB (287 ± 7 Ma) (by S. Meffre Pers. comm.), were used in relation to the general tectonic architecture of the KKFTB in order to estimate

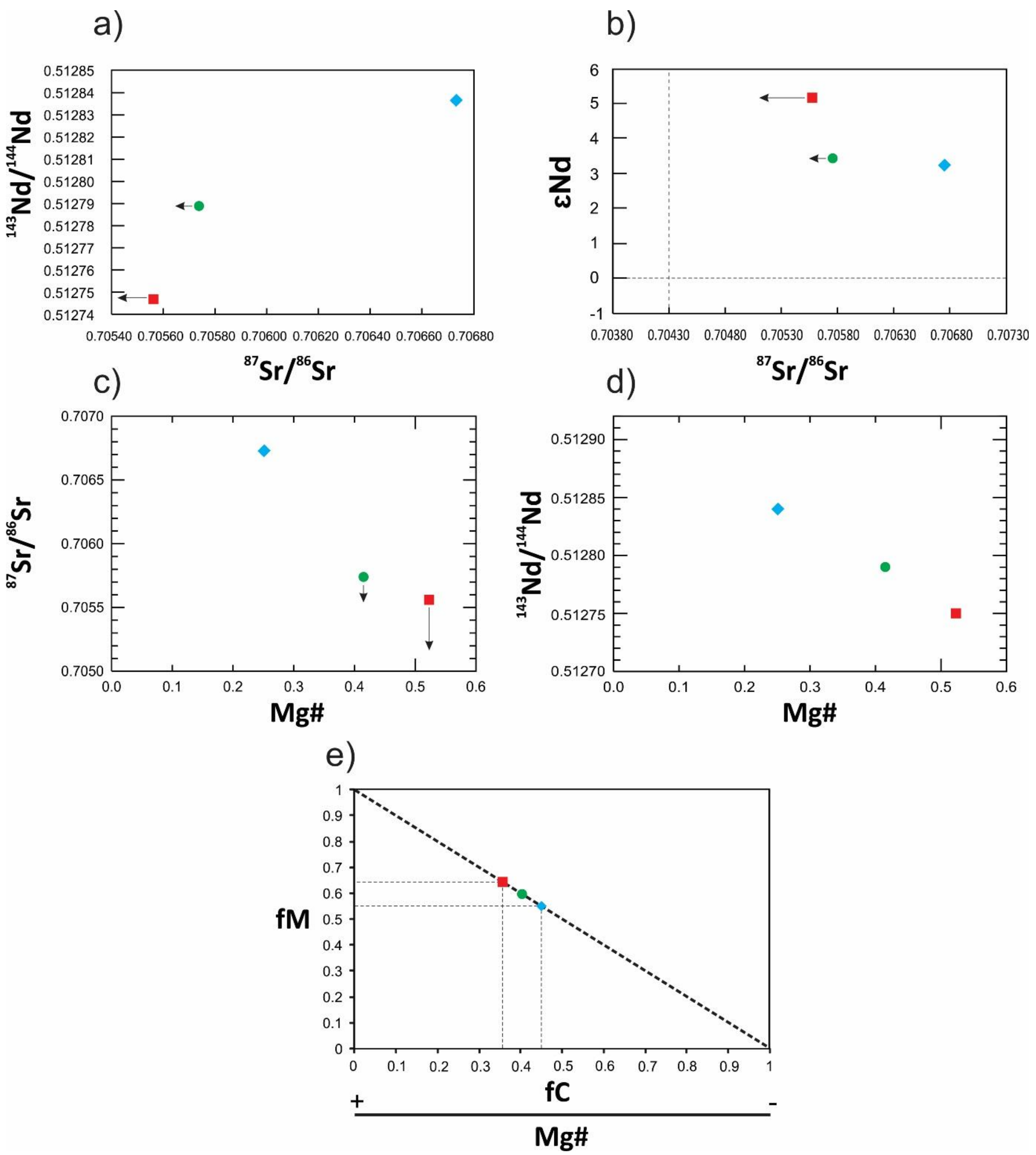

Figure 11. a) $^{143}Nd/^{144}Nd$ vs $^{87}Sr/^{86}Sr$; b) $^{87}Sr/^{86}Sr$ vs εNd; c) $^{87}Sr/^{86}Sr$; d) $^{143}Nd/^{144}Nd$ initial isotopic composition vs Mg-number; and e) plot showing the balancing of the isotopes masses and the relative trend with respect to the Mg-number. Black arrows in plots a, b, c point out the possibly lower values of $^{87}Sr/^{86}Sr$ in samples from group I and II, related to the level of alteration (high Loss Of Ignition

ages for each samples. All of them have a narrow range of *ε*Nd(*t*) values ranging from +5.16 (Sample T13_070, ±280 Ma) to +3.22 (Sample T13_027, ±230 Ma), with relative calculated mantle ages are in the range of *c.* 700-900 Ma. The *ε*Nd(*t*) values of the dykes that predate the main tectonic event are slightly higher and the model ages are younger than those reported for the less juvenile basaltic dyke within the Khao Yai Hill (Table 3 – Appendix C). All the samples have a relatively narrow range in Sr isotopic ratios ($^{87}Sr/^{86}Sr(t)$ = 0.705560– 0.706729), with the lowest values pairing with the highest *ε*Nd(*t*) in Group I while Group III stands out for the highest $^{87}Sr/^{86}Sr(t)$ and both the lowest Mg# and εNd(*t*). The trend of the εNd(*t*) and of the $^{87}Sr/^{86}Sr(t)$ in the dykes of the KKFTB might suggest that some of the magmas were either affected by crustal contamination or reflect a heterogeneous mantle source(s). Looking at the LOI of the rock samples it is possible to imply that the $^{87}Sr/^{86}Sr(t)$ might have been modified by alteration, resulting in values higher than its original isotopic composition (Figure 11a, b, c). One of the key differences between the volcanic groups is their quite constant and overlapping REE trends (Figure 10), these ratios seem to indicate similar depths of melting for the volcanic groups of the KKFTB. Both $^{87}Sr/^{86}Sr(t)$ and $^{143}Nd/^{144}Nd(t)$ correlate with Mg-number which rather suggest that these variations are related to crustal contamination processes. Balancing the isotopes masses (Faure, 2013) at 220 and 250 Ma we calculated that a slight increase of crustal contamination of only 10%, from about (65% fM - ±35% fC) to (55% fM - ±45% fC), is necessary to lower the ratio of εNd(*t*) from +5.16 to +3.22 (Figure 11e). Similar values of crustal component were calculated in the parental magma of the rocks of the Main Range in the Malay Peninsula (Ng et al., 2015a).

5.5. $^{40}Ar/^{39}Ar$ geochronology

$^{40}Ar/^{39}Ar$ analytical results for biotite and muscovite are shown in Figure 12. In this study, an age plateau is defined as a sequence of three or more consecutive steps corresponding to at least 70% of the total ^{39}Ar released that yield apparent ages reproducible at the 95% confidence level (2σ). The two samples, both of Group III, yielded well-defined plateau ages at 255 ± 6 Ma (MSWD 2.0, P=0.05), and 224 ± 1.9 Ma (MSWD 1.0, P=0.43), (Figure 11). The characteristics of the age spectra suggest that argon loss occurred in the samples from subsequent thermal event, but this event affected only the low-temperature extraction steps and allowed us to derive a crystallization age for those two samples.

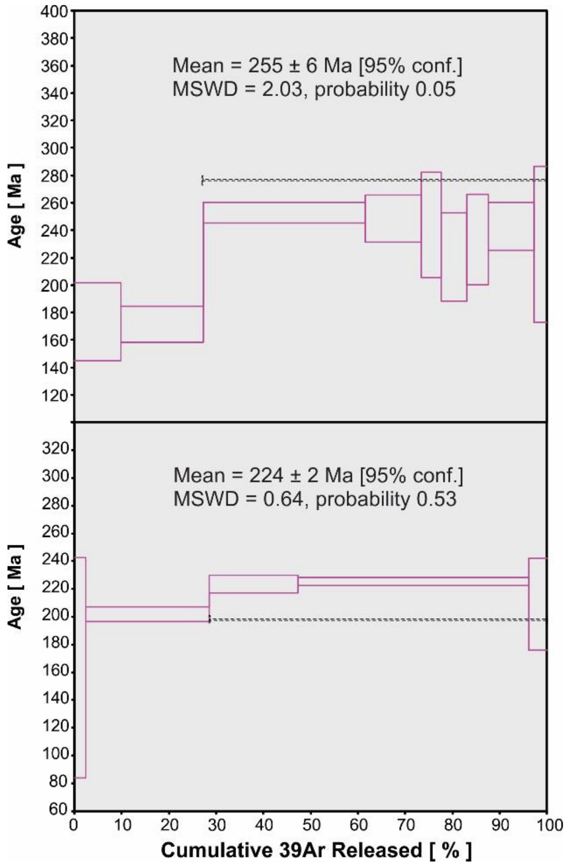

Figure 12. $^{40}Ar/^{39}Ar$ weighted mean plateau ages calculated for two andesites of Group III.

6. Discussions

6.1. SE Asia tectonic context

Perhaps the most outstanding feature of the Indosinian Orogeny in Thailand and Malaysia is the extensive, highly voluminous, nature of ‘I’ and ‘S’-type granites (Beckinsale, 1979) and Cobbing et al., 1986). With the Sibumasu granites west of the Raub-Bentong suture being predominantly ‘S-type’, while those east of the suture (Sukhothai-Indochina block) being predominantly ‘I-type’. Traditionally this division, following Chappell and White (1974), has been used to infer an Andean-type setting for the ‘I-type’ granites and continent collision, associated with considerable crustal thickening and melting of a sedimentary protolith, for the ‘S-type’ granites. This association would make the Sibumasu-Sukhothai/Indochina collision in Thailand and Malaysia appear to be more like a major continent-continent collision, and less like an accretionary orogen.

Accretionary orogens are characterized by a succession of collisional events, that if long-lived enough can involve seamount/plateau accretion, ridge-trench interaction, formation of supra-subduction ridges and back-arc basins, arc-arc, and arc-continent collision, oroclinal bending, and collision of island arcs and continental fragments. An example of an extremely long-lived accretionary orogeny is the Altaids of Central Asia that developed from 600 Ma to 250 Ma (see review in Wilhem et al., 2012). The accretion of narrow, ribbon-shaped terranes enables subduction to initiate or continue on the outboard side of the ribbon, thus permitting the accretionary orogen to continue growing. Whereas in a major continent-continent collision zone such as the Alps or the Himalayas subduction continues and ultimately terminates at the site of collision. Consequently a considerably greater degree of continental crust thickening, and subduction occurs in major continent-continent collision zones compared with accretionary orogens.

The Indosinian orogeny is virtually a continuation of processes seen earlier in the Altides to the north, and Sibumasu is a ribbon continental terrane, not a major continental block. Hence, the tin belt association with a major continental collision has not been an easy one to reconcile. Recently interpretation of the origin of the granites has become more nuanced because geochemically the two provinces in Malaysia actually only show slight differences in lithology, geochemistry and isotope values (e.g. Ghani et al., 2013, Searle et al., 2012, Ng et al., 2015b). The extensive occurrence of tin-bearing granites (~220-195 Ma) within the Sibumasu Terrane is interpreted to be a consequence of widespread crustal thickening (e.g. Cobbing et al., 1992; Cobbing, 2011). However, Ng et al. (2015b) note that although up to 40% crustal sources were incorporated into melts due to anatexis of metasedimentary basement, fluids driven off a subduction zone on the west side of Sibumasu remained an important factor in triggering partial melting of thickened Sibumasu crust. Granites in the eastern belt span ages around 290-220 Ma (Ng et al., 2015a). They are metaluminous to weakly peraluminous, with an enriched high field strength element (HFSE) signature, and are interpreted to have formed in a suprasubduction zone setting (Ng et al., 2015b). Around 20% crustal source contribution has been determined, with little difference in crustal signature between eastern and western Malaysia (Ng et al., 2015b).

The interpretation of Ng et al. (2015b), which minimizes the contribution of crustal thickening to the development of the tin-bearing granites in Malaysia (and by association, Thailand) and invokes subduction on the western side of Sibumasu, emphasizes the accretionary nature of the Indosinian orogen into the Early Jurassic.

The crustal thickness in Thailand ranges from 31 to 38 km (Noisagool et al., 2014). However, this measure provides no evidence for crustal thicknesses attained during the Indosinian orogeny, since it is well known that other ancient orogenic belts, particularly the Scandinavian Caledonides, have normalized their thicknesses post-collision (Blundell, 1984, 2002). In the case of the Caledonides a range of processes (erosion, plate divergence, gravity-driven collapse of the orogenic wedge, viscous flow of lower crust) are considered to be responsible (Fossen et al., 2014). While normalization has probably occurred in Thailand the preservation of low-grade metamorphism fold and thrust belts, and the widespread absence of exhumed high-grade terranes indicates that uplift and erosion during the orogeny was limited. One exposed region of high grade Indosinian metamorphism is Doi Inthanon, where P-T analysis indicates high temperatures (700-750°C) but moderate pressures (6-7 kbar), i.e. depths of 20-23 km, at peak metamorphism (Macdonald et al. 2010). These observations support the interpretation that the crust never became very thick (<50km?). The high grade (amphibolite-granulite) gneissic terranes that are exposed in Thailand, in most cases, were exhumed as a consequence of Late Cretaceous-Cenozoic tectonics, not Indosinian orogeny-related processes (Macdonald et al., 2010; see review in Morley et al., 2012). This tectonic complexity is well reflected within the KKFTB. The compositional variations amongst the three groups identified in the preceding sections most likely reflect complicated magmatic processes and/or the nature of the source(s). These characteristics can generally be attributed to: (1) various amounts of assimilation/fractional crystallization of mantle-derived magma and crustal contamination en route to the surface; (2) various degrees of partial melting of a homogeneous source at different pressures and temperatures; and (3) mantle source variability, e.g. metasomatised lithospheric mantle or hybridized source (Bell and Simonetti, 1996).

6.2. Effect of alterations

The mafic dykes in the region have commonly been altered to various degrees after intrusion, which can be determined from petrographic observations and exemplified by the relatively high loss on ignition in most of the sample with andesitic samples over basaltic samples having a LOI between 2 and 7 wt% (Figure 4). Some incompatible elements, such as Rb, Ba and K, are known to be mobile during weathering (Deniel, 1998), as demonstrated by the considerable scatter in the N-MORB multi-element variation diagrams. However, the consistency demonstrated by the data set (except for the most mobile elements) in primitive–mantle-normalized patterns (Figure 9d, e, f), suggests that absolute abundances and ratios of incompatible elements, such as LREE and HREE are the least sensitive to weathering. This is supported by a large number of studies (Jochum et al., 1991; Deniel, 1998; Kerrich et al., 1999; Xu et al., 2001). Accordingly, the following discussions focus mostly on the most immobile elements as well as the Mg#, εNd(t) values, although we will tentatively use the $^{87}Sr/^{86}Sr(t)$ ratio for supporting our hypothesis.

6.3. Magma sources

The Mg# is a differentiation proxy which monitors the chemical evolution of the magma (Lindh et al., 2001). The Ni, Cr and P contents show quite consistent correlation with the Mg#. The low SiO_2 contents (average 46.6 wt. %) suggests that the dykes of the KKFTB were possibly derived from a ultramafic mantle source (by opposition to anatectic melts derived from the crust). This is also supported by high concentrations of Ni (average 222 ppm) and Cr (average 688 ppm), in the most mafic dykes of the KKFTB. Crustal rocks might be ruled out as possible sources because experimental evidence shows that partial melting of any of the older, exposed crustal rocks (Hirajima et al., 1990; Yang et al., 1993; Zhang et al., 1994, 1995; Kato et al., 1997) and lower crustal intermediate granulites (Gao et al., 1998) in the deep crust would produce high-Si liquids (Rapp et al., 2003). However, the dykes probably do not represent primary melts, as judged from their

MgO (average <6.1%), Mg# (0.29–0.99) and Ni contents (1.5–320 ppm). The Mg# negative trend showed by the rock groups of the KKFTB, from Group I to Group III, suggests that the most evolved rocks might have undergone to crustal contamination as also indicated by the co-variation in $^{87}Sr/^{86}Sr(t)$, and in εNd(t) (Figure 11c, d). The differences between rocks of Group I and III might be also related to a degree of fractional crystallization prior to emplacement. Looking at the major and trace elements, Group III and partially Group II rocks may have experienced fractionation of olivine and clinopyroxene from the parental magmas, supported by the positive correlation between Mg# and Cr and Ni (Figure 7). The slight increase of CaO/Al_2O_3 with higher abundances of Mg# (not shown) indicates possible clinopyroxene fractionation. In primitive mantle normalized diagrams (Figure 9) all the rocks reveal very distinctive negative anomalies for Nb, Ta and Ti, and positive anomalies for Sr and Pb. HFSE-depletion indicates the involvement of components from the Tethyan/back-arc oceanic or ancient continental crust (Zhang et al., 2005a). Accordingly, the above observations suggest that continental materials were involved in the development of these mantle-derived magmas (Pearce, 1996; Jahn et al., 1999).

The Nd and Sr isotopic records help constraining the nature of the mafic parental magma. The slightly positive εNd values are similar to those in the 240 Ma rhyolitic tuff from the Phetchabun fold-thrust belt area (Figure 11b) (+4.8 to +5.8, Barr et al., 2000, 2006). However, a more complicated scenario appears when looking at the data from Intasopa (1993) and Intasopa and Dunn (1994), who reported εNd values from +0.39 to -1.35 for rhyolites in the Loei area. These rocks are Devonian-Carboniferous in age and are interpreted by Intasopa (1993) and Intasopa and Dunn (1994) to have been derived from crust on the edge of the Indochina Terrane. Hence, these are not directly comparable to those from the KKFTB. These geochemical and isotopic data suggest that the parental magma of the dykes is unlikely to be have derived from different depths of melting as indicated by the MREE/HREE (Figure 10), and probably arose from the lithospheric wedge after the metasomatism of the subducted back-arc basin between Sukhothai and Indochina. The younger and more evolved samples might have undergone to higher degrees of crustal contamination (Figure 11b) and this process possibly occurred during the late Permian to Late Triassic evolution of the Indosinian orogeny after the Sukhothai-Indochina collision and the relative slab break-off. Other similarities appear with volcanic belts within the Sukhothai terrane, in fact the *ε*Nd(*t*) values yield Neoproterozoic T_{DM} ages (ca. 600-900 Ma) similar to those from the Chiang Khong volcanic suite (Barr et al,. 2006).

6.4. Tectonic setting

As outlined above, geochemical features of the studied dykes suggest a LILE and LREE enriched mantle source, possibly modified through metasomatism of a lithospheric mantle component in a subduction-related environment (Pearce, 1982, 1996). The Th/Yb vs Nb/Yb (Pearce, 2008) plot indicates that the KKFTB volcanic suite is chemically affine to a continental volcanic arc tectonic setting. Figure 13a shows a spreading of the data from the IAT affine to MORB enriched rocks, and the drift in some calc-alkaline samples of Group III (Figure 13a), with the lowest values of Ti and V, seems to represents magnetite fractionation (Shervais, 1982). Therefore, the overall trend might not be compatible with an oversimplified tectonic framework, and any proposed geodynamic model must explain the following characteristics of the KKFTB mafic dykes: (1) high VAB geochemical affinity; (2) small volume; (3) isotopic evidences of crustal contamination in the late stages of the tectonic event, (5) signs of shallow spinel-bearing source for the dykes of the KKFTB, and (4) the temporal coincidence with a sequence of geologic events in central Thailand

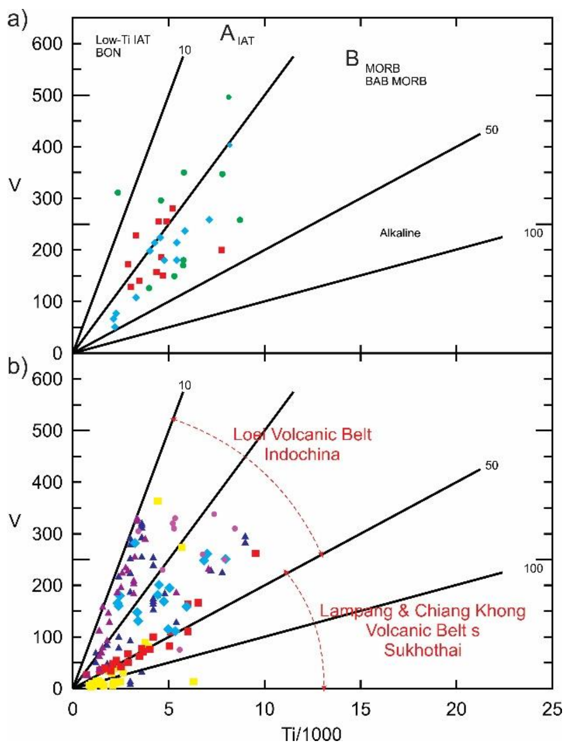

Figure 13. a) Binary plot of Ti/1000 vs V for the igneous and volcanic rocks of the KKFTB (Shervais, 1982); b) Binary plot of Ti/1000 vs V for the igneous and volcanic rocks of the Loei volcanic belt (see text for references) (Shervais, 1982).

6.4.1. Regional tectonic model

The previously discussed data might be representative of a tectonic setting within the KKFTB, where the arc-affinity rocks of the KKFTB represent the stage of the subduction of the slab (proximal BAB) between Sukhothai and Indochina. The post-collisional setting after the Sukhothai-Indochina collision, and the possible beginning of the collision between the westward Sibumasu terrane and the already amalgamated Indochina-Sukhothai might have caused break-up of the subducted back-arc slab in the Early Triassic. and the intrusion of a more MORB-like magma with higher levels of Ti depletion (Figure 9d,e,f; Figure 13a). This tectonic framework appears to be quite consistent throughout the entire Loei volcanic belt and the southwestern margin of Indochina (Figure 13b) (Panjasawatwong et al., 2006; Boonsoong et al., 2011; Salam et al., 2013; Vivatpinyo et al., 2014). However, on a more regional scale, the volcanic rocks in northern Thailand within the Sukhothai terrane (Lampang volcanic belt; Barr et al., 2000, 2006) seem to describe a more heterogeneous tectonic framework with a more MORB-like to alkaline affinity, probably describing the early stages of rifting between Sukhothai and Indochina during the Early Permian (Figure 13b). All these geochemical, isotopic and geochronological evidences make possible to constraint the evolution of the Indosinian tectonic on the southwestern margin of the Indochina block from the Mid-Permian with the emplacement of the dykes of Group I during the subduction of the back-arc basin between Sukhothai and Indochina. The $^{40}Ar/^{39}Ar$ ages on mica from the andesites of Group III move the early stages of the post-collisional setting to the Early Triassic (245 ± 6 Ma) and possibly the latest post-collisional stages to the Late Triassic (224± 1.9 Ma), as also constrained by $^{40}Ar/^{39}Ar$ ages of 238 ± 4 and 237 ± 12 Ma from andesitic samples near the northern Phetchabun fold-thrust and Loei volcanic belt (Intasopa, 1993). Increased basal heat flow due to mantle upwelling may have maintained relatively high temperatures during the latest stages of the post-tectonic exhumation. This might have driven to crustal partial melting and the consequent eruption of the Khao Yai rhyolite in the latest Triassic (207.1 ± 2.4 Ma) (Figure 14).

This model fits the available chronological data, but the lack of ages of highly mafic rocks from Group I means that this model is not unique. A second possible model would be that the different geochemical groups represent repeated injections of magma with increased crustal-component throughout the Permian and Triassic.

7. Conclusions

Our new geochemical, geochronological, and isotopic data reported in this study together with the geometrical relationship between the igneous rocks and the hosting stratigraphy; provide information on the petrogenesis and mantle source origins of the rocks that intruded the KKFTB within the southwestern margin of the Indochina block:

- Chemically the volcanic suite can be divided in three sub-groups. They share the distributions of elements such as HFSE (Nb, Ti, P), Th, Hf, Ta, Zr, and Y indicating high affinity with a continental volcanic arc tectonic setting. The KKFTB volcanic suite is associated with a range of stages in the development of the Indosinian Orogeny from the early tectonic stages in the Mid-Permian to the post collisional stages in the Late Triassic (Figure 14). These ages are in agreement with the end of Triassic deposition in the Mae Sariang and Fang formations on the eastern margin of the Sibumasu Block (Kamata et al., 2002; Srinak et al., 2007, Hara et al., 2013), and with the U-Pb zircon ages of 211-203 Ma for the Doi Inthanon orthogneisses and the granite (Dunning et al., 1995; Macdonald et al., 1993, 2010).

- The MREE/HREE ratios are explained by a similar spinel-bearing composition of the source for the whole KKFTB igneous suite that rose to the base of the lithosphere underneath the southwestern Indochina margin from the Mid Permian to Early Triassic. The isotopic variations show that the KKFTB igneous suite possibly underwent to degrees of crustal contamination, whereas the LREE/HFSE fractionation strengthens the dominance of a volcanic arc tectonic setting.

- In this slab break-off model, the detachment of a lithospheric slab allows the asthenosphere underlying the downgoing plate to flow up into the broken slab window above the sinking slab. The heat supply from the uprising asthenosphere can affect overlying thickened lithosphere, yielding characteristic isotopic trend. Asthenosphere upwelling induced partial melting of the overlying lithospheric mantle previously metasomatized during subduction. Thermal flux lowered the density of the remnant lithosphere of limited extent, with the possible consequent crustal melting. Heated crust facilitates the involvement of crustal components within mantle-derived melts through assimilation–fractionation–crystallization processes (von Blanckenburg and Davies, 1995). This geodynamic model might explain the extensive andesitic dyke swarm within the KKFTB, as well as the Khao Yai rhyolite south of the KKFTB.

$^{40}Ar/^{39}Ar$ ages from andesitic dykes of Group III (255 ± 6 Ma, 224 ± 1.9 Ma) and U-Pb crystallization age from rhyolite of Group III ($^{206}Pb/^{238}U$ zircon mean age of 207.1 ± 2.4 Ma) constrained the timing for the andesitic magmatism to the Late Triassic. These ages

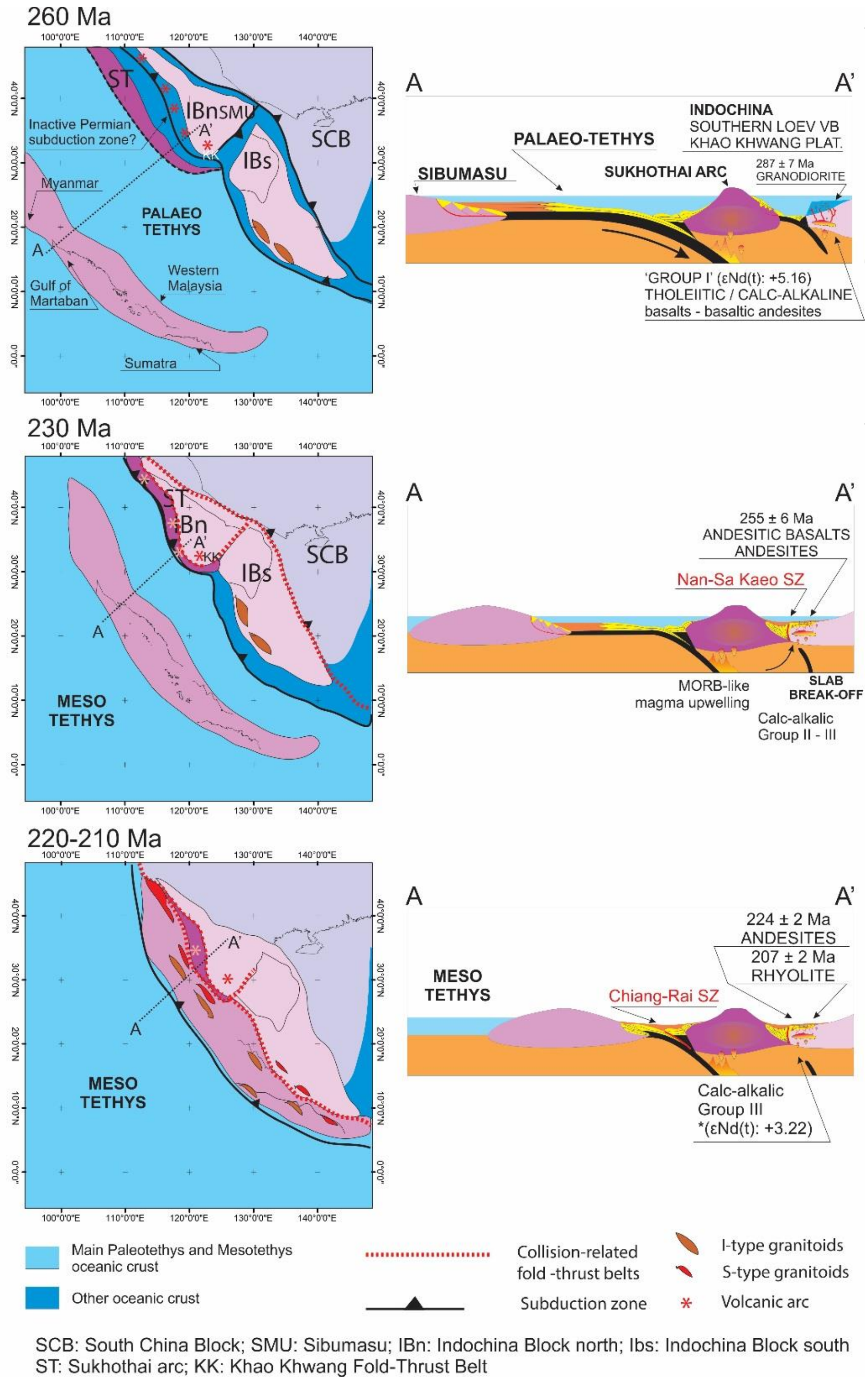

coupled with that of the dacite south of the KKFTB (213 ± 10 Ma) (By S. Meffre Pers. comm.) are interpreted to indicate that the break-up of the Sukhothai back-arc slab started during the Early Triassic following the complete subduction and Sukhothai-Indochina collision.

Figure 14. Palaeo-geographic schematic reconstructions of SE Asia based on the GPlate software reconstruction (rotation file in Supplementary data-3). The cross-sections show the tectonic development of the Indochina, Sukothai and Sibumasu blocks during the Early Permian to the Late Triassic; resulting in the emplacement of the Late Permian VAB to theTriassic MORB-like andesites ad rhyolites within the southern portion of the Loei volcanic belt

Acknowledgements

This work was funded by Australian Research Council Discovery Project #DP 120101460. ASC is funded by Australian Research Council grant #FT120100340. This is a contribution to IGCP projects #589 (Development of the Asian Tethyan Realm) and #628 (The Gondwana Map) and we gratefully acknowledge all the funding organizations. This publication forms TRaX Record #xxx.

References

Arboit, F., Collins, A. S., King, R., Morley, C. K., & Hansberry, R. 2014. Structure of the Sibumasu–Indochina collision, central Thailand: A section through the Khao Khwang Fold-Thrust belt.Journal of Asian Earth Sciences, 95, 182-191.

Arboit, F., Amrouch, K., Collins, A. S., King, R., & Morley, C. 2015. Determination of the tectonic evolution from fractures, faults and calcite twins on the south-western margin of the Indochina Block. Tectonics.

Barr S.M., Macdonald A.S. 1987. Nan River suture zone, northern Thailand, Geology, 15 907–910.

Barr, S. M., & Macdonald, A. S., 1991. Toward a late Paleozoic-early Mesozoic tectonic model for Thailand, Journal of Thai Geosciences, 1(1), 11-22.

Barr, S. M., Macdonald, A. S., Dunning, G. R., Ounchanum, P., & Yaowanoiyothin, W., 2000. Petrochemistry, U–Pb (zircon) age, and palaeotectonic setting of the Lampang volcanic belt, northern Thailand. Journal of the Geological Society, 157(3), 553-563.

Barr, S. M., Macdonald, A. S., Ounchanum, P., & Hamilton, M. A., 2006. Age, tectonic setting and regional implications of the Chiang Khong volcanic suite, northern Thailand. Journal of the Geological Society, 163(6), 1037-1046.

Beckinsale, R. D. 1979. Granite magmatism in the tin belt of south-east Asia. In Origin of granite batholiths (pp. 34-44). Birkhäuser Boston.

Bell, K., & Simonetti, A. 1996. Carbonatite magmatism and plume activity: implications from the Nd, Pb and Sr isotope systematics of Oldoinyo Lengai. Journal of Petrology, 37(6), 1321-1339.

Blundell, D. J. 1984. Deformation of the Caledonide lithosphere of Northwest Scotland. Tectonophysics, 109(1), 137-145.

Blundell, D. J. 2002. The timing and location of major ore deposits in an evolving orogen: the geodynamic context. Geological Society, London, Special Publications, 204(1), 1-12.

Boonsoong, A., Panjasawatwong, Y., & Metparsopsan, K. 2011. Petrochemistry and tectonic setting of mafic volcanic rocks in the Chon Daen–Wang Pong area, Phetchabun, Thailand. Island Arc, 20(1), 107-124.

Bunopas, S., 1982. Paleogeographic history of western Thailand and adjacent parts of South-east Asia: A plate tectonics interpretation. Geological Survey Division, Department of Mineral Resources, (No. 5).

Bunopas, S., Vella, P., 1983. in: Nutalaya, P. (Ed.), Tectonic and geologic evolution of Thailand Proceedings of the Workshop on Stratigraphic Correlation of Thailand and Malaysia, Haad Yai, Thailand, September 1983, vol. 1. Geological Society of Thailand and Geological Society of Malaysia, , pp. 212–232.

Chappell, B., & White, A. 1974. Two contrasting granite types. Pacific geology, 8(2), 173-174.

Charusiri, P., Chonglakmani, C., Daorerk, V., Supananthi, S., & Imasmut, S., 1994. Detailed stratigraphy of the Ban Thasi area, Lampang, northern Thailand: implications for paleoenvironments and tectonic history. In Bangkok Proc. Intern. Symp. Stratigraphic correlation of SE Asia (pp. 226-244).

Charusiri, P., Daorerk, V., Archibald, D., Hisada, K. I., & Ampaiwan, T., 2002. Geotectonic evolution of Thailand: a new synthesis. Journal of the Geological Society of Thailand, 1, 1-20.

Cho, D. L., Lee, S. R., & Armstrong, R. 2008. Termination of the Permo-Triassic Songrim (Indosinian) orogeny in the Ogcheon belt, South Korea: Occurrence of ca. 220 Ma post-orogenic alkali granites and their tectonic implications. Lithos, 105(3), 191-200.

Chutakositkanon, V., Hisada, K., Ueno, K., & Charusiri, P., 1997. New suture and terrane deduced from detrital chromian spinel in sandstone of the Nam Duk Formation, north-central Thailand. Preliminary report. In Intern. Conf. on Stratigraphy and Tectonic Evolution of Southeast Asia and the South Pacific, Bangkok (Vol. 368).

Cobbing, E. J., Mallick, D. I. J., Pitfield, P. E. J., & Teoh, L. H. 1986. The granites of the Southeast Asian tin belt. Journal of the Geological Society,143 (3), 537-550.

Cobbing, E. J. 1992. The granites of the South-East Asian tin belt (Vol. 10). HMSO.

Cobbing, E. J. 2011. Granitic rocks. The Geology of Thailand. The Geological Society, London, 441-457.

Della-Pasqua, F.N., Khin Zaw, 2002. Chemical affinities of Loei belt volcanic-intrusive rocks, Central Thailand. 16th Australian Geological Convention, Adelaide, Abstr. v.67, p.255.

Deniel, C., 1998. Geochemical and isotopic (Sr, Nd, Pb) evidence for plume-lithosphere interactions in the genesis of Grande Comore magmas (Indian Ocean). Chemical Geology, 144 (3-4), pp. 281-303.

Dunning, G. R., Macdonald, A. S., & Barr, S. M., 1996. Zircon and monazite U� Pb dating of the Doi Inthanon core complex, northern Thailand: implications for extension within the Indosinian Orogen. Tectonophysics, 251(1), 197-213.

Fossen, H., Gabrielsen, R. H., Faleide, J. I., & Hurich, C. A. 2014. Crustal stretching in the Scandinavian Caledonides as revealed by deep seismic data. Geology, 42(9), 791-794.

Gao, S., Luo, T. C., Zhang, B. R., Zhang, H. F., Han, Y. W., Zhao, Z. D., & Hu, Y. K., 1998. Chemical composition of the continental crust as revealed by studies in East China. Geochimica et Cosmochimica Acta, 62(11), 1959-1975.

Gardiner, N.J., Searle, M.P., Morley, C.K., Whitehouse, M.P., Spencer, C. J. and Robb, L.J., 2015. The closure of Paleo-Tethys in Eastern Myanmar and Northern Thailand from zircon U-Pb and Hf isotope data. Gondwana Research

Ghani, A. A., Searle, M., Robb, L., & Chung, S. L. 2013. Transitional IS type characteristic in the Main Range Granite, Peninsular Malaysia. Journal of Asian Earth Sciences, 76, 225-240.

Hansberry, R. L., King, R., Collins, A. S., & Morley, C. K. 2014. Complex structure of an upper-level shale detachment zone: Khao Khwang Fold-Thrust belt, Central Thailand. Journal of Structural Geology,67, 140-153.

Hara, H., Kon, Y., Usuki, T., Lan, C.-Y., Kamata, Y., Hisada, K.-I., Ueno, K., Charoentitirat, T., and Charusiri, P., 2013. U-Pb ages of detrital zircons within the Inthanon Zone of the Paleo-Tethyan subduction zone, northern Thailand: New constraints on accretionary age and arc activity. Journal of Asian Earth Sciences, 74, 50-61.

Hastie, A. R., Kerr, A. C., Pearce, J. A., & Mitchell, S. F., 2007. Classification of altered volcanic island arc rocks using immobile trace elements: development of the Th–Co discrimination diagram. Journal of Petrology, 48(12), 2341-2357.

Hirajima, T., Ishiwatari, A., Cong, B., Zhang, R., Banno, S., & Nozaka, T., 1990. Coesite from Mengzhong eclogite at Donghai county, northeastern Jiangsu province, China. Mineralogical Magazine, 54(377), 579-583.

Hutchison, C. S., 1975. Ophiolite in southeast Asia. Geological Society of America Bulletin, 86(6), 797-806.

Intasopa, S. B., 1993. Petrology and geochronology of the volcanic rocks of the central Thailand volcanic belt. University of New Brunswick (Canada).

Intasopa, S., Dunn, T., 1994. Petrology and Sr–Nd isotopic systems of the basalts and rhyolites, Loei, Thailand. Journal Southeast Asian Earth Sciences 9, 167–180.

Irvine, T., & Baragar, W. 1971. A guide to the chemical classification of the common volcanic rocks. Canadian journal of earth sciences, 8(5), 523-548.

Jackson, S.E., Pearson, N.J., Griffin, W.L., Belousova, E.A., 2004. The application of laser ablation-inductively coupled plasma-mass spectrometry to in-situ U/Pb zircon geochronology. Chemical Geology 211, 47–69.

Jochum, K.P., Arndt, N.T., Hofmann, A.W., 1991. NbThLa in komatiites and basalts: constraints on komatiite petrogenesis and mantle evolution. Earth and Planetary Science Letters, 107 (2), pp. 272-289.

Jourdan, F., Renne, P.R., 2007. Age calibration of the Fish Canyon sanidine 40Ar/39Ar dating standard using primary K–Ar standards. Geochimica et Cosmochimica Acta 71, 387–402.

Jourdan, F., Bertrand, H., Schärer, U., Blichert-Toft, J., Féraud, G., & Kampunzu, A. B., 2007. Major and trace element and Sr, Nd, Hf, and Pb isotope compositions of the Karoo large igneous province, Botswana–Zimbabwe: lithosphere vs mantle plume contribution. Journal of Petrology, 48(6), 1043-1077.

Jungyusuk, N., Khositanont, S., 1992. in: Piencharoen, C. (Ed.), Volcanic rocks and associated mineralization in Thailand Proceedings of the National Conference on Geologic Resources of Thailand—Potential for Future Development, Bangkok, Thailand, November 1992. Department of Mineral Resources, pp. 528–532.

Kamata, Y., Sashida, K., Ueno, K., Hisada, K. I., Nakornsri, N., & Charusiri, P., 2002. Triassic radiolarian faunas from the Mae Sariang area, northern Thailand and their paleogeographic significance. Journal of Asian Earth Sciences, 20(5), 491-506.

Kamvong T., Charusiri P. & Intasopa B. S. 2006. Petrochemical characteristics of igneous rocks from the Wang Pong area, Phetchabun, north central Thailand: Implication for tectonic setting. Journal of the Geological Society of Thailand **1**, 9–26.

Kelemen, P. B., Shimizu, N., & Dunn, T., 1993. Relative depletion of niobium in some arc magmas and the continental crust: partitioning of K, Nb, La and Ce during melt/rock reaction in the upper mantle. Earth and Planetary Science Letters, 120(3), 111-134.

Kepezhinskas, P., McDermott, F., Defant, M. J., Hochstaedter, A., Drummond, M. S., Hawkesworth, C. J., Bellon, H., 1997. Trace element and Sr Nd Pb isotopic constraints on a three-component model of Kamchatka Arc petrogenesis. Geochimica et Cosmochimica Acta, 61(3), 577-600.

Khositanont s., Panjasawatwong Y., Ounchanum P., Thanasuthipitak T., Khinz., Meffre S. 2008.

Petrochemistry and zircon age determination of Loei-Phetchabun volcanic rocks. In Chutakositkanon

V., Sutthirat C. and Charoentitirat T. (eds.) Proceedings of the International Symposia on Geoscience

Resources and Environments of Asian Terranes (GREAT 2008), pp. 272–8, 4th IGCP 516 and 5th

APSEG, Bangkok.

Koppers, A.A.P., 2002. ArArCALC — software for 40Ar/39Ar age calculations. Computers & Geosciences 28, 605–619.

Lindh, A., Andersson, U. B., Lundqvist, T., & Claesson, S., 2001. Evidence of crustal contamination of mafic rocks associated with rapakivi rocks: an example from the Nordingrå complex, Central Sweden. Geological Magazine, 138(04), 371-386.

Macdonald, A.S., Barr, S.M., Dunning, G.R., and Yaowanoiyothin, W., 1993. The Doi Inthanon metamorphic core complex in NW Thailand: age and tectonic significance. Journal of Southeast Asian Earth Sciences, 8, 117-125.

Macdonald, A.S., Barr, S.M., Miller, B.V., Reynolds, P.H., Rhodes, B.P. and Yokart, B. 2010. P-T-t constraints on the development of the Doi Inthanon metamorphic core complex domain and implications for the evolution of the western gneiss belt, northern Thailand. Journal of Asian Earth Sciences, 37, 82-104.

MacLean, W. H., & Barrett, T. J., 1993. Lithogeochemical techniques using immobile elements. Journal of geochemical exploration, 48(2), 109-133.

Marhotorn K., Mizuta T., Ishiyama D. et al. 2008. Petrochemistry of igneous rocks in the southern parts of the Chatree gold mine, Pichit, central Thailand. In Chutakositkanon V., Sutthirat C. and Charoentitirat T. (eds.) Proceedings of the International Symposia on Geoscience Resources and Environments of Asian Terranes (GREAT 2008), pp. 289–98, 4th IGCP 516 and 5th APSEG, Bangkok.

Meschede, M,. 1986. A method of discriminating between different types of mid-ocean ridge basalts and continental tholeiites with the Nb-Zr-Y diagram. Chemical geology, 56(3), 207-218.

Metcalfe, I. 2000. The Bentong–Raub suture zone. Journal of Asian Earth Sciences, 18(6), 691-712. Metcalfe, I., 2005. Asia: South-East. In: Selley, R.C., Cocks, L.R.M., Plimer, I.R. (Eds.), Encyclopedia of Geology, Elsevier, Oxford, vol. 1, 169–198.

Metcalfe, I., 2011. Tectonic framework and Phanerozoic evolution of Sundaland. Gondwana Research, 19(1), 3-21.

Metcalfe, I., 2013. Tectonic evolution of the Malay Peninsula. Journal of Asian Earth Sciences, 76, 195-213.

Metcalfe, I., and M. Sone, 2008. Biostratigraphy and palaeobiogeography of Lower Permian (lower Kungurian) conodonts from the Tak Fa Formation (Saraburi Limestone), Thailand. Palaeogeography, Palaeoclimatology, Palaeoecology 257.1, 139-151.

Miyashiro, A., Shido, F., 1975. Tholeiitic and calc-alkalic series in relation to the behaviors of titanium, vanadium, chromium, and nickel. American Journal of Science, 275(3), 265-277.

Morley, C. K. 2012. Late Cretaceous–early Palaeogene tectonic development of SE Asia. Earth-Science Reviews, 115(1), 37-75.

Morley, C.K., Ampaiwan, P., Thanudamrong, S., Kuenphan, N., Warren, J., 2013. Development of the Khao Khwang Fold and Thrust Belt: Implications for the geodynamic setting of Thailand and Cambodia during the Indosinian Orogeny. Journal of Asian Earth Sciences, 62, 705-719.

Nakamura, N., 1974. Determination of REE, Ba, Fe, Mg, Na and K in carbonaceous and ordinary chondrites. Geochimica et Cosmochimica Acta, 38(5), 757-775.

Nakchaiya, T., Mitzuta, T., Ishiyama, D., Takashima, I., Won-In, K., Lunwongsa, V., & Charusiri, P., 2008. Stratigraphy and petrochemistry of volcanic rocks in the Chatree gold mine, central Thailand: Implication for tectonic setting. In Proceedings of the International Symposia on Geoscience Resources and Environments of Asian Terranes (GREAT 2008), 4th IGCP526 and 5th APSEG, Bangkok, Thailand (pp. 302-311).

Ng, S. W. P., Whitehouse, M. J., Searle, M. P., Robb, L. J., Ghani, A. A., Chung, S. L., Roselee, M. H. 2015a. Petrogenesis of Malaysian tin granites: Part 1. Geochemistry and fractional crystallization of the Malaysian tin granites. Geological Society of America Bulletin.

Ng, S. W. P., Whitehouse, M. J., Searle, M. P., Robb, L. J., Ghani, A. A., Chung, S. L., Roselee, M. H. 2015b. Petrogenesis of Malaysian tin granites: Part 2. High precision U–Pb zircon geochronology of the Malaysian tin granites and tectonic model for their emplacement history. Geological Society of America Bulletin.

Noisagool, S., Boonchaisuk, S., Pornsopin, P., & Siripunvaraporn, W. 2014. Thailand's crustal properties from tele-seismic receiver function studies. Tectonophysics, 632, 64-75.

Pearce, J. A., 1982. Trace element characteristics of lavas from destructive plate boundaries. Andesites, 525-548.

Pearce, J. A., 1983. Role of the subcontinental lithosphere in magma genesis at active continental margins. (pp. 230-249).

Pearce, J. A., 1996. A user’s guide to basalt discrimination diagrams. Trace element geochemistry of volcanic rocks: applications for massive sulphide exploration. Edited by DA Wyman. Geological Association of Canada, Short Course Notes, 12, 79-113.

Pearce, J. A. 2008. Geochemical fingerprinting of oceanic basalts with applications to ophiolite classification and the search for Archean oceanic crust. Lithos, 100(1), 14-48.

Panjasawatwong, Y., Zaw, K., Chantaramee, S., Limtrakun, P., & Pirarai, K., 2006. Geochemistry and tectonic setting of the Central Loei volcanic rocks, Pak Chom area, Loei, northeastern Thailand. Journal of Asian Earth Sciences, 26 (1), 77-90.

Payne, J.L., Ferris, G.M., Barovich, K.M., Hand, M., 2010. Pitfalls of classifying ancient magmatic suites using tectonic discrimination diagrams: an example from the Paleoproterozoic Tunkillia Suite, Gawler Craton, Australia. Precambrian Research 177, 227–240.

Okamura, S., Wu, G.Y., Zhao, C.H., Kagami, H., Yoshida, T. & Kawana, Y. 1997. Geochemistry of Mesozoic intracontinental basalts from Yunnan, southern China: implications for geochemical evolution of the subcontinental lithosphere. Mineralogy and Petrology, 60, 81–98.

Rapp, R.P., Shimizu, N., Norman, M.D., 2003. Growth of early continental crust by partial melting of eclogite. Nature, 425 (6958), pp. 605-609.

Renne, P.R., Balco, G., Ludwig, K.R., Mundil, R., Min, K., 2011. Response to the comment by W.H. Schwarz et al. on “Joint determination of K-40 decay constants and Ar-40*/K-40 for the Fish Canyon sanidine standard, and improved accuracy for Ar-40/Ar-39 geochronology” by PR Renne et al. (2010). Geochimica et Cosmochimica Acta 75, 5097–5100.

Ricou, L. E., 1994. Tethys reconstructed: plates, continental fragments and their Boundaries since 260 Ma from Central

America to South-eastern Asia. Geodinamica Acta, 7(4), 169-218.

Ridd, M. F., & Morley, C. K., 2011. The Khao Yai Fault on the southern margin of the Khorat Plateau, and the pattern of faulting in Southeast Thailand. Proceedings of the Geologists' Association, 122(1), 143-156.

Robinson, P., 2003. XRF analysis of flux-fused discs. Geoanalysis 2003. InThe 5th International Conference on the Analysis of Geological and Environmental Materials. Geological Survey of Finland and International Association of Geoanalysis. Finland: Rovaniemi, Abstracts (p. 90).

Rollinson H., 1993. Using geochemical data: evaluation, presentation, interpretation: Longman scientific and technical. Harlow, pp. 352 .

Salam, A., Zaw, K., Meffre, S., McPhie, J., & Lai, C. K., 2014. Geochemistry and geochronology of the Chatree epithermal gold–silver deposit: Implications for the tectonic setting of the Loei Fold Belt, central Thailand. Gondwana Research, 26(1), 198-217.

Searle, M. P., Whitehouse, M. J., Robb, L. J., Ghani, A. A., Hutchison, C. S., Sone, M., Oliver, G. J. H. 2012. Tectonic evolution of the Sibumasu-Indochina terrane collision zone in Thailand and Malaysia: constraints from new U-Pb zircon chronology of SE Asian tin granitoids. Journal of the Geological Society, 169, 489.

Shervais, J. W., 1982. Ti-V plots and the petrogenesis of modern and ophiolitic lavas. Earth and planetary science letters, 59(1), 101-118.

Sláma, J., Kosler, J., Condon, D.J., Crowley, J.L., Gerdes, A., Hanchar, J.M., Horstwood,M.S.A., Morris, G.A., Nasdala, L., Norberg, N., Schaltegger, U., Schoene, B., Tubrett, M.N., Whitehouse, M.J., 2008. Plesovice zircon — a new natural reference material for U–Pb and Hf isotopic microanalysis. Chemical Geology, 249, 1–35.

Sone, M., Metcalfe, I., 2008. Parallel Tethyan sutures in mainland Southeast Asia: new insights for Palaeo-Tethys closure and implications for the Indosinian orogeny. Comptes Rendus Geoscience, 340(2), 166-179.

Srinak, N., Hisada, K.-I., Kamata, Y., and Charusiri, P., 2007. Stratigraphy of the Mae Sariang Group of Northwestern Thailand: Implication for palaeoenvironments and tectonic setting. The Natural History Journal of Chulalongkorn University, 7, 87-108.

Sun, S.S., McDonough, W.F., 1989. in: Saunders, A.D., Norry, M.J. (Eds.), Chemical and isotopic systematics of oceanic basalts—implications for mantle composition and processes Magmatism in Ocean Basins. Geological Society Special Publication 42, pp. 313–345.

Ueno, K., & Hisada, K., 1999. Closure of the Paleo-Tethys caused by the collision of Indochina and Sibumasu. Chikyu Monthly, 21, 832-839.

Ueno, K., & Hisada, K. I., 2001. The Nan-Uttaradit-Sa Kaeo Suture as a Main Paleo-Tethyan Suture in Thailand: Is it Real?. Gondwana Research, 4(4), 804-806.

Van Achterbergh, E., Ryan, C.G., Jackson, S.E., Griffin, W.L., 2001. Data reduction software for LA-ICP-MS. In: Sylvester, P.J. (Ed.), Laser-ablation-ICPMS in the Earth Sciences; Principles and Applications. Mineralogical Association of Canada, Short Course Handbook, Ottawa, pp. 239–243.

Vivatpinyo, J., Charusiri, P., & Sutthirat, C., 2014. Volcanic Rocks from Q-Prospect, Chatree Gold Deposit, Phichit Province, North Central Thailand: Indicators of Ancient Subduction. Arabian Journal for Science and Engineering, 39(1), 325-338.

von Blanckenburg, F., Davis, J.H., 1995. Slab breakoff: a model for syncollisional magmatism and tectonics in the Alps. Tectonics 14, 120–131.

Wilhem, C., Windley, B. F., & Stampfli, G. M. 2012. The Altaids of Central Asia: a tectonic and evolutionary innovative review. Earth-Science Reviews, 113(3), 303-341.

Winchester, J. A., & Floyd, P. A., 1977. Geochemical discrimination of different magma series and their differentiation products using immobile elements. Chemical geology, 20, 325-343.

Wood, D. A., 1979. A variably veined suboceanic upper mantle—genetic significance for mid-ocean ridge basalts from geochemical evidence. Geology, 7(10), 499-503.

Wood, D. A., 1980. The application of a Th-Hf-Ta diagram to problems of tectonomagmatic classification and to establishing the nature of crustal contamination of basaltic lavas of the British Tertiary volcanic province. Earth and Planetary Science Letters, 50, pp. 11 -30.

Yoder, H. S., JR. 1973. Contemporaneous basaltic and rhyolitic magmas. American Mineralogist, 58, pp. 153 - 17 1.

Xu, J.F., Wang, Q., Xu, Y.G., Zhao, Z.H., Xiong, X.L., 2001. Geochemistry of Anjishan intermediate-acid intrusive rocks in Ningzhen area: Constraint on the origin of the magma with HREE and Y depletion. Acta Petrologica Sinica, 17 (4), pp. 576-584.

Yang, K., Mo, X. & Zhu, Q. 1994. Tectono-volcanic belts and late Paleozoic–early Mesozoic evolution of southwestern Yunnan, China. Journal of Southeast Asian Earth Sciences, 10, 245–262.

Zhang J., Herzberg, C., 1994. Melting experiments on anhydrous peridotite KLB-1 from 5.0 to 22.5 GPa. Journal of Geophysical Research, 99 (B9), pp. 17,729-17,742.

Zhang, S. Q., Mahoney, J. J., Mo, X. X., Ghazi, A. M., Milani, L., Crawford, A. J., Zhao, Z. D., 2005. Evidence for a widespread Tethyan upper mantle with Indian-Ocean-type isotopic characteristics. Journal of Petrology, 46(4), 829-858.

Chapter VII

Arboit, F., Amrouch, K., Morley, C., Collins, A. S., & King, R. (2016). The effect of active margin tectonic on palaeostress magnitudes: Results after calcite twin analysis in central Thailand. *Tectonophysics*.

The effect of active margin tectonic on palaeostress magnitudes: Results after calcite twin analysis in central Thailand

ABSTRACT

Using the Khao Khwang fold–thrust belt in central Thailand as case study, we handled data from calcite twinning analysis in order to propose the quantification of the effective principal palaeostresses magnitudes since the onset of the early stages of the Indosinian orogeny. We also combined the differential stress estimates from mechanically-induced calcite twins with geochronological data in order to constrain the timing of the palaeoburial depth and subsequent uplift by folding within the Khao Khwang fold–thrust belt. The proposed mechanical scenario is based on the time-constrained kinematic sequence of fracturing, faulting, and folding in the strata of the carbonate formations of the Saraburi Group. Cross-checking the data on the palaeostress orientations, regimes, and differential stress magnitudes with rock mechanics analysis; we provided data on the principal stress magnitudes for each tectonic stage that developed during the Indosinian orogeny. Further, $^{40}Ar/^{39}Ar$ and U-Pb geochronological data allowed to place reliable constraints on the amount and rate of vertical uplift of the carbonate formations of the Saraburi-Group.

1. Introduction

The state of stress in rocks is generally anisotropic and is represented by the magnitudes of the principal axes of the stress ellipsoid. In positive compression, the longest axis is the ellipsoid's major stress (σ_1), the intermediate axis is the intermediate stress (σ_2), and the shortest axis is the minimum stress (σ_3) (Jaeger and Cook, 1969, Sibson, 1977; Price and Cosgrove, 1990). The distribution of the modern-day stress-field states (e.g. Zoback, 1992; Sandiford et al., 2004), as well as the palaeostress orientation and differential stress values (Lacombe et al., 1992; Lacombe and Laurent, 1996; Lacombe, 2001; Lacombe et al., 2007; Lacombe, 2007; Amrouch et al., 2010a), have been deeply investigated in the last decades. However, quantitative estimates of effective palaeostress magnitudes through geological time are difficult to make and have been well studied only in the last years (Lacombe et al., 2009; Amrouch et al., 2011). Never-the-less estimates of the palaeostress states from rocks affected by tectonic events are of fundamental importance for addressing unsettled problems such as the mechanical behaviour of geological materials and deciphering various tectonic mechanisms, from those related to plate motions at a large scale to those causing jointing and faulting or even microstructures at a smaller scale (Lacombe, 2007; Amrouch et al., 2010a, 2010b). For these purposes, several analytical methodologies were developed in the last decades (Etchecopar et al., 1981; Angelier et al., 1982; Armijo et al., 1982; Gephart and Forsyth, 1984; Michael, 1984; Carey-Gailhardis and Mercier, 1987; Reches, 1987; Angelier, 1990; Gephart, 1990; Marrett and Almandinger, 1990; Will and Powell, 1991; Yin and Ranalli, 1993). Dynamically recrystallized grain size, along with well-calibrated relationship between the stress state and the re-arrangement of crystal lattices, are parameters associated with dislocation creep of crystalline solids. This is especially important as a stress indicator via piezometer calibrations, where quantification of palaeostresses can be numerically expressed using calcite twinning (Lacombe, 2001; Amrouch et al., 2011). Here, following the analysis in Arboit et al. (2015), we use calcite twinning analysis using Etchecopar Method (Etchecopar, 1984) to provide estimates of maximum differential stress (Lacombe, 2007; Amrouch et al., 2010a). This contribution is aimed at presenting the effect of the differential stress, and constraining the effective principal stress magnitudes during the Indosinian orogeny, in order to better understand the complicate geodynamic evolution of the Khao Khwang fold-thrust belt since the Mid Permian in central Thailand.

2. Tectonic framework

The Khao Khwang fold-thrust belt (KKFTB) (Figure 1) lies in the Saraburi Province in central Thailand, and it is tectonically located on the SW margin of the Indochina Block (Bunopas, 1982; Metcalfe, 2011; Morley et al., 2013). It is bounded to the north and to the east by the Khorat Plateau, which trends NW-SE, and to the south by the Cenozoic Mae Ping strike-slip fault (Morley, 2007; Morley et al., 2013). This region has undergone a complex geological history, which mainly developed during the Indosinian tectonic event, this is characterised by two different subduction and collision episodes that covered the period from ca. 260 to 200 Ma (Late Permian to Late Triassic) (Sone and Metcalfe, 2008; Morley, 2007; Morley et al., 2013, Arboit et al., 2015). The resulting tectonic belts and suture zones in Thailand have a dominant N-S trend. The Indosinian orogeny in Thailand has been considered to involve two stages of collision during the Triassic-Early Jurassic between the three main terranes, which, from east to west, are: Indochina, Sukhothai and Sibumasu (Figure 1a) (Sone and Metcalfe, 2008; Metcalfe, 2013). Additionally, beyond Thailand, to the NE, coeval Triassic collision also occurred between both the Indochina/South China Blocks (Cai and Zhang, 2009) and the South/North China Cratons (Dong et al., 2015).

The Sukhothai Terrane is believed to have been a volcanic arc that rifted away from the south-western margin of Indochina in the Early Permian, as consequence of rollback above the subducting Paleo-Tethys, and opening of the back-arc basin between the volcanic arc (Sukhothai) and the Indochina Terrane (Sone and Metcalfe, 2008). However, the geodynamic evolution on the southwestern margin of the Indochina terrane has been poorly understood. The first tectonic event on the Indochina margin has been recently constrained as resulting from the latest Permian (255~4 Ma; Arboit et al., 2016) collision as the Sukhothai Terrane re-amalgamated with Indochina, with the related closure of the Permian back-arc basin (Metcalfe, 2005; Sone and Metcalfe, 2008; Metcalfe, 2013). Subsequently, in the Late Triassic, during the late stages of the Indosinian collision, the Sibumasu Terrane is thought to have collided with the now combined Indochina/Sukhothai Terrane, causing the complete closure of the Paleo-Tethys in this region. The Indosinian orogeny has usually been thought as resulting from the collisions between these two strongly linear terranes and Indochina. However, despite the common N-S trend of the suture zones (Nan-Sra Kaeo and Changning-Menglian S.Z.) (Figure 1a) between the blocks involved in the collision, in some areas the tectonic trend diverges from simply N-S to NW-SE and E-W trends. The most prominent of these regions is the Saraburi region (Morley et al., 2013; Arboit et al., 2014). One explanation for the different trend is that the belt was rotated from a N-S direction to a more E-W orientation by motion along the NW-SE trending Cenozoic Mae Ping Fault Zone; Tapponier et al. (1986) proposed sinistral displacement of about 150 km on this fault. However, even after restoring this offset, and applying a relative clockwise rotation of about 25°-30° (Charusiri, 2006; Cung and Geissman, 2013; Singsoupho et al. 2014) to the northern side of the fault, the boundary does not restore to a N-S orientation (Anchuelas et al., 2012; Mochales et al., 2012; Morley et al., 2013).

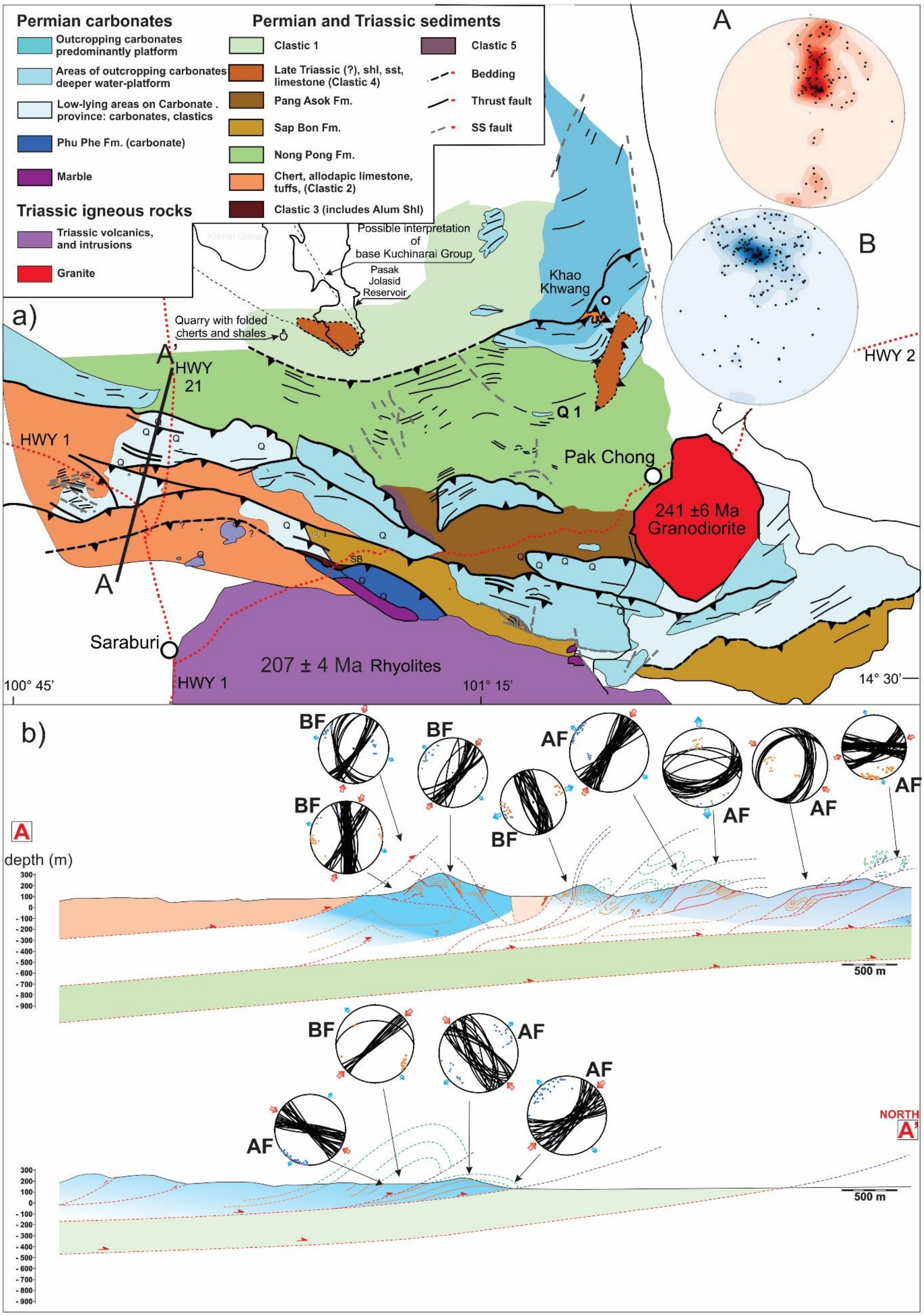

Figure 1. Geological map of the Khao Khwang Fold and Thrust Belt. It has been modified from Warren et al., (2014) to show possible interpretations of the stratigraphy as a consequence of this study. (A) Stereonet of poles to bedding for the region, (B) Stereonet of poles to main thrusts along Highway 21. b) N-S oriented regional cross-section A-A' through the southern portion of the Saraburi Region, the Khao Khwang Fold-and-Thrust Belt (see Figure 1a for location). BF: before folding; AF: after folding.

Alternatively, the deflection may be due to the original orientation of the continental margins, or possibly due to a poorly documented intra-Indochina suture, that strikes east-west, and lies close to the southern margin of the Khorat Plateau (Hutchinson, 1975; Morley et al. 2013). The sequence of deformation includes a layer-parallel shortening event (LPS) that is addressed to be the result of the Sukhothai-Indochina collision (Arboit et al., 2015). This sequence of fracturing has been recently constrained (Arboit et al., 2015), with the oldest system of conjugated fractures striking 035° to 055° at high angle to the bedding. The second set of conjugate fractures is the more widespread throughout the Saraburi region; it took place during the Indosinian stress build-up (LPS event) and was probably coeval to the Sukhothai-Indochina collision (Arboit et al., 2015). This set of fracture in the southern portion of the KKFTB seems to have formed under the same stress tensor that is responsible for the formation of conjugate sets of newly formed reverse faults that strike parallel to the major anticlines in the area. The majority of the folds in the southern portion of the KKFTB developed in response to thrusting as fault bend, detachment, and fault propagation folds (Morley et al., 2013; Arboit et al., 2014); hence, thrusting is interpreted as coeval with the growth of the major anticlines. The third stage of fractures developed during the Indosinian event with a general low angle and striking 200° to 240° appear to be almost synchronous or to have formed just after the main LPS event (Figure 1b). The subsequent stress tensor is associated with a stage of fold-tightening (Warren et al., 2015; Arboit et al,. 2015). This stage is characterised by the reactivation of fracture set-2 developed during the main LPS event, and by the newly formed fractures striking 070° to 090° mainly detected on the hinge zones and probably developed in response to the fold-tightening parallel to the fold axis. The fifth stage of fracturing is the latest brittle event that seems to have affected the southern portion of the KKFTB, it is marked by strike-slip faults, tail-cracks associated with shear veins and the reactivation of reverse faults previously emplaced during the main LPS event (Figure 1).

3. Methodologies

The palaeostresses that affected central Thailand since the Mid Permian were correlated to the stress that builded up mainly during the Indosinian event (Morley et al., 2013; Arboit et al., 2015). The orientations and the regimes were determined from fractures, faults, and calcite twinning analysis using the Calcite Stress Inversion Technique (CSIT) (Etchecopar, 1984; Lacombe and Laurent, 1992, 1996; Lacombe, 2001; Amrouch et al., 2010a; Amrouch et al., 2010c). This methodology computes the mean stress tensor with both the principal stress orientations and the associated differential stress magnitudes from mechanically developed sets of calcite twin data.

The sequence of tectonic events detected with the calcite twins has been constrained with respect to the fracturing/faulting development by the comparison of the reduced stress tensors T' recorded both within the matrix of the rock and in the successive vein sets that developed since the

Mid Permian (Arboit et al., 2015). Knowing the reduced stress tensors T', we quantified the deviatoric stress tensors T_D as (Lacombe, 2001) (1):

$$T_D = T - \left[\frac{\sigma_1+\sigma_2+\sigma_3}{3}\right] I \ (1)$$

The quantification of the deviatoric stress tensors T_D, depends upon: the complete stress tensor (T), the three principal stresses (σ_1, σ_2, σ_3), the unit matrix (I), and the determination of a fifth parameter of the complete stress tensor that is the scalar peak differential stress (σ_1–σ_3). This determination relies on the existence of a constant Critical Resolved Shear Stress (CRSS) for twinning τ_a (smallest resolved shear stress; for more details see Etchecopar, 1984), and on the accurate estimate of $\tau_a{}'$ that correspond to the normalized value of the CRSS for the reduced stress tensor used for calculation (Lacombe, 2001; Amrouch et al., 2010a).

However, the reduced stress tensor concept is based on the shape factor of the stress ellipsoid (Angelier, 1994), and it is independent of the absolute stress magnitudes, since it considers only the relative ratios of principal stress magnitudes. Therefore, it is independent of the pore-water pressure (σ_p) under hydrostatic conditions (i.e. pore-water pressure is smaller than the minimum principal stress magnitudes $\sigma_p < \sigma_3$), if we adhere to those conditions, the thickness of the sedimentary column and the relative overburden is the only effective influence. The T_D lacks in the isotropic module in order to define the complete stress tensor (e.g. Lacombe, 2001); hence, the palaeostress orientations and regimes were here combined with rock mechanics data; these data were successively plotted as a Mohr circle in order to extrapolate the effective principal stress magnitudes (Lacombe and Laurent, 1996; Lacombe et al., 2007, 2009; Amrouch et al., 2011). The values of the differential stresses (Table 1 – Appendix D) were estimate from calcite twin analyses (Arboit et al., 2015). For a specific tectonic event, the quantification of the complete stress tensor consists of determining the effective values of the vertical effective stress (σ_{veff}), σ_{e1}, σ_{e2}, and σ_{e3}, these values must be compatible with newly formed (Mohr-Coulomb criterion) and reactivated pre-existing planes (Byerlee's friction law; Byerlee, 1978) (Lacombe and Laurent, 1992; Lacombe, 2001; Amrouch et al., 2011).

The internal mechanical properties of the limestones outcropping in the southern and eastern portion of the KKFTB (Khao Khad formations and Saraburi marble) were here used to describe the intrinsic failure envelope of the Khao Khad Formation (Figure 2a) (Tepnarong, 2001).

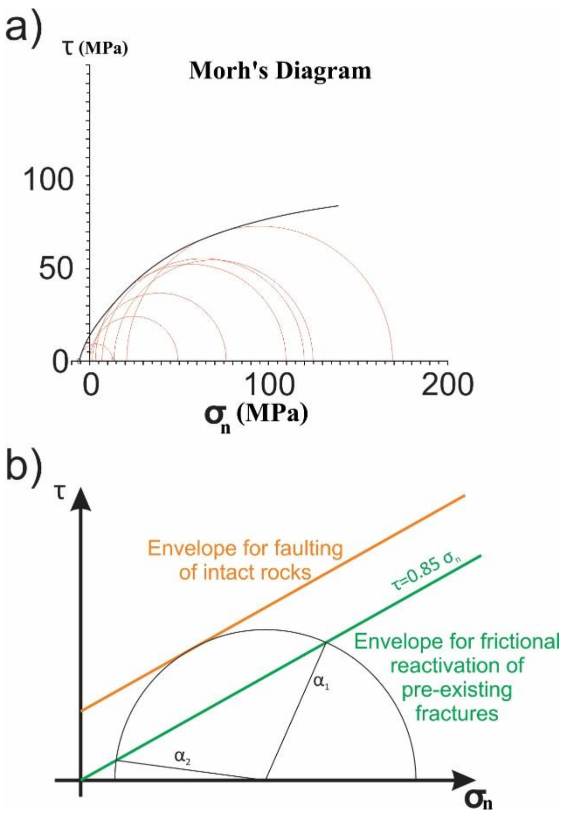

Figure 2. a) crack development curve (CDC) (red circles) from rock mechanic tests. b) Mohr circle representation of the orientations of planes that would reactivate in a given state of stress according to equations 3 and 4

given in the text. The angular range 2α2 - 2α1, shown at the intersection with the green line, defines the orientational spectrum of the reactivable planes.

The objective of the triaxial compressive strength test was to determine the compressive strengths of Saraburi limestones under various confining pressures. The sample preparation and test procedure followed the applicable ASTM (ASTM D2664-86) and ISRM suggested method (Brown, 1981). A total of 5 specimens have been tested under various confining pressures. The Length/Diameter of the specimen equals 2.0. The samples underwent to tension and compression under confining pressures of 1.7, 3.4, 6.9, 13.8 and 20.7 MPa, the deviatoric stress necessary to obtain failure within the samples were calculated at each step (Table 2 – Appendix C). The relationship between the applied stresses and the crack development is the physical expression of the equation (Hoek, 1990): $\tau = c_i + \sigma_n \tan \Phi$, where c_i is the cohesive internal strength calculated from the tangent to the envelope, and Φ is the Mohr-Coulomb friction angle. The data from Tepnarong (2001) were then used to calculate the Mohr circles corresponding to the crack and shear development at different confining pressures following the methodology of Lacombe(2001) and Amrouch et al. (2011).

4. Palaeostress conditions

Bergerat (1987), and Angelier (1989) proposed that palaeostress could be estimated based on determining the most easily derivable stress value, which is the vertical stress (σ_v). This value is controlled by the thickness of the overburden, the average density of the rock column (ρ= 2500 kg/m^3) under hydrostatic fluid pressure conditions, and the gravity acceleration (g= 9.82 ms^{-2}). Jaeger and Cook (1969); Byerlee (1970, 1978) and Sibson (1994) demonstrated that at intermediate pressures (5< σ_n<200 MPa; and τ= 50 MPa + 0.6 σ_n) rock type does not influence friction coefficient values in the failure criteria for reactivation of pre-existing shear surfaces. Additionally the initial surface roughness has little effect on friction values and the failure criteria for pre-existing shear surfaces can be approximated by equation (2):

$$\tau = [\mu_w|0.85|]\sigma_n \quad (2)$$

where τ, μ_ω and σ_n are respectively the shear stress, the coefficient of sliding friction and the normal stress. Palaeostress analysis of reactivated faults is based on the kinematic theory of reactivation for a given state of stress. This theory predicts: (I) the favourable orientations of the fault planes for reactivation, and (II) the direction along which slip is likely to occur on a given fault surface (Wallace, 1951; Bott, 1959). The angular range, α_1, α_2, defines the spectrum of the plane orientations that qualify for reactivation in a given stress state and can be predicted by equations 3 and 4 as follows (Jaeger and Cook, 1969) (Figure 2b):

$$\alpha_1 = \frac{1}{2\pi} - \cos^{-1}\left\{\frac{\frac{\mu_w}{(\mu_w^2+1)^1}}{2}\right\} + \frac{1}{2}\cos^{-1}\left\{\frac{\frac{\mu_w \sigma_m}{\tau_m(\mu_w^2+1)^1}}{2}\right\} \quad (3)$$

$$\alpha_2 = \frac{1}{2\pi} - \cos^{-1}\left\{\frac{\frac{\mu_w}{(\mu_w^2+1)^1}}{2}\right\} - \frac{1}{2}\cos^{-1}\left\{\frac{\frac{\mu_w \sigma_m}{\tau_m(\mu_w^2+1)^1}}{2}\right\} \quad (4)$$

Where β_1 or β_2 are the angles between the point, where the vector perpendicular to the normal stress axe intersect the plane $\{\tau = [\mu_w|0.85|]\sigma_n\}$, with $\sigma_m = (\frac{\sigma_1+\sigma_3}{2})$, and $\tau_m = (\frac{\sigma_1-\sigma_3}{2})$. These equations, which are independent of the degree of heterogeneity and rock type, help predict the orientations of faults that should reactivate in a given state of stress.

4.1. Stage 1

The samples yielding the effective principal stress tensor related to the first tectonic stage of the Indosinian orogeny represent an extensional event, and is well constrained by newly formed mode II veins. After unfolding calculations (Arboit et al., 2015) the veins are almost normal to the bedding with a θ angle of about 20°. The geometrical representation of the maximum differential stress (σ_{e1}- σ_{e3}) is tangent to the crack development curve with a magnitude of about 43 MPa (Table 2 – Appendix C). σ_{e1} is the vertical effective principal stress (σ_{veff}) during Stage I, with a magnitude of ~38 MPa and σ_{e3}~ –5 MPa. The negative σ_{e3} corresponds to the opening of fractures that occurred with the shearing caused by moderate fluid overpressure. The value of the stress ratio "Φ" drives σ_2 towards values of ~ 8 MPa. The calculated σ_{e1} principal stress axis lies within the two sets of conjugate fractures Set-AI (65°/150°) and Set-AII (65°/175°), at an angle β of ~20° to σ_1 (Figure 3a).

4.2. Stage 2

The second tectonic stage is interpreted to be the main compressive tectonic event in SE Asia during the Early Triassic in SE Asia and corresponds to the formation of a new set of faults (pure compressive stress regime) and to two new fracture sets (strike-slip stress regime): Set-AIII (80°/050°) and Set-AIV (90°/080°) (Arboit et al., 2015). The stress tensors detected with calcite twin analysis describe both the deformations observed in the field, both with a horizontal σ_1 axis oriented NE-SW that trends perpendicular to the mean fold hinge orientation. The emplacement during the Early Triassic throughout the KKFTB of newly formed conjugate set of strike-slip veins and of reverse faults containing the σ_2 axis and at an angle θ of 20° to 28° to the σ_1 axis (when unfolded) requires the Mohr circle to be tangent to the CDC (Figure 3). Differential stress in compressive conditions reaches the value of ~59 MPa with the effective principal stress values σ_{e1} = 54 MPa and (σ_{veff}) σ_{e3} = -5 (Figure 3a), and σ_{e2} = 27 MPa. Differential stress in strike-slip regime is calculated to be ~44 MPa, with the vertical effective stress (σ_{veff}) σ_{e2}= ~30 MPa, and the other effective principal stress values being σ_{e1} = 39 MPa and σ_{e3} = -5 (Figure 3b). The values of the σ_2-σ_3 differential stress obtained after CSIT calculation are the same for both the stress tensors (~34 MPa) with only the maximum horizontal stress (σ_{e1})being higher in the pure compressive tensor. In both the geometrical construction the Mohr circles corresponding to the two differential stresses present a negative minimum principal stress, indicating the increase of fluid overpressure from Stage 1 to Stage 2

4.3. Stage 3

The third stress event caused the left lateral shear reactivation of the pre-existing set of fractures formed during the extensional phase (stage 1), and the LPS (stage 2) under strike-slip regime, these reactivated veins are often associated with wing cracks and Riedel arrays (R and R') when reactivated under a strike-slip regime. The only pure compressive stress tensor yields a quite low stress ratio (Φ= 0.2) that might permit σ_2-σ_3 stress permutation. The reactivated strike-slip fractures sets are vertical and contain the principal stress σ_2. The Mohr circle representing the stress tensors in Stage 3 is secant to the reactivation friction curve ($\tau = 0.85\sigma_n$) at two points, with the lower α angle (~20°) representing the reactivated strike-slip fractures. The differential stress has same value in all the stress tensors (~66 MPa) and the absolute values of the effective principal stresses are: σ_{e1}= ~78 MPa, (σ_{veff}) σe2= ~12 MPa, and σ_{e3} =~46 MPa.

4.4. Stage 4

The fourth stress event is characterized by two compressive and one strike-slip stress tensors, the latter of which have a similar attitude to the strike-slip tensors of stage 3. The differential stress value of this stress tensor (~38 MPa) was high enough to allow right lateral shear reactivation of the pre-existing set of strike-slip fractures formed during Stage 1 and Stage 2. The two compressive stress tensors yield relatively low stress ratios (Φ= 0.1, 0.35), and values of high differential stress (~65 MPa) that reactivated some of the major north-verging reverse faults that created the most significant fault-related folds within the KKFTB during the LPS. The Mohr circle representing the compressive regime is secant to the reactivation friction curve ($\tau = 0.85\sigma_n$) at two points, with the higher α angle (~45°) representing reactivated thrusts throughout the KKFTB. The principal effective stresses are: σ_{e1}= ~77 MPa, σ_{e2}= ~18 MPa, and (σ_{veff}) σ_{e3} =~12 MPa. The strike-slip stress tensor is associated with reactivation of fractures with an average θ angle of ~20°. Consistently, the Mohr circle representing the reactivation of these fractures is tangent to the friction curve at an angle α of the same amount and present effective stress values of σ_{e1}= ~49 MPa, σe_3 =~11 MPa, and (σ_{veff}) σ_{e2}= ~43 MPa (Figure 3d).

4.5. Stage 5

This stage is associated with the peak differential stress (σ_{e1}-σ_{e3}) recorded by the calcite twins during the tectonic stage that has been interpreted as the only one not related to the Indosinian event. Both fractures and calcite twins recorded a consistent post-folding relationship. This stage is represented by two strike –slip and two compressive stress tensors. The stress ratios of the latter is lower (average Φ= 0.36) than those of the strike-slip tensors (average Φ= 0.66). Arboit et al. (2015) pointed out that several fractures and faults underwent a post-tilting reactivation with a high angle between the reactivated planes and the maximum horizontal stress σ_1 (Figure 3e). For the sake of semplicity we consider that all the strike-slip fractures were reactivated during Stage 5 with an angle α= ~25°, while the angle of the reactivated reverse faults is around ~47° (Figure 3e). The Mohr circle representing the pure compressive regime is secant to the reactivation friction curve at two points, with the pure compressive regime having higher differential stress (~61 MPa), whereas the strike-slip regime show a lower differential stress, quite similar to the values of the previous strike-slip stress tensors (~47 MPa). The effective principal stress values ranges from ~75 to ~60 MPa (σ_{e1}), with quite similar σ_{e3}= ~12 MPa (Figure 3e).

5. Discussion

5.1. Uncertainties

Before discussing the quantification of the stress magnitude, we will first review few underlying factors that are necessary to define a complete stress tensors. There are several criteria and inaccuracies that have to be taken in account for the final palaeostress quantification. For instance: 1) the values of differential stress detected with calcite twin analysis suffer of a level of uncertainties of ~20% (Lacombe et al., 2001). However, the accuracy of the quantification of the differential stress values might have increased after the statistical calibration between the critical resolved shear stress, twinning strain and grain size (Lacombe et al., 2009; Amrouch, 2010b). 2) It was not possible to construct the CDC directly from the samples that were used to extrapolate the stress tensors responsible for the deformation of the KKFTB. Therefore, uncertainties might be induced by using a proxy CDC from the

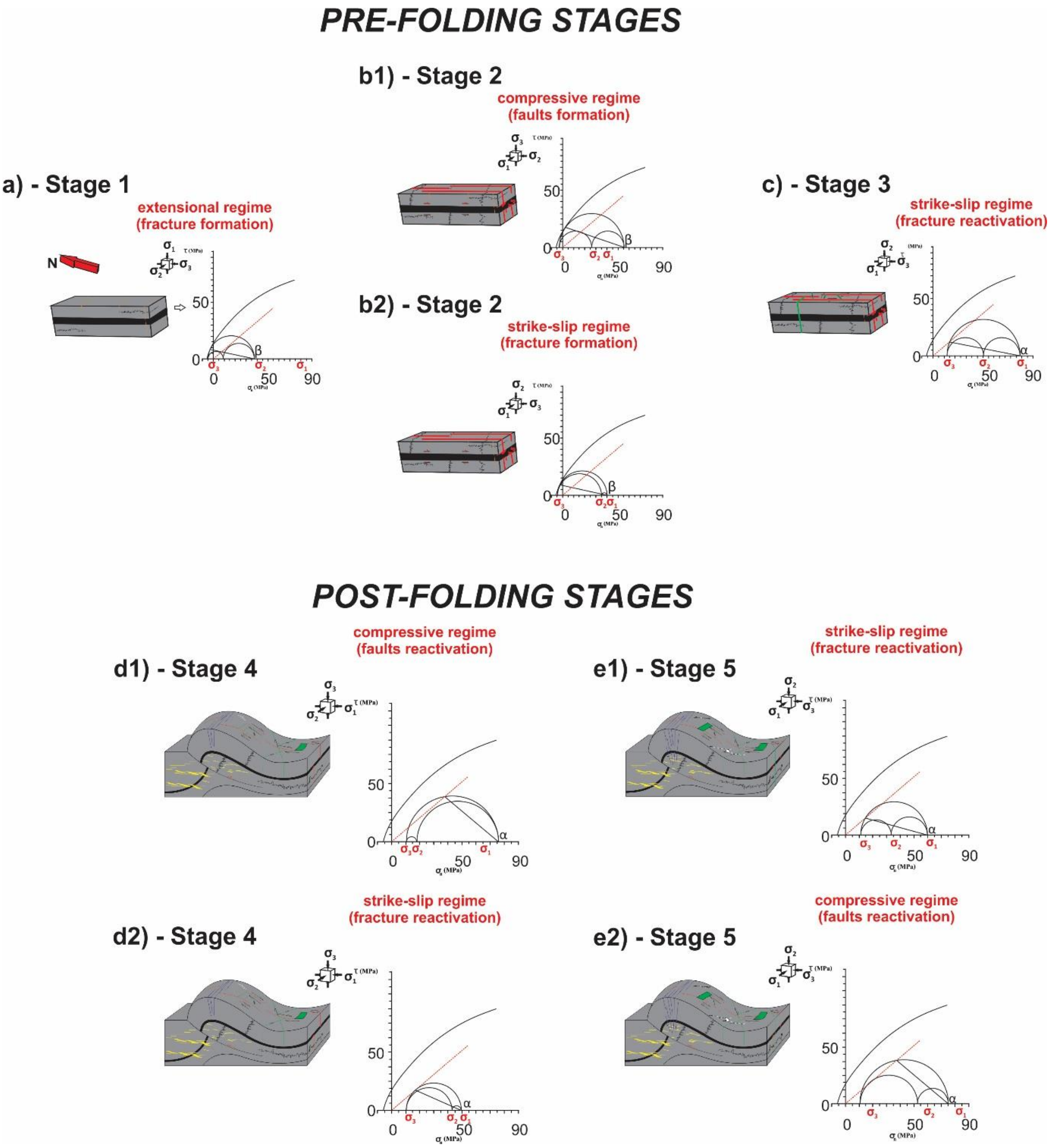

Figure 3. Mohr circles construction corresponding to each tectonic stage within the KKFTB since the Mid-Permian. For details on these kinematic and mechanical scenarios, see Tables 1 and 2

literature (Tepnarong, 2001) to constraint the position of the Mohr circles. 3) One principal stress is considered to be close to the vertical position. If one principal stress was not coaxial with gravity, this will result in an increase of vertical effective stress toward σ_{e1}. 4) The Mohr circles, representing the fractures sets at each tectonic stage, are assumed to be representative only if the fractures were coeval, either if newly formed or the results of reactivation of pre-existing discontinuities (Andrè et al., 2001).

As consequence of these considerations, the values obtained should be considered in the order of magnitudes rather than absolute values (Lacombe, 2001; Lacombe et al., 2009; Amrouch et al., 2011). However, these are the only available record for the uppermost crustal palaeostresses in central Thailand from the onset of the Indosinian deformation. Further, the validity of the methodology has already been proved by Lacombe (2001), Amrouch et al. (2010a, 2011).

5.2. Consistency of the of palaeostress results from calcite twins with Thailand regional tectonics

Each stress state revealed by the twinning analysis has been correlated to a specific tectonic event (Arboit et al., 2015). However, we need to take in consideration that the samples used for calculating the differential stress were collected within a fold-thrust belt, and might correspond to a local value (e.g. high stress concentrations related to asperities along major thrust in the area); and consequently might not be indicative of the far field stress conditions. However, the tight stress-strain relationships observed in Arboit et al. (2015) indicate that the palaeostress tensors can be related to regional tectonic events.

All the calculated maximum differential stress values (Table 2) fit reasonably with a bracket of values between 30 MPa and 65 Mpa. These values are higher than the average values in a common intraplate setting (Lacombe et al., 1996; Rocher et al., 2004) and possibly adequate for an active collisional setting. The (σ_1-σ_3) values for each tectonic event are:

- STAGE 1: (pre-folding setting) About 45 MPa for the N-S extension;
- STAGE 2: (pre-folding setting) About 60 MPa for the N-S compression, and about 40 MPa for S2 NS strike-slip;
- STAGE 3: (pre-folding setting) About 66 MPa for the E-W strike-slip;
- STAGE 4: (post-folding setting) About 59 MPa for the N-S compression and ~40 MPa strike-slip regime;
- STAGE 5: (post-folding setting) About 62 MPa for the ENE-SWS pure compressive state and ~48 MPa strike-slip regime.

Samples with insufficient untwinned planes can give overestimated differential stress values (Rocher et al., 2004). In the few samples with insufficient untwinned planes (values between square brackets, Table 2), the calculated differential stress values appears to be overestimated; hence, these samples are not taken in consideration. The formation of pre-folding extensional veins can be related to the overburden stress associated with burial, predating, or coeval with, formation of few bedding-parallel stylolites. All these fractures and bedding-parallel stylolites have a more restricted occurrence than the sets of fractures that developed during later stages. The relatively narrow strike of the fracture sets that took place during Stage 1 implies a uniform distribution of minimum stress σ_3 and a constant position through time of the vertical stress σ_1. We proposed that the sets of vein developed during the Permian extensional phase on the southwestern margin of the Indochina terrane, within the KKFTB before the main LPS event, and possibly in response to the N-S oriented flexure of the foreland in front of the advancing thrust sheets, contemporary with burial and possibly under high fluid pressures (Arboit et al., 2015).

The second tectonic stage is connected to a major N-S oriented collision, this compressional stage is consistent with the direction of tectonic transport within the KKFTB (Morley et al., 2013; Arboit et al., 2014), supporting the regional significance of the stress tensors. This tectonic stage is well represented by strike-slip and compressive stress tensors. These tensors link to the formation of both strike-slip fractures, and major reverse faults. The strike-slip tensors were mostly detected within the N-E striking veins and present lower differential stress values than the compression stress tensors that were recorded in the N-S striking veins. All the Mohr circles representing the stress tensors of Stage 2 have a negative σ_3 value; and these values are reflected by the high number of horizontal veins that opened during the LPS on Stage 2 (Arboit et al., 2015).

Stage 3 is represented by three strike-slip and one compressive stress tensors. The strike-slip stress tensors calculated on the calcite veins present distinctive differential stress values that resemble the magnitude of the average compressive stages (~65 MPa). These anomalously high strike-slip differential stress values allow to advance the hypothesis where Stage 3 might corresponds to a compressional tectonic stage; however, the high stress ratio does not justify this idea (Table 2). Also, it must be taken in consideration that the high fracturing and faulting activity in Stage 2 released huge amounts of fluid pressure. This drop in fluid pressure massively shifted the Mohr circle corresponding to Stage 3 towards higher effective stress values (Figure 3c), and this might be the reason of such high differential stress.

The macro deformation associated with Stage 4 is responsible for the reactivation of E-W striking thrusts, the tightening of pre-existing fault-propagation folds and reactivation of the fractures developed during the earlier events. During the latest Triassic, the half-graben basins in the Khorat Plateau (NE Thailand) containing the Kuchinarai Group (Late Triassic) ceased to subside and some were structurally inverted, and the degree of deformation associated with this event is very much less than the one that took place during the earlier Indosinian I event (Booth and Sattayarak, 2011). However the differential stress that was necessary to reactivate the fractures in the post-folding stress states was in the order of 50-60 MPa. This might be caused also by the complex polyphase pre-folding deformation that induced high levels of strain hardening in the crystal lattices, and this had a remarkable effect on the yield stress value of the post-folding events (Stage 4; Stage 5). These post-folding differential stresses range in the order of few MPa (Table 2), and this might be a consequence of the more homogeneous tectonic framework in central Thailand after the collision of Sibumasu with the amalgamated Sukhothai-Indochina terrane during the Late Triassic ~220 Ma (Sone and Metcalfe, 2008; Morley et al., 2013; Metcalfe, 2013; Arboit et al., 2015; Ng et al., 2015; Arboit et al., 2015).

Price and Cosgrove (1990) demonstrated that from equation (5) with a coefficient k= 4.0, that corresponds to a coefficient of friction (μ) of 0.75:

$$(\sigma_1 - \sigma_3) = (k-1)\left[(a)\sigma_2\ or\ (b)\frac{\sigma_1}{k}\ or\ (c)\frac{\sigma_2}{k}\right] \quad (5)$$

At a given depth, the ratios of differential stress required for reaching shear conditions are higher for (a) compressive conditions, (b) intermediate for strike-slip and lower for (c) extensional systems. This partially agrees with the differential stress values calculated within the KKFTB, except for the anomalous differential stress values in Stage 3. Indeed, the average differential stress values of the pure compressive tectonic stages have higher magnitude (average ~65 MPa) than those of strike-slip regimes (average ~50 MPa). Sibson (1977) assumed that if the angle (θ) between the plane of the fault and the principal stress (σ_1) increase, the magnitude of the stress tensor necessary to reactivate a fault plane has to be higher. This principle is reflected on the differential stresses that acted on the KKFTB, where the magnitudes increased from Stage 2 to Stage 5 (Table 2) because of the growth of the general bedding, and the consequent tilting of the faults, after the main folding event (Arboit et al., 2015).

5.3. Relationship between palaeostress, tectonic framework and palaeoburial in central Thailand from the Mid-Permian

The obtained values of differential stress are independent of the fluid pressure (Rowe and Rutter, 1990), and we can use this evidence in order to prove that the calculated values are the maximal values reached during the deformational cycles undergone by the calcite grains during the same tectonic event. Lacombe (2001, 2007), Lacombe et al. (2009) proved the relationship between palaeo-differential stress data and depth, deriving increasing values of differential stresses with depth. Since it is feasible to imply that the LPS was coeval with the onset of folding, the related stress tensors were probably recorded by twinning at the time of the maximum burial. After CSIT calculation we obtained differential stress for Stage 1 of ~45 MPa, with effective stress as σ_{e3}=~-5 MPa and σ_{e1}=~40 MPa (Figure 3a). These values imply a maximum burial depth of about 1.9 Km, the stratigraphic thickness at which the LPS occurred in the KKFTB is not well established; nonetheless, Ueno and Charoentitirat (2011) suggested similar burial depths for the Khao Khad Formation during the Early Triassic (1800 m). Stock et al. (1985) and Morris and Ferril (1996) modelled that within an extensional setting σ_2 is 50-70% of σ_1 and σ_3 is 20-30% of σ_1, in such case the effective stresses would be σ_{e3}= ~10 MPa, σ_{e2}= ~30 MPa, and σ_{e1}= ~55 MPa. Consequently the depth of burial would be ~2 km~, and we might consider these palaeoburial estimates as maximum values (Lacombe, 2007; Lacombe et al,. 2009, Amrouch et al., 2011).

The active folding within the KKFTB started when the flexure of the foreland basin shut off and the collision between Sukhothai and Indochina began. The basin on the edge of the southwestern margin of the Indochina terrane that was then filled by Late Permian foredeep and Triassic foreland deposits. The Mid Permian structural regime was, therefore, likely dominated by foreland flexure (Sone and Metcalfe, 2008; Morley et al., 2013), so that burial stylolites and the extensional veins in the foreland probably developed during the Early to Mid Permian.

Thrusting/folding in the KKFTB began during the Early Triassic, with maximum shortening probably at the time of the Sukhothai-Indochina collision. After Morley et al. (2013), and Arboit et al. (2014) it is possible to link the formation of the main anticlines to the first major folding episode, with possibly a later reactivation coeval with a phase of fold tightening that occurred during the Late Triassic after the Sibumasu-Indochina collision. Depending on the structural evolution during the Triassic, the maximum burial might have been reached at different times through the Triassic, depending on the position within the fold-thrust belt, however it is feasible to imply the LPS to have occurred while the KKFTB reached its maximum burial depth.

The ages of the syntectonic sedimentation of the foredeep ($^{206}Pb/^{238}U$ age= 251 ± 3 Ma) and foreland ($^{206}Pb/^{238}U$ age= 205 ± 6 Ma) deposit on top of the Khao Khwang carbonate platform (Arboit et al., 2016); the 208 ± 4 Ma $^{40}Ar/^{39}Ar$ ages on the orogenic illite collected on a reactivated thrust plane of the KKFTB (Hansberry et al., 2015); and the 255 ± 6 Ma, 224 ± 2 Ma $^{40}Ar/^{39}Ar$ crystallization ages on biotite and muscovite from andesitic dykes that intruded the core of a fault-propagation fold and propagated passively on a thrust of the KKFTB (Arboit et al., 2016) (Figure 4) provide a relatively good constraint on the timing of the several palaeostress states that deformed the KKFTB. As a result, the limestones of the KKFTB were buried in the Early Triassic at a depth that might range from ~1.9 up to ~2 km (Ueno and Charoentitirat, 2011) and on basis of this data it is possible to derive a mean rate of exhumation of the sedimentary Permian and Triassic cover of the KKFTB in the range 0.05–0.07 mm/yr.

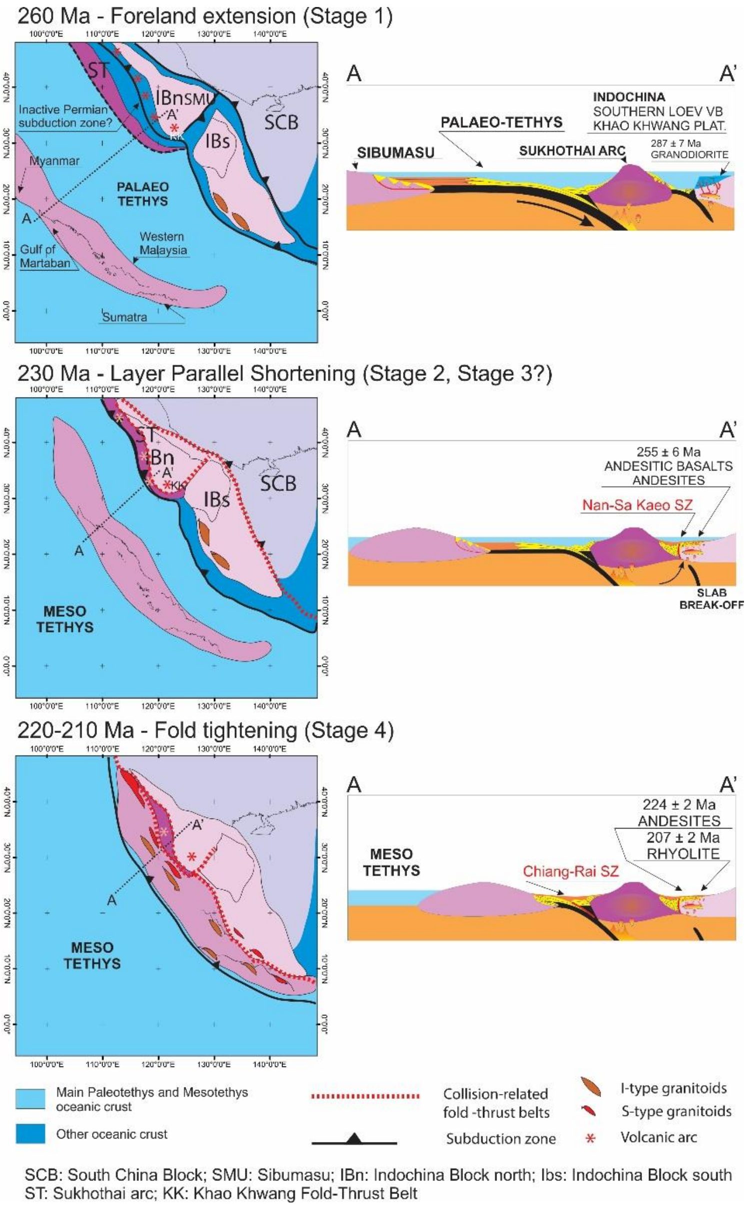

Figure 4. Modified from Arboit et al. (in press). Palaeo-geographic schematic reconstructions of SE Asia based on the GPlate software reconstruction (contour and rotation file in Supplementary data). The cross-sections show the tectonic development of the Indochina, Sukothai and Sibumasu blocks during the Early Permian to the Late Triassic; resulting in the LPS and fold-tightening deformations, within the southern portion of the KKFTB.

6. Conclusions

Quantitative estimates of crustal stresses and strength are central to many problems of rock mechanics. This paper presents a first attempt at comparing and combining palaeostress magnitude data together with geomechanical data in order to constraint the effective magnitude values of the principal axes that affected the sedimentary layers of the KKFTB in central Thailand mainly during the Triassic Indosinian orogeny, and feasible estimates of average denudation rates. Hence, this combination of stress data brings useful information on the strength and mechanical behaviour of the upper continental crust in central Thailand since the Mid Permian, and might be considered for future modelling.

Acknowledgements

This work was funded by Australian Research Council Discovery Project #DP 120101460. ASC is funded by Australian Research Council grant #FT120100340. This is a contribution to IGCP projects #589 (Development of the Asian

Tethyan Realm) and #628 (The Gondwana Map) and we gratefully acknowledge all the funding organizations. This publication forms TRaX Record #xxx.

References

Amrouch, K., Lacombe, O., Bellahsen, N., Daniel, J. M., & Callot, J. P. 2010a. Stress and strain patterns, kinematics and deformation mechanisms in a basement-cored anticline: Sheep Mountain Anticline, Wyoming. Tectonics, 29(1).

Amrouch, K., Robion, P., Callot, J. P., Lacombe, O., Daniel, J. M., Bellahsen, N., & Faure, J. L. 2010b. Constraints on deformation mechanisms during folding provided by rock physical properties: a case study at Sheep Mountain anticline (Wyoming, USA). Geophysical Journal International, 182(3), 1105-1123.

Amrouch, K. 2010c. Apport de l'analyse microstructuralea la comprehension des mecanismes de plissement: Exemples de structures plissees aux USA (Wyoming) et en Iran (Zagros) (Doctoral dissertation, Thèse).

Amrouch, K., Beaudoin, N., Lacombe, O., Bellahsen, N., & Daniel, J. M. 2011. Paleostress magnitudes in folded sedimentary rocks. Geophysical Research Letters, 38(17).

Anchuela, Ó. P., Pueyo, E. L., Juan, A. P., & Imaz, A. G. 2012. Vertical axis rotations in fold and thrust belts: Comparison of AMS and paleomagnetic data in the Western External Sierras (Southern Pyrenees). Tectonophysics, 532, 119-133.

André, A. S., Sausse, J., & Lespinasse, M. 2001. New approach for the quantification of paleostress magnitudes: application to the Soultz vein system (Rhine graben, France). Tectonophysics, 336(1), 215-231.

Angelier, J., Tarantola, A., Valette, B., & Manoussis, S. 1982. Inversion of field data in fault tectonics to obtain the regional stress—I. Single phase fault populations: a new method of computing the stress tensor. Geophysical Journal International, 69(3), 607-621.

Angelier, J. 1989. From orientation to magnitudes in paleostress determinations using fault slip data. Journal of structural geology, 11(1), 37-50.

Angelier, J., 1990. Inversion of field data in fault tectonics to obtain regional stress. III. A new rapid direct inversion method by analytical means. Geophysical Journal International 103, 363–376.

Angelier, J., 1994. Fault slip analysis and paleostress reconstruction. In: Hancock, P.L. (Ed.), Continental Deformation. Pergamon Press, pp. 53–100.

Arboit, F., Collins, A. S., King, R., Morley, C. K., & Hansberry, R. 2014. Structure of the Sibumasu–Indochina collision, central Thailand: A section through the Khao Khwang Fold-Thrust belt.Journal of Asian Earth Sciences, 95, 182-191.

Arboit, F., Amrouch, K., Collins, A. S., King, R., & Morley, C. 2015. Determination of the tectonic evolution from fractures, faults, and calcite twins on the southwestern margin of the Indochina Block. Tectonics, 34(8), 1576-1599.

Arboit, F., Collins, A. S., Morley, C., King, R., Amrouch, K. (in press.). Detrital zircon analysis of the southwest Indochina terrane, central Thailand: Unravelling the Indosinian orogeny, GSA Bulletin.

Arboit, F., Collins, A. S., Morley, C., King, R., Amrouch, K. (in press.). Geochronological and geochemical study of mafic dykes from the Khao Khwang Fold-Thrust Belt: Implications for petrogenesis and tectonic evolution, Journal of the Geological Society.

Armijo, R., Carey, E., Cisternas, A., 1982. The inverse problem in microtectonics and the separation of tectonic phases. Tectonophysics 82, 145–169.

Bergerat, F. 1987. Stress fields in the European platform at the time of Africa-Eurasia collision. Tectonics, 6(2), 99-132.

Booth, J., & Sattarayak, N. 2011. Cretaceous geology of NE Thailand. The Geology of Thailand, 185.

Bott, M. H. P. 1959. The mechanism of oblique slip faulting. Geol. Mag. 96, 109-117.

Brown, E.T. 1981. Rock characterization, testing and monitoring, ISRM suggested methods. Pergamon Press, Oxford, pp. 107–127.

Bunopas, S., 1982. Paleogeographic history of western Thailand and adjacent parts of South-east Asia: A plate tectonics interpretation. Geological Survey Division, Department of Mineral Resources, (No. 5).

Byerlee, J. D. 1970. The mechanics of stick-slip. Tectonophysics, 9(5), 475-486.

Byerlee. J.D., 1978. Friction of rocks. Pure Appl. Geophys., 116: 615-626

Cai, J. X., & Zhang, K. J. 2009. A new model for the Indochina and South China collision during the Late Permian to the Middle Triassic. Tectonophysics, 467(1), 35-43.

Carey-Gailhardis, E., Mercier, J.L., 1987. A numerical method for determining the state of stress using focal mechanisms of earthquake populations: application to Tibetan teleseisms and microseismicity of southern Peru. Earth and Planetary Science Letters 82, 165–179.

Charusiri, P., Imsamut, S., Zhuang, Z., Ampaiwan, T., & Xu, X. 2006. Paleomagnetism of the earliest Cretaceous to early late Cretaceous sandstones, Khorat Group, Northeast Thailand: implications for tectonic plate movement of the Indochina block. Gondwana Research, 9(3), 310-325.

Cung, T. C., & Geissman, J. W. 2013. A review of the paleomagnetic data from Cretaceous to lower Tertiary rocks from Vietnam, Indochina and South China, and their implications for Cenozoic tectonism in Vietnam and adjacent areas. J. Geodyn, 69(5).

Dong, Y., Zhang, X., Liu, X., Li, W. Chen, Q., Zhang, G., Zhang, H., Yang, Z., Sun, S., Zhang, F. 2015. Propagation tectonics and multiple accretionary processes of the Qinling Orogen. Journal of Asian Earth Sciences, 104, 84-98.

Etchecopar, A., Vasseur, G., & Daignieres, M. 1981. An inverse problem in microtectonics for the determination of stress tensors from fault striation analysis. Journal of Structural Geology, 3(1), 51-65.

Etchecopar, A. 1984. Etude des e tats de contraintes en tectonique cassante et simulation de de formation plastique (approche mathe matique), the se doctorates-sciences, 270 pp., Univ. Sci. et Tech. du Langue-doc, Montpellier, France.

Gephart, J.W., Forsyth, D.W., 1984. An improved method for determining the regional stress tensor using earthquake focal mechanism data. Journal of Geophysical Research B89, 9305–9320.

Gephart, J.W., 1990. Stress and direction of slip on fault planes. Tectonophysics 8, 845–858.

Hoek, E. 1990. Estimating Mohr-Coulomb friction and cohesion values from the Hoek-Brown failure criterion. In International

Journal of Rock Mechanics and Mining Sciences & Geomechanics Abstracts (Vol. 27, No. 3, pp. 227-229). Pergamon.

Hutchison, C.S., 1975. Ophiolite in southeast Asia. Geological Society of America Bulletin, 86(6), 797-806.

Jaeger, J. C., Cook, N. G., & Zimmerman, R., 1969. Fundamentals of rock mechanics. John Wiley & Sons.

Lacombe, O., Angelier, J., Laurent, P., Bergerat, F., & Tourneret, C. 1990. Joint analyses of calcite twins and fault slips as a key for deciphering polyphase tectonics: Burgundy as a case study. Tectonophysics, 182(3), 279-300.

Lacombe, O., Angelier, J., & Laurent, P. 1992. Determining paleostress orientations from faults and calcite twins: a case study near the Sainte-Victoire Range (southern France). Tectonophysics, 201(1), 141-156.

Lacombe, O., & Laurent, P. 1992. Determination of principal stress magnitudes using calcite twins and rock mechanics data. Tectonophysics,202(1), 83-93.

Lacombe, O., & Laurent, P. 1996. Determination of deviatoric stress tensors based on inversion of calcite twin data from experimentally deformed monophase samples: preliminary results. Tectonophysics, 255(3), 189-202.

Lacombe, O., Laurent, P., Rocher, M., 1996. Magnitude de la contrainte deviatorique pyreneenne dans l'avant-pays nord-pyreneen. C. R. Acad. Sci., Paris (IIa) 322, 229–235.

Lacombe, O. 2001. Paleostress magnitudes associated with development of mountain belts: Insights from tectonic analyses of calcite twins in the Taiwan Foothills. Tectonics, 20(6), 834-849.

Lacombe, O. 2007. Comparison of paleostress magnitudes from calcite twins with contemporary stress magnitudes and frictional sliding criteria in the continental crust: Mechanical implications. Journal of Structural Geology, 29(1), 86-99.

Lacombe, O., Amrouch, K., Mouthereau, F., & Dissez, L. 2007. Calcite twinning constraints on late Neogene stress patterns and deformation mechanisms in the active Zagros collision belt. Geology, 35(3), 263-266.

Lacombe, O., Malandain, J., Vilasi, N., Amrouch, K., & Roure, F. 2009. From paleostresses to paleoburial in fold–thrust belts: Preliminary results from calcite twin analysis in the Outer Albanides. Tectonophysics, 475(1), 128-141.

Marrett, R., Almandinger, R.W., 1990. Kinematic analysis of fault slip data. Journal of Structural Geology 12, 973–986.

Metcalfe, I., 2005. Asia: South-East. In: Selley, R.C., Cocks, L.R.M., Plimer, I.R. (Eds.), Encyclopedia of Geology, Elsevier, Oxford, vol. 1, 169–198.

Metcalfe, I., 2011. Tectonic framework and Phanerozoic evolution of Sundaland. Gondwana Research, 19(1), 3-21.

Metcalfe, I., 2013. Tectonic evolution of the Malay Peninsula. Journal of Asian Earth Sciences, 76, 195-213.

Michael, A.J., 1984. Determination of stress from slip data: faults and folds. Journal of Geophysical Research B89, 11517–11526.

Mochales, T., Casas, A. M., Pueyo, E. L., & Barnolas, A. 2012. Rotational velocity for oblique structures (Boltaña anticline, Southern Pyrenees). Journal of Structural Geology, 35, 2-16.

Morley, C.K., 2007. Variations in late Cenozoic–Recent strike-slip and oblique-extensional geometries, within Indochina: The influence of pre-existing fabrics. Journal of Structural Geology, 29(1), 36-58.

Morley, C.K., Ampaiwan, P., Thanudamrong, S., Kuenphan, N., Warren, J., 2013. Development of the Khao Khwang Fold-Thrust Belt: Implications for the geodynamic setting of Thailand and Cambodia during the Indosinian Orogeny. Journal of Asian Earth Sciences, 62, 705-719.

Morris, A., Ferrill, D. A., & Henderson, D. B. 1996. Slip-tendency analysis and fault reactivation. Geology, 24(3), 275-278.

Ng, S. W. P., Whitehouse, M. J., Searle, M. P., Robb, L. J., Ghani, A. A., Chung, S. L., Roselee, M. H. 2015b. Petrogenesis of Malaysian tin granites: Part 2. High precision U–Pb zircon geochronology of the Malaysian tin granites and tectonic model for their emplacement history. Geological Society of America Bulletin.

Price, N. J., & Cosgrove, J. W. 1990. Analysis of geological structures. Cambridge University Press.

Reches, Z., 1987. Determination of the tectonic stress tensor from slip along faults that obey the Coloumb yield criterion. Tectonics 6, 849–861.

Rocher, M., Cushing, M., Lemeille, F., Lozac'h, Y., & Angelier, J. 2004. Intraplate paleostresses reconstructed with calcite twinning and faulting: improved method and application to the eastern Paris Basin (Lorraine, France). Tectonophysics, 387(1), 1-21.

Rowe, K. J., & Rutter, E. H. 1990. Palaeostress estimation using calcite twinning: experimental calibration and application to nature. Journal of Structural Geology, 12(1), 1-17.

Sandiford, M., Wallace, M., & Coblentz, D. 2004. Origin of the in situ stress field in south-eastern Australia. Basin Research, 16(3), 325-338.

Sibson, R. H. 1977. Fault rocks and fault mechanisms. Journal of the Geological Society, 133(3), 191-213.

Sibson, R. H. 1994. Crustal stress, faulting and fluid flow. Geological Society, London, Special Publications, 78(1), 69-84.

Singsoupho, S., Bhongsuwan, T., & Elming, S. Å. 2014. Tectonic evaluation of the Indochina Block during Jurassic-Cretaceous from palaeomagnetic results of Mesozoic redbeds in central and southern Lao PDR. Journal of Asian Earth Sciences, 92, 18-35.

Sone, M., Metcalfe, I., 2008. Parallel Tethyan sutures in mainland Southeast Asia: new insights for Palaeo-Tethys closure and implications for the Indosinian orogeny. Comptes Rendus Geoscience, 340(2), 166-179.

Stock, J. M., Healy, J. H., Hickman, S. H., & Zoback, M. D. 1985. Hydraulic fracturing stress measurements at Yucca Mountain, Nevada, and relationship to the regional stress field. Journal of Geophysical Research: Solid Earth (1978–2012), 90(B10), 8691-8706.

Ueno, K., Charoentitirat, T., 2011. Carboniferous and Permian. In: Ridd, M.F., Barber,A.J. Crow, M.J. (eds.), The Geology of Thailand, The Geological Society of London, 71–136.

Tapponnier, P., Peltzer, G., & Armijo, R. 1986. On the mechanics of the collision between India and Asia. Geological Society, London, Special Publications, 19(1), 113-157.

Tepnarong, P. 2001. Theoretical and experimental studies to determine compressive and tensile strengths of rocks, using modified point load testing.M. Eng. Thesis, Suranaree University of Technology, Thailand.

Wallace, R. E. 1951. Geometry of shearing stress and relation to faulting. J. Geol. 59. 118-130.

Warren, J., Morley, C.K., Charoentitirat, T., Cartwright, I., Ampaiwan, P., Khositchaisri, P., Mirzaloo, M., Yingyuen, J., 2014. Structural and fluid evolution of Saraburi Group sedimentary carbonates, central Thailand: A tectonically driven fluid system. Marine and Petroleum Geology, Doi: 10.1016/j.marpetgo.2013.12.019.

Will, T.M., Powel, R., 1991. A robust approach to the calculation of paleostress fields from fault plane data. Journal of Structural Geology 13, 813–821.

Yin, Z.M., Ranalli, G., 1993. Determination of tectonic stress field from fault slip data, toward a probabilistic model. Journal of Geophysical Research 98, 12165–12176.

Zoback, M. L. 1992. First-and second-order patterns of stress in the lithosphere: the world stress map project. Journal of Geophysical Research, Vol. 97, no. b8, pages 11,703-11,728

Conclusions and Perspective

This study was set out to explore the geodynamic evolution of the southwestern margin of the Indochina terrane during the early stages of the Indosinian orogeny, using the KKFTB as case study. The revision of the rocks within the Saraburi region has sought to shed some light on their depositional history and the deformation they underwent, in order to fit them into a coherent pattern – a tectono-stratigraphic model. However, several analyses have shown that a clear-cut distinction on the type and driving mechanism of this FTB is still far to be achieved. Notwithstanding, it seems reasonable to assume that the KKFTB can be correlated to the development of the Sukhothai-Indochina collisional zone, and therefore to a far-field stress driven systems. The study has also sought to identify the various tectonic events that characterised the whole Indosinian event and to use the stratigraphic record as much as the igneous suite within the KKFTB to constrain their timing. Hence, we used the geological record of the KKFTB in order to answer few questions on the tectonic geodynamic evolution of the southwestern margin of Indochina, such as: 1. What driving mechanism deformed the Khao Khwang carbonate platform? 2 Is the KKFTB the final product of tectonic mechanisms that deformed the edge of the Indochina terrane or the Sukhothai volcanic arc? Is it possible to fit the E-W trend of the structures within the KKFTB with the contrasting N-S general present day setting of the Indosinian terranes in SE Asia?

The Palaeozoic and Mesozoic evolution of central Thailand and the adjacent regions of SE Asia involved the rifting and separation of three collages of continental terranes (probably as elongate micro-continents) from eastern Gondwana and the successive opening and closure of two oceans, the back-arc between Sukhothai and Indochina, and the Palaeotethys. The development of the KKFTB centres on the closure and subduction of the back-arc basin from the Middle Permian to the Early Triassic, where the slab under-ridded the accretionary complex on the southwestern margin of the Indochina terrane. Finally, once Sukhothai had collided, it started a phase of crustal shortening involving further thrusting until the Late Triassic. The subduction and consequent metasomatism of the subducted back-arc basin reflected in the emplacement of a large igneous province, the Loei-Petchabun volcanic belt on the edge of the Indochina terrane.

This province comprises several regions made of diverse igneous rock types and ages, which extends from Loei in the north to Khao Yai (or Saraburi) and Sa Kaeo in the south. The igneous rocks that intruded the KKFTB sedimentary sequence form part of the south portion of the Loei volcanic belt. Few $^{40}Ar/^{39}Ar$ mica and U–Pb zircon ages, along with both whole rock elemental and Sr–Nd isotopic data shed some light on the average crystallization age for the dykes that intruded the KKFTB. The most evolved igneous rocks constrained the age of the possible Sukhothai-Indochina collision in the Late Permian Early Triassic (255 ± 6 Ma), and possibly the latest post-collisional stages to the Late Triassic (224 ± 1.9 Ma). The latest stages of the Indosinian orogeny correspond to the Sibumasu-Sukhothai collision, and this compressive stress seems to have propagated towards the western margin of the Indochina margin triggering the effusion of the Khao Yai rhyolite. This volcanic body presents similar geochemical, geochronological, and isotopic characteristics to the Malaysian granitoids of the western Southeast Asian tin belt, which present a high degree of involvement of a predominantly sedimentary-sourced melt. Therefore, the effusive rhyolite body in the southern KKFTB seems to be linked to an increased basal heat flow due to mantle upwelling, which might have driven to crustal partial melting and the consequent eruption in the latest Triassic (207.1 ± 2.4 Ma).

The deformation that affected the KKFTB during the Sukhothai-Indochina collisional event – and especially the brittle dislocations that occurred within the crystal lattices of the carbonate rocks of the Saraburi Group – unravelled the stress-strain relationship of each Indosinian tectonic phase in space and time before and after the main folding event in central Thailand.

Within the western edge of the KKFTB, the comparison of major structures, such as large anticlines, with fracture patterns, and the palaeostress tensors from calcite twins (describing all the tectonic events developed during the Indosinian orogeny) revealed a consistent record of the tectonic stresses at the scale of the entire KKFTB. In central Thailand the closure of the back-arc basin has been studied by many researchers; however the characteristics of the paleostress evolution have never been investigated before. This analysis unravelled the polyphase tectonic history of the southwestern margin of Indochina, which revealed that the KKFTB underwent to a complex deformation and allowed the interpretation of a FTB developed on the southwestern margin of one of the Indochina continental fragments during the onset of the Indosinian orogeny.

The tectonic implications opened by the palaeostress history necessitated of further constraints to strengthen the possibility where the Indochina terrane was not a unique block with strongly linear boundary, as suggested in the previous models. Conversely, it might have consisted in a series of continental blocks, separated by Permian rifting that during the early stages of collision (particularly collision of the South China-Cathaysian Terrane with the Vietnam portion of Indochina) in the Early Triassic became amalgamated by closure along the older rifts.

Hence, we tried to constrain the provenance of the sedimentary sources in order to obtain a better idea of the palaeogeographic and tectonic setting of central Thailand during Permian and Triassic ages. This investigation involved the analysis of zircon U-Pb ages and Hf isotopes from detrital zircons of the arenaceous formations of the Saraburi Group, which were deposited during latest Palaeozoic-Early Mesozoic on the southwestern margin of the Indochina Terrane. Structural investigations on the KKFTB previously highlighted the northward direction of tectonic transport, and this structural architecture was imitated by the depositional setting that was active until the Late Permian in the southern KKFTB and until the Late Triassic in the northern KKFTB.

The U-Pb age peaks in the arenaceous lithologies of the KKFTB reflected the depositional influx after the Early Triassic Sukhothai-Indochina collision. However, the siliciclastic formations lying in the northern portion of the KKFTB recorded an unexpected Late Triassic, Early Jurassic sedimentary inflow, which is probably to be attributed to the Sibumasu/Sukhothai+Indochina amalgamation. Hence, the maximum depositional ages in the northern KKFTB opened to a tectono-sedimentary scenario in central Thailand that was active until at least 205 ± 6 Ma.

Moreover, the Hf-isotope data identified that different magma sources were feeding the depositional system before and during the subduction of the back-arc basin, and statistical analysis on SE Asian sedimentary record highlighted the mismatch of the sediments within Indochina. The sediments from the Khorat Plateau in the north are noticeably different from the Cambodian sediments in the southern portion of the Indochina terrane. The different sedimentary sources within Indochina strengthen the hypothesis suggested by the palaeostress analysis of a more complicated geometry within the Indochina terrane. Therefore, it is possible to speculate about the presence of a minor intra-continent ocean (Siem Reap-Stung Treng Line) that acted as provenance separation. The stress propagated into the carbonate rocks of the KKFTB from the welding of this suture, and might have caused the anomalous strike of the major structures within the KKFTB.

All these new data from the KKFTB emphasizes the accretionary nature of the Indosinian orogen from the Mid Permian early stages, to the Early Jurassic. Undeniably, we can assert that SE Asia was characterized by a succession of collisional events, that involved seamount/plateau accretion, ridge-trench interaction, formation of supra-subduction ridges and back-arc basins, and collision of island arcs with continental fragments. This tectonic complexity is well reflected within the KKFTB; the compositional variations of the igneous rocks, the polyphase palaeostress history and the complex pattern of the sedimentary sources are a fundamental data that helped – to some extent – in constraining the geodynamic evolution of the Indosinian orogeny.

Supplementary Data

Appendix A

Etchecopar’s calcite stress inversion technique (CSIT)

Stress Tensors extensional - Phase N*1

```
***** ECHANTILLON 20 *********************
*****************************************
POURCENTAGE: 50
 NOMBRE DE MACLES        200.
 NOMBRE DE NON MACLES      73.
 MACLES INCORPOREES       100
 POURCENTAGE DU NOMBRE DE NON MACLES SUR MACLES=   37. %
        *****************************************
     SIGMA 1   DIRECTION  312.   PENDAGE   54.      -2.178
     SIGMA 2   DIRECTION  108.   PENDAGE   34.      -1.372
     SIGMA 3   DIRECTION  206.   PENDAGE   11.      -2.686
        f=  .49  RAPPORT R= 0.7       .675

 421 501 226 504 520 401 408 521 102 416 309  10 414 506
 113 201 402 625 310 329 412 105 420 116 327 324 718 228
 323 204 508 427 315 106 104 107 526 509 119  13  29 123
 110  15-705 511 505 519 510 209 101-722 517 128 121 211
 316 516 523 108 715 314-804 313  26-707 230 502 616 130
 210 220 114   9  23  20 206-612 124 328  14 103 525 406
   6 308 127 126 131 529-713 317 407 207  21 115 528 216
 223 217 202  27  28  24 430 205
        *****************************************
     SIGMA 1   DIRECTION  321.   PENDAGE   58.      -2.086
     SIGMA 2   DIRECTION  115.   PENDAGE   29.      -1.366
     SIGMA 3   DIRECTION  211.   PENDAGE   12.      -2.594
        f=  .37  RAPPORT R= 0.6       .629

 520 226 504 521 421 408 309 501 113 102 201 625 416 327
 401 310 508 324 412 228  10 506 329 402 315 105 414 104
 323 526 106 116  29 427  13 204 316 509 119 420 110 523
 107 314 718-804 517 123 519 128 313 505  26  23 516 511
 230 211   9 308 209 101-722 328 502  15 317 616  14 121
 108 223-612 510 207 528-705 124 126  24 529  28 103 715
 525  21 407  27  20 114 130   6 210 406  25 326-824-818
 430-801 507 405-707 206 131 220 322 127
        *****************************************
        SEUIL INTERNE = 0.1184
        TAILLE DES CRISTAUX = 100 MICRONS
        SEUIL CALCULE =   11.5 MPa
        SIGMA1-SIGMA3 =    97.1
        SIGMA2-SIGMA3 =    61.1
        SIGMA1d =         44.4
```

```
***** ECHANTILLON 29 ********************
****************************************
POURCENTAGE: 50
 NOMBRE DE MACLES        365.
 NOMBRE DE NON MACLES     106.
 MACLES INCORPOREES       182
 POURCENTAGE DU NOMBRE DE NON MACLES SUR MACLES=   29. %; FAIBLE !
 POURCENTAGE DU NOMBRE DE NON MACLES SUR MACLES=   29. %
        ****************************************
    SIGMA 1   DIRECTION  186.   PENDAGE   55.     -1.077
    SIGMA 2   DIRECTION  320.   PENDAGE   26.     -1.962
    SIGMA 3   DIRECTION   61.   PENDAGE   22.     -2.075
        f= 1.03  RAPPORT R= 0.3       .344

 126 520 607 570 156 155 565 528 519 517 139 322 141 561
 547 603 223 626 527 321 154 328 571 306 558 546 630 304
 310 522 305 249 529 550 530 513 609 539 620 134 524 133
 536  24 564 221 613 202 562 509 555 624 146 435 504 118
 422 515 618  15 556 237  19 269 503 137 614 263 543  23
 616 502 559 516 204 268 312 103-538 119 824 534 260 153
 511 518 203-606 508 604 140  18 567 226 213 548 124 512
 125 127 214 617 417 563 569-818 240 542 130 443 301 147
-825 521 302-744 206   1 533 551 612 109 152 115  20 128
   5 248 621 217 329 145 510 537 430 505-501 545 142 229
 123 823 120 441 112 605  28 433 615  12 829-863 148 320
 707 318 323 423 445-804  25 506-608 315 415 303 108 261
-871 232 421 224-862 244-813 848 811 841 526-864 225  13
  22 557 201 868   3 405 264-712 205 218  29-812  21 514
 413
        ****************************************
    SIGMA 1   DIRECTION  181.   PENDAGE   53.     -1.046
    SIGMA 2   DIRECTION  316.   PENDAGE   28.     -1.950
    SIGMA 3   DIRECTION   58.   PENDAGE   22.     -2.128
        f=  .76  RAPPORT R= 0.3       .293

 520 126 607 528 570 141 322 156 565 519 155 139 561 328
 626 517 527 321 547 571 603 154 223 558 249 530 529 310
 609 134 133 630 536 522 539 306 305 524 564 546 550 304
 146 513 515 118 620 221 556 543  24 624 502 204 616 312
 503 422 613 555 509 435 119 518 562-538  15 618 559 504
 614 202 103 124 604 237 548 213 137 417 569 516 130 263
 269 534-606 147  19 153 533 260 268  18 824  23 127 125
 240 140 511 152 508 551 563 302 145 128 226 301 510 109
 203 567 217 512 115 123 443 537 214-825 545 112  20 329
 617-818 605 612 823 108 142 148-744   1 542 206 120 621
```

```
  5 430 521 303 248 505-501 421 261 205 201 445 557 441
 514 413 232 433 423 229 320 560  12 431 506 449 323 829
-863-608 811-862 615 318 415 868 121  13 315 848 212-804
-704 707 247  28 244-715 270-834 224 129-812 262 438 841
        *****************************************
        SEUIL INTERNE = 0.1314
        TAILLE DES CRISTAUX = 100 MICRONS
        SEUIL CALCULE =   11.5 MPa
        SIGMA1-SIGMA3 =    87.5
        SIGMA2-SIGMA3 =    25.7
        SIGMA1d =         49.8
```

```
***** ECHANTILLON 18 ********************
*****************************************
POURCENTAGE: 28
 NOMBRE DE MACLES        186.
 NOMBRE DE NON MACLES      81.
 MACLES INCORPOREES       52
 POURCENTAGE DU NOMBRE DE NON MACLES SUR MACLES=   44. %
        *****************************************
     SIGMA 1   DIRECTION  293.   PENDAGE   54.      -2.158
     SIGMA 2   DIRECTION  142.   PENDAGE   32.      -1.816
     SIGMA 3   DIRECTION   43.   PENDAGE   14.      -2.392
        f=  .69  RAPPORT R= 0.4        .366

 271 116 603 534 267 167 270 622-608 422 624-629 564 225
 513 129 309  30-611 202 141 256 214 553-605 536 563   2
 121 402 233 101 142 164 439 327 152 223   6 232 823 133
 263 626 318 512-627 532 149 554 413 411-621 404 212-616
-854 406 803-623 463
        *****************************************
     SIGMA 1   DIRECTION  288.   PENDAGE   57.      -2.098
     SIGMA 2   DIRECTION  139.   PENDAGE   29.      -1.820
     SIGMA 3   DIRECTION   41.   PENDAGE   14.      -2.429
        f=  .52  RAPPORT R= 0.3        .336

 271 116 534 603 422 622 167 267 624 225 270-608  30 513
-629 141 309 129-605 564 553 536   2 214-611 142 256 121
 202 327 402 563 101   6 164 152 133 823 439 232 223 413
 626 404 233 263 149 803 406 105 463 411 532-855 512 318
 844
        *****************************************
        SEUIL INTERNE = 0.2743
        TAILLE DES CRISTAUX = 100 MICRONS
        SEUIL CALCULE =   11.5 MPa
```

SIGMA1-SIGMA3 = 41.9
SIGMA2-SIGMA3 = 14.1
SIGMA1d = 23.3

Etchecopar's calcite stress inversion technique (CSIT)

Stress Tensors compressional / strike-slip - Phase N*2

```
***** ECHANTILLON 29 ********************
*****************************************
POURCENTAGE: 38
 NOMBRE DE MACLES        183.
 NOMBRE DE NON MACLES     106.
 MACLES INCORPOREES       69
 POURCENTAGE DU NOMBRE DE NON MACLES SUR MACLES=   58. %
         *****************************************
     SIGMA 1   DIRECTION   27.   PENDAGE  11.     -2.255
     SIGMA 2   DIRECTION  296.   PENDAGE   9.     -2.895
     SIGMA 3   DIRECTION  167.   PENDAGE  76.      -.222
         f= 2.16  RAPPORT R= 0.6       .604

 414 407 325 132-851 404-842-844 412 406 138-629 144 246
 436-743-713 708 619-831 455  30 456-737 235 408 710-865
-754 233-731 444-736 732 833 101 143 702 309 701 104 106
-852 623   8 326  16 149 706 231 255 622 854-729 307 242
 222 411 110 566 410 426 330 450 454 266 440-739 420 317
 314 327 102 439-705 116-628 860 402 254-730 451 271-850
  17 114-805-723 716-822 409
         *****************************************
     SIGMA 1   DIRECTION   23.   PENDAGE  16.     -2.237
     SIGMA 2   DIRECTION  290.   PENDAGE  13.     -2.778
     SIGMA 3   DIRECTION  163.   PENDAGE  69.      -.291
         f= 1.80  RAPPORT R= 0.5       .515

 414-842 132 325 407 404 246 144-851 436-844 406 408-865
 412 455   8 138-629 410-713 456 307 235-852  30-831 420
 706 622 143 326 101  17  16-850 833 732-729 619-743-736
-628 708 439 450 255 411 327 426 566 701 710-822 437 860
 116-737 402 623 106 233 454 314 857-705 105 271-731 113
 266-730 267-805-869 856 231 110 451-840 447 309-754 317
 242 311-855 854 444 149 131 716 702
         *****************************************
         SEUIL INTERNE = 0.1961
         SEUIL CALCULE =   11.5 MPa
         SIGMA1-SIGMA3 =   58.6
         SIGMA2-SIGMA3 =   30.2
```

```
       SIGMA1d =        29.0
```

```
***** ECHANTILLON 08 ********************
*****************************************
POURCENTAGE: 30
 NOMBRE DE MACLES        166.
 NOMBRE DE NON MACLES      87.
 MACLES INCORPOREES       49
 POURCENTAGE DU NOMBRE DE NON MACLES SUR MACLES=   52. %
       *****************************************
    SIGMA 1   DIRECTION  287.   PENDAGE   39.      -.905
    SIGMA 2   DIRECTION   44.   PENDAGE   30.     -2.216
    SIGMA 3   DIRECTION  159.   PENDAGE   37.      -.361
       f=  .42  RAPPORT R= 0.8       .813

   7 120   8-717-645 610 614 612   2 642  41 611   1 309
 603 305 234 244 403-707 532 601  37 631  24 547 341 629
 314 501  30 313 527-704 630   5 418 534 201 608  40-604
 544 342 516-621 618 104 235 426-606 617   9 607  18   6
       *****************************************
    SIGMA 1   DIRECTION  272.   PENDAGE   33.      -.693
    SIGMA 2   DIRECTION   37.   PENDAGE   41.     -2.118
    SIGMA 3   DIRECTION  159.   PENDAGE   31.      -.367
       f=  .30  RAPPORT R= 0.9       .914

 234 244 642   7 601   8 501 547 120  37 610 527 314 341
 532-717 614  30  24  41   2 603 608 403-645-707 607 305
 232   1 309 612 611 302 516 238 544 104 407 537 201   5
 247-606 631-704 534 618 303-621   9 629 237  42 235 426
       *****************************************
       SEUIL INTERNE = 0.3058
       SEUIL CALCULE =   11.5 MPa
       SIGMA1-SIGMA3 =    37.6
       SIGMA2-SIGMA3 =    34.4
       SIGMA1d =        13.6
```

```
***** ECHANTILLON 18 ********************
*****************************************
 POURCENTAGE: 34
 NOMBRE DE MACLES        152.
 NOMBRE DE NON MACLES      68.
 MACLES INCORPOREES       51
 POURCENTAGE DU NOMBRE DE NON MACLES SUR MACLES=   45. %
       *****************************************
    SIGMA 1   DIRECTION  237.   PENDAGE   28.      -.550
    SIGMA 2   DIRECTION    8.   PENDAGE   50.     -2.010
```

SIGMA 3   DIRECTION 133.   PENDAGE   25.   -.824
f= .98 RAPPORT R= 0.8   .816

316 315 14 113 732 730 325 121 124 115 122-610 117-719
525-628-601   7 723-721 709 422 736 28 107 321 626-717
412 135 25 120 724 726 712 130 126 132 326 429 301 311
305 424 430 225-615-735 625 133 307 403 114 701-720 528
123 520 119 136
****
SIGMA 1   DIRECTION 244.   PENDAGE   27.   -.552
SIGMA 2   DIRECTION   6.   PENDAGE   47.   -2.121
SIGMA 3   DIRECTION 136.   PENDAGE   32.   -.766
f= .67 RAPPORT R= 0.8   .769

14 316 730 325 315 709 124 107 122 121 525 321 429 732
113 626   7-628 723-717 117 736 726 132 422-601-719-610
115 712-735 520 114 412-721 701 305 28 135-720 130-615
306 625 120 123 301 724-616 802 136 126 25 225-733 133
326 521 311 516 320 307 424
****
SEUIL INTERNE = 0.2603
SEUIL CALCULE =   11.5 MPa
SIGMA1-SIGMA3 =   44.2
SIGMA2-SIGMA3 =   34.0
SIGMA1d =   18.1

Etchecopar's calcite stress inversion technique (CSIT)

Stress Tensors compressional / strike-slip - Phase N*3

***** ECHANTILLON 11 ********************
****
POURCENTAGE: 38
NOMBRE DE MACLES   249.
NOMBRE DE NON MACLES   86.
MACLES INCORPOREES   94
POURCENTAGE DU NOMBRE DE NON MACLES SUR MACLES=   35. %
****
SIGMA 1   DIRECTION 109.   PENDAGE   38.   -.890
SIGMA 2   DIRECTION 352.   PENDAGE   30.   -.924
SIGMA 3   DIRECTION 236.   PENDAGE   37.   -2.161
f= 1.17 RAPPORT R= 0.5   .482

529 226 305 808 29 125 121 324 212 717   7 18 427 25
6 23-739 404 506 105 204   3   9 450 118 307 507 423

```
 207 325 518-810 106  16 227 154 416 115 405 509 210 217
 215 142 102 103 516 801 114 144 510 219 511 513  13 214
 414 514-823-605 141-625 303 110 609 512 224 206  27 320
 441 222 425 221-825 418-805-804 229 419 508 143 119 402
 504 703 149 429 526 439 454-701-816 520 426-601-741 124
 607-616 123-807-732 442 108 503 445-757-455 705-746 421
      *****************************************
    SIGMA 1   DIRECTION  110.   PENDAGE   33.      -.749
    SIGMA 2   DIRECTION  353.   PENDAGE   36.      -.916
    SIGMA 3   DIRECTION  230.   PENDAGE   38.     -2.270
       f=  .65  RAPPORT R= 0.5        .515

 529 226 305  29 808 125 717  25  18 121 324 427 212  23
   6   7-739 506 404   3 507 307 207 423 518 204 115 210
 105 450 217   9 118 142 405 106 514 325  16 416  13 154
 441 510-810  27 509 103 504 801 215 221 703 425 511 119
 114 206 609 144 418 227 513 102-625 110 516 219-605 214
-741-757 454 141 402-823  12 705 508 224 520 222 124 607
 143 512 229 414-825 442 419 526 421 149 720-732 439 228
-816 429-621 156 320-805 116 123 303 502
       *****************************************
       SEUIL INTERNE = 0.1522
       SEUIL CALCULE =   11.5 MPa
       SIGMA1-SIGMA3 =    75.5
       SIGMA2-SIGMA3 =    38.9
       SIGMA1d =         37.4
```

```
***** ECHANTILLON 18 ********************
*****************************************
POURCENTAGE: 32
 NOMBRE DE MACLES        273.
 NOMBRE DE NON MACLES      81.
 MACLES INCORPOREES       87
 POURCENTAGE DU NOMBRE DE NON MACLES SUR MACLES=   30. %; FAIBLE !
 POURCENTAGE DU NOMBRE DE NON MACLES SUR MACLES=   30. %
       *****************************************
    SIGMA 1   DIRECTION  137.   PENDAGE   59.     -1.447
    SIGMA 2   DIRECTION   36.   PENDAGE    6.     -1.042
    SIGMA 3   DIRECTION  303.   PENDAGE   30.     -1.000
       f= 1.22  RAPPORT R= 0.4        .399

 868 451 428 407 409 440 427 465 448 454 435 865 857 166
-829 866 405 408   5 162 835 442 449  11 417 126   1-804
 410 313 870  10 467-811  24-826 441-730 426  18 834 117
  15 125 244   9 464  27 401-853 462 502 452 304  13 455
```

```
 466 533 421 312 416 832 801 319 429-613 224 106 824  29
-623-833 264 823 571 717-612-725-710 762 766-716 138 604
  21 310   2 565 867 263 303 254 524  17-308 128 864 110
 567-722 265   4
        *******************************************
    SIGMA 1   DIRECTION  133.   PENDAGE   49.      -1.459
    SIGMA 2   DIRECTION   37.   PENDAGE    5.      -.861
    SIGMA 3   DIRECTION  303.   PENDAGE   41.       -.995
        f=  .96  RAPPORT R= 0.4       .392

 427 435 409 166 428 440-829 407 866 857 868 451 835 162
 448 426 465  13 454 405 442 417   5 865 410 304 801-804
 441 455 834  18 452 421 126 224 571 125 425 502 467  10
 106 313  17  24-826 408 565 151  11 832 416 870 449   1
  27-722 867-716-853-748 856 836   9 265 319 429 464 268
-613 401 503 533 257-730 323-725 139  29  22 717 604 244
-739 466-811 203 329 302 762 138   8 567 556  12 568 303
 003
        *******************************************
        SEUIL INTERNE = 0.1614
        TAILLE DES CRISTAUX = 100 MICRONS
        SEUIL CALCULE =   11.5 MPa
        SIGMA1-SIGMA3 =    71.2
        SIGMA2-SIGMA3 =    27.9
        SIGMA1d =         38.2
```

```
***** ECHANTILLON 18 *********************
*******************************************
POURCENTAGE: 32
 NOMBRE DE MACLES        223.
 NOMBRE DE NON MACLES      68.
 MACLES INCORPOREES       71
 POURCENTAGE DU NOMBRE DE NON MACLES SUR MACLES=   30. %
        *******************************************
    SIGMA 1   DIRECTION  109.   PENDAGE   38.       -.890
    SIGMA 2   DIRECTION  352.   PENDAGE   30.       -.924
    SIGMA 3   DIRECTION  236.   PENDAGE   37.      -2.161
        f= 1.05  RAPPORT R= 0.5       .482

 323 304 319-809 227 302 322 330 303  22 406 101  13 116
 728 125 606  27 530 210 103 215  18  20 706 329   8-727
-806 519  12 618 431 131 411 105 515-714   5   3-630 522
 110 423 230  17 619-737  21 108 620 436 204 501 432 109
-734 224 415 104 413 512 214-612 829-613  23 830-823-602
 127-816 729 416  10 112 229 207  19-623 404 128 318-627
```

```
433
     *****************************************
   SIGMA 1   DIRECTION  112.   PENDAGE   33.      -.925
   SIGMA 2   DIRECTION    4.   PENDAGE   24.      -.757
   SIGMA 3   DIRECTION  246.   PENDAGE   47.     -1.994
     f=  .91  RAPPORT R= 0.5       .478

323 304 227  13 116 728 530-809 322 302  22 406-727 125
330 131 319 103 522 101 411 606  17 519 303 706 501 431
512 215 210   8 620-737 329-734  12 104-823-714 619  27
 18 230  20   3   5 110-630 214 127 423 437 729-613 105
204  23 502 830 222 416 618 207 432 415-806 109  10 515
-612 224 413 527 111-617  19 436 218 108 112 128
     *****************************************
     SEUIL INTERNE = 0.1478
     TAILLE DES CRISTAUX = 100 MICRONS
     SEUIL CALCULE =   11.5 MPa
     SIGMA1-SIGMA3 =    77.8
     SIGMA2-SIGMA3 =    37.2
     SIGMA1d =         39.5
```

```
***** ECHANTILLON 11 ********************
*****************************************
POURCENTAGE: 40
 NOMBRE DE MACLES        259.
 NOMBRE DE NON MACLES      86.
 MACLES INCORPOREES       103
 POURCENTAGE DU NOMBRE DE NON MACLES SUR MACLES=   33. %
     *****************************************
   SIGMA 1   DIRECTION  109.   PENDAGE   38.      -.890
   SIGMA 2   DIRECTION  352.   PENDAGE   30.      -.924
   SIGMA 3   DIRECTION  236.   PENDAGE   37.     -2.161
     f= 1.39  RAPPORT R= 0.5       .482

529 226 305 808  29 125 121 324 212 717   7  18 427  25
  6  23-739 404 506 105 204   3   9 450 118 307 507 423
207 325 518-810 106  16 227 154 416 115 405 509 210 217
215 142 102 103 516 801 114 144 510 219 511 513  13 214
414 514-823  10-605 141-625 303 110 609 512 224 206  27
320 441 222 425 221-825 418-805-804 229 419 508 143 119
402 504 703 149 429 526 439 454-701-816  12 520 426-601
-741 124 607-616 123-807-732 442 108  21 503 445-757-455
705-746 421 228-751 603 156 515 116 150
     *****************************************
   SIGMA 1   DIRECTION  107.   PENDAGE   34.      -.849
```

```
   SIGMA 2   DIRECTION  355.   PENDAGE   29.      -.837
   SIGMA 3   DIRECTION  234.   PENDAGE   42.     -2.195
      f=  .85  RAPPORT R= 0.5       .491

 529 305  29 226 808 717  18 324 212 125  23 427   6 121
  25   7 307 404-739 207 506   9   3 450 204 115 518 507
 217 423  16 210 106 142 105 514 215 118 405  13 516 214
 509-810 114 227 801 511 102 416 325 103 513 510 425 124
 154-625 402 441 221 414 144  12 222 206-741  27-757 609
 224-605-823 512 110  10 520 119 504 703 418 143 320 219
 442-746-816-805-732-701 508 229 141 454 526 720 705 419
 156 150 421 502 426 303 429-825  21 108 702 607-722 149
 603 439 228 123 515
      ******************************************
      SEUIL INTERNE = 0.1393
      TAILLE DES CRISTAUX = 100 MICRONS
      SEUIL CALCULE =   11.5 MPa
      SIGMA1-SIGMA3 =    82.6
      SIGMA2-SIGMA3 =    40.5
      SIGMA1d =          41.5
```

Etchecopar's calcite stress inversion technique (CSIT)

Stress Tensors compressional - Phase N*4

```
***** ECHANTILLON 08 *********************
******************************************
POURCENTAGE: 42
 NOMBRE DE MACLES        306.
 NOMBRE DE NON MACLES      84.
 MACLES INCORPOREES       128
 POURCENTAGE DU NOMBRE DE NON MACLES SUR MACLES=   27. %; FAIBLE !
      ******************************************
   SIGMA 1   DIRECTION   34.   PENDAGE   18.     -2.753
   SIGMA 2   DIRECTION  280.   PENDAGE   50.     -2.162
   SIGMA 3   DIRECTION  136.   PENDAGE   34.      -.762
      f= 1.16  RAPPORT R= 0.3       .260

 278  85 555  79  71 283  50  53 440  57  80  76 659 464
 261 567  47 687 565 438 290 554 661 547 466 289 469  78
 172 389 684 456 587 737 444 585 358 666  82  88 467  72
 750 552  63  49 551  81 272 451-743 771 454 452  48 690
 588 856 664 253 449 164  55 462 576-769-672 656 447 471
  68-647 161  52 593 560 268 442 739 768 168 648-670 669
 390 675 755 459 458  84 674  60-658 577  83 350 751 662
```

```
 657 287 288 550-763 455 767 443  64 295 359-170 285-738
 258 284 453-770-892  66 549 250-753  92-651 265 392 895
 379-758  67-677 583-676-680 292 387 376 568 450 362 386
 271-850  69 460 749  58
        *****************************************
    SIGMA 1   DIRECTION   35.   PENDAGE   20.      -2.738
    SIGMA 2   DIRECTION  275.   PENDAGE   54.      -2.071
    SIGMA 3   DIRECTION  136.   PENDAGE   29.       -.763
        f= 1.03  RAPPORT R= 0.4       .354

 278 555  71 283  79  50  85  76 464  80  53 567  57  47
 547 290 565 659 469 440 261 438 687 456 585 684 289 554
 272 666 552 661  72 737 358 466 467  81  63 587  88-743
 172 771 389  78  49 750 451  82 444 576 690 551 471-672
-769 164  48 664 454-647 268-658 588 168 452  55 657  68
 550 449 253 856 656  52 648 768 560 447 669 739 350 462
 285 390 161 675 443  84 593-680 265 287 250-670 459  83
 674 755 568  60 458 577 376 442 751 379  66 295 258 359
-892 284-738 767-763 366 288-676  64 455-850-170 583 662
 353 549-651 371-883 895  67 387 460 450 292 453  92 271
 559 849 362
        *****************************************
        SEUIL INTERNE = 0.1415
        TAILLE DES CRISTAUX = 100 MICRONS
        SEUIL CALCULE =   11.5 MPa
        SIGMA1-SIGMA3 =    81.3
        SIGMA2-SIGMA3 =    28.8
        SIGMA1d =         44.6
```

```
***** ECHANTILLON 08 ********************
*****************************************
POURCENTAGE: 40
 NOMBRE DE MACLES        294.
 NOMBRE DE NON MACLES      78.
 MACLES INCORPOREES       117
 POURCENTAGE DU NOMBRE DE NON MACLES SUR MACLES=   27. %; FAIBLE !
        *****************************************
    SIGMA 1   DIRECTION   28.   PENDAGE    7.      -2.880
    SIGMA 2   DIRECTION  294.   PENDAGE   28.      -2.643
    SIGMA 3   DIRECTION  131.   PENDAGE   61.       -.854
        f=  .86  RAPPORT R= 0.1       .061

  78 389 434 430  85 436 554 358 587 428 856 278 261  49
 253 155 157 593  63  81 452  82 551  57 441 552 289 661
 662 449  55 150 555  72  52 433 392 577 738  79  83 666
```

```
 585 754 148 283  48 156  80 390 375  88  50-740 659  53
  71 687 386-739 588 451 429 848 284 731 895-670  84  64
 664 565  47 560 272 292 270 144 684 356 268-886-677 443
  67  76 350 288 656 439 440-647 674  74 435 690 454 446
 370 549 572 290 359 756 437-850 453 567 132 138  68-445
 387  60 547 653-691  77 735-745 849 380-732-654 379 675
 271  92 131
         *****************************************
     SIGMA 1   DIRECTION   28.   PENDAGE    8.      -2.881
     SIGMA 2   DIRECTION  293.   PENDAGE   30.      -2.592
     SIGMA 3   DIRECTION  131.   PENDAGE   59.       -.860
         f=  .81  RAPPORT R= 0.1       .071

  78  85 389 434 430 436 554 358 587 428 278 856 261 155
  49 253 157  63  82 593 452  81  57 551 441 552 289 661
 555 150  72 449  55 662 433  52  79 392 738 577 666  83
 283 585  48  80 754  50 659 148  88  71  53 156 390 687
 375-740 386-739 451 588 664-670 429  84 284 565 848  64
  47 731 895 684 560 272 292-677 270 144  76 268 443 356
-886  67 439 350 288 656 440-647 674 690 435  74 454 290
 549 756 446 370 359 572 567 138  68-850 437 453 547 132
  60-445 387 653-691-745  77-732 735 675 849 379 380 271
-654  92 583
         *****************************************
         SEUIL INTERNE = 0.1805
         TAILLE DES CRISTAUX = 100 MICRONS
         SEUIL CALCULE =   11.5 MPa
         SIGMA1-SIGMA3 =    63.7
         SIGMA2-SIGMA3 =     4.5
         SIGMA1d =         41.0
```

```
***** ECHANTILLON 08 *********************
*****************************************
 POURCENTAGE: 38
 NOMBRE DE MACLES        188.
 NOMBRE DE NON MACLES      84.
 MACLES INCORPOREES       71
 POURCENTAGE DU NOMBRE DE NON MACLES SUR MACLES=   45. %
         *****************************************
     SIGMA 1   DIRECTION  287.   PENDAGE   39.       -.905
     SIGMA 2   DIRECTION   44.   PENDAGE   30.      -2.216
     SIGMA 3   DIRECTION  159.   PENDAGE   37.       -.361
         f=  .74  RAPPORT R= 0.8       .813

   7   8-645 610 614 404 612   2 642  41 611   1 432 309
```

```
 603 415 305 725 234 244 532 114 601 418  37 631 416  24
 547 341 419 629 435 314 501 704-733-718  30 313 527-713
 630   5 534 201-707 608  40-604 544 113-714 342 732 516
-621 618 429-712 235-606 617   9 607  18   6  10 247 302
 407 303 232  42 535 414 537 237-628-637 423 421 543
        *****************************************
     SIGMA 1   DIRECTION  282.   PENDAGE   36.      -.769
     SIGMA 2   DIRECTION   47.   PENDAGE   38.     -2.118
     SIGMA 3   DIRECTION  165.   PENDAGE   31.      -.255
        f=  .53  RAPPORT R= 0.8       .832

   7  41 532 642   8  37 244 614 234 404 432 601 114-733
 418 603   1 610 527 501 547 314 201-645 704 429   2 247
 612 611 415 725 309 435 305  40 341 238 237  30  24 608
 631 607 537 629 105 416 342 419-718   5 433 227 232   9
-713-606-729-714  10-637 113 302 313-712-707 732 115-621
 630 544 235 641  18 534 407 617 516 303 618 405   6
        *****************************************
        SEUIL INTERNE = 0.2638
        SEUIL CALCULE =   11.5 MPa
        SIGMA1-SIGMA3 =    43.6
        SIGMA2-SIGMA3 =    36.3
        SIGMA1d =         17.0
```

Etchecopar's calcite stress inversion technique (CSIT)

Stress Tensors compressional/strike-slip - Phase N*5

```
***** ECHANTILLON 08 ********************
*****************************************
  POURCENTAGE: 50
 NOMBRE DE MACLES        178.
 NOMBRE DE NON MACLES      84.
 MACLES INCORPOREES       89
 POURCENTAGE DU NOMBRE DE NON MACLES SUR MACLES=   47. %
        *****************************************
     SIGMA 1   DIRECTION  144.   PENDAGE   22.      -.388
     SIGMA 2   DIRECTION  341.   PENDAGE   67.     -1.464
     SIGMA 3   DIRECTION  237.   PENDAGE    6.     -2.153
        f= 1.37  RAPPORT R= 0.4       .392

 260 563 558 571 589 349 663 569 852 566 561 291 388 573
 579 137 355-365 368 146 369 277-880-888 155 562 592 575
-595 158  86 160 262 564 151 165 348 582 248 167 463-682
  87 381 140 256 382 557 144 148 138 468 254 266 367-752
```

```
 591 166 273 275-894 868 772  61 352 143 150 457 461 270
  56 884 574  62 282-745-748 572 761-770 364 152 383-875
-851 580 171 279 154 570  59 385 276-683 384 594-887 -65
 351  90 157-652-686 584-654 263 378

         *****************************************
     SIGMA 1   DIRECTION  140.   PENDAGE   15.      -.302
     SIGMA 2   DIRECTION   24.   PENDAGE   58.     -1.084
     SIGMA 3   DIRECTION  238.   PENDAGE   28.     -2.129
         f=  .92  RAPPORT R= 0.4       .364

 388 260 137 349 563 368 558 589 348 663  86 151 369 291
 566 468-595 382-752 571 167 573 561 138  87 160-888 592
 579 143 150 575 463 569  62 461 852  56 166 155 275 772
 570 171 140 364 158 144 277-887 256 146 384 355 266  90
 273  59-365 248 165 378 254-682 149 372 153 582 557 276
 761 562 455 591 270 159  70 262-770 385 279 152 282 457
  61 574 148-651 564 377  89 381 868 884 142 742 375 263
         *****************************************
         SEUIL INTERNE = 0.1980
         SEUIL CALCULE =   11.5 MPa
         SIGMA1-SIGMA3 =    58.1
         SIGMA2-SIGMA3 =    21.1
         SIGMA1d =         31.7
```

```
***** ECHANTILLON 08 ********************
*****************************************
POURCENTAGE: 46
 NOMBRE DE MACLES        177.
 NOMBRE DE NON MACLES      78.
 MACLES INCORPOREES       81
 POURCENTAGE DU NOMBRE DE NON MACLES SUR MACLES=   44. %
         *****************************************
     SIGMA 1   DIRECTION  123.   PENDAGE   23.      -.418
     SIGMA 2   DIRECTION  262.   PENDAGE   61.     -1.875
     SIGMA 3   DIRECTION   26.   PENDAGE   17.     -2.691
         f=  .96  RAPPORT R= 0.2       .243

 291-365 574 282 153 248 256 557 275 133 273 149 136 388
 140 564  86 154 139 348 266 130 581 279 364 260 152-595
 286 431 571-888 570 553  70-887  56-744 349 563  90 438
  62  87 377 293 729 276 277 558 135 384 663 368  54 592
 382 378 259 372 457 374 369 857  59-880 589  89 361 562
 734 351 569 251 743 254-851  91 264 852 267 893-728  61
 143 355-894 141 263 561
         *****************************************
```

```
   SIGMA 1   DIRECTION  126.   PENDAGE    9.      -.162
   SIGMA 2   DIRECTION  351.   PENDAGE   77.      -1.413
   SIGMA 3   DIRECTION  217.   PENDAGE    9.     -2.495
      f=  .47  RAPPORT R= 0.3       .315

291 276 382 557 275 574 248 388  62 348 273 260 368 282
 56 438 139 563 372 266-365 384 570-887  90 558  86 729
256 153 364 279  59 277  87 579 143 582 571 581-595 154
349 140 142-744  70 573 251 448  75  89 136 151 378 566
361 254 133 553 431 128 569 374 357-888 734 369 663 377
351 286 743 650 293-863 589 564 135 267 678 447 149 385
263 562-683 592 590
      ******************************************
      SEUIL INTERNE = 0.2164
      SEUIL CALCULE =   11.5 MPa
      SIGMA1-SIGMA3 =    53.1
      SIGMA2-SIGMA3 =    16.7
      SIGMA1d =         29.9
```

```
***** ECHANTILLON 08 *********************
******************************************
POURCENTAGE: 40
 NOMBRE DE MACLES        276.
 NOMBRE DE NON MACLES      87.
 MACLES INCORPOREES       110
 POURCENTAGE DU NOMBRE DE NON MACLES SUR MACLES=   32. %
      ******************************************
   SIGMA 1   DIRECTION  155.   PENDAGE   19.      -.592
   SIGMA 2   DIRECTION   54.   PENDAGE   29.      -.615
   SIGMA 3   DIRECTION  274.   PENDAGE   55.      -1.510
      f= 1.34  RAPPORT R= 0.6       .594

 101 802 323 102 333 332 119 410 424 114 320 412 126 526
 208 508 116 427 539-836 343 105 718 833 422 123 223  17
 408 413 125 306-518 107 106 226 316-823 511 506 515 110
 428 217 335  19 206 311-728-616 536 338 404 219   3 402
 411 121  25  35  33  29  31 321 122 225 127 521  22-623
 103 405 239 328 425 117 340 414  15 419 204 326 415  16
 211-818 331  38  32-619 108 236 329 720 519 312  39 837
 541-622 421-821-805  45 345-503 520-640 222 514 609 416
-643 113 529 710 317-835 218 809 504 842 613-701 605 210
      ******************************************
   SIGMA 1   DIRECTION  160.   PENDAGE   15.      -.645
   SIGMA 2   DIRECTION   64.   PENDAGE   20.      -.448
   SIGMA 3   DIRECTION  284.   PENDAGE   64.      -1.330
      f=  .95  RAPPORT R= 0.6       .580
```

```
 323 802 114 101 102 410 119 427 424 320 422  17 105 333
 413 332 126 123 412 506 306 208 428 116 408 343 311 125
 107 526 404  19 508 539 106-616 718 121 328  25 321 425
 226-818 411 405-518  16 331 206 833-836  15 415 108-823
  22 316-619 515 329 402 312 217   3 103 536  33 511 345
 223 419  39 609 421-622 326  29  31-503-728 110 710 613
 414 122 605-623 210 842-835  35-716 335 512 243 340 118
 510 541 218 245-701 706 225 514-639 720 317 117  28 416
-643 127  45  32 529-636  38  43 239 521 219 339 338 625
        *****************************************
        SEUIL INTERNE = 0.1908
        TAILLE DES CRISTAUX = 100 MICRONS
        SEUIL CALCULE =   11.5 MPa
        SIGMA1-SIGMA3 =    60.3
        SIGMA2-SIGMA3 =    35.0
        SIGMA1d =         28.5
```

```
***** ECHANTILLON 08 ********************
*****************************************
POURCENTAGE: 38
 NOMBRE DE MACLES        303.
 NOMBRE DE NON MACLES      84.
 MACLES INCORPOREES       115
 POURCENTAGE DU NOMBRE DE NON MACLES SUR MACLES=   28. %; FAIBLE !
        *****************************************
     SIGMA 1   DIRECTION  149.   PENDAGE   32.      -1.159
     SIGMA 2   DIRECTION   50.   PENDAGE   13.       -.616
     SIGMA 3   DIRECTION  301.   PENDAGE   55.      -1.037
        f= 1.28  RAPPORT R= 0.7       .692

 323 126 802 431 120 127 702 515 217 333 422 417 706 343
 206 406 710 320-836 130 136 128 316-518 332 208 722 112
 103  33 124 123 108  19  16  22 226  17 102 508  25 223
-818 536 326  39 335 111-436 809 202  32 328 339 711 125
  29 539 204  31 338  15-823 526 721 210 219 833 306 716
 311  35 134 245 506 517 322 214 331-806 427 514 215 122
 107 723 106 109-717 209 412 329 131 224 116 239-845   3
 321  43 511  28 842 502 426 317  45 129 312-616 225-821
 212 345 211-805 613 425 402 705-826 409-623-640 728  38
  26 222-619-810  11
        *****************************************
     SIGMA 1   DIRECTION  154.   PENDAGE   26.      -1.096
     SIGMA 2   DIRECTION   57.   PENDAGE   13.       -.509
     SIGMA 3   DIRECTION  303.   PENDAGE   61.       -.993
        f= 1.14  RAPPORT R= 0.7       .694
```

```
323 126 802 120 422 702 406 431 127 130 710 320 417 333
515 343 217 112 206 108 128  17  19 103 124  16 706  22
 25 332-518 208-818 316 111 123-836 136 508 328  39  33
125 226 722 306  15 326 311-436 506 134 536 721 210 102
107 711 339 245 331 526 223 202 321  29  31 809 716 116
329 539 723 322  32-616 514 209  43 833 312-823-806 335
  3 345  28-717 106 212 842 214 613 413 426-619-845  35
 45 317 338  26 122 609 219 412  23 109 239 511 728 224
204 409 724 121 605 427 517 225 425-503 243 541  12 131
       ****************************************
       SEUIL INTERNE = 0.1424
       TAILLE DES CRISTAUX = 100 MICRONS
       SEUIL CALCULE =   11.5 MPa
       SIGMA1-SIGMA3 =    80.8
       SIGMA2-SIGMA3 =    56.1
       SIGMA1d =         35.2
```

Appendix B

LA-ICP-MS U/Pb detrital zircon data

Analysis	$^{207}Pb/^{206}Pb$	±2σ	$^{206}Pb/^{238}U$	±2σ	$^{207}Pb/^{235}U$	±2σ	$^{208}Pb/^{232}Th$	±2σ	$^{207}Pb/^{206}Pb$	±2σ	$^{206}Pb/^{238}U$	±2σ	$^{207}Pb/^{235}U$	±2σ	$^{208}Pb/^{232}Th$	±2σ	Concordancy
Sample T15_PK1 – Volcanic Sandstones – Clastic Unit 4																	
PK1 - 1	0.10838	0.00171	0.3193	0.00421	4.77212	0.08037	0.0793	0.00449	1772.4	28.52	1786.3	20.56	1780	14.14	1542.4	84.16	101
PK1 - 2	0.05422	0.00087	0.05994	0.00079	0.44813	0.00763	0.01022	0.00035	380.1	35.6	375.3	4.83	376	5.35	205.6	7.08	99
PK1 - 3	0.05591	0.00121	0.07258	0.00105	0.5595	0.01236	0.01059	0.00044	448.6	47.19	451.7	6.31	451.2	8.05	212.9	8.9	101
PK1 - 4	0.05545	0.00101	0.06759	0.00092	0.51674	0.00981	0.0114	0.00042	430.2	39.64	421.6	5.55	423	6.57	229.1	8.46	98
PK1 - 5	0.05999	0.00249	0.09213	0.00187	0.76055	0.0297	0.0045	0.00036	603.2	87.38	568.1	11.03	574.3	17.13	90.7	7.23	94
PK1 - 6	0.05985	0.00465	0.09223	0.00314	0.75624	0.05433	0.00137	0.00015	598.2	159.79	568.7	18.53	571.8	31.41	27.7	3.03	95
PK1 - 7	0.13124	0.00223	0.38813	0.00531	7.02501	0.12703	0.09655	0.00649	2114.6	29.45	2114.2	24.67	2114.6	16.07	1862.9	119.64	100
PK1 - 8	0.1473	0.01203	0.43392	0.01503	8.80681	0.68605	0.14055	0.05827	2314.8	133.74	2323.4	67.59	2318.2	71.03	2658.1	1032.64	100
PK1 - 9	0.10989	0.00203	0.32189	0.00463	4.87645	0.09646	0.0661	0.00453	1797.5	33.32	1798.9	22.57	1798.2	16.67	1293.6	85.89	100
PK1 - 10	0.10364	0.00446	0.29916	0.00608	4.27705	0.17848	0.07329	0.01277	1690.2	77.31	1687.1	30.17	1689	34.34	1429.6	240.51	100
PK1 - 11	0.08845	0.00164	0.24058	0.00336	2.93436	0.05739	0.0636	0.00498	1392.2	34.98	1389.7	17.47	1390.8	14.81	1246.2	94.59	100
PK1 - 12	0.16286	0.00534	0.47052	0.00817	10.567	0.33663	0.1254	0.0184	2485.6	54.25	2485.8	35.8	2485.8	29.55	2387.8	330.48	100
PK1 - 13	0.09146	0.00872	0.25338	0.00924	3.18882	0.29196	0.0379	0.01021	1456	171.35	1455.9	47.5	1454.5	70.77	751.8	198.82	100
PK1 - 14	0.19009	0.00444	0.53059	0.00809	13.90687	0.33781	0.11844	0.01198	2742.9	37.93	2743.9	34.07	2743.4	23.01	2262.4	216.57	100
PK1 - 15	0.05494	0.00279	0.06473	0.00143	0.48957	0.02397	0.0036	0.00031	409.8	109.6	404.3	8.68	404.6	16.34	72.6	6.22	99
PK1 - 16	0.08665	0.00115	0.23374	0.00315	2.79257	0.04204	0.04371	0.00142	1352.8	25.35	1354.1	16.45	1353.5	11.26	864.8	27.42	100
PK1 - 17	0.05195	0.0015	0.04382	0.0007	0.31397	0.00899	0.00549	0.00022	283.1	64.67	276.5	4.33	277.3	6.94	110.6	4.44	98
PK1 - 18	0.05508	0.00136	0.06748	0.001	0.51243	0.01289	0.01942	0.001	415.5	53.64	421	6.06	420.1	8.66	388.8	19.87	101
PK1 - 19	0.05118	0.00246	0.03952	0.00082	0.27906	0.01286	0.00349	0.00023	249.1	106.83	249.8	5.09	249.9	10.21	70.4	4.56	100
PK1 - 20	0.0534	0.00206	0.05582	0.00095	0.41063	0.01557	0.01581	0.00115	345.6	84.74	350.2	5.8	349.3	11.21	317.1	22.87	101
PK1 - 21	0.16531	0.00262	0.47619	0.00684	10.85748	0.19247	0.10772	0.00619	2510.7	26.45	2510.7	29.87	2511	16.48	2067.7	113.04	100
PK1 - 22	0.06444	0.00466	0.12291	0.00462	1.09285	0.07124	0.0026	0.00027	756.2	145.64	747.3	26.54	749.9	34.56	52.4	5.36	99
PK1 - 23	0.05295	0.00485	0.05143	0.00142	0.3752	0.03333	0.01641	0.00189	326.6	195.32	323.3	8.73	323.5	24.61	328.9	37.62	99
PK1 - 24	0.15676	0.00229	0.45585	0.00644	9.85379	0.16388	0.08267	0.00376	2421	24.54	2421.2	28.52	2421.2	15.33	1605.4	70.13	100
PK1 - 25	0.07861	0.00227	0.19681	0.00321	2.13135	0.0615	0.05496	0.00509	1162.3	56.28	1158.2	17.28	1159	19.94	1081.4	97.54	100
PK1 - 26	0.0726	0.00139	0.16764	0.0025	1.67849	0.03417	0.02789	0.00135	1002.8	38.43	999.1	13.79	1000.4	12.95	555.9	26.51	100

PK1 - 27	0.06876	0.00322	0.051	0.00099	0.48332	0.02209	0.01656	0.00133	891.5	93.8	320.7	6.06	400.3	15.12	332	26.43	36
PK1 - 28	0.08763	0.00201	0.23767	0.00374	2.87132	0.06891	0.06763	0.00595	1374.5	43.44	1374.6	19.48	1374.4	18.07	1322.6	112.73	100
PK1 - 29	0.05653	0.00483	0.07654	0.00242	0.59504	0.04903	0.02156	0.00512	472.5	179.43	475.5	14.49	474.1	31.21	431.2	101.25	101
PK1 - 30	0.0539	0.00341	0.05793	0.00128	0.43054	0.02658	0.01538	0.00137	366.6	136.15	363	7.82	363.6	18.87	308.5	27.35	99
PK1 - 31	0.06208	0.00208	0.11071	0.00198	0.94711	0.0306	0.0159	0.00072	677	69.88	676.8	11.51	676.6	15.96	318.8	14.3	100
PK1 - 32	0.05488	0.00108	0.06504	0.00095	0.49232	0.01022	0.01318	0.00054	407.1	42.97	406.2	5.77	406.5	6.95	264.7	10.83	100
PK1 - 33	0.10375	0.00158	0.30052	0.0042	4.29938	0.07303	0.07554	0.00381	1692.3	27.78	1693.9	20.8	1693.2	13.99	1472	71.66	100
PK1 - 34	0.06703	0.00234	0.13743	0.00261	1.2689	0.04191	0.00831	0.00047	838.6	71.06	830.1	14.77	831.9	18.76	167.3	9.45	99
PK1 - 35	0.05413	0.00434	0.06135	0.00186	0.45823	0.035	0.00944	0.00126	376.4	171.07	383.8	11.27	383	24.37	190	25.26	102
PK1 - 36	0.09055	0.00223	0.24961	0.00405	3.1165	0.07694	0.03197	0.00155	1437.2	46.28	1436.5	20.88	1436.8	18.98	636.1	30.39	100
PK1 - 37	0.10228	0.00248	0.29485	0.00443	4.15512	0.10049	0.07316	0.00629	1665.9	44.14	1665.7	22.06	1665.2	19.79	1427.2	118.45	100
PK1 - 38	0.05517	0.00123	0.06736	0.001	0.51249	0.01179	0.01385	0.00071	418.8	48.55	420.2	6.01	420.1	7.91	278.1	14.13	100
PK1 - 39	0.07331	0.00194	0.17131	0.00279	1.72963	0.04411	0.01176	0.00052	1022.5	52.53	1019.3	15.35	1019.6	16.41	236.3	10.45	100
PK1 - 40	0.05561	0.00233	0.07095	0.00132	0.54442	0.02225	0.01788	0.00164	436.6	90.59	441.9	7.95	441.3	14.63	358.2	32.57	101
PK1 - 41	0.05852	0.00103	0.08908	0.00124	0.71866	0.01327	0.01282	0.00055	549.3	37.99	550.1	7.37	549.9	7.84	257.4	11	100
PK1 - 42	0.05787	0.00221	0.08305	0.00159	0.66139	0.02395	0.00474	0.00027	524.6	82.04	514.3	9.45	515.5	14.64	95.7	5.36	98
PK1 - 43	0.15216	0.00288	0.44452	0.00649	9.32226	0.18096	0.04526	0.00212	2370.4	31.88	2370.8	28.97	2370.2	17.8	894.8	40.93	100
PK1 - 44	0.07026	0.00128	0.15611	0.00218	1.51164	0.02846	0.02156	0.00097	935.9	36.86	935.1	12.14	935.1	11.51	431.1	19.11	100
PK1 - 45	0.08917	0.00245	0.24341	0.00398	2.98752	0.07927	0.01572	0.00085	1407.7	51.74	1404.4	20.65	1404.4	20.19	315.3	16.9	100
PK1 - 46	0.11363	0.00208	0.05541	0.00079	0.86802	0.01628	0.01569	0.00052	1858.3	32.77	347.7	4.8	634.5	8.85	314.7	10.32	19
PK1 - 47	0.07006	0.00124	0.04884	0.00067	0.47175	0.00863	0.00816	0.00023	930.1	35.84	307.4	4.09	392.4	5.95	164.2	4.68	33
PK1 - 48	0.05389	0.00297	0.05796	0.00153	0.43089	0.02167	0.00141	0.00008	366.4	119	363.2	9.33	363.8	15.38	28.4	1.71	99
PK1 - 49	0.09249	0.00137	0.25781	0.00342	3.28787	0.05291	0.04214	0.00149	1477.4	27.99	1478.6	17.54	1478.2	12.53	834.3	28.99	100
PK1 - 50	0.06925	0.00148	0.15083	0.00222	1.4405	0.03065	0.015	0.00059	906.3	43.5	905.6	12.44	905.9	12.75	301	11.82	100
PK1 - 51	0.06543	0.00212	0.13308	0.00254	1.20028	0.03508	0.00268	0.00017	788.2	66.71	805.4	14.45	800.7	16.19	54.1	3.48	102
PK1 - 52	0.08448	0.00179	0.22434	0.0033	2.61472	0.05495	0.01705	0.00069	1303.5	40.66	1304.8	17.39	1304.8	15.44	341.7	13.66	100
PK1 - 53	0.05523	0.00102	0.06815	0.00094	0.5194	0.00991	0.00843	0.00032	421.4	40.08	425	5.66	424.8	6.62	169.7	6.32	101
PK1 - 54	0.05568	0.00162	0.07122	0.00115	0.5475	0.0154	0.00495	0.00024	439.2	63.44	443.5	6.94	443.4	10.11	99.9	4.85	101
PK1 - 55	0.05557	0.00111	0.07077	0.00098	0.54265	0.01105	0.00882	0.00034	435	43.54	440.8	5.93	440.2	7.27	177.6	6.78	101

PK1 - 56	0.09101	0.0017	0.25178	0.00348	3.16116	0.06013	0.03494	0.00138	1446.7	35.07	1447.7	17.92	1447.7	14.67	694.1	27.03	100
PK1 - 57	0.05772	0.00117	0.08465	0.00116	0.67412	0.01384	0.0135	0.00061	519	43.99	523.8	6.88	523.2	8.4	271.1	12.1	101
PK1 - 58	0.07157	0.00208	0.16351	0.0027	1.61616	0.0444	0.00828	0.00045	973.7	58.05	976.3	14.96	976.5	17.23	166.7	8.93	100
PK1 - 59	0.12261	0.00268	0.36345	0.0053	6.15772	0.13281	0.0195	0.00095	1994.5	38.39	1998.5	25.07	1998.5	18.84	390.3	18.9	100
PK1 - 60	0.08854	0.00164	0.24201	0.00331	2.95896	0.05602	0.02973	0.00138	1394.2	35.07	1397.1	17.19	1397.1	14.37	592.2	27.18	100
PK1 - 61	0.05973	0.0014	0.097	0.00148	0.79897	0.01808	0.00389	0.00013	593.9	49.95	596.8	8.71	596.2	10.2	78.5	2.7	100
PK1 - 62	0.07721	0.00159	0.19078	0.00273	2.03061	0.04273	0.03438	0.00122	1126.6	40.41	1125.6	14.79	1125.8	14.32	683.2	23.91	100
PK1 - 63	0.05525	0.00129	0.06743	0.00099	0.51353	0.01201	0.00756	0.00025	422.1	50.57	420.7	5.98	420.8	8.06	152.2	4.94	100
PK1 - 64	0.15674	0.00506	0.45622	0.00775	9.8595	0.30844	0.11562	0.01478	2420.8	53.81	2422.9	34.33	2421.7	28.84	2211.5	267.83	100
PK1 - 65	0.05832	0.00261	0.08796	0.00199	0.70764	0.02917	0.00227	0.00014	541.1	95.71	543.5	11.77	543.3	17.34	45.9	2.8	100
PK1 - 66	0.06977	0.00111	0.15386	0.00206	1.47965	0.02531	0.03177	0.00133	921.6	32.4	922.6	11.5	922.1	10.36	632.1	25.99	100
PK1 - 67	0.05743	0.00345	0.07934	0.00248	0.62784	0.03364	0.00152	0.00012	507.5	127.51	492.2	14.81	494.8	20.99	30.7	2.37	97
PK1 - 68	0.06496	0.00369	0.12786	0.00349	1.14536	0.06009	0.00568	0.00042	773.1	115.17	775.6	19.97	775	28.44	114.5	8.51	100
PK1 - 69	0.05071	0.00154	0.03543	0.0006	0.24772	0.00719	0.0023	0.00011	227.8	68.89	224.4	3.72	224.7	5.85	46.5	2.22	99
PK1 - 70	0.13771	0.00237	0.40618	0.00562	7.70842	0.14187	0.107	0.00723	2198.7	29.56	2197.4	25.76	2197.6	16.54	2054.7	132.02	100
PK1 - 71	0.05624	0.00257	0.07238	0.00157	0.56125	0.02409	0.00301	0.00018	461.2	98.9	450.5	9.42	452.3	15.67	60.8	3.72	98
PK1 - 72	0.05645	0.00122	0.07464	0.00106	0.58071	0.01297	0.02097	0.00154	469.5	47.73	464.1	6.39	464.9	8.33	419.4	30.39	99
PK1 - 73	0.07845	0.00182	0.19627	0.003	2.1216	0.04913	0.01951	0.0009	1158.3	45.3	1155.3	16.16	1155.9	15.98	390.5	17.79	100
PK1 - 74	0.05436	0.00168	0.06157	0.00095	0.46123	0.01418	0.0192	0.00152	385.8	67.67	385.2	5.75	385.1	9.85	384.4	30.24	100
PK1 - 75	0.0558	0.00209	0.07142	0.00126	0.54927	0.02021	0.02302	0.003	444.2	81.27	444.7	7.58	444.5	13.24	459.9	59.24	100
PK1 - 76	0.0757	0.00261	0.18404	0.00368	1.91821	0.06003	0.00582	0.00026	1087.2	67.56	1089	20.05	1087.4	20.89	117.3	5.23	106
PK1 - 77	0.11454	0.00127	0.33799	0.00402	5.33518	0.06498	0.05556	0.0014	1872.6	19.88	1877	19.36	1874.5	10.41	1093	26.77	105
PK1 - 78	0.05535	0.00075	0.06823	0.00084	0.52059	0.00752	0.00914	0.00024	426.1	29.97	425.5	5.06	425.5	5.02	183.8	4.87	102
PK1 - 79	0.10019	0.00242	0.28735	0.00417	3.96872	0.09482	0.06729	0.0051	1627.7	44.19	1628.3	20.86	1627.8	19.38	1316.3	96.67	102
PK1 - 80	0.08134	0.00156	0.21013	0.00287	2.35682	0.04497	0.02237	0.00067	1229.6	37.18	1229.5	15.27	1229.6	13.6	447.1	13.29	102
PK1 - 81	0.05472	0.0027	0.06363	0.00149	0.47978	0.02177	0.00167	0.00009	401	106.44	397.7	9.05	397.9	14.94	33.7	1.74	100
PK1 - 82	0.10237	0.0018	0.29542	0.00394	4.17018	0.07293	0.02289	0.00081	1667.6	32.13	1668.6	19.59	1668.2	14.32	457.4	15.98	100
PK1 - 83	0.07855	0.00221	0.19806	0.00328	2.14449	0.0562	0.00482	0.00022	1160.9	54.73	1164.9	17.67	1163.3	18.15	97.2	4.49	100
PK1 - 84	0.08878	0.00216	0.23853	0.00319	2.89764	0.06806	0.07048	0.00709	1399.3	45.85	1379.1	16.61	1381.3	17.73	1376.6	133.8	100

PK1 - 85	0.057	0.00124	0.07736	0.00104	0.60778	0.01318	0.02076	0.00129	490.9	47.12	480.3	6.21	482.2	8.33	415.2	25.64	100
PK1 - 86	0.05564	0.00108	0.07196	0.00091	0.55134	0.01071	0.02207	0.00128	437.7	42.25	447.9	5.47	445.9	7.01	441.3	25.31	100
PK1 - 87	0.056	0.00169	0.07198	0.00113	0.55577	0.01611	0.00851	0.00042	452	65.61	448.1	6.78	448.8	10.52	171.2	8.37	100
PK1 - 88	0.09139	0.00227	0.25365	0.00385	3.19597	0.07626	0.0184	0.00085	1454.6	46.67	1457.3	19.79	1456.2	18.45	368.5	16.9	100
PK1 - 89	0.05637	0.00158	0.0752	0.00115	0.58431	0.01574	0.00596	0.00029	466	61.35	467.4	6.9	467.2	10.09	120.1	5.84	100
PK1 - 90	0.09979	0.00197	0.2856	0.00388	3.92956	0.07704	0.02974	0.00132	1620.3	36.34	1619.5	19.43	1619.8	15.87	592.4	25.95	100
PK1 - 91	0.07138	0.00145	0.16137	0.00223	1.58851	0.03117	0.01079	0.00037	968.4	40.83	964.4	12.36	965.7	12.23	216.9	7.49	100
PK1 - 92	0.05881	0.00271	0.09089	0.00206	0.73781	0.03115	0.00309	0.00018	560.1	97.52	560.8	12.17	561.1	18.2	62.3	3.55	100
PK1 - 93	0.05521	0.0009	0.06713	0.00085	0.51088	0.00852	0.00998	0.00031	420.4	35.65	418.8	5.11	419	5.73	200.7	6.11	100
PK1 - 94	0.05546	0.00086	0.07046	0.00087	0.53877	0.00867	0.01195	0.00032	430.7	33.67	438.9	5.25	437.6	5.72	240.1	6.35	100
PK1 - 95	0.06145	0.00319	0.10932	0.00287	0.92963	0.0432	0.00263	0.00016	655	107.48	668.8	16.69	667.4	22.73	53.2	3.25	100
PK1 - 96	0.05261	0.00172	0.04983	0.00085	0.36163	0.01082	0.002	0.00009	312	72.47	313.5	5.22	313.4	8.07	40.4	1.82	100
PK1 - 97	0.05273	0.00376	0.05313	0.00128	0.38623	0.02655	0.0137	0.0016	317.3	153.94	333.7	7.86	331.6	19.45	275	31.93	100
PK1 - 98	0.09932	0.0017	0.28385	0.00365	3.8869	0.06666	0.0261	0.00091	1611.5	31.47	1610.7	18.31	1611	13.85	520.8	17.99	100
PK1 - 99	0.0678	0.00153	0.14254	0.00198	1.33227	0.02907	0.01035	0.00039	862.5	46.12	859	11.2	859.9	12.66	208.2	7.9	100
PK1 - 100	0.074	0.00196	0.17501	0.00266	1.78547	0.04445	0.00848	0.00036	1041.6	52.43	1039.6	14.57	1040.2	16.2	170.7	7.27	100
PK1 - 101	0.07399	0.00219	0.12133	0.00187	1.23767	0.03585	0.03083	0.00257	1041.2	58.72	738.2	10.77	817.8	16.27	613.7	50.35	100
PK1 - 102	0.06066	0.00183	0.1014	0.00161	0.84787	0.02376	0.00456	0.00022	627.1	63.72	622.6	9.45	623.5	13.06	92	4.49	100
PK1 - 103	0.05814	0.00201	0.08627	0.00148	0.6914	0.02207	0.01195	0.00066	534.4	74.3	533.4	8.76	533.6	13.25	240.2	13.19	100
PK1 - 104	0.06569	0.0033	0.13126	0.00313	1.18904	0.05433	0.00779	0.00055	796.4	101.8	795.1	17.85	795.5	25.2	156.8	11.11	100
PK1 - 105	0.05548	0.00445	0.06353	0.00235	0.48726	0.03232	0.00089	0.0001	431.2	169.61	397	14.25	403	22.07	17.9	2.08	~~100~~
PK1 - 106	0.06599	0.00346	0.14224	0.00397	1.29333	0.06148	0.00386	0.00027	806.2	106.2	857.3	22.41	842.8	27.22	77.9	5.39	100
PK1 - 107	0.09721	0.00123	0.27582	0.00332	3.69606	0.05086	0.0578	0.00187	1571.3	23.54	1570.3	16.77	1570.5	11	1135.8	35.65	100
PK1 - 108	0.0779	0.00128	0.19416	0.0024	2.08483	0.03519	0.05237	0.00277	1144.3	32.34	1143.8	12.94	1143.8	11.58	1031.7	53.29	100
PK1 - 109	0.05495	0.00129	0.06585	0.00087	0.49877	0.01167	0.01935	0.00096	410.1	50.87	411.1	5.25	410.9	7.91	387.3	18.95	100
PK1 - 110	0.15076	0.00196	0.44094	0.00538	9.16309	0.12756	0.06051	0.00172	2354.5	22.03	2354.8	24.07	2354.4	12.74	1187.5	32.76	100
PK1 - 111	0.19542	0.00356	0.54172	0.00742	14.59914	0.26322	0.03075	0.0011	2788.3	29.5	2790.7	31.04	2789.5	17.13	612.2	21.51	100
PK1 - 112	0.11334	0.00232	0.33293	0.00469	5.20604	0.10397	0.01589	0.0006	1853.6	36.57	1852.6	22.69	1853.6	17.01	318.7	11.99	100
PK1 - 113	0.10035	0.0014	0.28779	0.00353	3.98085	0.0586	0.04287	0.00137	1630.6	25.67	1630.5	17.68	1630.3	11.95	848.5	26.56	100

PK1 - 114	0.06853	0.00165	0.05438	0.00074	0.5137	0.01221	0.0139	0.00082	884.7	48.92	341.4	4.5	420.9	8.19	279.1	16.25	100
PK1 - 115	0.05921	0.0044	0.07807	0.00205	0.63583	0.04523	0.01513	0.00278	574.7	154.01	484.6	12.27	499.7	28.07	303.4	55.42	100
PK1 - 116	0.06343	0.00103	0.11885	0.00151	1.03936	0.01739	0.01435	0.00053	722.7	33.95	724	8.69	723.6	8.66	288	10.58	100
PK1 - 117	0.06954	0.00112	0.15243	0.0019	1.46114	0.02432	0.02846	0.00113	914.8	32.76	914.6	10.64	914.5	10.04	567.2	22.13	100
PK1 - 118	0.06719	0.00151	0.1404	0.00196	1.30086	0.02897	0.01467	0.0006	843.8	45.97	846.9	11.09	846.1	12.78	294.3	11.97	100
PK1 - 119	0.07512	0.0012	0.18061	0.00225	1.87006	0.03101	0.03161	0.00135	1071.7	31.84	1070.3	12.26	1070.6	10.97	629	26.52	100
PK1 - 120	0.09002	0.00155	0.24774	0.00321	3.0747	0.05441	0.03075	0.00125	1425.9	32.53	1426.8	16.57	1426.4	13.56	612.1	24.61	100
PK1 - 121	0.10749	0.0017	0.31293	0.00404	4.63598	0.07325	0.03921	0.00109	1757.2	28.65	1755.1	19.85	1755.8	13.2	777.3	21.24	100
PK1 - 122	0.05637	0.00091	0.07499	0.00094	0.58271	0.00972	0.01055	0.00034	466.1	35.82	466.2	5.64	466.2	6.23	212.1	6.75	100
PK1 - 123	0.09644	0.00124	0.27284	0.0033	3.6269	0.04976	0.03916	0.001	1556.3	23.9	1555.2	16.72	1555.5	10.92	776.5	19.39	100
PK1 - 124	0.09983	0.0013	0.28601	0.00344	3.93589	0.05479	0.04848	0.00138	1620.9	24.1	1621.6	17.24	1621.1	11.27	956.8	26.54	100
PK1 - 125	0.10659	0.00138	0.31017	0.00373	4.55749	0.06271	0.03934	0.00106	1742	23.5	1741.5	18.35	1741.5	11.46	779.9	20.68	100
PK1 - 126	0.07339	0.0011	0.17217	0.00213	1.74161	0.02704	0.02202	0.00062	1024.7	29.77	1024	11.7	1024.1	10.01	440.3	12.19	100
PK1 - 127	0.06	0.00087	0.09809	0.00118	0.81143	0.01234	0.02055	0.00074	603.7	31.09	603.2	6.92	603.3	6.92	411.2	14.61	99
PK1 - 128	0.11061	0.00152	0.3239	0.00389	4.93881	0.07147	0.05692	0.00196	1809.4	24.78	1808.7	18.94	1808.9	12.22	1119	37.5	99
PK1 - 129	0.08892	0.00124	0.24283	0.00291	2.97662	0.04349	0.0407	0.00139	1402.5	26.47	1401.4	15.1	1401.7	11.1	806.4	26.92	99
PK1 - 130	0.12978	0.00222	0.38383	0.00497	6.86613	0.11735	0.03426	0.00124	2095	29.72	2094.1	23.17	2094.3	15.15	680.9	24.16	99
PK1 - 131	0.08899	0.0013	0.24317	0.00292	2.9835	0.04541	0.0537	0.0024	1403.9	27.62	1403.1	15.13	1403.4	11.58	1057.2	45.99	98
PK1 - 132	0.06664	0.00121	0.13695	0.00175	1.258	0.02272	0.02202	0.00094	826.7	37.47	827.4	9.92	827	10.22	440.2	18.68	92
PK1 - 133	0.12709	0.00229	0.37582	0.00482	6.58295	0.11758	0.03443	0.00135	2058.1	31.51	2056.7	22.57	2057.1	15.74	684.3	26.37	84
PK1 - 134	0.16474	0.00258	0.47476	0.00579	10.7839	0.17375	0.11889	0.00681	2504.9	26.08	2504.4	25.3	2504.7	14.97	2270.6	123.01	71
PK1 - 135	0.07622	0.00167	0.1859	0.00247	1.95445	0.04234	0.04642	0.00343	1100.8	43.2	1099.1	13.43	1100	14.55	917.2	66.26	39
Sample T15_PK3 – Immature Volcanic Sandstones – Clastic Unit 5																	
PK3 - 01	0.11629	0.00338	0.36135	0.00564	5.80425	0.16078	0.06232	0.00427	1899.9	51.36	1988.6	26.69	1947	23.99	1221.9	81.23	105
PK3 - 02	0.0873	0.001	0.2288	0.00247	2.75484	0.03249	0.04726	0.00105	1367.2	21.91	1328.2	12.94	1343.4	8.79	933.3	20.17	97
PK3 - 03	0.08792	0.00133	0.23695	0.00272	2.87716	0.04313	0.02194	0.0007	1380.8	28.84	1370.8	14.17	1375.9	11.29	438.7	13.93	99
PK3 - 04	0.12091	0.00482	0.36143	0.00697	6.07499	0.22882	0.01698	0.00133	1969.7	69.42	1988.9	33	1986.7	32.84	340.4	26.38	101
PK3 - 05	0.12698	0.00146	0.35008	0.00379	6.13013	0.07225	0.05834	0.00126	2056.6	20.1	1935	18.12	1994.5	10.29	1146	23.97	94
PK3 - 06	0.07254	0.00111	0.04498	0.00051	0.44981	0.0069	0.01412	0.00045	1001.2	30.88	283.6	3.17	377.1	4.83	283.4	8.96	28

PK3 - 07	0.06688	0.00112	0.04608	0.00054	0.42488	0.00708	0.01294	0.00049	833.9	34.41	290.4	3.32	359.5	5.04	260	9.7	35
PK3 - 08	0.05795	0.00091	0.04284	0.00049	0.34217	0.00538	0.0119	0.00042	527.4	34.31	270.4	3.02	298.8	4.07	239	8.46	51
PK3 - 09	0.0893	0.00206	0.23908	0.00317	2.94401	0.06646	0.06358	0.00472	1410.5	43.4	1381.9	16.47	1393.3	17.11	1245.9	89.68	98
PK3 - 10	0.0953	0.00176	0.25613	0.00316	3.36722	0.06067	0.01914	0.00066	1534	34.37	1470	16.22	1496.8	14.11	383.2	13.18	96
PK3 - 11	0.07011	0.00231	0.15094	0.00234	1.46027	0.04691	0.03931	0.00442	931.5	66.28	906.2	13.09	914.1	19.36	779.4	85.95	97
PK3 - 12	0.07328	0.00252	0.17313	0.00295	1.74993	0.05808	0.00944	0.00066	1021.8	68.21	1029.3	16.2	1027.1	21.45	189.8	13.21	101
PK3 - 13	0.08971	0.00132	0.22548	0.0026	2.78851	0.04169	0.05626	0.0022	1419.4	27.78	1310.8	13.67	1352.5	11.17	1106.4	42.19	92
PK3 - 14	0.08623	0.00149	0.23206	0.00282	2.75873	0.04771	0.04111	0.00164	1343.2	33	1345.3	14.75	1344.4	12.89	814.3	31.81	100
PK3 - 15	0.05499	0.00133	0.06555	0.00087	0.497	0.01176	0.00716	0.00031	411.7	52.47	409.3	5.29	409.7	7.98	144.3	6.25	99
PK3 - 16	0.0561	0.00112	0.07328	0.00089	0.56678	0.01119	0.01989	0.00068	456.1	43.69	455.9	5.36	455.9	7.25	398	13.52	100
PK3 - 17	0.05331	0.00583	0.05029	0.00176	0.36964	0.03864	0.01631	0.00216	341.9	230.31	316.3	10.81	319.4	28.64	327	43.05	93
PK3 - 18	0.08469	0.00126	0.22528	0.00264	2.6308	0.03921	0.03045	0.00088	1308.2	28.66	1309.7	13.88	1309.3	10.96	606.3	17.27	100
PK3 - 19	0.09618	0.00227	0.27339	0.00381	3.62663	0.08139	0.01835	0.00079	1551.3	43.77	1558	19.28	1555.4	17.86	367.6	15.67	100
PK3 - 20	0.06347	0.00265	0.11969	0.00241	1.0464	0.04013	0.00273	0.00016	723.9	86.22	728.8	13.89	727.1	19.91	55.2	3.17	101
PK3 - 21	0.05556	0.00082	0.07006	0.0008	0.53672	0.008	0.01288	0.00034	434.5	32.2	436.5	4.81	436.3	5.29	258.7	6.81	100
PK3 - 22	0.11011	0.00417	0.3218	0.00567	4.87986	0.17428	0.08464	0.0097	1801.1	67.31	1798.5	27.64	1798.8	30.1	1642.2	180.74	100
PK3 - 23	0.05448	0.00096	0.06209	0.00073	0.46641	0.00816	0.01341	0.00044	390.8	38.86	388.3	4.44	388.7	5.65	269.3	8.71	99
PK3 - 24	0.06993	0.00112	0.15616	0.00182	1.50574	0.02399	0.02899	0.00088	926.2	32.62	935.4	10.14	932.7	9.72	577.6	17.31	101
PK3 - 25	0.07332	0.00105	0.17118	0.00194	1.73055	0.02499	0.03668	0.00123	1022.7	28.73	1018.6	10.67	1020	9.29	728.2	23.99	100
PK3 - 26	0.05336	0.00206	0.05579	0.00089	0.41015	0.01522	0.01309	0.00096	344.2	85.03	350	5.44	349	10.96	262.9	19.21	102
PK3 - 27	0.0558	0.00196	0.06458	0.00097	0.49672	0.0168	0.00918	0.00035	444	76.42	403.4	5.86	409.5	11.4	184.7	6.97	91
PK3 - 28	0.0558	0.00095	0.07176	0.00083	0.55216	0.00929	0.01567	0.00058	444.2	36.98	446.7	5.02	446.4	6.08	314.3	11.59	101
PK3 - 29	0.05449	0.00138	0.06317	0.00081	0.47466	0.01172	0.01699	0.00083	391.2	55.75	394.9	4.93	394.4	8.07	340.5	16.54	101
PK3 - 30	0.06158	0.00212	0.10855	0.00174	0.92162	0.02997	0.0088	0.00039	659.7	72.15	664.3	10.09	663.2	15.84	177	7.78	101
PK3 - 31	0.05869	0.00169	0.08791	0.0013	0.70977	0.01936	0.00684	0.00026	555.8	61.53	543.1	7.7	544.6	11.5	137.9	5.2	98
PK3 - 32	0.07461	0.00161	0.17712	0.00227	1.82146	0.0382	0.04483	0.00186	1057.7	43.11	1051.2	12.41	1053.2	13.75	886.5	35.99	99
PK3 - 33	0.05373	0.00116	0.05679	0.00071	0.42043	0.00888	0.00979	0.00034	359.6	48.07	356.1	4.36	356.4	6.35	197	6.79	99
PK3 - 34	0.05891	0.00105	0.09177	0.0011	0.74504	0.01321	0.0252	0.00108	563.7	38.37	566	6.48	565.3	7.69	503	21.22	100
PK3 - 35	0.05624	0.00117	0.07442	0.00091	0.57686	0.01176	0.01865	0.00065	461	45.67	462.8	5.48	462.4	7.57	373.5	12.91	100

PK3 - 36	0.05568	0.00145	0.06985	0.00092	0.53612	0.01352	0.01991	0.00101	439.4	56.53	435.3	5.55	435.9	8.93	398.4	19.92	99
PK3 - 37	0.05525	0.00107	0.06788	0.00082	0.51698	0.00989	0.01844	0.00087	422.2	42.16	423.4	4.93	423.1	6.62	369.3	17.17	100
PK3 - 38	0.05	0.00376	0.03228	0.00099	0.22237	0.01563	0.0024	0.0003	195.2	165.85	204.8	6.19	203.9	12.99	48.5	6.1	105
PK3 - 39	0.05282	0.00119	0.05067	0.00064	0.36897	0.00816	0.01266	0.00053	321.2	50.34	318.7	3.92	318.9	6.05	254.2	10.62	99
PK3 - 40	0.05437	0.00115	0.06188	0.00077	0.46374	0.00961	0.01089	0.00038	386.2	46.59	387.1	4.68	386.9	6.67	218.9	7.56	100
PK3 - 41	0.09614	0.00172	0.27165	0.00334	3.6	0.06361	0.04283	0.00182	1550.6	33.21	1549.1	16.91	1549.5	14.04	847.7	35.36	100
PK3 - 42	0.05369	0.00119	0.05691	0.00072	0.42126	0.00913	0.01029	0.00042	358.1	49.3	356.8	4.39	357	6.52	206.9	8.31	100
PK3 - 43	0.08883	0.00143	0.24259	0.00285	2.97044	0.04788	0.05991	0.00278	1400.4	30.49	1400.2	14.8	1400.1	12.24	1176.1	53.06	100
PK3 - 44	0.06833	0.0029	0.05425	0.00097	0.51106	0.02067	0.01464	0.00111	878.7	85.4	340.5	5.91	419.2	13.89	293.8	22.17	39
PK3 - 45	0.08793	0.00438	0.23951	0.00492	2.90234	0.13718	0.0645	0.01093	1380.9	92.66	1384.1	25.61	1382.5	35.69	1263.3	207.56	100
PK3 - 46	0.08687	0.00337	0.23264	0.00428	2.78488	0.10225	0.04346	0.00348	1357.7	72.95	1348.3	22.38	1351.5	27.43	859.9	67.46	99
PK3 - 47	0.08172	0.0033	0.18524	0.00339	2.08876	0.08033	0.02213	0.00195	1238.9	77.11	1095.5	18.43	1145.1	26.41	442.4	38.52	88
PK3 - 48	0.08871	0.00121	0.24256	0.00279	2.9662	0.04145	0.04854	0.00146	1397.8	25.8	1400	14.45	1399	10.61	958.1	28.16	100
PK3 - 49	0.09127	0.00141	0.21457	0.00255	2.69974	0.04227	0.0538	0.00195	1452.1	29.11	1253.1	13.56	1328.4	11.6	1059.1	37.45	86
PK3 - 50	0.087	0.00164	0.23461	0.00299	2.81375	0.05216	0.03602	0.00128	1360.4	35.79	1358.6	15.59	1359.2	13.89	715.2	24.92	100
PK3 - 51	0.05632	0.00168	0.04711	0.00066	0.36578	0.01057	0.00849	0.00034	464.2	65.12	296.7	4.08	316.5	7.85	170.9	6.88	64
PK3 - 52	0.0508	0.00142	0.03538	0.00051	0.2479	0.00666	0.00249	0.00012	231.7	63.23	224.2	3.18	224.9	5.42	50.4	2.51	97
PK3 - 53	0.05347	0.00184	0.0547	0.00081	0.4032	0.01341	0.0161	0.00099	348.5	75.69	343.3	4.94	344	9.7	322.8	19.69	99
PK3 - 54	0.05343	0.00115	0.05342	0.00067	0.39352	0.00838	0.01186	0.00049	346.9	48.08	335.5	4.11	336.9	6.11	238.3	9.72	97
PK3 - 55	0.05519	0.00264	0.06622	0.00122	0.50386	0.02313	0.02179	0.00322	419.9	103.46	413.3	7.4	414.3	15.62	435.7	63.76	98
PK3 - 56	0.14253	0.00603	0.41998	0.00928	8.33149	0.33852	0.0092	0.00083	2258.1	71.22	2260.4	42.12	2267.8	36.84	185.1	16.7	100
PK3 - 57	0.05528	0.00097	0.06802	0.0008	0.51838	0.00907	0.01309	0.00041	423.2	38.12	424.2	4.85	424.1	6.06	262.9	8.13	104
PK3 - 58	0.0552	0.00122	0.06685	0.00086	0.50906	0.01115	0.01884	0.00114	420.3	48	417.2	5.19	417.8	7.5	377.2	22.68	103
PK3 - 59	0.08175	0.00448	0.14505	0.00381	1.65981	0.08117	0.00338	0.00031	1239.6	103.88	873.2	21.46	993.3	30.99	68.2	6.29	103
PK3 - 60	0.07091	0.00163	0.16019	0.00209	1.56679	0.03463	0.01465	0.00071	954.7	46.42	957.8	11.62	957.2	13.7	294	14.13	103
PK3 - 61	0.08962	0.00324	0.23891	0.00427	2.9656	0.09676	0.00561	0.00035	1417.4	67.47	1381	22.22	1398.8	24.78	113	7.03	102
PK3 - 62	0.05235	0.00141	0.04731	0.00065	0.34154	0.00881	0.00549	0.00029	300.6	60.26	298	3.98	298.3	6.67	110.6	5.91	102
PK3 - 63	0.06631	0.00156	0.13495	0.00179	1.23407	0.02818	0.01635	0.00075	816.1	48.41	816.1	10.18	816.2	12.81	327.8	14.87	102
PK3 - 64	0.08436	0.00173	0.2235	0.0029	2.59969	0.05239	0.03024	0.00136	1300.7	39.36	1300.3	15.28	1300.6	14.78	602.2	26.6	101

PK3 - 65	0.07328	0.00193	0.17171	0.00235	1.73434	0.0433	0.01346	0.0007	1021.7	52.38	1021.5	12.94	1021.4	16.08	270.3	13.99	101
PK3 - 66	0.05708	0.00163	0.07994	0.00113	0.62887	0.01707	0.00763	0.00043	493.9	62.32	495.8	6.76	495.4	10.64	153.6	8.66	101
PK3 - 67	0.05509	0.00103	0.06669	0.00081	0.50656	0.00951	0.01576	0.00073	415.8	40.99	416.2	4.88	416.1	6.41	316	14.61	101
PK3 - 68	0.05308	0.00277	0.05221	0.00086	0.38211	0.01956	0.01645	0.00122	332.3	113.97	328.1	5.26	328.6	14.37	329.9	24.28	101
PK3 - 69	0.08542	0.00196	0.22815	0.0031	2.68709	0.06061	0.03291	0.00176	1324.9	43.84	1324.8	16.28	1324.9	16.69	654.4	34.41	101
PK3 - 70	0.06366	0.00116	0.07647	0.00093	0.67117	0.01229	0.01657	0.00078	730.5	38.11	475	5.57	521.4	7.47	332.2	15.5	101
PK3 - 71	0.05199	0.00226	0.04134	0.00075	0.29624	0.01257	0.01345	0.00197	284.8	96.13	261.1	4.66	263.5	9.84	270	39.37	100
PK3 - 72	0.05551	0.00144	0.06901	0.00096	0.52851	0.01322	0.00571	0.0002	432.7	56.42	430.2	5.77	430.8	8.78	115.1	4.02	100
PK3 - 73	0.07864	0.00168	0.19778	0.00268	2.14681	0.04439	0.01412	0.00045	1163	41.84	1163.4	14.45	1164	14.32	283.3	9.02	100
PK3 - 74	0.0762	0.00166	0.18649	0.00254	1.96127	0.0411	0.01351	0.00047	1100.4	42.99	1102.3	13.83	1102.3	14.09	271.1	9.4	100
PK3 - 75	0.07476	0.00123	0.17842	0.00219	1.83865	0.03086	0.04738	0.00202	1062.1	32.63	1058.3	11.97	1059.4	11.04	935.6	39.07	100
PK3 - 76	0.07298	0.00146	0.17049	0.00224	1.71724	0.03336	0.00924	0.0003	1013.3	40.06	1014.8	12.34	1015	12.47	185.9	6.05	100
PK3 - 77	0.06682	0.00165	0.06826	0.00094	0.62843	0.01523	0.02072	0.0014	832	50.58	425.7	5.67	495.1	9.5	414.6	27.8	100
PK3 - 78	0.05795	0.00333	0.08411	0.00167	0.67182	0.03732	0.02663	0.00204	527.6	121.71	520.6	9.93	521.8	22.67	531.2	40.14	100
PK3 - 79	0.09601	0.0017	0.27142	0.00349	3.59701	0.06275	0.016	0.0005	1547.9	32.85	1548	17.69	1548.9	13.86	320.8	10.04	100
PK3 - 80	0.07763	0.00153	0.19348	0.00256	2.07236	0.04031	0.00656	0.00024	1137.5	38.7	1140.2	13.85	1139.7	13.32	132.1	4.74	100
PK3 - 81	0.11922	0.0032	0.34952	0.00523	5.74297	0.14877	0.09804	0.00894	1944.5	47.27	1932.3	25	1937.9	22.4	1890.5	164.49	100
PK3 - 82	0.08437	0.00246	0.22326	0.0037	2.59899	0.07235	0.01239	0.00052	1300.9	55.73	1299.1	19.5	1300.4	20.41	248.8	10.48	100
PK3 - 83	0.05022	0.00225	0.03346	0.00082	0.23194	0.00994	0.00105	0.00007	205.3	100.91	212.2	5.08	211.8	8.19	21.1	1.35	100
PK3 - 84	0.10908	0.00171	0.31128	0.00377	4.68063	0.07575	0.0783	0.00439	1784	28.4	1747	18.54	1763.8	13.54	1523.7	82.27	100
PK3 - 85	0.05667	0.00115	0.07763	0.00099	0.60666	0.01214	0.00871	0.00027	477.9	44.56	481.9	5.95	481.5	7.67	175.3	5.33	100
PK3 - 86	0.05273	0.00166	0.04856	0.00077	0.35301	0.01069	0.0031	0.00012	317	69.81	305.7	4.71	307	8.02	62.5	2.47	100
PK3 - 87	0.10456	0.00148	0.30322	0.00369	4.37205	0.06351	0.03693	0.00097	1706.6	25.9	1707.3	18.24	1707.1	12	732.9	18.83	100
PK3 - 88	0.13359	0.00206	0.39517	0.00503	7.28074	0.11259	0.03441	0.00106	2145.7	26.75	2146.8	23.24	2146.5	13.81	683.7	20.76	100
PK3 - 89	0.06261	0.00304	0.11348	0.00289	0.98041	0.04279	0.00324	0.0002	695.1	100.11	692.9	16.73	693.8	21.94	65.3	4.06	100
PK3 - 90	0.05127	0.00089	0.04083	0.0005	0.28867	0.00501	0.00568	0.00017	252.9	39.27	257.9	3.09	257.5	3.95	114.6	3.42	100
PK3 - 91	0.05173	0.00123	0.04321	0.00059	0.30838	0.00709	0.00372	0.00013	273.4	53.48	272.7	3.65	272.9	5.5	75.1	2.69	100
PK3 - 92	0.05195	0.00165	0.04458	0.00061	0.31933	0.01	0.00991	0.00044	283.1	71.1	281.2	3.74	281.4	7.7	199.3	8.76	100
PK3 - 93	0.07101	0.00101	0.16011	0.00188	1.56805	0.02289	0.02843	0.00103	957.6	28.8	957.4	10.47	957.7	9.05	566.7	20.22	100

PK3 - 94	0.0567	0.00415	0.07761	0.00214	0.60735	0.04215	0.00329	0.00026	479	154.84	481.8	12.83	481.9	26.63	66.3	5.23	100
PK3 - 95	0.05515	0.00116	0.06726	0.00084	0.51141	0.01063	0.02014	0.00119	418.2	45.49	419.6	5.05	419.4	7.14	403	23.55	100
PK3 - 96	0.15271	0.0029	0.44578	0.00594	9.39625	0.17433	0.03466	0.00136	2376.5	31.98	2376.5	26.5	2377.5	17.03	688.8	26.5	100
PK3 - 97	0.05306	0.00336	0.0522	0.00109	0.38175	0.02332	0.01558	0.00189	331.3	136.83	328	6.68	328.3	17.14	312.5	37.7	100
PK3 - 98	0.0868	0.00135	0.23402	0.00279	2.80139	0.04413	0.03789	0.00155	1356	29.68	1355.5	14.55	1355.9	11.79	751.6	30.17	100
PK3 - 99	0.05185	0.00316	0.04457	0.00097	0.31823	0.01856	0.01425	0.00262	278.7	133.84	281.1	5.97	280.5	14.29	286	52.25	100
PK3 - 100	0.08902	0.01176	0.24122	0.01245	2.95935	0.37194	0.06388	0.01463	1404.4	233.91	1393.1	64.67	1397.2	95.38	1251.6	277.95	100
PK3 - 101	0.07376	0.00195	0.17437	0.00253	1.77493	0.04524	0.01729	0.00095	1035	52.47	1036.1	13.9	1036.3	16.55	346.5	18.95	100
PK3 - 102	0.09098	0.00183	0.25134	0.00329	3.15213	0.06331	0.07351	0.0047	1446.2	37.81	1445.4	16.96	1445.5	15.48	1433.8	88.54	100
PK3 - 103	0.05491	0.00416	0.06614	0.00225	0.5009	0.03461	0.00214	0.00018	408.5	161.12	412.9	13.62	412.3	23.41	43.3	3.54	100
PK3 - 104	0.05863	0.00478	0.08795	0.00366	0.70637	0.05097	0.00151	0.00013	553.4	168.57	543.4	21.66	542.6	30.33	30.5	2.6	100
PK3 - 105	0.10521	0.00237	0.05654	0.00077	0.82024	0.01784	0.01178	0.0004	1718	40.81	354.6	4.68	608.2	9.95	236.8	8.07	100
PK3 - 106	0.0933	0.00221	0.26038	0.00372	3.35003	0.07591	0.02294	0.00101	1493.9	44.16	1491.8	19.04	1492.8	17.72	458.5	20.05	100
PK3 - 107	0.06289	0.00104	0.11541	0.00141	1.0007	0.01675	0.01962	0.00072	704.4	34.73	704.1	8.13	704.2	8.5	392.7	14.36	100
PK3 - 108	0.05607	0.00126	0.07395	0.00094	0.57165	0.01273	0.02214	0.00111	454.8	48.88	459.9	5.62	459.1	8.22	442.7	22.02	100
PK3 - 109	0.05437	0.00127	0.05976	0.00076	0.44795	0.01034	0.01796	0.00103	386.4	51.37	374.1	4.63	375.8	7.25	359.9	20.38	100
PK3 - 110	0.10741	0.00185	0.31324	0.00394	4.63872	0.08039	0.04631	0.00207	1756	31.09	1756.6	19.35	1756.3	14.48	915	39.98	100
PK3 - 111	0.06786	0.00158	0.14392	0.00197	1.34639	0.03028	0.01596	0.00082	864.4	47.62	866.8	11.08	866	13.1	320	16.31	100
PK3 - 112	0.09209	0.00261	0.25544	0.00397	3.24278	0.08739	0.02525	0.0015	1469	52.93	1466.5	20.4	1467.5	20.91	504.1	29.63	100
PK3 - 113	0.08825	0.00177	0.23989	0.00311	2.91837	0.05901	0.05756	0.0042	1388	38.01	1386.1	16.19	1386.7	15.29	1131.2	80.29	100
PK3 - 114	0.15889	0.00329	0.46108	0.0061	10.09936	0.20624	0.05542	0.00311	2443.9	34.61	2444.3	26.92	2443.9	18.87	1090.3	59.47	100
PK3 - 115	0.06813	0.00216	0.1447	0.00231	1.35857	0.04022	0.00943	0.00059	872.5	64.2	871.2	12.99	871.3	17.31	189.7	11.88	100
PK3 - 116	0.08014	0.00161	0.20449	0.00258	2.25929	0.04516	0.06037	0.00447	1200.5	39.13	1199.4	13.79	1199.7	14.07	1184.7	85.2	100
PK3 - 117	0.16218	0.00205	0.46854	0.00546	10.47572	0.13933	0.0832	0.00241	2478.5	21.12	2477.1	23.98	2477.8	12.33	1615.3	44.97	100
PK3 - 118	0.09455	0.00125	0.26573	0.00312	3.46352	0.04814	0.04454	0.00137	1519	24.81	1519.1	15.91	1519	10.95	880.8	26.51	100
PK3 - 119	0.07243	0.00205	0.16737	0.00255	1.67172	0.04378	0.0041	0.00021	998.2	56.14	997.6	14.09	997.8	16.64	82.7	4.21	100
PK3 - 120	0.08228	0.00157	0.21461	0.00279	2.43482	0.04589	0.0252	0.00101	1252.2	36.76	1253.3	14.78	1252.9	13.56	503	19.86	100
PK3 - 121	0.05467	0.00123	0.06344	0.00084	0.47826	0.01044	0.0062	0.00025	398.8	49.16	396.5	5.12	396.9	7.17	124.9	5	100
PK3 - 122	0.07123	0.00146	0.16078	0.00211	1.57899	0.03183	0.01624	0.00067	964	41.41	961.1	11.74	962	12.53	325.7	13.39	99

PK3 - 123	0.05276	0.00167	0.0496	0.00077	0.36078	0.0107	0.00335	0.00018	318.3	70.51	312	4.76	312.8	7.98	67.5	3.67	99
PK3 - 124	0.05183	0.00095	0.04387	0.00054	0.31342	0.00579	0.00799	0.0003	277.7	41.59	276.8	3.31	276.8	4.48	160.9	6.01	99
PK3 - 125	0.13483	0.00293	0.39858	0.00533	7.40927	0.15664	0.03277	0.00171	2161.8	37.48	2162.5	24.56	2162.1	18.91	651.8	33.5	99
PK3 - 126	0.0536	0.003	0.05615	0.00143	0.41438	0.02107	0.00215	0.00017	354.2	121.06	352.1	8.71	352	15.12	43.3	3.36	99
PK3 - 127	0.05459	0.00166	0.06362	0.00096	0.47886	0.01403	0.00625	0.00034	395.5	66.22	397.6	5.79	397.3	9.63	126	6.89	99
PK3 - 128	0.05633	0.00095	0.07521	0.0009	0.58403	0.00999	0.01558	0.00069	464.5	37.37	467.4	5.4	467	6.4	312.4	13.69	99
PK3 - 129	0.05152	0.00201	0.04289	0.00067	0.30467	0.0116	0.00717	0.00041	264.3	87.24	270.7	4.12	270	9.03	144.5	8.14	99
PK3 - 130	0.05239	0.00221	0.04889	0.00087	0.35315	0.01412	0.00384	0.00025	302.5	93.2	307.7	5.35	307.1	10.59	77.4	5.11	99
PK3 - 131	0.0835	0.00157	0.21975	0.00278	2.52974	0.04737	0.0346	0.00166	1280.8	36.28	1280.5	14.69	1280.6	13.63	687.4	32.52	99
PK3 - 132	0.05533	0.00153	0.06837	0.00097	0.5217	0.01395	0.00663	0.00024	425.2	60.09	426.3	5.84	426.3	9.31	133.6	4.92	99
PK3 - 133	0.10797	0.00467	0.31399	0.00668	4.66848	0.19236	0.09421	0.01118	1765.4	76.95	1760.3	32.75	1761.6	34.46	1819.8	206.58	99
PK3 - 134	0.0548	0.00574	0.067	0.00219	0.50592	0.05106	0.01759	0.00238	404	219.03	418	13.26	415.7	34.43	352.4	47.3	98
PK3 - 135	0.07473	0.00306	0.17925	0.00343	1.84679	0.07165	0.01299	0.00051	1061.3	80.14	1062.9	18.73	1062.3	25.56	260.8	10.12	98
PK3 - 136	0.07114	0.0018	0.16064	0.00225	1.57425	0.03766	0.00704	0.00031	961.5	50.71	960.3	12.5	960.1	14.85	141.8	6.14	98
PK3 - 137	0.08679	0.00167	0.23419	0.00297	2.80153	0.05267	0.01803	0.00071	1355.8	36.63	1356.4	15.52	1355.9	14.07	361.2	14.12	98
PK3 - 138	0.08714	0.0012	0.24693	0.00288	2.96631	0.04233	0.04307	0.0014	1363.6	26.3	1422.6	14.91	1399	10.84	852.4	27.19	97
PK3 - 139	0.07514	0.00309	0.17694	0.00377	1.82438	0.06895	0.00343	0.00024	1072.1	80.53	1050.3	20.64	1054.3	24.79	69.1	4.86	97
PK3 - 140	0.05339	0.00376	0.05676	0.00125	0.41766	0.02856	0.01793	0.00154	345.2	151.62	355.9	7.6	354.4	20.46	359.1	30.63	96
PK3 - 141	0.08875	0.00133	0.24204	0.00289	2.96128	0.04571	0.05344	0.00225	1398.6	28.36	1397.3	14.99	1397.7	11.72	1052.3	43.25	96
PK3 - 142	0.15461	0.00259	0.45026	0.00563	9.59503	0.16366	0.06397	0.00286	2397.5	28.26	2396.4	25.03	2396.7	15.68	1253.2	54.31	96
PK3 - 143	0.05568	0.00433	0.06738	0.00179	0.51705	0.03856	0.02019	0.00366	439.3	164.66	420.3	10.83	423.2	25.81	404	72.54	92
PK3 - 144	0.05551	0.00295	0.06688	0.00174	0.50903	0.02521	0.00121	0.0001	432.5	114.48	417.3	10.52	417.8	16.97	24.5	2.04	70
PK3 - 145	0.05565	0.00168	0.06973	0.00103	0.53479	0.01579	0.01762	0.00147	438.1	65.51	434.5	6.23	435	10.45	353.1	29.22	65
PK3 - 146	0.08037	0.00174	0.20557	0.00274	2.27651	0.04891	0.01954	0.00103	1206.1	42.16	1205.2	14.66	1205	15.16	391	20.38	51
PK3 - 147	0.05597	0.00236	0.07221	0.00123	0.55723	0.02257	0.02664	0.00359	451	90.6	449.5	7.37	449.7	14.71	531.5	70.68	21
Sample T15_PK4 –Volcanic Sandstones – Clastic Unit 4																	
PK4 - 01	0.05568	0.00249	0.06966	0.00141	0.53503	0.02346	0.01506	0.00103	439.4	96.46	434.1	8.5	435.1	15.52	302.2	20.46	105
PK4 - 02	0.08113	0.00104	0.20875	0.00303	2.3347	0.03731	0.03712	0.0009	1224.7	25.03	1222.2	16.16	1222.9	11.36	736.8	17.5	102
PK4 - 03	0.07622	0.00207	0.18855	0.00326	1.98121	0.05512	0.05218	0.00259	1100.9	53.51	1113.5	17.66	1109.1	18.77	1028	49.7	102

PK4 - 04	0.14124	0.00246	0.41465	0.00653	8.06964	0.14858	0.03099	0.00095	2242.4	29.77	2236.2	29.74	2238.9	16.63	616.9	18.67	101
PK4 - 05	0.05822	0.00084	0.08621	0.00128	0.69193	0.01128	0.00743	0.00016	537.4	31.79	533.1	7.62	534	6.77	149.6	3.15	101
PK4 - 06	0.05692	0.00073	0.08012	0.00117	0.62868	0.01015	0.02285	0.00057	487.8	28.27	496.9	6.99	495.3	6.33	456.6	11.19	101
PK4 - 07	0.10616	0.00121	0.30903	0.00455	4.52277	0.06805	0.05435	0.00108	1734.5	20.76	1735.9	22.4	1735.2	12.51	1069.7	20.75	101
PK4 - 08	0.05577	0.00102	0.06839	0.00105	0.52572	0.01079	0.01944	0.00072	442.9	39.61	426.4	6.35	429	7.18	389.1	14.23	101
PK4 - 09	0.06039	0.00371	0.06299	0.00169	0.52346	0.0301	0.00346	0.00037	617.4	127.41	393.8	10.25	427.5	20.06	69.8	7.4	101
PK4 - 10	0.05476	0.00156	0.0624	0.00107	0.47075	0.01289	0.00265	0.0001	402.5	61.67	390.2	6.51	391.7	8.9	53.6	1.96	101
PK4 - 11	0.09041	0.00232	0.24722	0.00426	3.08004	0.08173	0.06086	0.00465	1434	48.25	1424.1	21.99	1427.7	20.34	1194.2	88.6	101
PK4 - 12	0.06837	0.00245	0.14458	0.0028	1.36348	0.04575	0.00712	0.00038	879.8	72.51	870.5	15.79	873.4	19.66	143.3	7.61	101
PK4 - 13	0.07604	0.00096	0.1751	0.00261	1.83533	0.0299	0.04505	0.00137	1096.2	25.13	1040.1	14.32	1058.2	10.71	890.6	26.44	101
PK4 - 14	0.07246	0.00178	0.16768	0.00276	1.67681	0.0413	0.0116	0.00047	998.8	49.2	999.3	15.25	999.8	15.66	233.2	9.48	101
PK4 - 15	0.05529	0.00508	0.06778	0.00228	0.51636	0.04549	0.01872	0.00521	423.6	192.94	422.8	13.78	422.7	30.46	374.8	103.33	101
PK4 - 16	0.05709	0.00099	0.07933	0.00124	0.62416	0.01243	0.0204	0.00084	494.3	38.05	492.1	7.38	492.4	7.77	408.1	16.64	101
PK4 - 17	0.0565	0.00068	0.07627	0.00116	0.59389	0.00945	0.01289	0.00023	471.1	26.69	473.8	6.97	473.3	6.02	258.9	4.57	101
PK4 - 18	0.05614	0.00299	0.06781	0.00155	0.52508	0.02729	0.02234	0.00208	457.4	114.28	423	9.36	428.5	18.17	446.6	41.19	100
PK4 - 19	0.08192	0.00144	0.06908	0.0011	0.78009	0.01548	0.01765	0.00036	1243.7	33.79	430.6	6.65	585.5	8.83	353.5	7.06	100
PK4 - 20	0.06825	0.00129	0.14508	0.00233	1.36445	0.0278	0.01444	0.00037	876.3	38.76	873.3	13.13	873.8	11.94	289.8	7.31	100
PK4 - 21	0.05554	0.00214	0.06875	0.00134	0.52615	0.01972	0.00576	0.00028	433.7	83.73	428.6	8.07	429.3	13.12	116	5.59	100
PK4 - 22	0.05191	0.00154	0.0427	0.00073	0.30566	0.00871	0.00187	0.00007	281.5	66.27	269.5	4.51	270.8	6.77	37.7	1.35	100
PK4 - 23	0.05416	0.00085	0.05997	0.00094	0.4478	0.00841	0.01138	0.00025	377.7	35.11	375.5	5.73	375.7	5.9	228.7	4.98	100
PK4 - 24	0.13697	0.0025	0.40433	0.00615	7.63576	0.14181	0.01677	0.00054	2189.2	31.45	2188.9	28.25	2189.1	16.67	336.2	10.71	100
PK4 - 25	0.05305	0.00315	0.05292	0.00144	0.38742	0.02094	0.00183	0.00013	331	128.55	332.4	8.83	332.5	15.32	37	2.57	100
PK4 - 26	0.06817	0.00136	0.14439	0.00237	1.35653	0.02909	0.01441	0.00053	873.7	40.77	869.5	13.36	870.4	12.54	289.3	10.6	100
PK4 - 27	0.05255	0.0014	0.04936	0.00084	0.35759	0.00953	0.00328	0.00012	309.2	59.32	310.6	5.17	310.4	7.13	66.2	2.4	100
PK4 - 28	0.06385	0.00107	0.12102	0.002	1.06506	0.02159	0.02411	0.001	736.6	34.95	736.4	11.53	736.3	10.62	481.5	19.64	100
PK4 - 29	0.05518	0.00085	0.06758	0.00108	0.51403	0.00968	0.01407	0.00038	419.2	33.66	421.6	6.53	421.2	6.49	282.4	7.51	100
PK4 - 30	0.05475	0.00076	0.0646	0.00103	0.48762	0.00866	0.01196	0.00032	401.9	30.38	403.6	6.26	403.3	5.91	240.3	6.46	100
PK4 - 31	0.05159	0.00161	0.04103	0.00074	0.29182	0.00903	0.0027	0.00012	267.1	70.16	259.2	4.6	260	7.09	54.5	2.45	100
PK4 - 32	0.07383	0.00092	0.17425	0.0026	1.77349	0.02818	0.03015	0.00072	1036.8	24.91	1035.5	14.29	1035.8	10.32	600.4	14.17	100

PK4 - 33	0.05486	0.00077	0.06554	0.00105	0.49566	0.00894	0.0141	0.00042	406.4	30.75	409.2	6.36	408.8	6.07	283.1	8.32	100
PK4 - 34	0.12308	0.00148	0.36388	0.00542	6.17446	0.09522	0.05567	0.00122	2001.4	21.16	2000.5	25.61	2000.8	13.48	1095.1	23.39	100
PK4 - 35	0.05025	0.00177	0.03428	0.00065	0.23697	0.0076	0.00082	0.00004	206.5	79.57	217.3	4.03	215.9	6.24	16.6	0.8	100
PK4 - 36	0.08056	0.00151	0.20573	0.00323	2.28394	0.04479	0.01456	0.00047	1210.7	36.38	1206	17.25	1207.3	13.85	292.2	9.41	100
PK4 - 37	0.06683	0.00119	0.13844	0.00214	1.27603	0.02413	0.01166	0.0003	832.5	36.69	835.9	12.14	835.1	10.76	234.2	5.91	100
PK4 - 38	0.11495	0.0013	0.33803	0.00494	5.35744	0.08138	0.09317	0.0022	1879.1	20.18	1877.2	23.79	1878.1	13	1800.5	40.63	100
PK4 - 39	0.05646	0.00214	0.0751	0.00142	0.58479	0.02198	0.02	0.00122	469.9	82.4	466.8	8.53	467.5	14.08	400.3	24.2	100
PK4 - 40	0.08585	0.00133	0.23028	0.00342	2.72731	0.04403	0.01255	0.00028	1334.8	29.71	1335.9	17.92	1335.9	11.99	252	5.67	100
PK4 - 41	0.05647	0.00184	0.07611	0.00137	0.59288	0.01793	0.0023	0.00008	470.2	70.76	472.9	8.21	472.7	11.43	46.5	1.7	100
PK4 - 42	0.05912	0.00066	0.09329	0.00135	0.76055	0.01111	0.01526	0.00027	571.3	23.58	575	7.97	574.3	6.41	306.1	5.47	100
PK4 - 43	0.06394	0.00203	0.12215	0.00223	1.07726	0.03207	0.00707	0.00028	739.8	65.88	742.9	12.8	742.3	15.68	142.4	5.66	100
PK4 - 44	0.08003	0.001	0.20496	0.00302	2.26304	0.03464	0.0315	0.00059	1197.8	24.4	1201.9	16.17	1200.9	10.78	626.9	11.61	100
PK4 - 45	0.05745	0.00141	0.08226	0.00133	0.65214	0.01553	0.00418	0.00012	508.5	53.44	509.6	7.91	509.8	9.55	84.3	2.39	100
PK4 - 46	0.05683	0.0008	0.0777	0.00115	0.60907	0.01038	0.01852	0.00042	484.4	31.16	482.4	6.88	483	6.55	370.9	8.38	100
PK4 - 47	0.05482	0.0013	0.06529	0.00104	0.49403	0.01149	0.00377	0.0001	405	51.87	407.7	6.29	407.7	7.81	76.1	2.11	100
PK4 - 48	0.06845	0.0017	0.14641	0.00238	1.3832	0.03236	0.00626	0.00019	882.3	50.5	880.8	13.39	881.8	13.79	126	3.86	100
PK4 - 49	0.05574	0.00089	0.0705	0.00105	0.5423	0.00959	0.00762	0.00017	441.6	34.66	439.2	6.34	439.9	6.31	153.5	3.32	100
PK4 - 50	0.05488	0.00075	0.06615	0.00097	0.50105	0.00808	0.00823	0.00017	407.3	30	412.9	5.88	412.4	5.46	165.6	3.5	100
PK4 - 51	0.05451	0.00138	0.06287	0.00102	0.47324	0.01163	0.00338	0.0001	392.1	55.4	393.1	6.16	393.4	8.02	68.1	2.03	100
PK4 - 52	0.07219	0.00139	0.16604	0.00258	1.65482	0.03231	0.01087	0.00023	991.4	38.55	990.3	14.24	991.4	12.36	218.5	4.69	100
PK4 - 53	0.0708	0.00132	0.15893	0.00237	1.55383	0.02841	0.00607	0.00014	951.6	37.61	950.8	13.19	952	11.3	122.3	2.86	100
PK4 - 54	0.05764	0.00164	0.08121	0.00133	0.64575	0.0168	0.00359	0.00013	515.7	61.49	503.4	7.95	505.9	10.37	72.4	2.53	100
PK4 - 55	0.05568	0.00076	0.07067	0.00105	0.54254	0.00919	0.02172	0.0006	439.5	29.62	440.2	6.32	440.1	6.05	434.3	11.81	100
PK4 - 56	0.05589	0.0007	0.07098	0.00105	0.54707	0.00881	0.01728	0.00038	447.7	27.16	442.1	6.34	443.1	5.78	346.2	7.51	100
PK4 - 57	0.06917	0.00145	0.15099	0.00221	1.44159	0.02811	0.00526	0.00017	903.9	42.52	906.5	12.4	906.4	11.69	106	3.43	100
PK4 - 58	0.0912	0.00106	0.25284	0.00372	3.17998	0.04809	0.04388	0.00083	1450.7	22.02	1453.1	19.15	1452.3	11.68	868	16.08	100
PK4 - 59	0.05838	0.00266	0.0704	0.0016	0.56667	0.02333	0.00252	0.00013	544.2	96.46	438.6	9.61	455.9	15.12	51	2.72	100
PK4 - 60	0.11135	0.00139	0.32663	0.00485	5.01653	0.07614	0.03336	0.00073	1821.6	22.42	1822	23.57	1822.1	12.85	663.2	14.36	100
PK4 - 61	0.10635	0.00134	0.30955	0.00463	4.54031	0.07061	0.03428	0.0008	1737.8	23.01	1738.5	22.81	1738.4	12.94	681.2	15.58	100

PK4 - 62	0.08832	0.00119	0.24102	0.00363	2.9354	0.04748	0.02489	0.00061	1389.4	25.64	1392	18.87	1391.1	12.25	496.9	11.94	100
PK4 - 63	0.1123	0.00149	0.33011	0.00499	5.11176	0.08234	0.03996	0.00098	1837	23.82	1838.9	24.19	1838.1	13.68	791.9	18.98	100
PK4 - 64	0.09029	0.00123	0.24847	0.00374	3.09319	0.05011	0.02695	0.00067	1431.5	25.83	1430.6	19.33	1431	12.43	537.5	13.11	100
PK4 - 65	0.06845	0.00168	0.1461	0.00236	1.37964	0.03241	0.00765	0.00027	882.3	49.95	879	13.27	880.3	13.83	154	5.47	100
PK4 - 66	0.05908	0.00087	0.09276	0.0014	0.75558	0.01318	0.01607	0.0004	570.2	31.61	571.8	8.27	571.5	7.62	322.3	8.04	100
PK4 - 67	0.06651	0.00123	0.13568	0.00208	1.24454	0.02392	0.01014	0.00025	822.3	38	820.2	11.83	820.9	10.82	203.9	5.03	100
PK4 - 68	0.08482	0.00125	0.22566	0.00336	2.63922	0.04302	0.01801	0.00042	1311.4	28.42	1311.7	17.7	1311.6	12	360.9	8.28	100
PK4 - 69	0.09354	0.00138	0.2619	0.00394	3.37731	0.05592	0.02334	0.00052	1498.9	27.59	1499.6	20.15	1499.1	12.97	466.3	10.35	100
PK4 - 70	0.07818	0.00248	0.15521	0.00289	1.67322	0.05249	0.01663	0.00094	1151.5	61.62	930.1	16.11	998.4	19.94	333.4	18.68	100
PK4 - 71	0.17213	0.00215	0.44833	0.00669	10.63547	0.16545	0.05567	0.00126	2578.4	20.68	2387.8	29.79	2491.8	14.44	1094.9	24.05	100
PK4 - 72	0.05416	0.00157	0.06139	0.00103	0.45945	0.01261	0.00175	0.00006	377.5	63.82	384	6.26	383.9	8.78	35.4	1.28	100
PK4 - 73	0.0553	0.00446	0.06662	0.00197	0.50752	0.03931	0.01703	0.00224	424.2	170.49	415.7	11.92	416.8	26.48	341.2	44.43	100
PK4 - 74	0.05796	0.00122	0.06615	0.00101	0.52863	0.01188	0.01918	0.00093	527.9	45.74	412.9	6.12	430.9	7.89	383.9	18.4	100
PK4 - 75	0.05517	0.00146	0.0664	0.0011	0.505	0.01299	0.00309	0.00011	419.1	57.36	414.4	6.65	415.1	8.77	62.4	2.17	100
PK4 - 76	0.05594	0.00088	0.07235	0.00109	0.55784	0.00995	0.00821	0.0002	449.6	34.28	450.3	6.56	450.1	6.48	165.4	4.08	100
PK4 - 77	0.05524	0.00089	0.06827	0.00104	0.51989	0.00939	0.00706	0.0002	422	35.4	425.7	6.25	425.1	6.27	142.1	4	100
PK4 - 78	0.07468	0.00253	0.1714	0.0033	1.75988	0.05599	0.006	0.00029	1059.8	66.72	1019.8	18.17	1030.8	20.6	121	5.78	100
PK4 - 79	0.15337	0.00185	0.3585	0.00525	7.58031	0.11723	0.0586	0.00138	2383.8	20.38	1975.1	24.9	2182.5	13.87	1151	26.32	100
PK4 - 80	0.07268	0.00103	0.16905	0.00254	1.69369	0.02885	0.02621	0.00074	1005	28.58	1006.9	14	1006.2	10.87	522.9	14.48	100
PK4 - 81	0.07445	0.00115	0.1774	0.00269	1.82065	0.03251	0.02449	0.00073	1053.5	31.26	1052.7	14.73	1052.9	11.7	488.9	14.31	100
PK4 - 82	0.0625	0.0008	0.11303	0.00169	0.97404	0.01568	0.0195	0.00038	691.3	27.18	690.3	9.77	690.5	8.06	390.3	7.61	100
PK4 - 83	0.07276	0.00143	0.16922	0.00273	1.69812	0.0348	0.01331	0.00033	1007.2	39.4	1007.8	15.03	1007.8	13.1	267.2	6.5	100
PK4 - 84	0.07072	0.0009	0.15866	0.00236	1.54707	0.02474	0.02722	0.0005	949.3	25.74	949.3	13.11	949.3	9.86	542.8	9.85	100
PK4 - 85	0.05385	0.00088	0.05885	0.0009	0.43701	0.00802	0.00613	0.00013	364.7	36.71	368.6	5.5	368.1	5.67	123.5	2.52	100
PK4 - 86	0.09139	0.00122	0.25353	0.00384	3.19545	0.05061	0.02265	0.00047	1454.7	25.15	1456.7	19.76	1456.1	12.25	452.8	9.23	100
PK4 - 87	0.05634	0.00109	0.07453	0.00118	0.57905	0.01208	0.00926	0.00024	465	42.46	463.4	7.06	463.8	7.77	186.4	4.8	100
PK4 - 88	0.05839	0.0013	0.07412	0.00116	0.59667	0.01407	0.0208	0.00091	544.6	48.38	460.9	6.95	475.1	8.95	416.1	18.03	99
PK4 - 89	0.08047	0.00135	0.20666	0.00323	2.293	0.04103	0.00743	0.00021	1208.5	32.73	1211	17.25	1210.1	12.65	149.7	4.19	99
PK4 - 90	0.05563	0.00106	0.07097	0.00113	0.54448	0.01095	0.00484	0.00012	437.4	41.44	442	6.78	441.4	7.2	97.6	2.36	99

PK4 - 91	0.08484	0.00128	0.22529	0.00347	2.63536	0.04366	0.01143	0.00032	1311.9	29.03	1309.8	18.23	1310.6	12.19	229.8	6.49	99
PK4 - 92	0.07145	0.0009	0.16203	0.00242	1.59635	0.02519	0.02254	0.00047	970.3	25.44	968.1	13.44	968.8	9.85	450.5	9.28	99
PK4 - 93	0.09003	0.00117	0.24739	0.0037	3.07107	0.05065	0.0671	0.00211	1426.1	24.56	1425	19.15	1425.5	12.63	1312.7	39.89	99
PK4 - 94	0.05803	0.00107	0.08608	0.00137	0.68882	0.01343	0.00573	0.00017	530.3	40.13	532.3	8.13	532.1	8.07	115.4	3.4	99
PK4 - 95	0.05533	0.00091	0.06922	0.00108	0.5281	0.00972	0.007	0.00018	425.3	35.66	431.5	6.48	430.5	6.46	141	3.54	99
PK4 - 96	0.06388	0.00105	0.12142	0.00189	1.06959	0.01979	0.01412	0.00036	737.7	34.35	738.8	10.89	738.5	9.71	283.5	7.2	99
PK4 - 97	0.05606	0.00066	0.07271	0.00107	0.56213	0.00856	0.01285	0.00021	454.5	25.51	452.5	6.44	452.9	5.56	258.1	4.18	99
PK4 - 98	0.10479	0.00112	0.30404	0.00449	4.39366	0.06373	0.04088	0.00068	1710.6	19.54	1711.3	22.2	1711.1	12	809.8	13.13	99
PK4 - 99	0.08973	0.00106	0.24657	0.00368	3.05158	0.04604	0.0315	0.00056	1419.8	22.37	1420.8	19.03	1420.6	11.54	626.9	11.07	99
PK4 - 100	0.0549	0.00081	0.0653	0.00099	0.49441	0.00862	0.00921	0.00018	407.9	32.6	407.8	5.99	407.9	5.86	185.3	3.56	98
PK4 - 101	0.0589	0.00141	0.0915	0.00144	0.74272	0.01669	0.00379	0.00013	563.5	51.17	564.4	8.5	564	9.72	76.5	2.66	98
PK4 - 102	0.05553	0.00139	0.06942	0.00114	0.53143	0.01388	0.02087	0.00101	433.4	54.29	432.6	6.85	432.8	9.2	417.4	20.08	98
PK4 - 103	0.06022	0.00089	0.09203	0.00138	0.76419	0.01359	0.02593	0.00073	611.6	31.54	567.5	8.16	576.4	7.82	517.4	14.39	97
PK4 - 104	0.10766	0.00122	0.31383	0.0046	4.65912	0.06998	0.05462	0.0011	1760.2	20.56	1759.5	22.57	1759.9	12.56	1074.9	21.14	97
PK4 - 105	0.063	0.00159	0.1146	0.00179	0.99615	0.02284	0.00202	0.00008	708.1	52.76	699.4	10.33	701.9	11.62	40.7	1.53	96
PK4 - 106	0.06251	0.00267	0.11344	0.00243	0.97842	0.03834	0.003	0.00016	691.5	88.63	692.7	14.09	692.8	19.68	60.6	3.27	96
PK4 - 107	0.05779	0.00217	0.08371	0.00161	0.66791	0.02288	0.00178	0.00008	521.6	80.6	518.2	9.6	519.4	13.93	35.9	1.66	96
PK4 - 108	0.0588	0.00084	0.09101	0.00136	0.7379	0.01259	0.01395	0.00032	559.6	31	561.5	8.06	561.2	7.35	280.1	6.39	96
PK4 - 109	0.05468	0.00298	0.06148	0.0014	0.46356	0.02452	0.01662	0.00165	399	117.29	384.6	8.48	386.7	17.01	333.2	32.86	95
PK4 - 110	0.08017	0.00158	0.20482	0.00314	2.26515	0.0447	0.01412	0.00045	1201.2	38.43	1201.2	16.81	1201.5	13.9	283.5	9.06	93
PK4 - 111	0.06545	0.00189	0.13025	0.0022	1.17566	0.0317	0.00619	0.00026	788.9	59.62	789.3	12.56	789.3	14.8	124.8	5.15	93
PK4 - 112	0.05588	0.00319	0.07224	0.00168	0.55627	0.03082	0.0222	0.00169	447.2	122.4	449.7	10.12	449.1	20.11	443.9	33.32	92
PK4 - 113	0.0666	0.00212	0.13583	0.00247	1.24727	0.03784	0.00709	0.00021	825.2	65.17	821.1	14.04	822.2	17.1	142.7	4.22	85
PK4 - 114	0.06117	0.00084	0.10684	0.00161	0.90101	0.01545	0.02795	0.00064	645.4	29.15	654.4	9.38	652.3	8.25	557.1	12.63	83
PK4 - 115	0.08029	0.00124	0.20535	0.00309	2.27382	0.0391	0.01501	0.00039	1204.2	30.09	1204	16.55	1204.2	12.13	301.1	7.67	81
PK4 - 116	0.05645	0.00073	0.07364	0.00109	0.57303	0.0093	0.01411	0.00027	469.2	28.58	458	6.57	460	6	283.1	5.39	81
PK4 - 117	0.05605	0.00309	0.0727	0.00162	0.56184	0.02994	0.02587	0.00219	453.9	118.22	452.4	9.75	452.7	19.46	516.3	43.13	78
PK4 - 118	0.06096	0.0012	0.07531	0.00118	0.63285	0.01377	0.02394	0.00078	637.7	41.87	468.1	7.09	497.9	8.56	478.3	15.5	73
PK4 - 119	0.11254	0.00247	0.33084	0.00517	5.13309	0.10703	0.01162	0.00045	1840.9	39.27	1842.4	25.04	1841.6	17.72	233.6	9.04	64

PK4 - 120	0.06505	0.0014	0.12818	0.00196	1.14997	0.02422	0.00496	0.00017	776.1	44.67	777.5	11.2	777.2	11.44	100	3.42	35
Pang Asok Formation																	
Sample T13_003 –Slaty Sandstones																	
T13_003 - 1	0.05366	0.00168	0.05749	0.00092	0.42529	0.01321	0.01718	0.00077	356.6	68.92	360.4	5.62	359.8	9.41	344.2	15.24	120
T13_003 - 2	0.09243	0.00125	0.25005	0.00332	3.18625	0.04908	0.07685	0.00212	1476	25.55	1438.7	17.11	1453.8	11.91	1496.6	39.76	114
T13_003 - 3	0.05645	0.00171	0.04263	0.00066	0.33178	0.00997	0.01477	0.00056	469.5	65.93	269.1	4.09	290.9	7.6	296.3	11.18	108
T13_003 - 4	0.05608	0.00073	0.05599	0.00072	0.43282	0.00646	0.01851	0.00048	455	28.35	351.2	4.41	365.2	4.58	370.6	9.43	106
T13_003 - 5	0.05729	0.00091	0.07538	0.00098	0.59543	0.01016	0.02347	0.00077	502.4	34.38	468.5	5.9	474.3	6.47	468.9	15.22	105
T13_003 - 6	0.05371	0.00084	0.06086	0.0008	0.45066	0.00769	0.01986	0.00063	358.9	34.97	380.8	4.89	377.7	5.38	397.4	12.41	104
T13_003 - 7	0.05356	0.00238	0.04337	0.00079	0.32004	0.01376	0.01474	0.00093	352.6	97	273.7	4.9	281.9	10.59	295.8	18.53	103
T13_003 - 8	0.05377	0.0011	0.0525	0.0007	0.38919	0.00814	0.01719	0.00049	361.3	45.68	329.8	4.27	333.8	5.95	344.5	9.66	103
T13_003 - 9	0.10242	0.00117	0.15138	0.00191	2.13711	0.02891	0.04312	0.00102	1668.4	21.06	908.7	10.69	1160.9	9.36	853.3	19.74	103
T13_003 - 10	0.12053	0.00138	0.18815	0.00234	3.12616	0.04171	0.07683	0.00184	1964.1	20.25	1111.4	12.69	1439.2	10.26	1496.2	34.51	101
T13_003 - 11	0.07852	0.00145	0.09262	0.00134	1.0019	0.01981	0.06044	0.00355	1160.1	36.18	571	7.88	704.8	10.05	1186.1	67.7	101
T13_003 - 12	0.05856	0.002	0.0609	0.00101	0.49155	0.0166	0.02105	0.00099	550.7	72.97	381.1	6.17	406	11.3	421.1	19.64	101
T13_003 - 13	0.06963	0.00112	0.06251	0.00086	0.60014	0.01055	0.01987	0.00081	917.5	32.62	390.9	5.2	477.3	6.69	397.7	16.12	101
T13_003 - 14	0.06786	0.00091	0.06491	0.00084	0.60725	0.00922	0.02681	0.00095	864.2	27.57	405.4	5.08	481.8	5.82	534.7	18.64	101
T13_003 - 15	0.09047	0.00109	0.23618	0.00288	2.94553	0.0399	0.06561	0.00189	1435.3	22.78	1366.8	14.99	1393.7	10.27	1284.5	35.76	101
T13_003 - 16	0.05614	0.00086	0.07106	0.00096	0.54998	0.00933	0.02246	0.00059	457.4	33.32	442.6	5.76	445	6.11	449	11.65	101
T13_003 - 17	0.08979	0.00105	0.24981	0.00321	3.09202	0.0429	0.07238	0.00178	1420.9	22.1	1437.5	16.53	1430.7	10.64	1412.5	33.5	100
T13_003 - 18	0.05064	0.00084	0.04284	0.00058	0.29909	0.00539	0.01327	0.00043	224.7	37.75	270.4	3.59	265.7	4.21	266.4	8.56	100
T13_003 - 19	0.05534	0.00087	0.05599	0.00074	0.42717	0.0073	0.01776	0.00059	425.9	34	351.2	4.54	361.2	5.19	355.8	11.7	100
T13_003 - 20	0.09006	0.00106	0.23179	0.0029	2.87781	0.0392	0.07234	0.00173	1426.8	22.23	1343.9	15.18	1376.1	10.26	1411.7	32.53	100
T13_003 - 21	0.1144	0.00283	0.04605	0.00075	0.72613	0.01782	0.01996	0.00089	1870.5	44.01	290.2	4.62	554.3	10.48	399.5	17.55	100
T13_003 - 22	0.06826	0.00091	0.0874	0.00114	0.82251	0.01246	0.02315	0.00072	876.6	27.24	540.1	6.75	609.4	6.94	462.6	14.32	100
T13_003 - 23	0.0945	0.00146	0.24117	0.00339	3.14186	0.05489	0.05349	0.00236	1518.2	28.9	1392.8	17.61	1443	13.46	1053.2	45.34	100
T13_003 - 24	0.09054	0.00106	0.24138	0.00306	3.01257	0.04155	0.09124	0.00262	1436.9	22.17	1393.9	15.89	1410.8	10.51	1764.7	48.5	100
T13_003 - 25	0.06038	0.00095	0.09481	0.0013	0.78937	0.01376	0.02853	0.00093	617.4	33.44	583.9	7.68	590.8	7.81	568.5	18.24	100
T13_003 - 26	0.05134	0.00116	0.04276	0.0006	0.30268	0.00698	0.01399	0.00048	256.3	50.9	269.9	3.73	268.5	5.44	280.7	9.5	100

T13_003 - 27	0.05587	0.00093	0.07033	0.00093	0.54172	0.00968	0.02249	0.00092	447	36.37	438.2	5.62	439.6	6.38	449.5	18.17	100
T13_003 - 28	0.1067	0.00136	0.30471	0.00396	4.48249	0.06585	0.08495	0.00249	1743.8	23.1	1714.6	19.58	1727.7	12.2	1648	46.3	100
T13_003 - 29	0.18418	0.00228	0.51322	0.00671	13.03219	0.18936	0.14223	0.0044	2690.9	20.3	2670.4	28.57	2682	13.7	2687.8	77.89	99
T13_003 - 30	0.0566	0.00097	0.05992	0.00084	0.46766	0.00873	0.02151	0.00095	475.3	37.69	375.1	5.08	389.6	6.04	430.2	18.88	99
T13_003 - 31	0.10006	0.0014	0.29787	0.00381	4.10868	0.06292	0.1034	0.0037	1625.1	25.81	1680.8	18.94	1656	12.51	1988.8	67.84	99
T13_003 - 32	0.09431	0.00119	0.233	0.00316	3.02922	0.04565	0.07706	0.00188	1514.4	23.7	1350.2	16.52	1415	11.5	1500.4	35.27	99
T13_003 - 33	0.08436	0.00116	0.16818	0.00231	1.95561	0.0312	0.07552	0.00211	1300.7	26.59	1002.1	12.76	1100.4	10.72	1471.5	39.6	99
T13_003 - 34	0.05307	0.00097	0.0533	0.00073	0.38986	0.00758	0.01684	0.0004	331.6	40.73	334.7	4.49	334.3	5.54	337.5	7.86	98
T13_003 - 35	0.11297	0.00127	0.33317	0.00431	5.1889	0.07088	0.0963	0.0021	1847.8	20.18	1853.7	20.84	1850.8	11.63	1858.3	38.67	98
T13_003 - 36	0.05571	0.00076	0.06744	0.0009	0.51799	0.00816	0.0211	0.00053	440.7	29.78	420.7	5.44	423.8	5.46	422.1	10.51	98
T13_003 - 37	0.0563	0.00074	0.06902	0.00092	0.53573	0.00818	0.02141	0.00054	463.5	28.86	430.3	5.55	435.6	5.41	428.2	10.76	98
T13_003 - 38	0.09043	0.00106	0.24932	0.00324	3.10804	0.04363	0.07516	0.00182	1434.5	22.22	1435	16.7	1434.7	10.78	1464.8	34.16	97
T13_003 - 39	0.09045	0.00115	0.24067	0.00314	3.00089	0.0441	0.07457	0.00213	1434.9	23.97	1390.2	16.33	1407.8	11.19	1453.6	40.01	97
T13_003 - 40	0.05646	0.00074	0.07173	0.00094	0.55832	0.00839	0.02174	0.00064	469.8	28.87	446.6	5.64	450.4	5.47	434.8	12.59	97
T13_003 - 41	0.05189	0.00097	0.0431	0.00058	0.30831	0.00606	0.01358	0.00035	280.4	42.32	272	3.58	272.9	4.7	272.7	7.05	97
T13_003 - 42	0.08002	0.00099	0.03825	0.0005	0.42194	0.00614	0.01722	0.00048	1197.6	24.26	242	3.1	357.4	4.38	345.1	9.52	97
T13_003 - 43	0.05218	0.00099	0.04483	0.00061	0.32251	0.00645	0.01389	0.00041	293.2	42.89	282.7	3.77	283.8	4.95	278.9	8.12	97
T13_003 - 44	0.1701	0.00269	0.49309	0.00684	11.55986	0.20063	0.13037	0.00636	2558.7	26.26	2584	29.53	2569.4	16.22	2477	113.69	97
T13_003 - 45	0.05694	0.00094	0.07928	0.00101	0.62243	0.01079	0.02317	0.00099	488.7	36.45	491.8	6.05	491.4	6.75	463	19.63	97
T13_003 - 46	0.05194	0.00145	0.04183	0.00064	0.29935	0.00838	0.01355	0.00055	282.8	62.49	264.2	3.98	265.9	6.55	272	10.96	96
T13_003 - 47	0.05332	0.00072	0.0589	0.00075	0.43309	0.00655	0.0187	0.00041	342.6	30.35	369	4.55	365.4	4.64	374.5	8.16	96
T13_003 - 48	0.10308	0.00131	0.29609	0.00388	4.2071	0.06208	0.08998	0.00268	1680.3	23.31	1671.9	19.28	1675.4	12.1	1741.5	49.72	95
T13_003 - 49	0.10893	0.00133	0.28773	0.00348	4.32303	0.05851	0.08948	0.00264	1781.6	22.09	1630.2	17.43	1697.8	11.16	1732.2	48.97	95
T13_003 - 50	0.06744	0.00094	0.03872	0.00051	0.35986	0.00562	0.01432	0.00046	851.5	28.68	244.9	3.15	312.1	4.2	287.4	9.1	95
T13_003 - 51	0.06344	0.00128	0.07329	0.00103	0.64091	0.01341	0.02363	0.0009	722.9	42.37	455.9	6.18	502.9	8.3	472.1	17.81	95
T13_003 - 52	0.09104	0.00133	0.17605	0.00209	2.20974	0.03335	0.04145	0.0018	1447.4	27.59	1045.3	11.44	1184.1	10.55	821	34.92	95
T13_003 - 53	0.05632	0.00109	0.07091	0.00097	0.55062	0.01104	0.02092	0.00105	464.4	42.48	441.7	5.86	445.4	7.23	418.4	20.75	94
T13_003 - 54	0.05106	0.00106	0.0397	0.0005	0.27962	0.00578	0.0131	0.00049	243.5	47.05	251	3.11	250.4	4.59	263	9.84	94
T13_003 - 55	0.05472	0.00111	0.05827	0.00079	0.43941	0.00913	0.01873	0.00068	400.1	45.06	365.1	4.79	369.8	6.44	375	13.56	93

T13_003 - 56	0.0788	0.00131	0.19457	0.00242	2.11551	0.03586	0.06286	0.0026	1167	32.62	1146.1	13.07	1153.9	11.69	1232.1	49.51	93
T13_003 - 57	0.05895	0.00086	0.07935	0.00098	0.64497	0.00997	0.02384	0.00079	565.1	31.39	492.3	5.85	505.4	6.15	476.3	15.59	93
T13_003 - 58	0.18902	0.00259	0.5061	0.00628	13.18884	0.19298	0.13913	0.00508	2733.7	22.4	2640	26.9	2693.3	13.81	2633	90.2	92
T13_003 - 59	0.11659	0.00148	0.33367	0.00404	5.36441	0.07418	0.09816	0.00325	1904.6	22.58	1856.2	19.51	1879.2	11.84	1892.6	59.88	92
T13_003 - 60	0.11289	0.0017	0.32512	0.00419	5.05662	0.08123	0.09164	0.00395	1846.4	27.05	1814.7	20.36	1828.9	13.62	1772.2	73.13	92
T13_003 - 61	0.05693	0.00099	0.07601	0.00103	0.59641	0.01112	0.02275	0.00061	488.3	38.29	472.3	6.19	475	7.07	454.6	12.14	92
T13_003 - 62	0.09345	0.00128	0.26198	0.00331	3.3756	0.05059	0.07862	0.00196	1497.1	25.74	1500	16.92	1498.7	11.74	1529.8	36.74	91
T13_003 - 63	0.07043	0.00081	0.1584	0.00196	1.53827	0.0207	0.04854	0.00105	940.8	23.5	947.9	10.92	945.8	8.28	958	20.21	91
T13_003 - 64	0.05918	0.00155	0.07777	0.00119	0.63354	0.01675	0.01701	0.00106	573.8	55.85	482.8	7.1	498.3	10.41	340.9	21.04	90
T13_003 - 65	0.05651	0.00101	0.07304	0.00091	0.56934	0.01042	0.02326	0.00073	471.7	39.48	454.5	5.49	457.6	6.74	464.7	14.5	89
T13_003 - 66	0.09099	0.00105	0.25112	0.00309	3.15074	0.04198	0.0746	0.00167	1446.2	21.72	1444.3	15.94	1445.2	10.27	1454.2	31.45	89
T13_003 - 67	0.05925	0.00111	0.09351	0.00124	0.76459	0.01487	0.02993	0.00143	576.3	40.23	576.3	7.28	576.7	8.56	596.1	27.98	87
T13_003 - 68	0.05475	0.00115	0.05877	0.00079	0.44364	0.00947	0.01932	0.00061	402.2	45.85	368.1	4.8	372.8	6.66	386.7	12	86
T13_003 - 69	0.09047	0.00114	0.21824	0.00282	2.72222	0.03976	0.06808	0.00212	1435.3	23.76	1272.6	14.91	1334.5	10.85	1331.3	40.1	84
T13_003 - 70	0.05755	0.00116	0.07583	0.00112	0.60193	0.01302	0.03337	0.00319	512.4	44.09	471.2	6.68	478.5	8.25	663.4	62.38	82
T13_003 - 71	0.1174	0.00162	0.34618	0.00443	5.60314	0.08524	0.10387	0.00337	1917	24.58	1916.3	21.19	1916.6	13.11	1997.4	61.71	79
T13_003 - 72	0.06357	0.00096	0.11973	0.00153	1.04937	0.0171	0.03794	0.00117	727.3	31.63	729	8.81	728.6	8.47	752.6	22.82	78
T13_003 - 73	0.05568	0.0009	0.06975	0.00089	0.53552	0.0092	0.02167	0.00067	439.4	35.27	434.7	5.34	435.5	6.08	433.4	13.32	77
T13_003 - 74	0.07186	0.00096	0.16419	0.0021	1.6268	0.02451	0.05054	0.00163	982	26.97	980	11.62	980.6	9.47	996.6	31.41	77
T13_003 - 75	0.05774	0.00145	0.07137	0.00109	0.56812	0.0146	0.02211	0.00099	519.7	54.46	444.4	6.56	456.8	9.45	442	19.52	76
T13_003 - 76	0.09181	0.00109	0.2635	0.00327	3.33552	0.04541	0.07794	0.00181	1463.3	22.42	1507.7	16.66	1489.4	10.63	1517	33.94	72
T13_003 - 77	0.10208	0.0013	0.29399	0.00373	4.13753	0.05969	0.08653	0.00239	1662.3	23.32	1661.4	18.58	1661.7	11.8	1677.3	44.55	69
T13_003 - 78	0.07682	0.00108	0.04125	0.00051	0.43688	0.00655	0.01815	0.00055	1116.4	27.83	260.6	3.13	368	4.63	363.5	10.99	63
T13_003 - 79	0.05755	0.00114	0.06238	0.00087	0.49499	0.01022	0.02086	0.00079	512.3	43.23	390.1	5.27	408.3	6.94	417.3	15.73	62
T13_003 - 80	0.06462	0.00101	0.12554	0.00163	1.1185	0.0188	0.04057	0.0012	762.1	32.62	762.4	9.34	762.3	9.01	803.8	23.39	57
T13_003 - 81	0.06369	0.00125	0.03854	0.00053	0.3384	0.00685	0.01754	0.00097	731.4	41.04	243.7	3.27	296	5.2	351.5	19.29	57
T13_003 - 82	0.07054	0.00098	0.1401	0.00181	1.36242	0.02115	0.04364	0.00136	944.1	28.21	845.2	10.25	872.9	9.09	863.4	26.27	54
T13_003 - 83	0.08178	0.00145	0.21024	0.00292	2.37066	0.04461	0.06185	0.00237	1240.3	34.18	1230.1	15.56	1233.8	13.44	1212.9	45.13	49
T13_003 - 84	0.05733	0.00101	0.08075	0.00115	0.6382	0.01229	0.02496	0.00112	503.8	37.99	500.6	6.87	501.2	7.62	498.4	22.11	47

T13_003 - 85	0.14093	0.00169	0.41409	0.00529	8.04474	0.11305	0.11794	0.00341	2238.6	20.62	2233.6	24.13	2236.1	12.69	2253.3	61.57	43
T13_003 - 86	0.08832	0.00201	0.25109	0.00341	3.05757	0.06916	0.06735	0.00524	1389.5	42.92	1444.1	17.54	1422.1	17.31	1317.4	99.3	33
T13_003 - 87	0.05642	0.00103	0.07605	0.00101	0.59153	0.01127	0.02357	0.00086	468.2	40.13	472.5	6.07	471.8	7.19	470.9	17.01	29
T13_003 - 88	0.05487	0.00084	0.07432	0.00098	0.56224	0.00947	0.02204	0.00074	407.1	33.64	462.2	5.9	453	6.15	440.6	14.65	23
T13_003 - 89	0.05942	0.00116	0.08884	0.00117	0.72768	0.01445	0.02806	0.00117	582.7	41.71	548.7	6.91	555.2	8.49	559.4	22.98	20
T13_003 - 90	0.07329	0.00098	0.17018	0.00223	1.71948	0.02627	0.05202	0.00183	1022.1	26.82	1013.1	12.26	1015.8	9.81	1025	35.14	16
Sample T13_005 –Slaty Sandstones																	
T13_005 - 1	0.10234	0.00116	0.30517	0.0041	4.30551	0.06102	0.09206	0.00197	1666.9	20.85	1716.9	20.27	1694.4	11.68	1780	36.47	84
T13_005 - 2	0.1348	0.00289	0.27573	0.0044	5.11948	0.11482	0.03201	0.00173	2161.4	36.96	1569.8	22.22	1839.3	19.05	636.8	33.94	40
T13_005 - 3	0.09097	0.00109	0.25177	0.00337	3.15768	0.04583	0.07279	0.00183	1445.9	22.6	1447.6	17.37	1446.9	11.19	1420.1	34.55	97
T13_005 - 4	0.07457	0.00105	0.04463	0.00063	0.45878	0.00754	0.01722	0.00041	1056.6	28.51	281.5	3.87	383.4	5.25	345.1	8.06	95
T13_005 - 5	0.14595	0.0017	0.42842	0.00584	8.62008	0.12541	0.11922	0.00314	2299	19.87	2298.6	26.34	2298.7	13.24	2276.5	56.68	56
T13_005 - 6	0.05213	0.00081	0.0439	0.00063	0.31551	0.00563	0.01335	0.00043	291.3	35.12	277	3.88	278.4	4.35	268.1	8.59	97
T13_005 - 7	0.12	0.00175	0.22021	0.00308	3.64283	0.06027	0.04352	0.00153	1956.2	25.75	1283	16.26	1558.9	13.18	861.1	29.56	84
T13_005 - 8	0.0701	0.00085	0.0907	0.00122	0.87653	0.01289	0.0269	0.00071	931.3	24.7	559.7	7.19	639.1	6.97	536.6	13.88	68
T13_005 - 9	0.10629	0.0016	0.18772	0.00256	2.75069	0.04591	0.02711	0.00103	1736.7	27.36	1109	13.91	1342.3	12.43	540.6	20.19	104
T13_005 - 10	0.07102	0.00091	0.12833	0.00177	1.25646	0.01956	0.04039	0.00134	957.9	26.09	778.4	10.14	826.3	8.8	800.2	25.94	102
T13_005 - 11	0.09156	0.00153	0.2533	0.00374	3.19719	0.06038	0.07098	0.00383	1458.2	31.53	1455.5	19.26	1456.5	14.61	1386.1	72.25	97
T13_005 - 12	0.06912	0.00104	0.11684	0.00164	1.11348	0.01906	0.02111	0.00075	902.4	30.6	712.4	9.44	759.8	9.16	422.2	14.8	84
T13_005 - 13	0.09101	0.00112	0.25049	0.00343	3.14301	0.04743	0.07208	0.00232	1446.7	23.27	1441	17.68	1443.3	11.62	1406.8	43.7	98
T13_005 - 14	0.07885	0.00102	0.18408	0.00256	2.00107	0.03124	0.04725	0.00151	1168.5	25.29	1089.2	13.96	1115.9	10.57	933.2	29.14	90
T13_005 - 15	0.08617	0.00164	0.06196	0.00094	0.73596	0.01531	0.01911	0.00118	1342.1	36.41	387.5	5.69	560	8.95	382.7	23.39	89
T13_005 - 16	0.05369	0.00116	0.04184	0.00062	0.30967	0.00702	0.01416	0.00047	357.8	48.08	264.2	3.81	273.9	5.44	284.2	9.34	100
T13_005 - 17	0.09017	0.00139	0.24846	0.00348	3.08914	0.05369	0.07464	0.00338	1429	29.14	1430.5	17.96	1430	13.33	1454.9	63.56	95
T13_005 - 18	0.05672	0.00085	0.07666	0.00107	0.59946	0.01025	0.02319	0.00067	479.8	33.16	476.2	6.39	476.9	6.51	463.4	13.3	98
T13_005 - 19	0.12703	0.00191	0.37628	0.00557	6.59028	0.11669	0.08916	0.00366	2057.3	26.23	2058.9	26.08	2058	15.61	1726.2	68	108
T13_005 - 20	0.05894	0.00108	0.0729	0.00104	0.59248	0.01171	0.02307	0.0012	564.9	39.53	453.6	6.24	472.5	7.46	460.9	23.72	85
T13_005 - 21	0.08847	0.00272	0.2386	0.00427	2.90181	0.09013	0.06373	0.00664	1392.7	57.77	1379.4	22.22	1382.4	23.46	1248.7	126.15	87
T13_005 - 22	0.05443	0.00139	0.04293	0.00066	0.32218	0.00848	0.01262	0.00043	389	56.14	271	4.05	283.6	6.52	253.4	8.61	103

T13_005 - 23	0.09213	0.00137	0.23526	0.00344	2.98821	0.05231	0.05295	0.00203	1470	28.16	1362	17.95	1404.6	13.32	1042.8	39.05	84
T13_005 - 24	0.05138	0.00101	0.04228	0.00062	0.2995	0.00633	0.01356	0.00049	257.8	44.53	267	3.81	266	4.94	272.2	9.68	137
T13_005 - 25	0.19532	0.00738	0.53911	0.01074	14.51129	0.54392	0.18489	0.02804	2787.5	60.54	2779.7	44.98	2783.7	35.61	3429	478.33	102
T13_005 - 26	0.05643	0.00081	0.07424	0.00105	0.57765	0.00976	0.02277	0.00084	468.6	31.74	461.7	6.31	462.9	6.28	455	16.55	108
T13_005 - 27	0.08954	0.00116	0.25813	0.00366	3.18679	0.05071	0.06618	0.00218	1415.7	24.63	1480.3	18.75	1454	12.3	1295.3	41.27	102
T13_005 - 28	0.05652	0.00185	0.07301	0.00122	0.56904	0.01852	0.02197	0.00203	472	71.49	454.3	7.34	457.4	11.99	439.3	40.19	96
T13_005 - 29	0.10816	0.00217	0.31248	0.00465	4.66046	0.09979	0.08987	0.00641	1768.5	36.33	1752.9	22.84	1760.2	17.9	1739.4	118.86	64
T13_005 - 30	0.14726	0.00523	0.43181	0.00824	8.76621	0.30823	0.12128	0.01678	2314.3	59.69	2313.9	37.11	2314	32.05	2313.6	302.42	92
T13_005 - 31	0.0805	0.00098	0.1876	0.0026	2.08182	0.03152	0.05525	0.00156	1209.3	23.72	1108.3	14.13	1142.8	10.39	1087	29.82	85
T13_005 - 32	0.05555	0.00086	0.07007	0.00101	0.53661	0.00961	0.02143	0.00062	434.3	33.64	436.6	6.09	436.2	6.35	428.5	12.18	77
T13_005 - 33	0.08914	0.00112	0.23453	0.00327	2.88194	0.0446	0.07646	0.00223	1407.1	23.92	1358.2	17.08	1377.2	11.67	1489.3	41.82	106
T13_005 - 34	0.05742	0.00082	0.07852	0.00113	0.62144	0.01053	0.02093	0.0007	507.3	30.82	487.3	6.73	490.8	6.59	418.7	13.78	97
T13_005 - 35	0.09407	0.00143	0.24926	0.00355	3.23227	0.05613	0.06479	0.00256	1509.5	28.52	1434.6	18.31	1464.9	13.47	1268.9	48.59	101
T13_005 - 36	0.10982	0.00137	0.31666	0.00446	4.79399	0.07423	0.09473	0.00286	1796.4	22.52	1773.4	21.84	1783.8	13.01	1829.3	52.87	92
T13_005 - 37	0.07998	0.00144	0.19454	0.00298	2.14481	0.04309	0.0498	0.00206	1196.5	35.19	1145.9	16.07	1163.4	13.91	982.3	39.74	89
T13_005 - 38	0.06227	0.00089	0.04167	0.00061	0.35767	0.00613	0.02132	0.00082	683.5	30.28	263.1	3.75	310.5	4.58	426.4	16.14	77
T13_005 - 39	0.05551	0.00077	0.06886	0.00097	0.52695	0.00872	0.02199	0.00072	432.7	30.22	429.3	5.87	429.8	5.8	439.7	14.29	98
T13_005 - 40	0.10528	0.00174	0.23608	0.00348	3.42609	0.06372	0.08372	0.00412	1719.2	30.15	1366.3	18.13	1510.4	14.62	1625.1	76.89	94
T13_005 - 41	0.05637	0.00094	0.07168	0.00101	0.55701	0.01028	0.02288	0.00089	466.1	36.68	446.3	6.1	449.6	6.7	457.3	17.65	97
T13_005 - 42	0.07188	0.00145	0.15119	0.00235	1.49692	0.03279	0.04506	0.00312	982.6	40.65	907.6	13.16	929.1	13.33	890.8	60.33	96
T13_005 - 43	0.14916	0.00607	0.43378	0.00882	8.91624	0.36682	0.07691	0.01198	2336.3	68.07	2322.7	39.64	2329.5	37.56	1497.6	224.76	104
T13_005 - 44	0.05217	0.00465	0.04213	0.00128	0.30292	0.02588	0.01232	0.00183	292.8	191.14	266	7.93	268.7	20.17	247.6	36.44	91
T13_005 - 45	0.07806	0.00168	0.05822	0.00087	0.6262	0.01404	0.01604	0.00122	1148.4	42.1	364.8	5.31	493.7	8.77	321.7	24.29	102
T13_005 - 46	0.11193	0.00188	0.27474	0.00411	4.24022	0.08073	0.06059	0.00331	1831	30.17	1564.8	20.8	1681.8	15.64	1189	63.03	102
T13_005 - 47	0.06672	0.00133	0.06164	0.00094	0.56707	0.01219	0.01759	0.00054	829.1	40.91	385.6	5.73	456.1	7.9	352.4	10.77	101
T13_005 - 48	0.06029	0.00087	0.1003	0.00143	0.83374	0.01413	0.03158	0.001	614	30.89	616.2	8.37	615.7	7.82	628.5	19.66	54
T13_005 - 49	0.08992	0.00371	0.2553	0.00516	3.17085	0.12726	0.03858	0.00447	1423.8	77.01	1465.7	26.51	1450.1	30.98	765.2	87.04	103
T13_005 - 50	0.09962	0.00118	0.24686	0.00334	3.39099	0.04963	0.07268	0.00207	1616.9	21.97	1422.3	17.28	1502.3	11.48	1418.1	39.03	101
T13_005 - 51	0.10755	0.00133	0.28355	0.00398	4.20432	0.06471	0.0641	0.00198	1758.2	22.37	1609.2	20.01	1674.9	12.62	1255.7	37.6	85

T13_005 - 52	0.05977	0.00254	0.05985	0.00117	0.49347	0.02053	0.01734	0.00144	595	90.12	374.7	7.1	407.3	13.96	347.6	28.57	107
T13_005 - 53	0.11032	0.00139	0.25109	0.0035	3.81967	0.05892	0.06304	0.00215	1804.7	22.67	1444.1	18.02	1596.9	12.41	1235.6	40.88	74
T13_005 - 54	0.0515	0.00173	0.04153	0.00069	0.29491	0.0098	0.01386	0.00088	263.2	75.29	262.3	4.25	262.4	7.68	278.1	17.45	104
T13_005 - 55	0.25411	0.00352	0.64436	0.00904	22.57718	0.36766	0.16731	0.00695	3210.5	21.72	3206.1	35.45	3208.9	15.83	3126.9	120.26	89
T13_005 - 56	0.05692	0.00084	0.07742	0.00107	0.60781	0.01023	0.02451	0.00097	487.8	32.72	480.7	6.41	482.2	6.46	489.4	19.14	102
T13_005 - 57	0.10145	0.00153	0.28739	0.00416	4.01952	0.07016	0.07712	0.00322	1650.8	27.65	1628.5	20.82	1638.2	14.19	1501.5	60.37	99
T13_005 - 58	0.11031	0.00177	0.32287	0.00467	4.91118	0.08929	0.08254	0.0044	1804.5	28.93	1803.7	22.78	1804.2	15.34	1603	82.06	104
T13_005 - 59	0.11189	0.00153	0.32897	0.00461	5.07539	0.08221	0.07269	0.0029	1830.4	24.64	1833.4	22.35	1832	13.74	1418.2	54.59	83
T13_005 - 60	0.17173	0.00237	0.49138	0.00677	11.63883	0.1863	0.13265	0.00554	2574.5	22.85	2576.6	29.28	2575.8	14.97	2517.7	98.88	106
T13_005 - 61	0.09811	0.00142	0.28573	0.00427	3.86489	0.06703	0.07777	0.00231	1588.5	26.88	1620.1	21.4	1606.4	13.99	1513.7	43.33	101
T13_005 - 62	0.11276	0.00144	0.33191	0.00456	5.15923	0.07902	0.09278	0.00299	1844.4	22.9	1847.6	22.07	1845.9	13.03	1793.4	55.32	119
T13_005 - 63	0.05656	0.00162	0.07641	0.00126	0.59555	0.01725	0.02278	0.00196	473.7	62.13	474.7	7.53	474.4	10.98	455.3	38.69	129
T13_005 - 64	0.05179	0.00087	0.04451	0.00067	0.31781	0.00611	0.01456	0.00056	276.1	38.01	280.7	4.11	280.2	4.71	292.2	11.25	168
T13_005 - 65	0.05607	0.00095	0.07309	0.00098	0.56503	0.01021	0.02058	0.00089	454.8	36.77	454.7	5.9	454.8	6.63	411.8	17.59	118
T13_005 - 66	0.10729	0.00144	0.32249	0.00456	4.77034	0.07647	0.09391	0.00315	1753.9	24.29	1801.9	22.25	1779.7	13.46	1814.2	58.17	128
T13_005 - 67	0.05198	0.00108	0.04442	0.00064	0.31829	0.00692	0.01323	0.00067	284.5	46.94	280.2	3.95	280.6	5.33	265.6	13.33	138
T13_005 - 68	0.05331	0.00085	0.05444	0.00079	0.40007	0.00733	0.01698	0.0006	341.8	35.6	341.7	4.85	341.7	5.31	340.4	11.83	103
T13_005 - 69	0.05718	0.00125	0.0804	0.0013	0.63378	0.01495	0.02206	0.00128	497.9	48.1	498.5	7.75	498.4	9.29	441.1	25.34	100
T13_005 - 70	0.05505	0.00081	0.05944	0.00084	0.45111	0.00768	0.01756	0.00068	414	32.21	372.2	5.11	378.1	5.37	351.9	13.46	104
T13_005 - 71	0.08763	0.00125	0.23804	0.00339	2.87594	0.04802	0.07529	0.00303	1374.4	27.06	1376.5	17.66	1375.6	12.58	1467.2	57.03	103
T13_005 - 72	0.11161	0.00141	0.36963	0.00523	5.68745	0.08882	0.09525	0.00336	1825.7	22.69	2027.7	24.64	1929.5	13.49	1839	61.92	97
T13_005 - 73	0.08096	0.00127	0.21172	0.00319	2.36363	0.04344	0.0644	0.00297	1220.6	30.45	1238	16.98	1231.7	13.11	1261.5	56.37	103
T13_005 - 74	0.06394	0.00124	0.11758	0.00174	1.03649	0.02163	0.03709	0.00212	739.5	40.59	716.6	10.05	722.2	10.79	736.2	41.37	101
T13_005 - 75	0.05361	0.00105	0.04254	0.00066	0.31443	0.00682	0.01399	0.00077	354.5	43.86	268.6	4.1	277.6	5.27	280.7	15.32	102
T13_005 - 76	0.16508	0.00195	0.36798	0.00525	8.37409	0.12845	0.06252	0.00165	2508.4	19.71	2019.9	24.72	2272.4	13.91	1225.7	31.37	106
T13_005 - 77	0.05657	0.00093	0.07186	0.00101	0.56042	0.01026	0.02332	0.00081	474	36.19	447.3	6.09	451.8	6.68	466	16.03	97
T13_005 - 78	0.05623	0.00092	0.0744	0.00108	0.57674	0.01076	0.02343	0.0008	460.9	36.01	462.6	6.5	462.4	6.93	468	15.8	99
T13_005 - 79	0.14376	0.00189	0.40996	0.00606	8.12305	0.13461	0.09927	0.00315	2273	22.45	2214.7	27.71	2244.8	14.98	1913	57.88	109
T13_005 - 80	0.09043	0.00222	0.25051	0.00378	3.12392	0.07764	0.07888	0.00749	1434.5	46.1	1441.1	19.46	1438.6	19.12	1534.6	140.29	97

T13_005 - 81	0.05953	0.00141	0.06697	0.00109	0.54949	0.01379	0.01636	0.00118	586.5	50.47	417.9	6.61	444.7	9.04	328	23.53	98
T13_005 - 82	0.09277	0.00137	0.25822	0.00384	3.3017	0.05883	0.07917	0.00324	1483.1	27.76	1480.7	19.68	1481.5	13.89	1540	60.75	106
T13_005 - 83	0.19399	0.00263	0.43703	0.00643	11.6857	0.19664	0.12067	0.00425	2776.3	22.02	2337.3	28.86	2579.6	15.74	2302.7	76.58	101
T13_005 - 84	0.05948	0.00134	0.06292	0.001	0.51585	0.01248	0.02157	0.00097	584.6	48.3	393.4	6.06	422.4	8.36	431.3	19.26	107
T13_005 - 85	0.08018	0.00123	0.2036	0.00297	2.25041	0.04031	0.06034	0.00255	1201.4	29.88	1194.7	15.89	1196.9	12.59	1184.2	48.59	98
T13_005 - 86	0.07985	0.00118	0.19624	0.00282	2.15999	0.03777	0.06223	0.00266	1193.2	28.97	1155.1	15.21	1168.3	12.14	1220.2	50.67	100
T13_005 - 87	0.05934	0.00423	0.05658	0.00156	0.4629	0.03158	0.01604	0.00289	579.8	147.82	354.8	9.51	386.3	21.92	321.5	57.55	103
T13_005 - 88	0.05634	0.0011	0.05949	0.00088	0.46205	0.00982	0.0205	0.00095	465.1	43.05	372.5	5.36	385.7	6.82	410.1	18.82	107
T13_005 - 89	0.05437	0.00087	0.04418	0.00064	0.33109	0.0061	0.01427	0.00059	386.2	35.24	278.7	3.96	290.4	4.65	286.3	11.73	101
T13_005 - 90	0.05532	0.00131	0.04278	0.00068	0.32628	0.00821	0.01323	0.00063	425.1	51.56	270.1	4.18	286.7	6.28	265.7	12.63	96

Siam cement Quarry lithological unit

Sample T13_016 –Silty Sandstones

T13_016 - 1	0.05751	0.00076	0.07883	0.00115	0.62498	0.01026	0.02395	0.00056	510.6	28.59	489.1	6.88	493	6.41	478.5	11.06	106
T13_016 - 2	0.05818	0.00078	0.07714	0.00106	0.61859	0.00981	0.02558	0.00055	535.8	29.72	479	6.35	489	6.16	510.5	10.84	79
T13_016 - 3	0.05738	0.00073	0.07806	0.0011	0.61741	0.00973	0.0248	0.00063	505.6	27.87	484.5	6.6	488.2	6.11	495.1	12.44	93
T13_016 - 4	0.07292	0.00094	0.16517	0.00229	1.66005	0.02576	0.05325	0.00122	1011.6	25.84	985.4	12.68	993.4	9.83	1048.7	23.34	98
T13_016 - 5	0.0561	0.00094	0.06922	0.00101	0.53516	0.01015	0.02176	0.00078	455.8	36.66	431.5	6.11	435.2	6.71	435.1	15.4	99
T13_016 - 6	0.18086	0.00191	0.50866	0.00691	12.6871	0.17285	0.12472	0.0025	2660.8	17.36	2650.9	29.54	2656.7	12.82	2375.6	44.94	76
T13_016 - 7	0.07226	0.00083	0.1668	0.00227	1.66128	0.024	0.04872	0.00119	993.3	23.2	994.4	12.54	993.9	9.16	961.6	22.9	95
T13_016 - 8	0.06996	0.0014	0.1541	0.00216	1.48603	0.03085	0.0499	0.00283	927.1	40.65	923.9	12.07	924.7	12.6	984.3	54.49	108
T13_016 - 9	0.08428	0.00097	0.22343	0.00329	2.59968	0.03883	0.05235	0.00123	1299	22.14	1299.9	17.34	1300.5	10.95	1031.3	23.6	94
T13_016 - 10	0.05824	0.00099	0.04246	0.00062	0.34057	0.0065	0.01378	0.00055	538.1	37.47	268	3.81	297.6	4.92	276.7	10.94	103
T13_016 - 11	0.07515	0.00089	0.18372	0.00254	1.90298	0.02837	0.05406	0.00158	1072.4	23.68	1087.3	13.82	1082.1	9.92	1064.2	30.32	97
T13_016 - 12	0.07924	0.00093	0.19777	0.00281	2.16047	0.03266	0.05904	0.00157	1178	22.95	1163.3	15.11	1168.4	10.49	1159.5	29.99	81
T13_016 - 13	0.0708	0.00091	0.15137	0.00224	1.47749	0.02431	0.0351	0.00117	951.5	26.17	908.7	12.55	921.2	9.96	697.3	22.9	103
T13_016 - 14	0.05702	0.00087	0.07031	0.00106	0.55277	0.01006	0.02132	0.00076	491.9	33.46	438	6.39	446.8	6.58	426.3	15.04	98
T13_016 - 15	0.12074	0.00316	0.35719	0.00589	5.94228	0.16339	0.11058	0.01131	1967.2	45.99	1968.9	28	1967.4	23.9	2119.9	205.89	95
T13_016 - 16	0.06973	0.00082	0.15556	0.00225	1.49541	0.02298	0.04423	0.00123	920.4	23.88	932	12.57	928.5	9.35	874.8	23.76	92
T13_016 - 17	0.05906	0.00074	0.09987	0.00146	0.81316	0.013	0.03123	0.00082	569.1	26.88	613.7	8.59	604.2	7.28	621.6	16.08	97

T13_016 - 18	0.06074	0.00108	0.06986	0.00111	0.58518	0.01194	0.02266	0.00084	629.9	37.82	435.3	6.67	467.8	7.65	452.9	16.55	100
T13_016 - 19	0.05688	0.001	0.08082	0.00126	0.63373	0.0128	0.02019	0.00079	486.3	38.78	501	7.52	498.4	7.96	404.1	15.58	95
T13_016 - 20	0.05275	0.00079	0.04593	0.00066	0.33404	0.00582	0.015	0.0006	318.2	33.74	289.5	4.04	292.6	4.43	300.9	12	101
T13_016 - 21	0.05459	0.00077	0.07184	0.00109	0.54075	0.00946	0.02145	0.00063	395.5	31.11	447.2	6.56	438.9	6.23	428.9	12.56	87
T13_016 - 22	0.06644	0.00088	0.13484	0.002	1.23509	0.02056	0.03916	0.00116	820.2	27.5	815.4	11.36	816.7	9.34	776.4	22.56	94
T13_016 - 23	0.05759	0.00088	0.08053	0.00123	0.63934	0.01179	0.02676	0.00107	513.7	33.68	499.3	7.35	501.9	7.3	533.8	21.02	87
T13_016 - 24	0.1748	0.00199	0.49458	0.00719	11.92039	0.18111	0.11297	0.00335	2604.2	18.84	2590.5	31	2598.2	14.23	2163.4	60.9	100
T13_016 - 25	0.19895	0.00226	0.47884	0.007	13.13643	0.19949	0.11568	0.00313	2817.6	18.47	2522.2	30.51	2689.5	14.33	2212.5	56.71	105
T13_016 - 26	0.09363	0.00139	0.24318	0.00359	3.13905	0.05491	0.0712	0.0027	1500.7	27.72	1403.2	18.63	1442.3	13.47	1390.2	50.98	101
T13_016 - 27	0.07518	0.00093	0.18422	0.00267	1.90944	0.03021	0.05603	0.00211	1073.4	24.54	1090	14.54	1084.4	10.54	1101.8	40.39	92
T13_016 - 28	0.07682	0.001	0.18197	0.00277	1.92826	0.03222	0.04477	0.00151	1116.6	25.68	1077.7	15.13	1090.9	11.17	885.2	29.26	89
T13_016 - 29	0.08084	0.00125	0.21667	0.00331	2.41474	0.04436	0.06568	0.0028	1217.5	30.02	1264.2	17.52	1247	13.19	1285.7	53.02	100
T13_016 - 30	0.05351	0.0008	0.05317	0.00079	0.39227	0.00699	0.01545	0.00062	350.5	33.28	334	4.81	336	5.1	309.9	12.27	89
T13_016 - 31	0.05763	0.00099	0.08515	0.00134	0.67662	0.01358	0.02563	0.00106	515.4	37.6	526.8	7.97	524.7	8.22	511.4	20.86	88
T13_016 - 32	0.05593	0.0009	0.07511	0.00115	0.57916	0.011	0.02316	0.00075	449.4	35.05	466.9	6.89	463.9	7.08	462.7	14.89	94
T13_016 - 33	0.05732	0.00075	0.0793	0.00117	0.6266	0.01041	0.02338	0.00071	503.6	28.7	491.9	7.01	494	6.5	467.1	14.02	88
T13_016 - 34	0.05633	0.0008	0.07414	0.00109	0.57566	0.00987	0.02344	0.00085	464.6	31.29	461.1	6.51	461.7	6.36	468.3	16.86	86
T13_016 - 35	0.0598	0.00079	0.08872	0.0013	0.73143	0.01205	0.02429	0.00137	596.5	28.33	548	7.68	557.4	7.07	485.1	27.02	70
T13_016 - 36	0.11337	0.00135	0.33319	0.00486	5.20751	0.08144	0.09003	0.00304	1854.2	21.39	1853.8	23.52	1853.8	13.32	1742.4	56.36	92
T13_016 - 37	0.10336	0.00173	0.3051	0.00492	4.3476	0.08619	0.07559	0.00406	1685.3	30.59	1716.6	24.28	1702.4	16.36	1472.9	76.26	87
T13_016 - 38	0.07975	0.00121	0.20142	0.00294	2.2142	0.03905	0.06032	0.00272	1190.9	29.57	1182.9	15.76	1185.5	12.34	1183.8	51.84	83
T13_016 - 39	0.05268	0.00102	0.05196	0.00081	0.37733	0.00811	0.01699	0.0008	314.9	43.33	326.5	4.96	325.1	5.98	340.6	15.84	89
T13_016 - 40	0.0706	0.001	0.16191	0.00246	1.57596	0.02754	0.04904	0.00205	945.8	28.75	967.4	13.62	960.8	10.86	967.6	39.51	94
T13_016 - 41	0.05281	0.00111	0.05701	0.00092	0.4151	0.00957	0.01615	0.00065	320.4	46.87	357.4	5.58	352.5	6.87	323.8	12.86	88
T13_016 - 42	0.05613	0.00078	0.07223	0.00107	0.55905	0.00954	0.02004	0.00079	457.3	30.24	449.6	6.44	450.9	6.22	401	15.65	95
T13_016 - 43	0.05815	0.00088	0.07828	0.00115	0.62756	0.0112	0.02483	0.0012	534.8	33.31	485.9	6.9	494.6	6.99	495.8	23.6	93
T13_016 - 44	0.06031	0.00088	0.10456	0.00158	0.86947	0.01546	0.02823	0.00115	614.8	31.28	641.1	9.24	635.3	8.39	562.7	22.7	79
T13_016 - 45	0.09449	0.00174	0.26536	0.00443	3.45869	0.07271	0.06288	0.00322	1518	34.32	1517.2	22.54	1517.9	16.56	1232.5	61.28	95
T13_016 - 46	0.15724	0.00319	0.42173	0.00657	9.14336	0.20263	0.10705	0.00872	2426.2	34.05	2268.3	29.81	2352.5	20.28	2055.5	159.17	98

T13_016 - 47	0.16182	0.00216	0.46087	0.00702	10.28363	0.17485	0.11644	0.00461	2474.8	22.37	2443.4	30.97	2460.6	15.73	2226.4	83.55	98
T13_016 - 48	0.0712	0.00119	0.1568	0.00241	1.53941	0.02971	0.04621	0.00221	963.3	33.64	939	13.41	946.3	11.88	913.1	42.78	101
T13_016 - 49	0.05774	0.00091	0.08887	0.00136	0.70754	0.01329	0.02382	0.00101	519.6	34.61	548.9	8.07	543.3	7.9	475.8	20	104
T13_016 - 50	0.06577	0.00254	0.05683	0.00111	0.51525	0.0198	0.01831	0.00141	799	78.8	356.3	6.79	422	13.27	366.8	27.95	123
T13_016 - 51	0.05554	0.00094	0.07874	0.0012	0.60304	0.01178	0.02354	0.00118	433.9	36.77	488.6	7.16	479.2	7.46	470.3	23.24	163
T13_016 - 52	0.07386	0.00117	0.188	0.00297	1.91453	0.03641	0.04846	0.00232	1037.6	31.7	1110.5	16.1	1086.2	12.69	956.6	44.7	98
T13_016 - 53	0.05893	0.00108	0.07584	0.00118	0.61619	0.01272	0.0229	0.00117	564.6	39.27	471.2	7.05	487.5	7.99	457.7	23.08	99
T13_016 - 54	0.05686	0.00122	0.07893	0.00126	0.61887	0.01449	0.02163	0.00102	485.6	46.89	489.7	7.53	489.1	9.09	432.6	20.12	91
T13_016 - 55	0.05118	0.0008	0.04449	0.00068	0.31394	0.00586	0.01182	0.00052	248.8	35.62	280.6	4.22	277.2	4.53	237.5	10.45	95
T13_016 - 56	0.07918	0.00323	0.2022	0.00426	2.2103	0.08908	0.04205	0.00394	1176.6	78.65	1187.1	22.84	1184.3	28.17	832.5	76.44	93
T13_016 - 57	0.08997	0.00145	0.24739	0.0038	3.0686	0.05818	0.06721	0.00389	1424.8	30.38	1425	19.64	1424.9	14.52	1314.7	73.72	91
T13_016 - 58	0.0654	0.00142	0.0461	0.00077	0.41575	0.00985	0.01535	0.00102	787.2	45.04	290.5	4.74	353	7.07	307.9	20.28	102
T13_016 - 59	0.10938	0.00161	0.31832	0.00493	4.80036	0.08669	0.07574	0.00357	1789.1	26.63	1781.5	24.09	1785	15.17	1475.6	67.11	100
T13_016 - 60	0.06993	0.0011	0.16406	0.0025	1.58162	0.02958	0.0435	0.00237	926.2	32.07	979.3	13.82	963	11.63	860.7	46	101
T13_016 - 61	0.10946	0.0014	0.33103	0.005	4.99518	0.0831	0.08836	0.00313	1790.3	23.18	1843.4	24.19	1818.5	14.07	1711.5	58.06	104
T13_016 - 62	0.05521	0.00103	0.07266	0.00118	0.55293	0.01183	0.01975	0.00083	420.5	40.39	452.2	7.07	446.9	7.73	395.3	16.46	104
T13_016 - 63	0.0518	0.00088	0.04472	0.00069	0.31934	0.00631	0.01336	0.00053	276.6	38.58	282	4.23	281.4	4.86	268.3	10.64	98
T13_016 - 64	0.14134	0.00176	0.38188	0.0057	7.44136	0.1207	0.10475	0.00369	2243.7	21.35	2085.1	26.61	2166	14.52	2013.5	67.59	103
T13_016 - 65	0.0601	0.00115	0.054	0.00087	0.44743	0.0097	0.01481	0.0006	607.3	40.69	339	5.34	375.5	6.81	297.2	12.03	105
T13_016 - 66	0.05343	0.0009	0.06054	0.00092	0.44596	0.00872	0.01773	0.00071	347.1	37.72	378.9	5.57	374.4	6.12	355.3	14.17	99
T13_016 - 67	0.06582	0.00203	0.1142	0.00208	1.03632	0.03277	0.06863	0.00764	800.5	63.27	697.1	12.05	722.1	16.34	1341.6	144.51	103
T13_016 - 68	0.05613	0.00083	0.0717	0.00109	0.55482	0.01002	0.02047	0.00083	457	32.19	446.4	6.55	448.1	6.54	409.6	16.4	97
T13_016 - 69	0.08146	0.00107	0.13376	0.00202	1.50213	0.02543	0.03811	0.00162	1232.5	25.68	809.3	11.5	931.3	10.32	756	31.58	102
T13_016 - 70	0.0726	0.0013	0.16812	0.00275	1.68227	0.03526	0.0467	0.00267	1002.7	35.9	1001.8	15.18	1001.8	13.35	922.6	51.49	99
T13_016 - 71	0.05545	0.00091	0.07072	0.0011	0.54062	0.01052	0.02173	0.00112	430	35.71	440.5	6.63	438.8	6.93	434.5	22.2	108
T13_016 - 72	0.05313	0.00148	0.04855	0.00085	0.35551	0.0103	0.01581	0.00138	334.4	61.78	305.6	5.21	308.9	7.72	317	27.53	98
T13_016 - 73	0.05329	0.00138	0.05478	0.00092	0.40252	0.01102	0.01693	0.001	341.3	57.57	343.8	5.6	343.5	7.98	339.3	19.85	95
T13_016 - 74	0.05684	0.00108	0.07571	0.00118	0.59329	0.01266	0.02331	0.00129	484.8	41.73	470.4	7.07	473	8.07	465.6	25.56	112
T13_016 - 75	0.07943	0.00123	0.20719	0.00324	2.26888	0.04273	0.06028	0.00325	1182.8	30.4	1213.9	17.28	1202.7	13.27	1183	61.97	99

Sample T13_065 –Silty Sandstones																
T13_065 - 1	0.11356	0.00124	0.26304	0.00335	4.11822	0.05483	0.07704	0.00152	1857.2	19.67	1505.4	17.09	1657.9	10.88	1500.1	28.49	97
T13_065 - 2	0.12169	0.00134	0.36014	0.00459	6.04194	0.08068	0.10879	0.00235	1981.2	19.51	1982.8	21.75	1981.9	11.63	2087.2	42.93	101
T13_065 - 3	0.0619	0.00089	0.09104	0.00119	0.77691	0.0124	0.02986	0.00064	670.7	30.41	561.7	7.05	583.7	7.09	594.7	12.6	99
T13_065 - 4	0.0721	0.00081	0.05769	0.00074	0.57347	0.00777	0.06825	0.00151	988.8	22.72	361.6	4.48	460.3	5.01	1334.4	28.6	96
T13_065 - 5	0.13156	0.00148	0.35808	0.00457	6.49479	0.08786	0.10986	0.0025	2119	19.53	1973.1	21.71	2045.2	11.9	2106.8	45.52	75
T13_065 - 6	0.16361	0.00192	0.44216	0.00571	9.97335	0.13845	0.13502	0.00323	2493.3	19.6	2360.3	25.52	2432.3	12.81	2559.8	57.44	84
T13_065 - 7	0.05791	0.00074	0.07702	0.001	0.61487	0.00908	0.02496	0.00062	525.9	28.15	478.3	5.96	486.6	5.71	498.4	12.22	74
T13_065 - 8	0.10551	0.00128	0.08162	0.00105	1.18732	0.01686	0.05071	0.00131	1723.3	22.12	505.8	6.28	794.7	7.82	999.8	25.29	91
T13_065 - 9	0.06966	0.00098	0.12779	0.00168	1.22722	0.01933	0.03913	0.00104	918.4	28.68	775.2	9.59	813.1	8.81	775.8	20.27	71
T13_065 - 10	0.05789	0.00076	0.06777	0.00088	0.54089	0.00813	0.02215	0.00062	525.5	28.84	422.7	5.3	439	5.36	442.8	12.21	82
T13_065 - 11	0.06913	0.00103	0.13958	0.00185	1.33015	0.02182	0.04146	0.00122	902.5	30.36	842.3	10.46	858.9	9.51	821	23.77	44
T13_065 - 12	0.07014	0.00096	0.13829	0.00181	1.33727	0.02062	0.04858	0.00146	932.5	27.74	835	10.24	862	8.96	958.8	28.13	102
T13_065 - 13	0.16375	0.00201	0.46351	0.006	10.4637	0.1503	0.13621	0.00413	2494.7	20.54	2455	26.42	2476.7	13.31	2581	73.52	96
T13_065 - 14	0.06056	0.00079	0.0609	0.00079	0.50849	0.00761	0.02037	0.00064	623.7	27.89	381.1	4.8	417.4	5.12	407.6	12.63	82
T13_065 - 15	0.05563	0.00144	0.05369	0.00079	0.41177	0.0107	0.01739	0.00063	437.1	56.21	337.2	4.85	350.2	7.7	348.5	12.55	103
T13_065 - 16	0.05962	0.0007	0.05793	0.00074	0.47616	0.00667	0.01892	0.00042	589.7	25.37	363	4.53	395.4	4.59	378.9	8.23	68
T13_065 - 17	0.09996	0.00116	0.27443	0.00352	3.78207	0.05227	0.07921	0.00181	1623.4	21.41	1563.2	17.82	1588.9	11.1	1540.7	33.84	40
T13_065 - 18	0.06154	0.00076	0.09209	0.00118	0.78136	0.01121	0.02875	0.0007	658.2	26.14	567.9	6.99	586.3	6.39	572.9	13.75	55
T13_065 - 19	0.09984	0.00116	0.28531	0.00365	3.92706	0.0541	0.08441	0.00195	1621.1	21.39	1618.1	18.3	1619.3	11.15	1637.9	36.39	97
T13_065 - 20	0.15909	0.00182	0.3954	0.00504	8.67189	0.11823	0.10974	0.0026	2446	19.18	2147.8	23.29	2304.1	12.41	2104.6	47.32	97
T13_065 - 21	0.11047	0.00133	0.30889	0.00397	4.70423	0.06638	0.07646	0.00191	1807.1	21.79	1735.3	19.55	1768	11.82	1489.2	35.78	63
T13_065 - 22	0.05668	0.0009	0.07726	0.00102	0.60369	0.01038	0.02392	0.00063	478.3	35.08	479.8	6.1	479.6	6.57	477.8	12.48	93
T13_065 - 23	0.09934	0.00121	0.28683	0.00368	3.92828	0.05567	0.08035	0.00208	1611.8	22.55	1625.7	18.41	1619.5	11.47	1562.1	38.88	98
T13_065 - 24	0.07119	0.0009	0.16116	0.00206	1.5817	0.02289	0.05426	0.00178	962.9	25.18	963.2	11.46	963	9	1067.9	34.11	60
T13_065 - 25	0.08031	0.00104	0.19309	0.00248	2.1379	0.03139	0.05798	0.00157	1204.7	25.19	1138.1	13.41	1161.1	10.16	1139.3	30.04	105
T13_065 - 26	0.09819	0.00119	0.25531	0.00325	3.4559	0.04872	0.08332	0.00231	1590	22.55	1465.8	16.7	1517.2	11.1	1617.7	43.04	100
T13_065 - 27	0.11848	0.00148	0.34227	0.00438	5.59024	0.07996	0.10355	0.00298	1933.4	22.14	1897.6	21.03	1914.6	12.32	1991.6	54.5	53

T13_065 - 28	0.05778	0.00095	0.07641	0.00101	0.60868	0.0107	0.02351	0.00072	521.4	35.91	474.7	6.03	482.7	6.75	469.7	14.17	99
T13_065 - 29	0.11381	0.00144	0.33045	0.00422	5.18459	0.07477	0.09217	0.00279	1861.1	22.69	1840.6	20.45	1850.1	12.28	1782.1	51.65	102
T13_065 - 30	0.10915	0.00149	0.06515	0.00084	0.98025	0.01483	0.02605	0.00081	1785.2	24.71	406.9	5.09	693.7	7.6	519.7	15.96	107
T13_065 - 31	0.06297	0.00104	0.06793	0.0009	0.58981	0.01038	0.02228	0.00052	707.4	34.81	423.7	5.4	470.7	6.63	445.4	10.29	90
T13_065 - 32	0.05797	0.00085	0.0735	0.00095	0.58747	0.0094	0.02147	0.00047	528.4	32.04	457.2	5.68	469.3	6.01	429.3	9.39	91
T13_065 - 33	0.0584	0.00123	0.07151	0.00099	0.57581	0.01239	0.02184	0.00056	544.9	45.33	445.2	5.93	461.8	7.98	436.7	11.16	88
T13_065 - 34	0.05553	0.00074	0.05951	0.00075	0.45563	0.00679	0.01828	0.00042	433.2	28.82	372.7	4.58	381.2	4.73	366.1	8.24	93
T13_065 - 35	0.0665	0.00086	0.07479	0.00095	0.68578	0.01003	0.01587	0.00038	822.2	26.89	464.9	5.67	530.3	6.04	318.3	7.58	102
T13_065 - 36	0.09583	0.00112	0.12012	0.0015	1.5872	0.02161	0.02852	0.00068	1544.4	21.88	731.3	8.64	965.2	8.48	568.3	13.36	50
T13_065 - 37	0.10981	0.00135	0.32079	0.00404	4.857	0.06815	0.08838	0.00216	1796.2	22.22	1793.6	19.73	1794.8	11.81	1711.7	40.02	54
T13_065 - 38	0.10803	0.00145	0.3172	0.00407	4.72468	0.07029	0.08755	0.00229	1766.4	24.32	1776	19.9	1771.6	12.47	1696.4	42.52	105
T13_065 - 39	0.12137	0.00147	0.29891	0.00374	5.00213	0.06922	0.08608	0.00222	1976.5	21.35	1685.9	18.55	1819.7	11.71	1668.9	41.23	103
T13_065 - 40	0.07349	0.0009	0.1466	0.00183	1.48538	0.0208	0.04204	0.00112	1027.4	24.65	881.9	10.28	924.4	8.5	832.4	21.69	104
T13_065 - 41	0.06083	0.0008	0.06785	0.00085	0.56902	0.00834	0.02124	0.00058	633.1	28.02	423.2	5.13	457.4	5.4	424.8	11.48	57
T13_065 - 42	0.06021	0.00094	0.07333	0.00094	0.60879	0.01015	0.02232	0.00065	611.3	33.32	456.2	5.65	482.8	6.41	446.3	12.86	102
T13_065 - 43	0.11008	0.00202	0.06638	0.00091	1.00742	0.01882	0.03816	0.00121	1800.7	32.99	414.3	5.51	707.6	9.52	757	23.59	87
T13_065 - 44	0.05439	0.00131	0.05884	0.00082	0.44121	0.01067	0.01744	0.00059	387	52.95	368.6	5.01	371.1	7.52	349.4	11.72	86
T13_065 - 45	0.0737	0.00094	0.12341	0.00153	1.25404	0.01796	0.03687	0.00116	1033.4	25.31	750.1	8.8	825.2	8.09	731.8	22.68	88
T13_065 - 46	0.19995	0.00224	0.46769	0.00564	12.89114	0.16551	0.1431	0.00291	2825.8	18.17	2473.4	24.77	2671.7	12.1	2703.4	51.42	73
T13_065 - 47	0.08019	0.00097	0.17292	0.0021	1.91158	0.0259	0.056	0.00115	1201.8	23.66	1028.2	11.53	1085.1	9.03	1101.3	22.03	95
T13_065 - 48	0.05742	0.00094	0.07055	0.00089	0.55843	0.0096	0.01999	0.00044	507.2	36.11	439.5	5.36	450.5	6.25	400	8.78	23
T13_065 - 49	0.07175	0.00085	0.16681	0.00202	1.64968	0.02209	0.04697	0.00104	978.7	24.04	994.5	11.14	989.4	8.46	927.7	19.99	75
T13_065 - 50	0.06258	0.00077	0.06325	0.00077	0.54564	0.00751	0.0171	0.00038	694.1	26.15	395.4	4.65	442.1	4.94	342.7	7.5	67
T13_065 - 51	0.10582	0.00122	0.3219	0.00389	4.69503	0.06163	0.08455	0.0019	1728.6	21.09	1799	18.97	1766.4	10.99	1640.5	35.4	86
T13_065 - 52	0.10508	0.00125	0.31536	0.00383	4.56725	0.06122	0.08673	0.00208	1715.7	21.78	1767	18.79	1743.3	11.17	1681.2	38.65	85
T13_065 - 53	0.05517	0.00094	0.07084	0.0009	0.53864	0.00951	0.02053	0.00051	419	37.23	441.2	5.41	437.5	6.28	410.8	10.18	101
T13_065 - 54	0.07226	0.00171	0.08737	0.00124	0.8702	0.02047	0.02744	0.00079	993.4	47.48	540	7.33	635.7	11.11	547.1	15.59	100
T13_065 - 55	0.05739	0.00079	0.03968	0.00049	0.31384	0.00466	0.01105	0.00028	506.3	29.7	250.8	3.02	277.2	3.6	222.2	5.54	47
T13_065 - 56	0.07044	0.00116	0.16017	0.00205	1.55495	0.02666	0.0439	0.00117	941.3	33.31	957.7	11.4	952.5	10.59	868.4	22.74	57

T13_065 - 57	0.07929	0.00096	0.18496	0.00225	2.02105	0.02737	0.04893	0.00131	1179.3	23.75	1094	12.22	1122.6	9.2	965.6	25.21	86
T13_065 - 58	0.10724	0.00132	0.27199	0.00332	4.01955	0.055	0.07107	0.00196	1753	22.27	1550.9	16.83	1638.2	11.13	1387.7	36.9	82
T13_065 - 59	0.06925	0.00087	0.13575	0.00166	1.29542	0.01804	0.03879	0.00111	906.1	25.72	820.6	9.4	843.7	7.98	769.2	21.62	87
T13_065 - 60	0.14276	0.00172	0.37222	0.00452	7.32263	0.09876	0.08284	0.00243	2261	20.63	2039.8	21.25	2151.6	12.05	1608.6	45.37	60
T13_065 - 61	0.07135	0.00091	0.17487	0.00219	1.71987	0.02464	0.05033	0.00123	967.5	25.73	1038.9	12.01	1016	9.2	992.6	23.68	23
T13_065 - 62	0.16644	0.00196	0.49094	0.00612	11.26347	0.15303	0.12596	0.00313	2522.2	19.65	2574.7	26.46	2545.2	12.67	2397.9	56.16	99
T13_065 - 63	0.07115	0.00085	0.15995	0.00198	1.56877	0.02151	0.04972	0.00175	961.8	24.16	956.5	11.02	957.9	8.5	980.8	33.7	91
T13_065 - 64	0.06134	0.00087	0.05493	0.00069	0.46448	0.00718	0.01729	0.00047	651.1	29.99	344.7	4.24	387.4	4.98	346.5	9.37	98
T13_065 - 65	0.08344	0.00108	0.21953	0.00276	2.52486	0.03663	0.06789	0.00204	1279.2	25.1	1279.4	14.58	1279.2	10.55	1327.6	38.62	92
T13_065 - 66	0.07051	0.00088	0.16575	0.00207	1.611	0.02288	0.05004	0.00142	943.2	25.47	988.6	11.43	974.5	8.9	986.8	27.35	94
T13_065 - 67	0.09946	0.00124	0.16264	0.00203	2.22996	0.0315	0.03868	0.00111	1614	23.02	971.4	11.26	1190.5	9.9	767.1	21.52	100
T13_065 - 68	0.07761	0.00098	0.18867	0.00235	2.01858	0.02877	0.05521	0.00163	1137	24.86	1114.2	12.77	1121.8	9.68	1086.1	31.24	101
T13_065 - 69	0.05373	0.00116	0.05328	0.00073	0.3946	0.0087	0.01668	0.00056	359.4	48.24	334.6	4.44	337.7	6.33	334.4	11.2	100
T13_065 - 70	0.08524	0.00108	0.13672	0.00171	1.60649	0.02303	0.04776	0.00153	1320.8	24.48	826.1	9.68	972.7	8.97	943	29.42	96
T13_065 - 71	0.08355	0.00111	0.21309	0.00268	2.45444	0.03625	0.06116	0.002	1281.9	25.65	1245.3	14.23	1258.7	10.66	1199.8	38.1	88
T13_065 - 72	0.07692	0.00103	0.18277	0.0023	1.93814	0.02888	0.04257	0.00146	1119.1	26.49	1082.1	12.52	1094.4	9.98	842.6	28.25	100
T13_065 - 73	0.11098	0.00147	0.16828	0.00211	2.57483	0.03803	0.05977	0.00208	1815.6	23.87	1002.6	11.67	1293.5	10.8	1173.3	39.69	86
T13_065 - 74	0.06826	0.00117	0.05525	0.00072	0.51997	0.00934	0.01829	0.0007	876.6	35	346.7	4.42	425.1	6.24	366.3	13.85	96
T13_065 - 75	0.06302	0.00101	0.07749	0.001	0.67322	0.01147	0.02606	0.001	708.8	33.59	481.1	5.97	522.7	6.96	520	19.72	62
T13_065 - 76	0.06077	0.00089	0.10659	0.00134	0.89292	0.01412	0.0315	0.00069	631.1	31.3	652.9	7.8	647.9	7.57	626.8	13.57	77
T13_065 - 77	0.0723	0.00086	0.1347	0.00165	1.3425	0.01823	0.04886	0.00116	994.4	24.08	814.6	9.38	864.3	7.9	964.3	22.44	61
T13_065 - 78	0.07759	0.00096	0.18501	0.00228	1.9789	0.02748	0.05036	0.00118	1136.5	24.31	1094.3	12.42	1108.3	9.37	993.1	22.8	98
T13_065 - 79	0.0914	0.00116	0.25749	0.00321	3.24416	0.04614	0.07468	0.00183	1454.9	24.04	1477	16.46	1467.8	11.04	1455.8	34.5	90
T13_065 - 80	0.06459	0.00079	0.05319	0.00066	0.47357	0.00655	0.01527	0.00038	761.1	25.55	334.1	4.01	393.7	4.52	306.3	7.59	93
T13_065 - 81	0.05935	0.00081	0.07673	0.00096	0.62771	0.00947	0.02295	0.00059	579.9	29.55	476.6	5.75	494.7	5.91	458.6	11.65	80
T13_065 - 82	0.11495	0.00139	0.22951	0.00285	3.63647	0.04992	0.07097	0.00189	1879.1	21.57	1331.9	14.92	1557.6	10.93	1385.8	35.65	84
T13_065 - 83	0.05787	0.00088	0.07694	0.00098	0.61366	0.01	0.02317	0.00066	524.5	33.15	477.8	5.86	485.9	6.29	463	13	29
T13_065 - 84	0.05871	0.00092	0.06631	0.00085	0.53653	0.00897	0.02126	0.00064	556.2	33.73	413.9	5.14	436.1	5.92	425.2	12.76	91
T13_065 - 85	0.07132	0.00109	0.13378	0.00172	1.31499	0.02157	0.04171	0.00124	966.5	30.9	809.4	9.8	852.3	9.46	825.9	24.1	95

T13_065 - 86	0.06163	0.00089	0.0802	0.00102	0.68127	0.01074	0.02398	0.00073	661.5	30.74	497.3	6.09	527.5	6.49	478.9	14.42	93
T13_065 - 87	0.05432	0.00075	0.0588	0.00074	0.44015	0.00668	0.01989	0.00065	384.2	30.56	368.3	4.52	370.4	4.71	398	12.96	37
T13_065 - 88	0.10648	0.00136	0.3049	0.00384	4.47395	0.06452	0.09187	0.00295	1739.9	23.34	1715.6	18.99	1726.2	11.97	1776.5	54.66	84
T13_065 - 89	0.05592	0.00081	0.07301	0.00093	0.56266	0.00892	0.02233	0.00074	449	31.54	454.3	5.6	453.3	5.8	446.3	14.69	100
T13_065 - 90	0.13545	0.00175	0.38591	0.00489	7.20283	0.10495	0.11063	0.00377	2169.8	22.37	2103.8	22.76	2136.9	12.99	2120.9	68.56	81
Sap Bon Formation																	
Sample T14_002 – Carbonatic/silty Sandstones																	
T14_002 - 1	0.05573	0.00089	0.06789	0.00094	0.52157	0.00927	0.02019	0.0005	441.5	34.7	423.4	5.67	426.2	6.18	404.1	9.99	98
T14_002 - 2	0.15682	0.00249	0.41062	0.00575	8.87777	0.15397	0.1046	0.00461	2421.7	26.74	2217.8	26.26	2325.5	15.83	2010.7	84.35	99
T14_002 - 3	0.07137	0.00131	0.15308	0.00211	1.50614	0.02902	0.04571	0.00188	968.1	36.92	918.2	11.82	932.9	11.76	903.4	36.31	93
T14_002 - 4	0.10669	0.00121	0.31095	0.00399	4.5739	0.06245	0.0822	0.00165	1743.7	20.57	1745.4	19.63	1744.5	11.38	1596.7	30.75	96
T14_002 - 5	0.05187	0.00078	0.04483	0.00061	0.32055	0.00546	0.01453	0.00037	279.8	34.22	282.7	3.76	282.3	4.2	291.5	7.35	90
T14_002 - 6	0.20085	0.00296	0.55249	0.00761	15.29666	0.25371	0.15054	0.00626	2833.1	23.83	2835.5	31.61	2833.9	15.81	2834.4	110.04	102
T14_002 - 7	0.05752	0.00113	0.05865	0.00084	0.46518	0.00965	0.0162	0.00063	511.3	42.88	367.4	5.09	387.9	6.69	324.7	12.56	78
T14_002 - 8	0.08309	0.00109	0.21707	0.00289	2.48662	0.03792	0.06348	0.0016	1271.3	25.3	1266.4	15.3	1268.1	11.04	1244	30.36	88
T14_002 - 9	0.09287	0.00138	0.25941	0.00362	3.32111	0.05609	0.07512	0.00258	1485.1	28	1486.8	18.54	1486	13.18	1464	48.46	84
T14_002 - 10	0.05819	0.00095	0.07152	0.00097	0.57377	0.01017	0.02145	0.00057	536.3	35.73	445.3	5.81	460.5	6.56	429	11.23	64
T14_002 - 11	0.07825	0.00097	0.20179	0.00269	2.17695	0.03233	0.05759	0.00161	1153.3	24.36	1184.9	14.41	1173.7	10.33	1131.8	30.67	55
T14_002 - 12	0.07549	0.00174	0.1446	0.00204	1.50503	0.03454	0.04222	0.00182	1081.6	45.64	870.6	11.48	932.4	14	835.9	35.25	92
T14_002 - 13	0.0573	0.00078	0.06988	0.00092	0.552	0.0086	0.02274	0.00064	502.6	29.6	435.4	5.56	446.3	5.63	454.6	12.72	93
T14_002 - 14	0.18597	0.00228	0.47492	0.0063	12.17643	0.17911	0.10596	0.00322	2706.8	20.09	2505.1	27.52	2618.1	13.8	2035.6	58.85	93
T14_002 - 15	0.0605	0.00152	0.05577	0.00086	0.46521	0.01195	0.01705	0.00072	621.6	53.38	349.9	5.25	387.9	8.28	341.7	14.4	79
T14_002 - 16	0.07846	0.00108	0.17804	0.00246	1.92531	0.03088	0.04644	0.0015	1158.6	26.98	1056.3	13.47	1089.9	10.72	917.6	28.96	87
T14_002 - 17	0.05902	0.00124	0.0576	0.00082	0.46854	0.01016	0.01245	0.00034	568	44.91	361	4.99	390.2	7.03	250.1	6.82	109
T14_002 - 18	0.12462	0.00142	0.35837	0.00456	6.15574	0.08327	0.05583	0.00128	2023.3	20.05	1974.4	21.63	1998.2	11.82	1098	24.59	105
T14_002 - 19	0.09767	0.00119	0.29269	0.00379	3.93971	0.05629	0.07679	0.00207	1580	22.65	1654.9	18.89	1621.9	11.57	1495.4	38.95	116
T14_002 - 20	0.08802	0.00137	0.22634	0.00328	2.74581	0.04885	0.06353	0.00239	1382.9	29.6	1315.3	17.22	1341	13.24	1245	45.34	90
T14_002 - 21	0.07618	0.00112	0.18368	0.00245	1.92881	0.03134	0.05166	0.00147	1099.9	29.11	1087.1	13.34	1091.1	10.86	1018	28.24	98
T14_002 - 22	0.0752	0.00124	0.16532	0.00216	1.7131	0.02974	0.04051	0.00201	1074	32.73	986.3	11.97	1013.4	11.13	802.6	39.01	102

T14_002 - 23	0.05467	0.0008	0.07367	0.00095	0.55518	0.0089	0.02265	0.00061	398.8	32.25	458.2	5.69	448.4	5.81	452.6	12.03	69
T14_002 - 24	0.07141	0.00108	0.16589	0.00219	1.63285	0.02679	0.0473	0.00144	969.1	30.43	989.4	12.08	983	10.33	934.2	27.82	91
T14_002 - 25	0.16918	0.00222	0.44533	0.00592	10.38388	0.15642	0.09182	0.0031	2549.6	21.81	2374.4	26.41	2469.6	13.95	1775.6	57.43	83
T14_002 - 26	0.26176	0.00307	0.63918	0.00804	23.06287	0.31221	0.15296	0.00418	3257.3	18.36	3185.8	31.61	3229.6	13.17	2876.9	73.24	101
T14_002 - 27	0.09818	0.00125	0.27784	0.00361	3.75979	0.05521	0.06174	0.00211	1589.9	23.68	1580.5	18.2	1584.2	11.78	1210.9	40.08	96
T14_002 - 28	0.0791	0.00113	0.17025	0.00226	1.85627	0.02963	0.0417	0.00154	1174.7	28.07	1013.5	12.47	1065.7	10.53	825.7	29.81	97
T14_002 - 29	0.06076	0.0008	0.0596	0.00075	0.49921	0.00728	0.01574	0.00047	630.6	27.97	373.2	4.56	411.2	4.93	315.6	9.39	86
T14_002 - 30	0.08812	0.00113	0.21989	0.00277	2.67111	0.03837	0.05818	0.00192	1385.1	24.42	1281.3	14.64	1320.5	10.61	1142.9	36.74	96
T14_002 - 31	0.10554	0.00145	0.30777	0.00408	4.47745	0.06906	0.09718	0.00299	1723.7	24.94	1729.7	20.12	1726.8	12.8	1874.5	55	89
T14_002 - 32	0.05921	0.00132	0.09661	0.00134	0.78847	0.01779	0.03115	0.00081	575	47.89	594.5	7.88	590.3	10.1	620	15.83	105
T14_002 - 33	0.08515	0.0011	0.13273	0.00175	1.55802	0.0233	0.05647	0.00133	1318.9	24.95	803.4	9.98	953.7	9.25	1110.2	25.41	101
T14_002 - 34	0.05454	0.00098	0.05068	0.00065	0.38093	0.00704	0.01464	0.00045	393.6	39.59	318.7	3.97	327.7	5.18	293.7	9.01	96
T14_002 - 35	0.05598	0.00074	0.06987	0.00087	0.53925	0.00792	0.02144	0.00047	451.3	28.75	435.4	5.26	437.9	5.22	428.8	9.22	104
T14_002 - 36	0.12317	0.00156	0.36079	0.00453	6.12468	0.08687	0.10546	0.0033	2002.6	22.28	1985.9	21.44	1993.8	12.38	2026.5	60.26	113
T14_002 - 37	0.08789	0.00119	0.12848	0.00178	1.55645	0.02494	0.03322	0.00122	1380	25.74	779.2	10.19	953.1	9.9	660.6	23.81	97
T14_002 - 38	0.06083	0.00073	0.09786	0.00124	0.82066	0.01144	0.02777	0.00066	633.3	25.61	601.8	7.27	608.4	6.38	553.6	13.05	78
T14_002 - 39	0.07131	0.00086	0.14438	0.00183	1.41938	0.01992	0.03744	0.00093	966.4	24.53	869.4	10.32	897.1	8.36	742.9	18.05	76
T14_002 - 40	0.05377	0.00138	0.05641	0.00079	0.41813	0.01071	0.01788	0.00052	361.2	56.76	353.8	4.83	354.7	7.66	358.2	10.29	102
T14_002 - 41	0.05169	0.00075	0.04364	0.00057	0.31099	0.00501	0.0132	0.00038	271.9	32.76	275.3	3.54	274.9	3.88	265.1	7.55	103
T14_002 - 42	0.07904	0.00095	0.19791	0.00252	2.15662	0.03018	0.0577	0.00152	1173.2	23.6	1164.1	13.55	1167.2	9.71	1133.9	28.97	97
T14_002 - 43	0.15192	0.00253	0.37164	0.00541	7.78357	0.1419	0.09884	0.00429	2367.6	28.18	2037.1	25.44	2206.3	16.4	1905.2	78.83	96
T14_002 - 44	0.0603	0.0008	0.0993	0.00127	0.82537	0.01234	0.0296	0.00089	614.2	28.47	610.3	7.42	611	6.86	589.6	17.52	93
T14_002 - 45	0.05551	0.00098	0.0721	0.00094	0.55173	0.01017	0.02133	0.00061	432.5	38.4	448.8	5.64	446.1	6.66	426.5	11.99	79
T14_002 - 46	0.05832	0.00095	0.08384	0.00108	0.67413	0.01164	0.02468	0.00072	541.1	35.92	519	6.44	523.2	7.06	492.8	14.19	89
T14_002 - 47	0.11741	0.00138	0.35287	0.00447	5.71173	0.07814	0.09985	0.00223	1917.1	20.86	1948.3	21.31	1933.1	11.82	1923.6	41.07	90
T14_002 - 48	0.05944	0.00096	0.07308	0.00098	0.59892	0.01052	0.02116	0.00056	583.3	34.72	454.7	5.9	476.5	6.68	423.2	11.13	82
T14_002 - 49	0.1675	0.00192	0.43675	0.00551	10.08603	0.13626	0.12194	0.00295	2532.8	19.14	2336.1	24.73	2442.7	12.48	2325.6	53.16	92
T14_002 - 50	0.06416	0.00093	0.10365	0.00141	0.91685	0.01506	0.0366	0.00128	746.8	30.23	635.8	8.22	660.7	7.98	726.6	24.86	91
T14_002 - 51	0.05657	0.00079	0.08262	0.00104	0.64439	0.00979	0.02535	0.00067	474	30.71	511.7	6.16	505	6.05	505.9	13.25	83

T14_002 - 52	0.09756	0.00135	0.28168	0.00353	3.78893	0.05638	0.07236	0.00194	1578	25.6	1599.8	17.78	1590.4	11.95	1412.1	36.55	86
T14_002 - 53	0.18351	0.00237	0.51993	0.00596	13.15528	0.1769	0.15032	0.00573	2684.9	21.22	2698.9	25.29	2690.9	12.69	2830.5	100.59	90
T14_002 - 54	0.08306	0.00131	0.21264	0.00267	2.43536	0.04007	0.06468	0.00258	1270.6	30.43	1242.9	14.22	1253.1	11.84	1266.9	49.04	74
T14_002 - 55	0.05241	0.00094	0.04372	0.0006	0.31595	0.00606	0.01333	0.00049	303.3	40.16	275.9	3.72	278.8	4.67	267.7	9.74	78
T14_002 - 56	0.0553	0.00107	0.06849	0.00088	0.52235	0.01027	0.02231	0.00088	424.2	42.17	427.1	5.31	426.7	6.85	445.9	17.42	85
T14_002 - 57	0.06758	0.00092	0.12777	0.00164	1.19044	0.01816	0.04533	0.00157	855.6	28.08	775.1	9.4	796.2	8.42	896.1	30.34	73
T14_002 - 58	0.05611	0.00092	0.05721	0.00072	0.44261	0.00761	0.01797	0.00057	456.3	35.83	358.6	4.39	372.1	5.35	360	11.23	85
T14_002 - 59	0.16849	0.0021	0.24166	0.00304	5.61441	0.07917	0.07679	0.00256	2542.7	20.79	1395.3	15.77	1918.3	12.15	1495.4	47.99	90
T14_002 - 60	0.09638	0.00125	0.17558	0.00223	2.33335	0.03404	0.04702	0.00166	1555.2	24.13	1042.8	12.21	1222.5	10.37	928.7	32.1	85
T14_002 - 61	0.0582	0.00128	0.07915	0.00099	0.63535	0.01365	0.02552	0.00112	536.7	48.06	491.1	5.9	499.4	8.47	509.3	22.03	103
T14_002 - 62	0.07004	0.00118	0.15229	0.00197	1.4706	0.02576	0.04783	0.00124	929.4	34.13	913.8	11.04	918.4	10.59	944.4	23.92	103
T14_002 - 63	0.05642	0.00087	0.06937	0.00093	0.5396	0.0092	0.02125	0.00058	468.2	34.09	432.4	5.62	438.2	6.07	425	11.51	103
T14_002 - 64	0.05889	0.00151	0.09029	0.0013	0.73307	0.01876	0.02678	0.00082	563	54.9	557.3	7.69	558.4	10.99	534.2	16.08	109
T14_002 - 65	0.05719	0.00092	0.0802	0.00108	0.63225	0.01111	0.02317	0.00065	498.3	35.16	497.3	6.45	497.5	6.91	462.9	12.78	107
T14_002 - 66	0.05788	0.00074	0.06696	0.00083	0.53435	0.00766	0.01706	0.00041	524.8	28.04	417.8	5.04	434.7	5.07	341.9	8.12	98
T14_002 - 67	0.09699	0.00129	0.27059	0.00336	3.61872	0.05229	0.07872	0.00211	1567.1	24.66	1543.8	17.04	1553.7	11.49	1531.5	39.45	98
T14_002 - 68	0.07741	0.00092	0.19163	0.00237	2.04527	0.02781	0.05546	0.00145	1131.8	23.48	1130.2	12.83	1130.7	9.27	1090.9	27.75	100
T14_002 - 69	0.05606	0.00083	0.07726	0.00098	0.59718	0.00958	0.02153	0.00058	454.4	32.25	479.8	5.88	475.4	6.09	430.5	11.48	107
T14_002 - 70	0.05723	0.00079	0.07585	0.00096	0.59848	0.00908	0.01959	0.00053	499.8	30.05	471.3	5.74	476.3	5.76	392.1	10.52	103
T14_002 - 71	0.16239	0.00197	0.47602	0.00589	10.6579	0.14596	0.12598	0.0037	2480.7	20.28	2509.9	25.71	2493.8	12.71	2398.3	66.4	99
T14_002 - 72	0.07642	0.00104	0.19358	0.00235	2.03972	0.02991	0.05621	0.00195	1106.2	27.07	1140.7	12.71	1128.9	9.99	1105.4	37.33	97
T14_002 - 73	0.0902	0.00117	0.25273	0.00315	3.14312	0.04523	0.05954	0.0019	1429.7	24.54	1452.5	16.2	1443.3	11.08	1169	36.23	105
T14_002 - 74	0.17507	0.00217	0.50657	0.00624	12.22739	0.16955	0.12299	0.00407	2606.7	20.49	2642	26.69	2622	13.02	2344.5	73.17	100
T14_002 - 75	0.07176	0.00102	0.16622	0.00213	1.64442	0.0256	0.0449	0.00145	979.2	28.55	991.2	11.79	987.4	9.83	887.7	27.98	104
T14_002 - 76	0.05411	0.00083	0.04532	0.00062	0.33802	0.00582	0.01212	0.00034	375.5	34.07	285.7	3.85	295.7	4.42	243.4	6.77	103
T14_002 - 77	0.05425	0.00119	0.06115	0.00083	0.4574	0.01017	0.01758	0.00044	381.5	48.3	382.6	5.02	382.4	7.08	352.2	8.75	101
T14_002 - 78	0.05275	0.00098	0.05187	0.00068	0.37725	0.00731	0.01467	0.00035	318.2	41.72	326	4.17	325	5.39	294.3	7.06	102
T14_002 - 79	0.05796	0.00074	0.08271	0.00105	0.66085	0.00957	0.02151	0.00049	527.8	27.93	512.3	6.26	515.1	5.85	430.1	9.6	100
T14_002 - 80	0.05589	0.00099	0.0724	0.00097	0.55781	0.01042	0.01938	0.00053	447.6	38.46	450.6	5.83	450.1	6.79	388	10.59	103

T14_002 - 81	0.07192	0.00146	0.16524	0.00233	1.6385	0.03411	0.04475	0.00196	983.7	40.7	985.8	12.88	985.1	13.13	884.9	37.99	102
T14_002 - 82	0.06527	0.00139	0.07752	0.00115	0.69669	0.01548	0.01972	0.00134	783	44.14	481.3	6.88	536.8	9.27	394.7	26.48	103
T14_002 - 83	0.0769	0.00098	0.19636	0.00242	2.08192	0.02931	0.04523	0.00115	1118.6	25.22	1155.7	13.01	1142.9	9.66	894.1	22.23	108
T14_002 - 84	0.05603	0.00152	0.07346	0.00103	0.5675	0.01529	0.01936	0.00058	453.4	59.23	457	6.18	456.4	9.9	387.5	11.52	99
T14_002 - 85	0.05912	0.00145	0.07899	0.00112	0.64375	0.01575	0.01841	0.0006	571.5	52.33	490.1	6.7	504.6	9.73	368.7	12	107
T14_002 - 86	0.07374	0.00183	0.17682	0.00255	1.7975	0.04394	0.04481	0.00177	1034.4	49.36	1049.6	13.99	1044.5	15.95	886	34.25	97
T14_002 - 87	0.30749	0.00375	0.72348	0.00902	30.67105	0.41998	0.16819	0.0048	3508.4	18.71	3509.1	33.73	3508.6	13.46	3142.1	82.99	99
T14_002 - 88	0.05415	0.00096	0.0585	0.00073	0.43677	0.00795	0.01557	0.00045	377.1	39.46	366.5	4.48	368	5.62	312.2	9	104
T14_002 - 89	0.06303	0.00098	0.09999	0.00129	0.86891	0.0144	0.02195	0.00083	709.1	32.62	614.4	7.58	635	7.83	438.8	16.39	104
T14_002 - 90	0.11114	0.00152	0.33353	0.00409	5.11024	0.07431	0.08283	0.00288	1818.1	24.6	1855.5	19.76	1837.8	12.35	1608.5	53.79	100

Table 1. Sample details with locations and summary on the U/Pb data carried out in this work. A) stratigraphic unit; b) lithology; c) sample; d) Hf analysis; e) number of samples on which has been done Hf analysis; f) Major U-Pb detrital age Peaks (Ma); g) N* of U-Pb analyses; h) N*of > 10% conc. U-Pb analyses; i) Youngest > 10% concentration U-Pb analysis Ma (MDA).

a	b	c	d	e	f	g	h	i
Sap Bon Fm	Qtz ssn	T14_002	Y	32	~400, 1100	90	53	275 ± 4
Pang Asok Fm	Qtz ssn	T13_003 - T13_005	Y - Y	42	~250, 450, 1400, 1700	180	120	251 ± 3
Siam City Cement Quarry	Qtz ssn	T13_016 - T13_065	Y - Y	36	~300, 450, 900, 1200, 1800	165	93	268 ± 4
Clastic 4	volc ssn	T15_PK1	Y	68	~450, 900, 1400, 1650	135	128	224 ± 4
Clastic 5	volc ssn	T15_PK3	Y	55	~450, 1000, 1400	147	136	205 ± 6
Clastic 4	volc ssn	T15_PK4	Y	38	~450, 850, 1100, 1400	120	112	217 ± 4

Table 2. KS Dissimilarity Matrix

	Indochina	C Vietnam	Sukhothai	East Malaysia	Ailaoshan	Sibumasu	Loei	Inthanon	Phuket	Khorat P	T15_PK1	T15_PK3	T15_PK4	T13_003-005	T13_016-065	T14_002	S China	NE Vietnam	Truong Son
Indochina	0	0.438461538	0.336184891	0.230769231	0.758055152	0.807692308	0.19736326	0.713204119	0.807692308	0.395738046	0.707331731	0.641855204	0.709203297	0.597435897	0.687758478	0.674165457	0.635034273	0.610989011	0.554476671
C Vietnam	0.438461538	0	0.550879614	0.6	1	1	0.597733711	0.940944882	1	0.753378378	0.984375	0.963235294	0.982142857	0.983333333	1	1	0.99009901	0.959183673	0.93442623
Sukhothai	0.336184891	0.550879614	0	0.330941704	0.780269058	0.802690583	0.313342395	0.705465909	0.807174888	0.459504908	0.747862948	0.694539699	0.744514734	0.686733931	0.747094845	0.730941704	0.700306354	0.669717214	0.649538092
East Malaysia	0.230769231	0.6	0.330941704	0	0.75	0.75	0.181303116	0.688582677	0.78902439	0.39527027	0.703125	0.626470588	0.705357143	0.591666667	0.667741935	0.643396226	0.631188119	0.607142857	0.485245902
Ailaoshan	0.758055152	1	0.780269058	0.75	0	0.150943396	0.755465284	0.145297876	0.215830649	0.386537481	0.201356132	0.297308546	0.341981132	0.281289308	0.217285453	0.301886792	0.241173174	0.29283789	0.407000722
Sibumasu	0.807692308	1	0.802690583	0.75	0.150943396	0	0.83286119	0.102362205	0.155600723	0.493243243	0.28125	0.397058824	0.357142857	0.408333333	0.33781362	0.341020266	0.376237624	0.308012094	0.423952641
Loei	0.19736326	0.597733711	0.313342395	0.181303116	0.755465284	0.83286119	0	0.738997569	0.841359773	0.386704693	0.63653063	0.51812198	0.646575273	0.554532578	0.667001736	0.591319686	0.590946063	0.583453778	0.430919983
Inthanon	0.713204119	0.940944882	0.705465909	0.688582677	0.145297876	0.102362205	0.738997569	0	0.152871135	0.40777293	0.194512795	0.316755442	0.303922947	0.339304462	0.273981881	0.297652652	0.273875419	0.302346135	0.382384579
Phuket	0.807692308	1	0.807174888	0.78902439	0.215830649	0.155600723	0.841359773	0.152871135	0	0.510135135	0.32183689	0.419117647	0.412238676	0.441666667	0.376344086	0.429590428	0.376237624	0.401443504	0.523723844
Khorat P	0.395738046	0.753378378	0.459504908	0.39527027	0.386537481	0.493243243	0.386704693	0.40777293	0.510135135	0	0.317778716	0.257551669	0.314430502	0.238288288	0.298823017	0.284612443	0.25140487	0.222007722	0.223877566
T15_PK1	0.707331731	0.984375	0.747862948	0.703125	0.201356132	0.28125	0.63653063	0.194512795	0.32183689	0.317778716	0	0.173253676	0.188616071	0.144791667	0.095430108	0.129716981	0.268177599	0.233418367	0.278645833
T15_PK3	0.641855204	0.963235294	0.694539699	0.626470588	0.297308546	0.397058824	0.51812198	0.316755442	0.419117647	0.257551669	0.173253676	0	0.144957983	0.190196078	0.202403542	0.134850166	0.231581246	0.210984394	0.239392478
T15_PK4	0.709203297	0.982142857	0.744514734	0.705357143	0.341981132	0.357142857	0.646575273	0.303922947	0.412238676	0.314430502	0.188616071	0.144957983	0	0.22202381	0.193068356	0.124494609	0.138702263	0.144132653	0.290690867
T13_003-005	0.597435897	0.983333333	0.686733931	0.591666667	0.281289308	0.408333333	0.554532578	0.339304462	0.441666667	0.238288288	0.144791667	0.190196078	0.22202381	0	0.147849462	0.165251572	0.312953795	0.245918367	0.269672131
T13_016-065	0.687758478	1	0.747094845	0.667741935	0.217285453	0.33781362	0.667001736	0.273981881	0.376344086	0.298823017	0.095430108	0.202403542	0.193068356	0.147849462	0	0.113613309	0.217076546	0.217467632	0.280980081
T14_002	0.674165457	1	0.730941704	0.643396226	0.301886792	0.341020266	0.591319686	0.297652652	0.429590428	0.284612443	0.129716981	0.134850166	0.124494609	0.165251572	0.113613309	0	0.164206987	0.192144782	0.223321992
S China	0.635034273	0.99009901	0.700306354	0.631188119	0.241173174	0.376237624	0.590946063	0.273875419	0.376237624	0.25140487	0.268177599	0.231581246	0.138702263	0.312953795	0.217076546	0.164206987	0	0.105071732	0.214521452
NE Vietnam	0.610989011	0.959183673	0.669717214	0.607142857	0.29283789	0.308012094	0.583453778	0.302346135	0.401443504	0.222007722	0.233418367	0.210984394	0.144132653	0.245918367	0.217467632	0.192144782	0.105071732	0	0.204193153
Truong Son	0.554476671	0.93442623	0.649538092	0.485245902	0.407000722	0.423952641	0.430919983	0.382384579	0.523723844	0.223877566	0.278645833	0.239392478	0.290690867	0.269672131	0.280980081	0.223321992	0.214521452	0.204193153	0

Appendix C

Table 1. Locations and petrographic descriptions for analysed samples from the KKFTB igneous and volcanic suite

Sample Number	Rock Name	Coordinates	Field Description	Petrographic Description
T13_015	Basalt	14°37'24.2" - 101°06'22.5"	Massive green to gray flow next to massive volcanic-lapilli tuffaceous body	Abundant volcanic glass (largely altered in chlorite) in a fine groundmass of fine-grained to cryptocrystalline plagiocalse and scattered altered horneblende. Pronounced opacity probably related to formation of magnetite/ilmenite by iron oxidation
T13_075	Basalt	14°37'34.1" - 101°04'40.9"	Massive volcaninc (Sill) layer bounded by carbonates of the Khao Khad Fm. both at top and bottom	Abundant volcanic glass surrounding sericized plagioclase, relict orthopyroxene and rare olivine and poly-cristalline quartz
T13_027	Basalt	14°42'00.8" - 100°53'02.1"	Metric Dyke running through the hinge of a fault bend fold after the main folding event	Groundmass of alkali with abundant volcanic glass. Cryptocrystalline plagioclase and subordinate feldspar, secondary hematite and sericite alteration, rare microcrystals of pyroxene (?)
T13_029	Andesite porphyry	14°42'01.1" - 100°53'02.8"	Green dyke partially folded in some parts by fold bend fold	Sanidine and plagiocalse phenocristals altered in sericite in a fine-grained equigranular quartzofeldspatic groundmass with volcanic glass altered in chlorites
T13_040	Gabbro	14°34'51.6" - 101°06'16.9"	Intruasion within an isolate quarry	Plagioclase, orthpyroxene, olivine and accessory cryptic hornblende. Hornblende partially turned in cummingtonite/epidote indicating a lower degree of regional metamorphism (green shist facies), accessory magnetite and ilmenite
T13_042	Gabbro	14°34'51.6" - 101°06'16.9"	Intruasion within an isolate quarry	Plagioclase, orthpyroxene, olivine and accessory cryptic hornblende. Hornblende partially turned in epidote,actinolite and chlorite indicating a lower degree of regional metamorphism (green shist facies), accessory magnetite
T13_049	Basaltic andesitic	14°37'40.5" - 101°04'26.7"	Folded layer within shale outcrop	Massive orthpyroxene, hornblende accessory augire and ploycristalline quartz in a matrix of cryptic quartzofeldspatic groundmass
T13_060	Basaltic tuff	14°37'38.4" - 101°04'25.0"	Layer of green to gray tuff folded parallel to layers of shale	Abundant plagioclase in a groundmass of alkali and rare cryptocrystalline augite
T13_072	Basaltic andesitic	14°45'55.5" - 100°53'48.1"	Layer of dark tuff folded parallel to thrust	Hornblende and minor orthopyroxene in a fine grained plagioclase groundmass, accessory magnetite and ilmenite
T13_074	Gabbroic basalt	14°37'34.1" - 101°04'40.9"	Massive volcanic body partially metamorphosed, evidence of weathering	plagiocalse and feldspar in an alkali fine grained groundmass, minor relict pyroxene and hematite
T13_076	Basaltic tuff	14°42'42.1" - 100°53'13.1"	Dyke running through the hinge of a fault propagation fold	Mostly fine grained groundmass of plagioclase and scattered cryptocrystalline olivine and pyroxene, presence of amygdales and voids filled by chalcedony roses
T13_055	Andesite	14°42'05.7" - 100°53'07.9"	Dyke running through carbomates of the Khao Khad Fm without being folded	Groundmass and microcrystals alkali in composition with relict felspar phenocrysts and biotite with sericite alteration has more abundant carbonate crystals
T13_081	Andesite	14°43'43.6" - 100°53'49.8"	Volcanic body intruded within a secondary thrust	Groundmass of feldspar and alkali with relict felspar phenocrysts and muscovite with sericite alteration. Hematite that seems to have replaced feldspar
T14_004	Rhyolite	14°32'16.7" - 100°57'03.4"	Massive volcanic body south of Highway 2	Quartz and altered feldspar with euhedral to sub-euhedral plagiocase altered in sericite, scattered clynopiroxene in a cryptocrystalline matrix of polycristalline quartz and alkali, scattered amygdales partially rimmed by plagioclase and filled by quartz

Table 2. XRF and ICP-MS for analysed samples from the KKFTB igneous and volcanic suite, values of trace elements and REE (ppm), of major elements (% wt)

Sample	SiO_2	TiO_2	Al_2O_3	Fe_2O_3	MnO	MgO	CaO	Na_2O	K_2O	P_2O_5	Loss	Sum	S%	Sc	Ba	V	Cr	Co	Ni	Cu	Zn	Ga	As	Rb	Sr	Y	Zr	Nb	Mo	Sn	W	Pb	U	Th	La	Ce	Nd
T-13-1	47.6	0.728	13.6	7.29	0.129	10.3	12.8	2.20	0.91	0.238	3.62	99.44	0.03	21.3	267	181	616	60.7	325	45.6	78.9	14.2	<3	23.0	725	16.7	98.7	2.8	<0.5	<1	62.4	7.7	<2	4.5	17.6	36.1	14.5
T-13-2	62.2	0.376	17.0	4.21	0.076	2.68	2.29	6.53	0.57	0.168	3.61	99.72	0.06	11.2	268	90.4	26.6	40.0	9.0	19.1	47.9	16.8	<3	10.2	1024	12.7	110	1.2	<0.5	<1	84.2	<1	<2	<2	8.3	24.1	6.1
T-13-7	49.3	0.482	15.0	5.63	0.071	6.22	8.27	5.52	0.43	0.129	4.72	95.74	0.04	30.6	166	237	744	53.0	228	64.1	68.3	16.7	<3	20.0	442	17.4	68.4	1.0	<0.5	<1	43.1	64.9	<2	<2	9.3	15.9	<4
T-13-9	41.8	0.869	15.8	11.6	0.184	12.2	11.1	0.89	0.73	0.228	4.72	100.20	<0.01	35.8	175	324	1168	78.1	404	79.5	81.6	14.3	<3	6.1	502	13.6	61.1	1.1	0.7	<1	20.5	<1	<2	<2	7.7	16.7	5.2
T-13-13	40.9	0.782	13.8	10.2	0.129	10.8	9.04	2.75	0.58	0.252	1.23	90.52	<0.01	36.1	104	182	880	64.8	310	17.3	61.8	13.4	5.5	5.4	201	13.0	52.7	1.2	0.8	<1	10.7	2.9	<2	<2	7.1	14.5	<4
T-13-15	47.5	1.455	16.0	11.3	0.149	6.73	8.88	3.15	0.93	0.393	3.67	100.20	<0.01	32.8	134	295	201	48.9	91.2	30.3	95.0	16.0	<3	7.8	452	23.3	131	4.4	<0.5	<1	47.8	1.6	<2	<2	9.2	24.4	8.9
T-13-17	47.3	0.717	18.1	10.2	0.206	3.69	7.80	4.76	0.14	0.504	6.74	100.12	0.34	17.6	38.7	262	2.5	26.9	<1	23.6	104	18.3	<3	2.8	1114	18.0	67.1	1.4	<0.5	1.8	8.1	4.3	<2	2.4	8.1	19.8	10.8
T-13-20	48.4	0.767	16.7	9.95	0.129	7.90	2.97	3.20	3.57	0.140	6.17	99.94	<0.01	39.6	369	358	324	30.4	75.9	34.1	56.8	14.2	<3	26.8	122	9.7	54.1	1.0	0.9	<1	24.6	<1	<2	<2	7.4	13.8	4.7
T-13-21	45.0	0.963	15.5	8.71	0.094	4.86	10.6	2.81	0.47	0.185	1.20	90.36	0.08	32.8	202	223	244	51.7	65.4	60.8	81.1	16.0	7.0	10.2	1013	16.6	85.7	4.7	<0.5	<1	41.6	2.3	<2	<2	7.1	19.5	7.1
T-13-25	38.9	0.961	14.6	8.72	0.121	4.98	13.9	0.10	0.67	0.207	4.03	87.23	0.31	32.7	94.1	216	369	29.9	95.0	51.6	93.7	15.5	13.0	17.7	479	18.0	93.9	8.1	3.7	1.6	<2	<1	<2	<2	12.0	23.3	7.4
T-13-27	46.3	0.799	15.9	8.68	0.137	3.36	8.51	2.92	1.32	0.446	3.53	91.91	3.12	17.5	247	237	34.3	21.3	16.1	119	127	20.0	<3	30.5	1571	20.5	129	4.1	<0.5	2.2	32.5	<1	<2	<2	20.3	39.3	17.4
T-13-30	49.4	0.905	17.6	9.76	0.194	3.60	8.64	3.20	0.12	0.414	5.79	99.71	0.26	17.9	47.3	246	4.4	35.8	<1	31.5	103	20.1	<3	3.0	735	17.0	86.5	3.3	<0.5	1.7	44.0	4.4	<2	<2	10.0	25.7	10.9
T-13-35	52.4	0.506	15.7	6.02	0.062	6.70	5.23	3.45	0.27	0.110	3.49	93.87	<0.01	22.9	62.8	171	224	46.2	128	36.8	60.5	16.8	<3	5.1	290	13.1	65.6	1.3	0.6	<1	20.4	<1	<2	<2	5.2	8.7	<4
T-13-40	42.5	1.356	15.3	14.2	0.202	8.60	14.3	1.46	0.54	0.166	1.54	100.20	0.19	56.1	118	585	207	58.4	62.6	106	93.9	18.4	<3	5.9	646	18.9	37.5	2.0	0.5	<1	57.3	<1	<2	<2	<4	7.2	<4
T-13-42	41.6	1.365	19.2	14.0	0.224	6.65	14.7	1.41	0.28	0.508	0.51	100.41	0.10	36.5	64.9	456	31.4	57.1	14.5	44.9	104	22.9	<3	1.4	879	20.5	35.6	1.7	<0.5	1.4	72.9	<1	<2	<2	6.4	12.0	<4
T-13-43	45.8	0.387	14.0	6.02	0.165	5.20	24.7	0.12	0.01	0.765	3.31	100.49	0.14	31.2	5.4	393	55.5	38.1	25.6	29.4	55.7	13.2	<3	<0.5	128	18.8	22.1	2.5	1.3	<1	65.7	<1	<2	2.9	11.0	21.7	7.6
T-13-44	51.7	0.554	17.7	7.74	0.162	2.74	8.88	5.08	0.04	0.636	5.17	100.36	0.44	10.1	35.7	122	3.0	19.3	<1	28.8	79.1	15.9	<3	<0.5	1352	21.0	84.0	1.7	0.5	<1	40.1	5.0	<2	<2	12.4	31.8	14.5
T-13-49	45.4	0.967	14.3	11.9	0.235	9.11	12.1	1.76	0.98	0.319	3.01	100.08	0.14	56.4	212	414	163	45.7	60.4	52.6	83.9	15.2	<3	17.9	698	15.4	48.7	1.5	<0.5	1.3	40.2	<1	<2	<2	4.2	16.4	7.1
T-13-51	40.9	0.818	13.3	10.3	0.163	10.0	10.3	0.02	0.21	0.274	1.08	87.45	0.32	42.5	40.6	348	593	46.1	195	61.6	74.0	15.3	<3	10.0	194	14.0	53.9	4.8	0.8	3.2	<2	<1	<2	<2	6.3	17.4	5.1
T-13-54	48.5	0.665	16.0	6.44	0.105	6.75	5.96	0.01	0.72	0.158	1.57	86.88	<0.01	17.2	57.9	172	126	39.8	66.2	26.9	105	18.7	<3	17.7	120	15.3	87.5	2.4	0.5	1.2	19.0	<1	<2	<2	4.3	14.8	<4
T-13-55	59.1	0.366	15.7	3.88	0.075	2.15	5.04	1.74	1.31	0.128	1.10	90.53	0.01	10.2	464	71.2	16.5	19.1	12.5	7.8	48.7	17.0	<3	33.5	333	12.8	90.1	2.0	0.5	<1	33.9	1.8	<2	<2	7.6	18.7	4.5
T-13-57	47.5	0.762	19.3	11.0	0.137	3.82	4.60	5.13	0.44	0.509	6.21	99.40	1.03	18.3	66.0	292	1.7	33.5	<1	16.8	98.1	19.9	<3	9.7	771	15.8	64.6	1.9	<0.5	<1	23.4	3.6	<2	<2	10.4	22.6	9.2
T-13-60	47.4	0.674	17.6	9.80	0.211	3.55	7.34	4.97	0.24	0.490	5.50	97.76	0.61	16.3	38.3	246	1.5	9.7	<1	22.2	96.2	16.4	4.5	4.3	2093	16.9	82.3	0.7	<0.5	1.0	26.7	<1	<2	<2	9.8	21.9	7.4
T-13-62	46.4	1.294	15.9	9.67	0.147	7.95	7.80	3.12	0.26	0.306	6.73	99.52	0.09	22.0	111	235	414	47.4	171	21.5	86.5	18.2	<3	2.3	938	13.6	86.7	4.9	<0.5	<1	21.0	<1	<2	<2	10.4	23.8	6.5
T-13-66	47.5	1.187	17.9	9.57	0.179	3.59	6.24	4.26	1.76	0.322	6.64	99.16	0.94	24.1	324	326	2.9	17.8	12.2	15.8	92.9	17.4	<3	32.7	1318	22.3	89.1	2.7	1.2	<1	27.5	3.2	<2	<2	12.9	25.6	11.3
T-13-68	41.9	0.905	16.9	8.67	0.187	3.15	11.4	2.65	1.70	0.340	1.21	89.03	0.31	19.3	357	240	3.7	29.0	<1	18.3	71.5	15.5	<3	41.3	502	20.5	86.9	3.9	<0.5	1.7	17.1	1.1	<2	<2	14.2	31.3	13.6
T-13-70	44.5	0.782	14.2	6.18	0.075	7.83	12.9	1.65	0.26	0.260	1.91	90.52	0.38	24.2	179	237	670	45.4	266	53.9	109	15.7	96.7	5.3	518	17.7	104	3.2	<0.5	<1	13.5	6.8	<2	4.5	20.7	41.6	17.9
T-13-71	44.3	0.976	16.9	9.57	0.130	3.64	7.20	1.57	1.75	0.450	1.96	88.46	4.21	24.7	339	310	50.6	36.8	25.8	183	200	22.6	3.5	41.3	876	21.3	120	4.9	1.2	1.6	24.4	2.4	<2	3.2	14.8	39.8	17.7
T-13-72	44.3	1.301	15.0	12.1	0.191	7.93	10.1	2.47	0.63	0.288	5.24	99.53	0.34	44.2	254	452	166	50.9	65.8	78.1	85.8	17.8	<3	8.2	1059	18.7	85.2	2.8	<0.5	<1	19.6	1.4	<2	<2	10.1	22.9	7.7
T-13-74	44.5	0.745	12.7	10.2	0.169	14.1	9.97	1.37	1.09	0.231	4.57	99.68	<0.01	31.2	169	302	1303	60.7	438	143	68.1	13.1	<3	18.8	272	14.9	72.4	1.5	1.1	<1	19.4	1.4	<2	<2	12.4	26.5	13.3
T-13-75	31.2	0.551	9.8	7.54	0.164	8.13	20.5	1.90	1.405	0.210	1.94	83.42	0.01	28.5	172	283	1114	73.2	184	28.7	57.2	9.6	<3	13.7	190	11.6	57.0	1.2	0.9	3.1	12.4	<1	<2	<2	7.9	22.1	5.9
T-13-76	45.3	0.577	13.3	6.60	0.088	7.49	10.6	1.77	0.48	0.274	2.87	89.39	0.32	21.6	216	189	504	49.1	288	43.1	74.9	14.2	<3	8.4	1220	10.6	99.2	1.7	<0.5	<1	12.5	6.1	<2	<2	23.8	45.3	16.5
T-13-79	47.9	0.884	17.0	7.90	0.064	5.77	9.50	2.49	0.08	0.115	4.89	96.59	0.26	30.6	56.8	191	164	43.3	26.6	56.2	63.0	16.2	<3	<0.5	1043	15.5	82.2	2.0	<0.5	1.1	35.7	<1	<2	<2	4.3	11.8	<4
T-13-81	60.2	0.355	16.2	3.82	0.060	2.29	3.79	3.09	1.13	0.157	2.39	93.46	0.22	12.5	72.7	86.4	63.8	24.6	13.5	14.2	112	17.0	3.7	19.4	273	12.0	98.3	1.9	0.5	<1	53.4	3.2	<2	<2	8.7	15.2	<4

10046

Sample	Ba	Be	Co	Cs	Ga	Hf	Nb	Rb	Sn	Sr	Ta	Th	U	V	Cr	W	Zr	Y	La	Ce	Pr	Nd	Sm	Eu	Gd	Tb	Dy	Ho	Er	Tm	Yb	Lu	Mo	Cu	Pb	Zn	Ni	As	Cd	Sb	Bi	Ag	Au	Hg	Ti	Se
T-13-1	271	<1	37.2	1.9	13.5	2.5	2.6	21.6	<1	742.5	0.1	4.5	0.9	157	616	49.4	84.3	16.4	19.1	37.7	5.03	19.7	4.05	1.12	3.80	0.50	2.88	0.52	1.56	0.23	1.38	0.22	0.8	46.1	5.3	43	202.3	2.2	<0.1	<0.1	<0.1	<0.1	3.2	<0.01	11.13	<0.5
T-13-2	290	3	19.4	0.6	14.4	2.7	1.7	10.2	<1	1028.5	0.2	2.0	0.6	77	26.6	85.7	94.3	12.6	9.9	20.4	2.86	11.5	2.49	0.77	2.49	0.34	2.10	0.46	1.25	0.19	1.30	0.21	0.7	21.4	0.8	44	13.6	<0.5	<0.1	<0.1	<0.1	<0.1	<0.5	<0.01	4.96	<0.5
T-13-7	181	<1	33.1	0.9	14.3	1.7	1.1	17.8	<1	435.7	0.1	1.9	0.5	172	744	32.6	58.1	15.8	9.3	17.9	2.44	10.9	2.67	0.87	2.93	0.40	2.41	0.49	1.51	0.21	1.33	0.22	0.2	62.0	2.1	53	198.2	<0.5	0.1	<0.1	<0.1	<0.1	1.9	0.02	6.89	<0.5
T-13-9	143	<1	51.4	1.5	10.8	1.6	0.9	6.5	<1	528.8	<0.1	1.1	0.3	280	1168	14.1	52.2	14.2	9.2	21.0	2.96	13.7	3.00	1.03	3.27	0.41	2.65	0.48	1.38	0.20	1.19	0.19	0.1	66.1	0.3	46	319.4	<0.5	<0.1	<0.1	<0.1	<0.1	0.6	<0.01	13.36	<0.5
T-13-13	100	<1	43.7	1.7	10.7	1.3	0.7	5.1	<1	201.5	<0.1	0.9	0.3	150	880	6.8	46.2	11.9	8.1	17.7	2.53	12.3	2.83	0.89	2.69	0.35	2.30	0.43	1.19	0.18	1.06	0.16	<0.1	7.8	0.8	26	257.3	1.0	<0.1	<0.1	<0.1	<0.1	3.0	<0.01	12.32	<0.5
T-13-15	112	4	42.3	0.6	14.9	3.0	3.7	7.0	1	468.1	0.3	0.8	0.2	258	201	50.7	122.7	22.9	11.3	25.3	3.75	17.3	4.08	1.45	4.74	0.69	4.42	0.77	2.43	0.35	2.30	0.32	0.2	25.2	0.5	71	64.2	<0.5	<0.1	<0.1	<0.1	<0.1	1.7	<0.01	18.78	<0.5
T-13-17	34	<1	26.0	0.7	17.6	1.3	1.5	2.9	<1	1137.9	<0.1	1.5	0.7	213	2.5	22.1	48.6	16.9	10.9	23.7	3.50	16.5	3.97	1.42	3.99	0.53	3.38	0.63	1.87	0.28	1.85	0.25	0.5	24.3	2.6	91	0.4	1.7	0.1	<0.1	<0.1	<0.1	<0.5	<0.01	10.76	<0.5
T-13-20	393	<1	35.0	1.7	12.0	1.5	0.7	26.0	<1	128.4	<0.1	1.9	0.5	296	324	23.2	50.9	9.4	8.0	16.7	2.57	11.5	2.75	0.77	2.56	0.35	2.17	0.39	1.15	0.15	0.96	0.15	<0.1	26.5	1.0	41	53.3	<0.5	<0.1	<0.1	<0.1	<0.1	2.7	<0.01	10.37	<0.5
T-13-21	193	<1	35.5	6.1	13.5	1.7	4.2	10.3	<1	1031.5	0.3	0.9	0.4	180	244	39.8	68.1	16.6	7.9	16.7	2.59	12.1	3.04	0.99	3.34	0.48	3.12	0.62	1.74	0.26	1.63	0.25	0.4	52.4	1.0	62	53.7	3.9	<0.1	0.4	<0.1	<0.1	<0.5	<0.01	13.12	<0.5
T-13-25	84	<1	27.6	6.4	12.4	2.1	6.4	16.5	<1	490.9	0.4	1.0	0.5	170	369	7.8	82.1	15.8	9.9	21.4	3.09	14.0	3.32	1.08	3.62	0.50	3.21	0.62	1.78	0.25	1.59	0.25	2.9	46.2	1.3	63	79.7	13.1	<0.1	0.4	<0.1	<0.1	0.5	<0.01	13.32	<0.5
T-13-27	245	<1	24.2	2.8	15.3	2.7	4.3	26.5	<1	1508.4	0.3	2.5	0.8	180	34.3	27.9	100.1	18.4	18.5	37.7	4.96	22.0	4.49	1.30	4.42	0.57	3.51	0.69	1.85	0.29	1.83	0.28	0.7	104.9	3.4	103	15.9	3.8	0.3	0.1	0.2	<0.1	3.8	<0.01	10.26	1.7
T-13-30	41	3	27.7	0.7	18.0	2.2	2.5	2.6	<1	771.7	0.2	1.4	0.7	214	4.4	47.5	74.4	17.5	12.0	26.7	3.95	17.9	4.32	1.36	4.19	0.54	3.40	0.62	1.66	0.27	1.57	0.25	<0.1	30.2	2.1	89	1.5	1.8	0.2	0.2	<0.1	<0.1	1.3	<0.01	13.69	<0.5
T-13-35	60	<1	24.1	2.9	12.8	1.8	0.7	4.5	<1	285.2	0.1	0.3	<0.1	128	224	10.6	57.8	11.0	4.6	9.7	1.40	6.7	1.96	0.66	2.30	0.33	2.17	0.43	1.29	0.18	1.35	0.18	0.2	36.5	0.3	45	98.9	0.5	<0.1	<0.1	<0.1	<0.1	<0.5	<0.01	6.54	<0.5
T-13-40	106	<1	52.7	0.6	16.2	0.9	1.6	6.0	<1	666.6	<0.1	<0.2	<0.1	496	207	57.8	26.9	18.3	5.0	11.3	2.08	11.5	3.33	1.12	4.10	0.61	3.73	0.69	1.99	0.23	1.55	0.22	<0.1	100.3	0.7	33	33.0	<0.5	<0.1	<0.1	<0.1	<0.1	<0.5	<0.01	18.97	<0.5
T-13-42	61	<1	40.9	0.1	19.3	1.0	1.6	1.9	<1	897.7	<0.1	<0.2	<0.1	403	31.4	61.4	22.7	19.9	5.5	13.4	2.38	13.1	3.74	1.32	4.28	0.62	3.94	0.72	2.02	0.28	1.55	0.24	<0.1	39.2	0.8	31	7.9	<0.5	<0.1	<0.1	<0.1	<0.1	0.5	<0.01	17.34	<0.5
T-13-43	4	<1	21.6	<0.1	11.9	1.0	1.4	<0.1	<1	136.9	0.1	1.5	0.5	310	55.5	73.4	25.8	18.6	12.7	24.2	3.87	17.4	4.45	1.12	4.46	0.60	3.68	0.65	1.75	0.23	1.38	0.20	0.2	23.5	0.4	11	14.5	<0.5	<0.1	<0.1	<0.1	<0.1	<0.5	<0.01	5.73	<0.5
T-13-44	36	<1	19.7	0.1	13.4	1.8	1.9	0.5	<1	1375.8	0.1	2.1	0.8	107	3.0	37.0	61.2	20.0	15.4	32.0	4.64	20.4	4.52	1.64	4.85	0.64	4.15	0.75	2.18	0.32	1.99	0.32	1.1	29.9	3.3	72	0.2	<0.5	<0.1	<0.1	0.2	<0.1	<0.5	<0.01	7.47	<0.5
T-13-49	240	<1	42.5	0.3	13.6	1.3	1.2	17.8	<1	749.6	<0.1	0.9	0.4	350	163	31.9	38.2	15.3	8.1	17.3	2.53	12.4	3.29	1.07	3.55	0.48	3.06	0.56	1.49	0.21	1.34	0.22	0.2	57.4	1.1	50	32.5	1.5	<0.1	<0.1	<0.1	<0.1	<0.5	<0.01	12.47	<0.5
T-13-51	30	<1	43.0	2.0	12.8	1.3	3.1	8.5	<1	195.4	0.2	0.9	0.3	255	593	5.9	47.3	12.3	9.6	17.8	2.44	11.0	2.42	0.89	2.71	0.41	2.66	0.47	1.33	0.21	1.20	0.19	0.1	59.7	0.6	58	182.3	1.1	<0.1	<0.1	<0.1	<0.1	1.4	<0.01	12.25	<0.5
T-13-54	59	<1	21.6	6.5	15.3	2.4	1.6	15.7	<1	116.7	0.1	0.8	0.2	126	126	18.0	79.6	13.6	5.9	13.8	2.02	9.5	2.16	0.68	2.68	0.37	2.43	0.44	1.36	0.20	1.41	0.21	0.1	22.5	0.6	67	42.6	<0.5	<0.1	<0.1	<0.1	<0.1	<0.5	<0.01	9.91	<0.5
T-13-55	448	<1	14.1	11.8	14.9	2.4	1.6	30.0	<1	331.0	0.1	1.4	0.4	51	16.5	37.7	82.2	12.4	7.1	16.2	2.11	9.5	2.05	0.67	2.32	0.32	2.13	0.39	1.18	0.19	1.33	0.21	<0.1	4.5	0.9	34	8.6	0.6	<0.1	0.2	<0.1	<0.1	<0.5	<0.01	5.47	<0.5
T-13-57	61	2	27.9	1.4	16.8	1.6	1.5	9.3	<1	787.0	<0.1	1.5	0.7	224	1.7	30.3	51.6	16.1	11.1	23.8	3.61	17.2	3.84	1.03	3.92	0.49	2.95	0.62	1.54	0.24	1.60	0.26	0.9	17.1	4.8	84	2.4	2.4	<0.1	<0.1	<0.1	<0.1	1.3	<0.01	10.06	<0.5
T-13-60	37	4	24.4	0.8	14.6	1.4	1.2	4.7	<1	2124.9	<0.1	1.6	0.6	197	1.5	26.5	48.7	17.4	10.6	23.6	3.56	16.4	3.95	1.29	3.90	0.54	3.32	0.64	1.73	0.26	1.70	0.24	0.5	18.2	2.2	82	0.7	1.8	<0.1	<0.1	<0.1	<0.1	0.9	<0.01	9.50	<0.5
T-13-62	109	<1	39.8	1.2	15.9	2.2	4.5	3.1	<1	958.4	0.3	0.8	0.2	200	414	20.4	72.5	13.7	11.0	23.3	3.23	14.5	3.39	1.27	3.83	0.48	2.65	0.52	1.35	0.18	1.16	0.16	0.4	22.0	0.5	57	158.5	0.7	<0.1	<0.1	<0.1	<0.1	1.6	<0.01	17.42	<0.5
T-13-66	338	4	26.2	2.9	15.2	1.8	2.5	30.3	<1	1321.2	0.2	1.4	2.1	259	2.9	16.5	68.2	22.6	11.9	23.7	3.45	15.5	4.03	1.31	4.46	0.67	4.26	0.80	2.23	0.34	2.18	0.32	0.8	14.6	4.6	77	8.8	1.4	0.2	<0.1	<0.1	<0.1	<0.5	<0.01	16.82	1.3
T-13-68	356	2	21.8	3.1	12.8	2.0	3.1	38.0	<1	516.1	0.2	1.6	0.7	180	3.7	18.4	77.0	19.0	13.1	28.4	3.89	17.3	4.12	1.33	4.49	0.58	3.61	0.71	2.08	0.28	1.78	0.29	0.2	16.0	0.8	56	2.4	0.9	<0.1	<0.1	<0.1	<0.1	<0.5	<0.01	12.41	<0.5
T-13-70	172	<1	36.1	4.6	13.4	2.6	2.2	5.1	<1	523.4	0.2	5.0	0.9	183	670	13.8	91.3	17.1	21.1	42.2	5.41	22.1	4.56	1.29	4.32	0.53	3.23	0.57	1.67	0.24	1.49	0.23	0.4	50.0	4.2	81	261.9	107.8	0.1	1.6	<0.1	<0.1	1.0	0.10	11.25	<0.5
T-13-71	298	<1	27.2	3.1	17.5	2.8	4.1	35.2	<1	855.5	0.2	2.3	0.7	237	50.6	22.7	97.3	20.2	17.9	35.4	4.83	21.2	4.30	1.14	4.63	0.60	3.87	0.74	2.05	0.30	1.96	0.30	0.9	157.9	4.8	158	24.9	5.3	0.3	0.1	0.4	<0.1	<0.5	<0.01	12.93	1.5
T-13-72	300	<1	41.9	1.6	15.8	2.0	2.7	8.7	1	1106.1	0.2	1.6	0.4	347	166	17.0	69.1	18.2	12.8	26.2	3.64	16.7	4.37	1.36	4.45	0.59	3.41	0.68	1.81	0.25	1.51	0.25	0.4	77.8	1.9	65	29.9	1.0	0.1	<0.1	<0.1	<0.1	0.8	<0.01	17.05	<0.5
T-13-74	156	<1	53.1	1.1	12.0	2.0	1.1	18.0	<1	281.4	<0.1	1.1	0.4	255	1303	21.5	65.5	14.3	13.6	29.5	4.30	19.9	4.61	1.28	4.41	0.51	3.09	0.52	1.34	0.20	1.20	0.17	<0.1	130.0	0.4	37	319.8	<0.5	<0.1	<0.1	<0.1	<0.1	1.9	<0.01	10.54	<0.5
T-13-75	185	<1	44.7	1.0	6.8	1.4	0.5	12.3	<1	190.5	<0.1	0.7	0.6	228	1114	12.6	48.3	10.1	10.3	21.7	3.13	14.5	3.14	0.97	3.06	0.36	2.06	0.36	1.00	0.14	0.87	0.13	0.1	16.2	0.8	29	149.8	1.7	0.1	<0.1	<0.1	<0.1	1.2	<0.01	7.73	<0.5
T-13-76	200	<1	33.4	3.0	12.8	1.9	2.5	7.3	<1	1163.4	0.1	3.1	0.7	139	504	18.0	71.7	10.2	24.0	45.9	5.62	21.7	3.62	1.08	2.90	0.35	2.09	0.36	1.10	0.16	0.98	0.16	0.4	40.5	4.0	57	290.7	0.8	<0.1	<0.1	<0.1	<0.1	2.2	<0.01	9.03	<0.5
T-13-79	54	<1	33.1	1.2	14.8	1.7	1.8	0.7	<1	1019.3	0.1	0.5	0.2	149	164	21.7	60.5	15.6	4.1	10.4	1.52	7.0	2.04	0.82	2.66	0.43	2.91	0.59	1.67	0.25	1.67	0.24	0.3	51.9	0.9	58	27.8	<0.5	0.2	<0.1	<0.1	<0.1	<0.5	<0.01	12.63	<0.5
T-13-81	78	<1	17.6	4.0	13.8	2.5	1.7	17.5	<1	261.8	0.2	1.6	0.6	66	63.8	59.2	84.1	11.5	7.8	17.9	2.39	10.1	1.99	0.66	2.19	0.34	2.12	0.42	1.14	0.18	1.19	0.20	0.6	15.0	1.9	89	9.5	1.0	0.3	<0.1	0.5	<0.1	<0.5	<0.01	5.12	<0.5
T-14-04	593	<1	32.6	9.7	9.2	2.8	4.9	167.1	<1	46.5	0.4	21.2	3.3	<8		219.7	86.3	14.8	16.0	39.9	2.60	9.8	1.82	0.32	2.02	0.35	2.46	0.49	1.74	0.26	2.06	0.32	<0.1	1.1	4.3	7	0.3	4.1	<0.1	0.2	<0.1	<0.1	<0.5	0.04		<0.5
T-14-31	78	<1	23.8	<0.1	3.7	<0.1	0.4	0.6	<1	92.9	<0.1	<0.2	0.6	38		84.3	3.0	7.4	6.2	8.4	1.20	5.4	0.79	0.37	0.84	0.10	0.62	0.13	0.41	0.04	0.26	0.05	1.8	1264.1	9.2	92	6.8	53.2	2.2	1.4	<0.1	0.7	2.4	0.03		0.5
T-14-07	123	4	5.7	3.3	9.8	7.7	5.3	22.6	<1	388.1	0.4	3.6	1.7	84		14.4	298.8	52.0	22.2	38.6	6.34	28.7	6.41	1.40	7.17	1.17	7.64	1.64	4.85	0.67	4.64	0.70	3.0	12.0	6.5	79	21.8	22.4	0.9	1.3	0.1	<0.1	<0.5	0.05		0.5
T-14-10	369	<1	14.3	0.9	16.2	2.9	6.8	28.8	<1	1444.2	0.6	3.2	1.7	62		66.2	124.5	13.5	21.1	41.6	4.98	19.1	3.47	1.05	3.07	0.41	2.23	0.43	1.29	0.21	1.27	0.20	1.8	13.5	7.1	59	6.4	0.6	<0.1	<0.1	0.1	<0.1	<0.5	<0.01		<0.5
T-14-05	136	<1	24.1	2.5	7.8	1.8	4.2	61.1	<1	21.2	0.4	5.1	1.7	80		34.8	62.6	15.1	17.4	19.5	3.56	13.7	2.50	0.56	2.41	0.38	2.43	0.55	1.39	0.22	1.45	0.22	0.5	26.2	6.0	36	13.1	13.2	<0.1	0.4	0.2	<0.1	0.5	<0.01		<0.5

10047

Table 3. Results from the Sm-Nd isotope analyses

Rock type		Rb	Sr	Sm	Nd	measured	measured	measured	measured		εNd(0)	εNd(T)		T_{DM}
		[ppm]	[ppm]	[ppm]	[ppm]	$^{143}/^{144}Nd$	$^{150}/^{144}Nd$	$^{147}/^{149}Sm$	$^{152}/^{149}Sm$					(Ma)
basalts	-	5.1	523.4	4.56	22.1	.512747	.492876	5.43335	1.88552	-	**1.03**	3.22	-	758
microgabbro	-	3.1	958.4	3.39	14.5	.512789	.496912	4.77357	1.85985	-	**1.83**	3.41	-	974
andesite	-	26.5	1508.4	4.49	22.0	.512837	.472676	4.81292	1.87726	-	**2.87**	5.16	-	679

Supplementary data 1. Results from the U-Pb analysis

Analysis	$^{207}Pb/^{206}Pb$	±2σ	$^{206}Pb/^{238}U$	±2σ	$^{207}Pb/^{235}U$	±2σ	$^{208}Pb/^{232}Th$	±2σ	$^{207}Pb/^{206}Pb$	±2σ	$^{206}Pb/^{238}U$	±2σ	$^{207}Pb/^{235}U$	±2σ	$^{208}Pb/^{232}Th$	±2σ	Concordancy
004_01	0.07184	0.00118	0.03336	0.00046	0.33042	0.00587	0.01095	0.00022	981.3	33.17	211.6	2.85	289.9	4.48	220.1	4.4	76
004_02	0.09707	0.00113	0.03463	0.00046	0.46342	0.00654	0.01113	0.00022	1568.6	21.65	219.5	2.85	386.6	4.53	223.8	4.45	58
004_03	0.05002	0.00175	0.03215	0.00055	0.22169	0.00773	0.00949	0.00038	195.9	79.3	204	3.45	203.3	6.42	191	7.67	94
004_04	0.05025	0.00088	0.03135	0.00041	0.21723	0.00399	0.01015	0.00026	206.8	39.99	199	2.56	199.6	3.33	204	5.17	102
004_05	0.05211	0.00069	0.03258	0.00043	0.23403	0.00356	0.01073	0.00024	290.4	29.82	206.6	2.67	213.5	2.93	215.6	4.89	101
004_06	0.05028	0.00076	0.03268	0.00044	0.22653	0.00384	0.01008	0.00025	207.8	34.8	207.3	2.76	207.3	3.18	202.8	4.9	98
004_07	0.05007	0.00186	0.03232	0.00057	0.22307	0.00822	0.00855	0.00039	198	84.02	205	3.59	204.5	6.82	172.1	7.81	84
004_08	0.04992	0.00111	0.03294	0.00044	0.22672	0.00506	0.01057	0.00043	191.4	50.96	209	2.72	207.5	4.19	212.5	8.53	102
004_09	0.05226	0.00255	0.03828	0.00077	0.2758	0.01311	0.012	0.00085	297	107.7	242.1	4.79	247.3	10.43	241.1	16.89	97
004_10	0.05127	0.00084	0.03284	0.00046	0.2321	0.00423	0.00953	0.00028	252.9	37.34	208.3	2.87	211.9	3.48	191.6	5.55	90
004_11	0.05075	0.00084	0.03369	0.00048	0.2357	0.00436	0.00871	0.00028	229.3	37.94	213.6	3	214.9	3.59	175.3	5.54	82
004_12	0.05061	0.00095	0.03281	0.00046	0.22889	0.00457	0.00924	0.00028	223	42.65	208.1	2.88	209.3	3.78	185.8	5.65	89
004_13	0.0514	0.00229	0.03313	0.00063	0.2347	0.01026	0.00939	0.00081	258.7	99.33	210.1	3.95	214.1	8.44	188.9	16.26	88
004_14	0.08256	0.00193	0.03332	0.00052	0.37922	0.00915	0.0105	0.00059	1258.9	44.87	211.3	3.26	326.5	6.74	211.1	11.72	65
004_15	0.05055	0.0015	0.03364	0.00054	0.23442	0.00699	0.01067	0.00079	220.4	67.04	213.3	3.4	213.8	5.75	214.4	15.87	100
004_16	0.05016	0.00331	0.03358	0.00081	0.23195	0.01482	0.01053	0.00115	202.4	146.49	212.9	5.05	211.8	12.21	211.7	22.92	100
004_17	0.05021	0.00103	0.03354	0.00051	0.23211	0.00515	0.00911	0.00037	204.7	47.05	212.7	3.19	211.9	4.24	183.2	7.37	86
004_18	0.05078	0.00105	0.03396	0.00048	0.23771	0.00515	0.01047	0.00029	230.7	46.86	215.3	3.02	216.5	4.22	210.6	5.86	97
004_19	0.05036	0.00244	0.03228	0.00065	0.22387	0.01064	0.00976	0.00076	211.5	108.58	204.8	4.05	205.1	8.83	196.4	15.19	96
004_20	0.06982	0.00105	0.03338	0.00047	0.32129	0.00554	0.00786	0.00024	922.9	30.67	211.7	2.94	282.9	4.25	158.3	4.85	56
004_21	0.05037	0.0011	0.03349	0.00051	0.23255	0.00541	0.00986	0.00039	212.2	49.96	212.4	3.17	212.3	4.45	198.4	7.89	93
004_22	0.05114	0.00117	0.03257	0.00049	0.22964	0.00548	0.01059	0.00039	247	51.76	206.6	3.05	209.9	4.53	212.9	7.76	101
004_23	0.0557	0.00121	0.03432	0.00051	0.26356	0.00601	0.01082	0.00039	440.1	47.22	217.5	3.18	237.5	4.83	217.5	7.8	92
004_24	0.21322	0.00513	0.03748	0.00063	1.1016	0.02542	0.00529	0.00028	2930.2	38.38	237.2	3.94	754.1	12.28	106.6	5.65	14
004_25	0.0505	0.00155	0.03264	0.00053	0.2273	0.00702	0.01047	0.00061	217.9	69.75	207.1	3.3	208	5.81	210.5	12.11	101
004_26	0.11427	0.00376	0.0339	0.00065	0.53397	0.01734	0.01041	0.00087	1868.3	58.23	214.9	4.05	434.4	11.48	209.3	17.33	48
004_27	0.051	0.00158	0.03699	0.0006	0.26006	0.00807	0.01118	0.0006	240.8	69.96	234.1	3.7	234.7	6.51	224.7	11.91	96
004_28	0.05071	0.00108	0.03608	0.00051	0.25227	0.00559	0.01098	0.00049	227.7	48.61	228.5	3.17	228.4	4.53	220.8	9.79	97
004_29	0.05048	0.00088	0.03576	0.0005	0.24887	0.00473	0.01084	0.00042	217	39.88	226.5	3.11	225.7	3.85	217.9	8.38	97
004_30	0.05175	0.00155	0.03354	0.00056	0.23928	0.00727	0.00975	0.00086	274.2	67.36	212.7	3.5	217.8	5.96	196	17.16	90

Appendix D

Table 1. Experimental determination of the brittle strength of the Saraburi limestone and marble

Saraburi Limestone and Marble					
Diameter (mm)	Length (mm)	D/L ratio	Load at failure (kN)	Confining Pressure (Mpa)	Axial Stress at Failure (Mpa)
see capt.	see capt.	0.5	0	0	-8.5
53.9	100.7	0.5	174	1.7	76.2
53.9	100.8	0.5	250	3.4	109.5
54.1	100.1	0.5	274	6.9	119.8
54	102.8	0.5	284	13.8	124.4
54	100.3	0.5	386	20.7	169.1

Table 2. Parameters and data set used in Mohr construction to quantify effective principal stress magnitudes

Stress Stage	Sample Number	Bedding (Dip Dir - Dip)	Vein (Dip Dir - Dip)	Stress Ratio (Φ)	Differential Stress (σ1- σ3) (MPa)	Stress Regime	Magnitude of σ3 (MPa)	Magnitude of σ2 (MPa)	Magnitude of σ1 (MPa)
SI	T020	174/14	068/88	0.6	84±17	EXT	[-2]	[42]	[78]
SI	T029	352/39	235/80	0.4	76±15	EXT	"	"	"
SI	T019b	160/40	251/72	0.3	37±7	EXT	-5	8	38
SII	T029b	352/39	358/82	0.4	58±12	PC	-4	26	54
SII	T083b	175/59	HOST	0.9	35±7	SS	-4	±30	40
SII	T018vb	160/40	138/25	0.8	38±7	SS	"	"	"
SIII	T011b	178/60	HOST	0.5	66±13	SS	13	21	87
SIII	T019	160/40	322/71	0.2	62±12	PC	"	"	"
SIII	T018v	160/40	322/71	0.5	68±13	SS	"	"	"
SIII	T011	178/60	HOST	0.5	72±15	SS	"	"	"
SIV	T081	175/59	140/78	0.3	71±14	PC	12	16	66
SIV	T082	175/59	217/75	0.1	55±11	PC	"	"	"
SIV	T080b	175/59	255/52	0.8	38±7	SS	12	55	66
SV	T081b	175/59	281/42	0.4	51±10	SS	46	30	72
SV	T082b	175/59	261/49	0.3	46±9	SS	"	"	"
SV	T083	175/59	045/87	0.6	52±11	PC	"	"	"
SV	T080	175/59	337/85	0.7	70±14	PC	"	"	"

Appendix E

Structure of the Sibumasu-Indochina collision, Central Thailand: A section through the Khao Khwang Fold-Thrust Belt

Francesco Arboit [a], Alan S. Collins [a], Rosalind King [a], Christopher K. Morley [b] and Rowan Hansberry [a]

[a] Centre for Tectonics Resources and Exploration (TRaX), Department of Earth Sciences, The University of Adelaide, SA 5005, Australia.
[b] PTT Exploration and Production Public Company Limited, 555 Vibhavadi-Rangsit Road, 10 Bangkok 10900, Thailand.

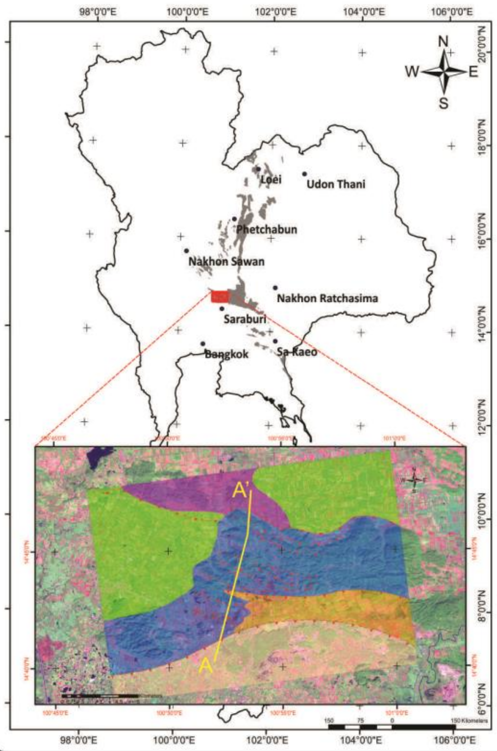

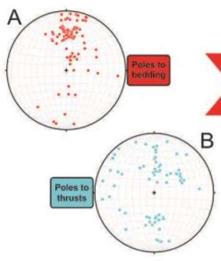

Geological map of the portion of the Khao Khwang Fold-Thrust Belt along Highway 21. Considerably modified from the original Map in Ueno and Charoentitirat (2011), based on fieldwork and Landsat imagery interpretation. Stereonets are representative of poles to bedding (A), and of poles to mappable thrusts (B).

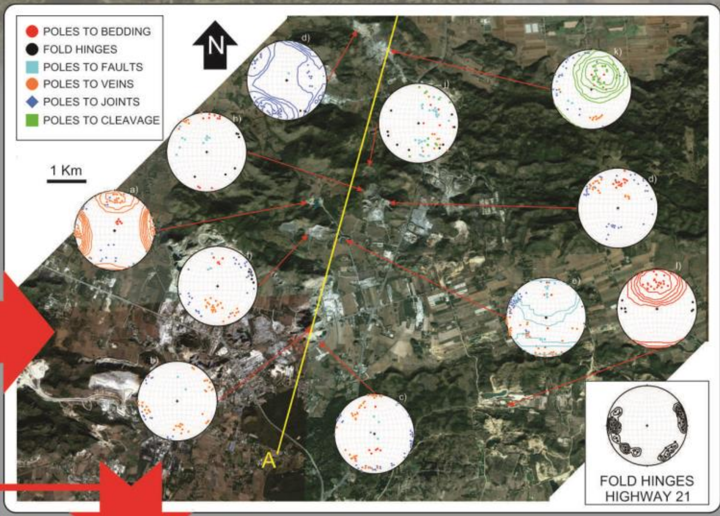

Project Outline

- South-East Asia is the final results of the collision of several continental blocks.
- These collisions were caused by the Early Triassic event of the Indosinian Orogeny in the range of 250–240 Ma.
- A detailed study of the Khao Khwang Fold-Thrust Belt revealed as many aspects of the Indosinian Orogeny remain unclear.
- This project therefore aims to identify and characterise the geo-dynamic evolution of the Khao Khwang Fold-Thrust belt in order to unravel unknown aspects of the Indosinian Orogeny.
- An integrated approach utilising field-based data, thin sections, geochemistry (XRF and ICP-MS) and geochronology are pursued in order to achieve this.

Poles to bedding, faults, veins, joints and cleavage at a section through the Khao Khwang Fold-Thrust Belt. Lower hemisphere projection data reveal the E-W trend of the major structural features as bedding, folds and related thrusts. Analysis of rotated data show three main set of joints and veins, striking E-W, N-S and NNW-SSE. Vein orientations correspond dominantly to join orientations and, to a lesser degree, pressure solution surfaces (not plotted here due to the lack of data).

Cross Section: Highway 21

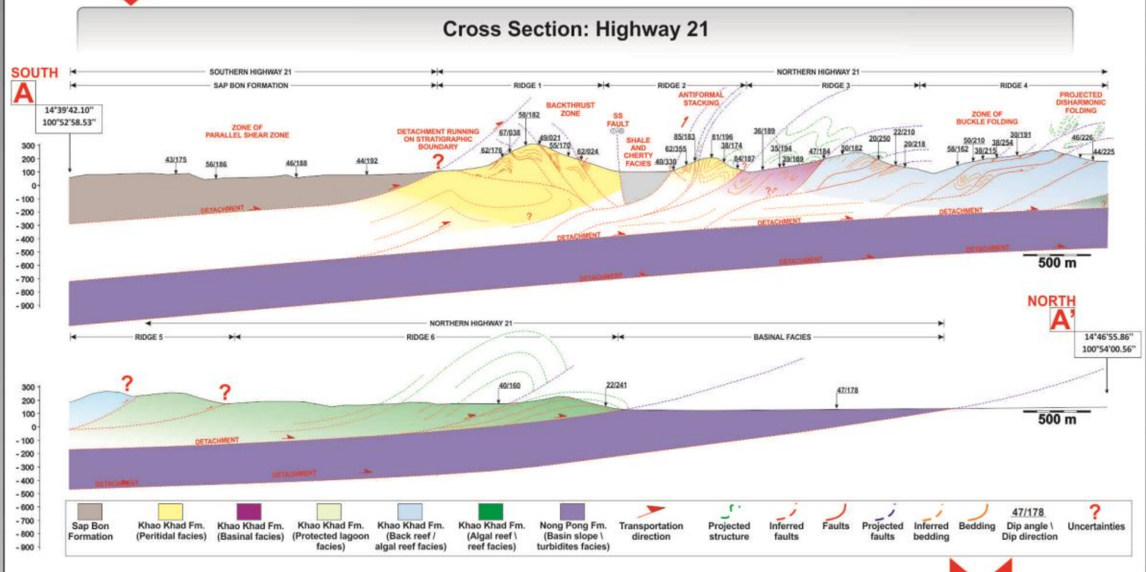

Methodologies

- Field observation and structural mapping.
- Measurements of any present structural features related to the Indosinian Orogeny as: veins, joints, faults, pressure solution surfaces, deformation bands.
- Scan lines and geomechanic stations on major folds and over related thrusts.
- Sampling of intruded volcanic and igneous rocks to assign the most probable tectonic setting at the time of emplacement (ICP-MS and XRF analysis).
- Sampling of carbonate rocks for analysis of calcite twinning in order to obtain a deeper understanding of stress orientation and magnitude during the Triassic phases of the Indosinian Orogeny.

Raw and Rotated Data

- Poles to bedding at the upper bench of the Khao Yai Hill with slickenside data along layer-parallel faults.
- Bedding with slickenside lineations
- Poles to Bedding

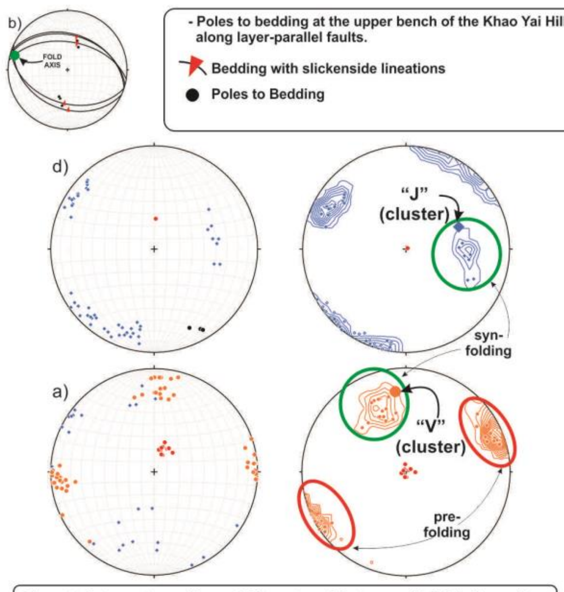

The rotated stereonet reveal the pre-folding nature of the two roughly N-S (orthogonal to bedding) main clusters of veins and joints and the possibly syn- or post-folding of the NE-SW (oblique to bedding), confirming the presumed N-S orientation of the main paleostress (δ¹) during the Triassic phase of the Indosinian Orogeny.

Lower hemisphere stereonet projection of raw data and rotated poles to structural elements: V, J, B. Data cluster are marked according to field observation with cluster analysis for J and V. Rotated data show that for horizontal bedding, both V and J strike: E-W, N-S and NNW-SSE. These three main sets are dominantly orthogonal to bedding

Simplified Cross Section: Highway 21

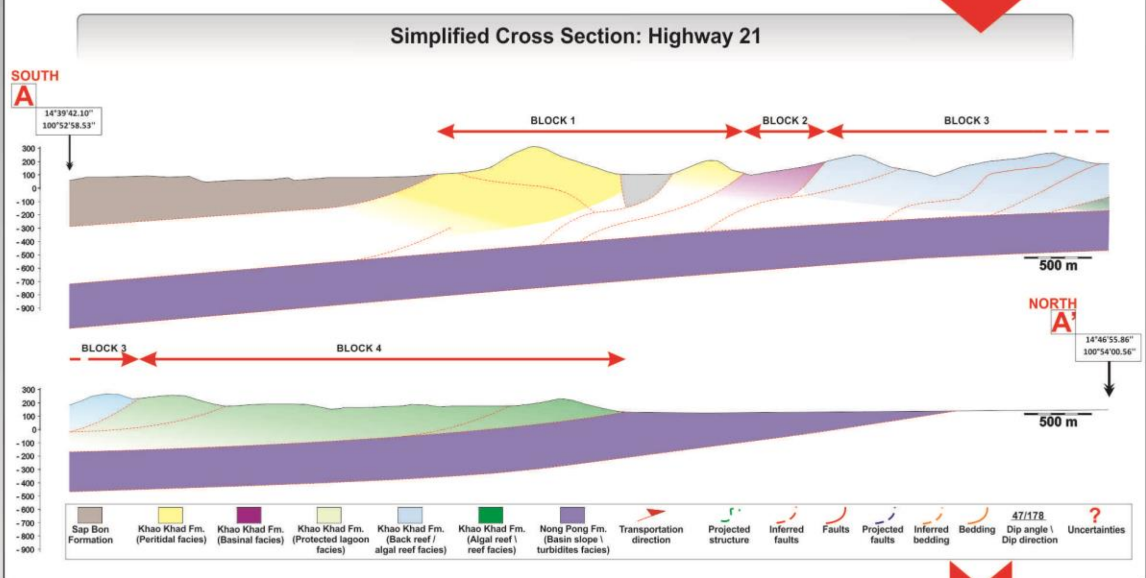

Cross Section Highway 21, restored section

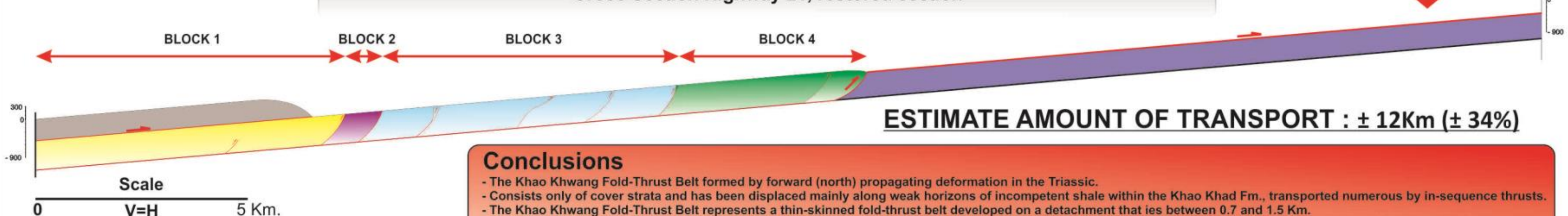

ESTIMATE AMOUNT OF TRANSPORT : ± 12Km (± 34%)

Conclusions

- The Khao Khwang Fold-Thrust Belt formed by forward (north) propagating deformation in the Triassic.
- Consists only of cover strata and has been displaced mainly along weak horizons of incompetent shale within the Khao Khad Fm., transported numerous by in-sequence thrusts.
- The Khao Khwang Fold-Thrust Belt represents a thin-skinned fold-thrust belt developed on a detachment that lies between 0.7 and 1.5 Km.
- The in-sequence, thin-skinned, deformation demonstrates that deformation has migrated from S-SSE to N-NNW along a zone as wide as the fold and thrust belt itself, with lateral variations probably attributed to lateral facies variations.
- The KKF&T Belt represents a significant kink in the collision between Sibumasu and Indochina, which may be due to either the original geometry of the Indochina margin, or due to a poorly recognised ocean strand that split Indochina into two or more late Palaeozoic continents.

S3 Stress Structure Seismic

TRaX

THE UNIVERSITY of ADELAIDE

Determination of the tectonic evolution from fractures, faults and calcite twins on the south-western margin of the Indochina Block

Francesco Arboit [a]*, Khalid Amrouch [b], Alan S. Collins [a], Rosalind King [a] and Christopher Morley [c]

[a] Centre for Tectonics Resources and Exploration (TRaX), Department of Earth Sciences, The University of Adelaide, SA 5005, Australia.

[b] The Australian School of Petroleum, The University of Adelaide, SA 5005, Australia.

[c] Chiang Mai University, 239 Huaykaew Road, Tumbol Suthep Amphur Muang, Chiang Mai, Thailand.

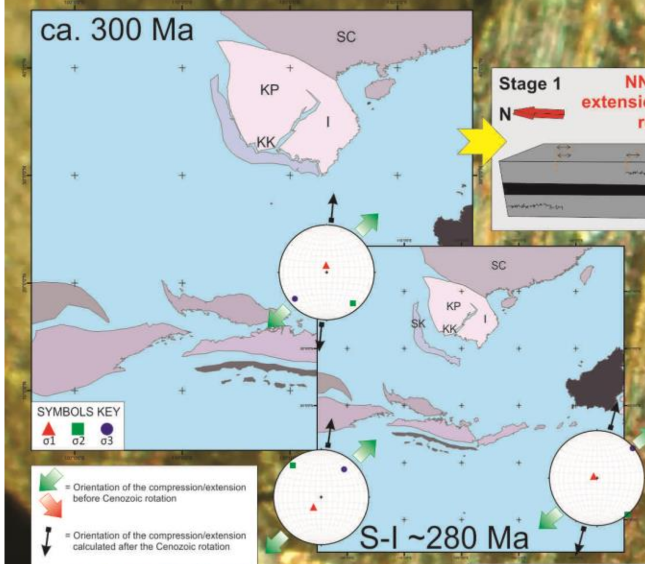

Introduction

South East Asia is formed from a number of continental fragments and volcanic arcs, separated by oceanic suture zones, which accreted to the growing Asian continent during the latest Paleozoic-early Mesozoic Indosinian Orogeny. In Thailand, this tectonic event, developed mainly during the Triassic and is the result of the collision between the Sibumasu, Sukhothai and Indochina Terranes. Models for the tectonic evolution of Thailand from the Indosinian Orogeny to the present have been defined using biostratigraphical, petrological, structural and geochronological data, and involve broadly N-S trending tectonic domains converging in E-W directions (with respect to the present-day orientation). However, these are based on the present day orientations of the tectonic domains and little constraints on the original orientations or paleo-stress determinations have been previously attempted.

Objectives

Central Thailand, and more specifically the Khao Khwang Fold-Thrust Belt (KKFTB), provides a natural laboratory to obtain the necessary information. In order to develop a permissive model for the dynamic evolution of the region, we took advantage of the rocks of the Khao Khad Formation to compare fracture and fault sets with a paleostress analysis carried out using calcite twins. In combination, these data provide an accurate estimate on the evolving stress orientation and resulting deformation before, during, and after, the Indosinian Orogeny.

Correlating palaeostress determinations with tectonic environment

Based on the results of previous studies on regional tectonics and paleogeographic reconstructions of SE Asia, the Permian-Recent history of Thailand began with Early-Mid Permian subduction of Paleo-Tethys underneath the south-western margin of Indochina. This initiated upper-plate extension and subsequent contraction as a back-arc basin first opened, then closed as the arc (represented by the Sukhothai terrane) collided with Indochina. This contractional event was followed by the Late Permian – Early Triassic collision between Sibumasu and the Indochina Block, which during the Mid-Late Triassic itself collided with South China (Cathaysia) to form a large amalgamated continent. The next major deformation to affect the region after the Indosinian occurred in the Cenozoic, and are associated with upper-crustal deformation (Mae-Ping and Three Pagodas fault zones). The KKFTB lies close to the trace of the Mae-Ping Fault, so we expect to see deformation, in the form of meso-scale faults and calcite twins, in the KKFTB limestones.

The stress states determined here are characterised by five tectonic systems have been recorded by structures both at the macro- and micro-scale, which are respectively represented as major anticlines and calcite twins. We present conceptual block models to illustrate the fracture evolution within the KKFTB. These models are composed of three layers, idealized from the stratigraphy of the Khao Khad Formation, including a black layer representing the shale between two grey layers representing limestone, which, being relatively stiffer (higher Young's modulus), can support greater amounts of stress than softer layers when subject to same effective stress. The limestone layer of the Khao Khad Formation responded to the stress by fracturing and shearing, while the black layers acted in a more ductile manner, dominantly by plastic flow (detachments), resulting in a less fractured framework. The bedding parallel slip at the interfaces between the ductile and brittle layers played an important role for the stress distribution. The stress tensors that resulted in the deformation observed are herein described.

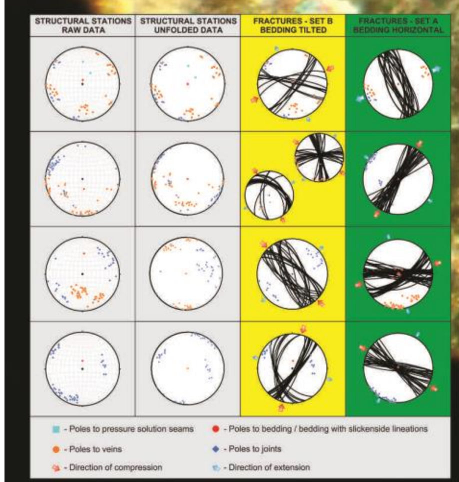

Stage I

Stage I is represented at the meso-scale by the fracture Set-AI/AII along with the RST at the micro-scale obtained from samples T_14_020/029/019b that are consistent with a pre-folding extensional stage, with a vertical σ_1 and an almost N-S oriented σ_3. The minimum principal stress lies in the plane of the bedding and is oriented ~N-S, sub-perpendicular to the trend of the KKFTB. These fracture sets pre-date all the other detected fracture sets as suggested by few macroscopic and microscopic observations along with calcite twin analysis. We suggest that this deformation reflects either pre-Indosinian extension, possibly related to, extension foreland -ward of an evolving contractional orogeny, created due to flexure in the peripheral bulge, or Permian supra-subduction zone extension.

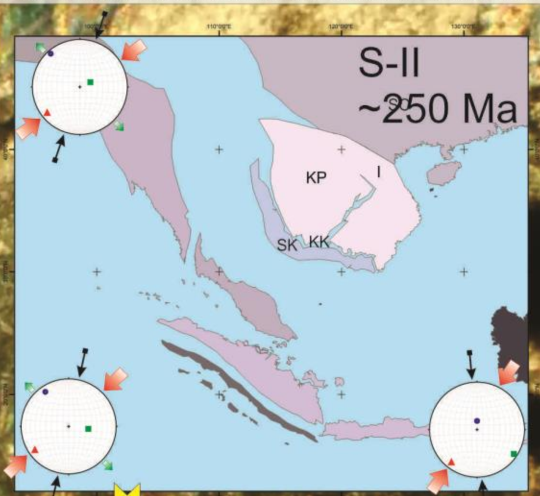

Stage II

Stage II corresponds to fracture Set-AIII/AIV along with some calcite twin results, yielding paleostress tensors of both strike-slip and pure compression, from the samples T_14_029b/083b/018a are consistent with a pre-folding compression. These yield N-S oriented σ_1 that is perpendicular to the fold-axis and is interpreted as related to the first phase of the Indosinian collisional event (Indosinian I) between the Sukhothai and Indochina terranes. This tectonic phase is interpreted to represent the main layer-parallel shortening event, and therefore to be the stress state responsible for the emplacement of the KKFTB. The range of orientations of fracture of Set II is in very good agreement with both the fault-slip and calcite derived stress state. These suggest a range of shortening direction from 020° to 340° with a mean shortening direction of 005°, which is quite consistent with the general trend of the major folds in the western portion of the KKFTB. Andesite intrusions in the Saraburi – Khao Yai area post-date major KKFTB deformation and have recently been dated as crystallising between 250 and 240 Ma in the Pak Choi granodiorite east of the KKFTB. This constrains the timing of this stress tensor to occurring in the Late Permian-Early Triassic. This collision is thought to have affected the entire Indochina Block. In the sub-surface of NE Thailand there is a major regional unconformity, which was clearly established by the uplift and the consequent erosion associated with major compressional deformation of the Saraburi Group at around the Permian – Triassic boundary. The RST is here presented by three tensors, two of them with σ_3 close to vertical, indicating a strike-slip fault stress regime. The apparent interchange between the vertical stress being σ_2 or σ_3 is likely due to the similarity in magnitude of these stresses during the Indosinian I event.

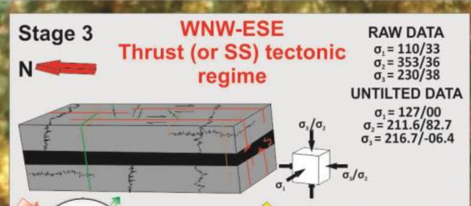

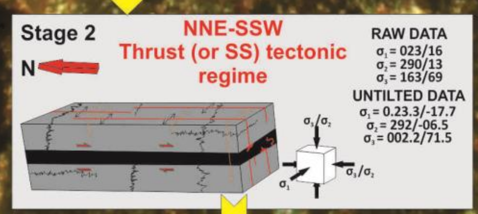

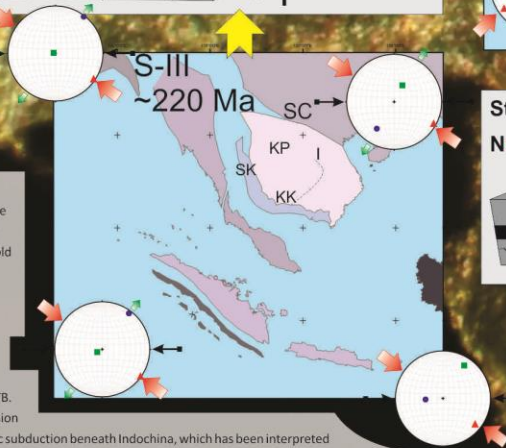

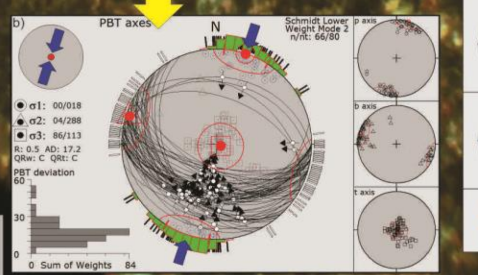

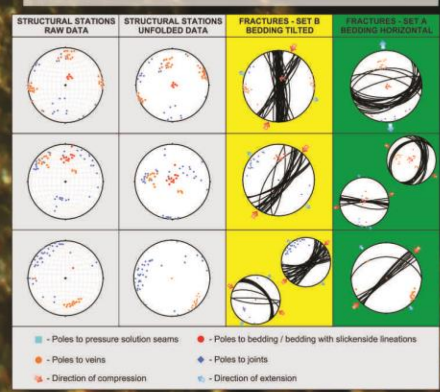

Stage III

Fracture Set–AV/AVI is represented by veins and joints that formed in both pure compressional and strike slip regimes. These represent an E-W oriented compressional (Figure 9c), strike-slip fault stress regime, which could represent either a pre- or syn-folding event. The σ_1 direction is almost parallel to the main fold axes of the KKFTB. This regime may reflect stress evolution during the early Indosinian Orogeny. However, in the last decade came out the possibility that the Indochina Block was actually more than one continental terrane or at least did not have strongly linear boundaries before the "Indosinian I" Orogeny with the possible presence of an intra-Indochina ocean that may have closed during the main phase of the "Indosinian I". The tensor described here would be in a favourable orientation to result from the closure of this proposed ocean. Clearly a wider, more regional, view is needed before this RST is attributed to a specific tectonic event. The Ailao Shan region lies 800 km NE of the KKFTB. Here, outcrops of mafic and ultramafic rocks interpreted as a suture zone were associated with the collision between Indochina and South China. This collision is thought to have started as a south-directed oceanic subduction beneath Indochina, which has been interpreted to have been active at ca. 236 Ma, based on $^{40}Ar/^{39}Ar$ dating. Syn- to post-tectonic granites have been U-Pb zircon dated to ca. 252-245 Ma dating the major compression in the region. This is consistent with the orientation and timing of the third RST.

Stage IV

The Indosinian event also probably marked the emplacement of fracture Set-BVII/BVIII. These fractures, ranging in orientation between 355° and 030°, are similar in orientation to Sets-AI/AII. However, these fractures are clearly shear fractures (Type 3). The similarity between these fracture sets suggests that many of the fractures belonging to Set-AIV are reactivated fractures emplaced during the early stages of the Indosinian orogeny. In such a case, sets of the fourth deformation phase in those parts of the KKFTB with near horizontal bedding could not always be distinguishable from fractures active during the second phase of the Indosinian orogeny. In most cases, though, Set-BVII/BVIII fractures consistently abut fractures of the second deformational phase. This later stage of the Indosinian Orogeny is further represented by fracture Set-BVIIa/BVIIIa; indeed, these fractures reflect the increasing intensity of folding. Fracture sets developed during the fourth stage of deformation are interpreted to be associated to the syn-folding bending of the layers. This is because they strike almost parallel to the fold axes and are most abundant in the hinge zones of the tight chevron folds in the core of north-verging fault -propagation folds. There is no clear calcite twin regime detected with this orientation but permutations of σ_1 and σ_2 axes in some of the samples provide an extensional stress regime with a horizontal σ_3 axis oriented at high angle to the major fold hinges. We interpret this resumption of ~N-S compression to correspond to the latest Indosinian Orogeny (Indosinian II). Macro deformation associated with this phase is responsible for the tightening of pre-existing fault-propagation folds and partial reactivation of the fractures developed during the earlier event (i.e. Set AII/AIII fractures). During the latest Triassic, the half -graben basins in the Khorat Plateau (NE Thailand) containing the Kuchinarai Group (Late Triassic) ceased to subside and were structurally inverted. The degree of deformation associated with this event is very much less than that which took place during the earlier Indosinian I event.

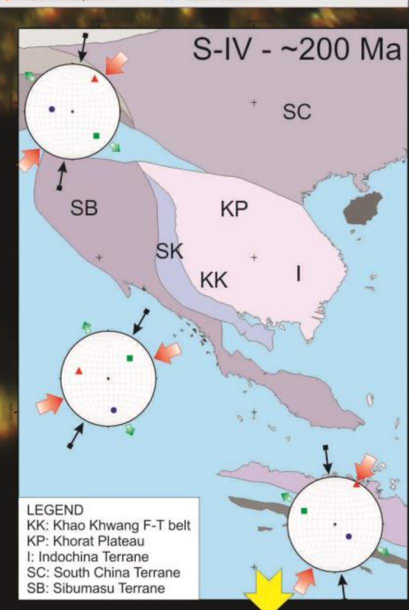

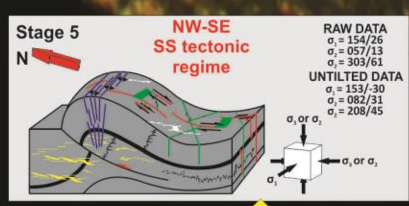

Stage V

The last fracture Sets BIX/BX are interpreted as the only fracture sets not related to the Indosinian event. Both fractures and calcite twins recorded a consistent post-folding relationship for the RST. The vertical stress vector was σ_2 and σ_1 was oriented NW-SE, consistent with the rupture of post-folding E-W oriented strike-slip faults. These strike-slip faults were detected in the field, and calcite twins from ~150° striking veins, few samples yielded results consistent with this stress state. We consider that these fracture sets represent the last event because of the strike slip faults deforming the region, which have similar orientation to Sets-BIX/BX, and cross-cut previous structures emplaced during the main Indosinian Orogeny. These age constraints limit these sets and their relative stress field to being post-Indosinian (i.e. post Triassic). However, the modern stress tensor has a similar orientation to the fifth RST detected by calcite twin analysis, with the modern maximum horizontal stress ranging from N-S to NW-SE. The modern stress field has been responsible for the nearby continental-scale NW-SE to NNW-SSE oriented Mae Ping Fault. We therefore assert that this stress tensor might represent Cenozoic deformation related to the India-Asia collision.

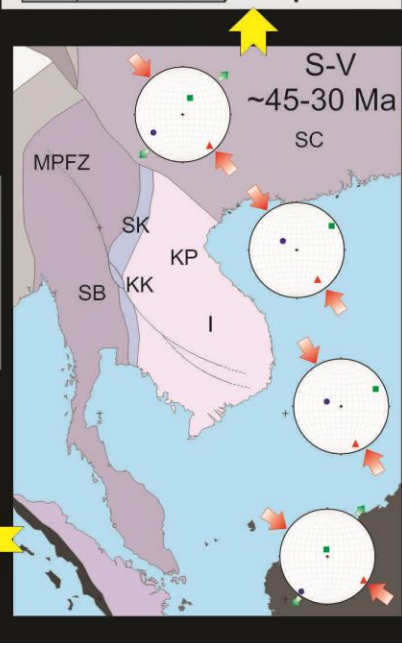

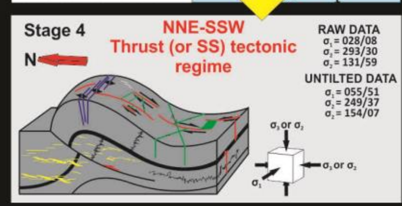

Conclusions

In this study, we have performed qualitative and quantitative tectonic analysis of the brittle deformation at meso- and micro-scales in order to unravel the distribution of the stress in space and time before and after the main folding event in the KKFTB. This has been possible due to the strain acquisition in the folded strata and the stress build-up in the carbonate layers of the Khao Khad Formation. The analyses yielded reliable paleostress states similar and consistent with those from fault-slip and fracture data collected throughout the western margin of the KKFTB. At the meso-scale, the observed fracture population are gathered into six different sets formed during five main events that are interpreted to be developed during the Indosinian I & II tectonic events and subsequent Cenozoic deformation. At the scale of the western margin of the KKFTB, the comparison of major structures, such as major folds, fracture patterns, and the RSTs derived from the calcite twin inversion for each of the detected events demonstrate a consistent record of the tectonic stresses at the scale of the entire KKFTB. Dominant and common stress states throughout the whole study area are characterised by a N-S trending σ_1 and vertical, to ENE-WSW plunging, σ_3 with variable values of stress ratio Φ; which made it possible to link different RSTs obtained with stress tensors coming from distinct samples through σ_1-σ_2 and σ_2-σ_3 permutations. Unfortunately, there are no syn-deformational sedimentary rocks preserved in the region, restricting the resolution of more precise age constraints on the age of the various deformations. Notwithstanding this, the characteristics of the paleostress regimes, from the calcite twins,

and the very good correlation with the distribution of the overall deformation, allowed us to provide a relative chronology of the tectonic events. Calcite twins revealed significant variations of paleostress orientation and regime across the KKFTB, providing a reliable picture of paleostress distribution on the edge of the southern Indochina Block. Beyond regional implications, this study enhance the potential of an analysis based on fault and calcite twin observations which has the potential to lead to a more exhaustive understanding of regional and local stress and stress patterns.

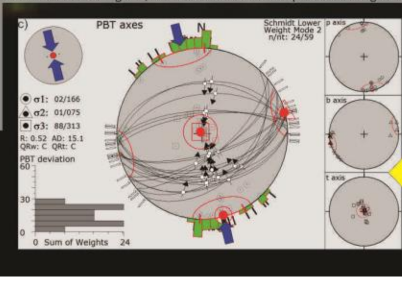

PLATE RECONSTRUCTION PERFORMED ON "GPLATE 1.5.0 & GIS" SOFTWARE ENVIRONMENTS
FOR REFERENCES SEE:
Arboit, F., Amrouch, K., Collins, A. S., King, R., & Morley, C., 2015. Determination of the tectonic evolution froM fractures, faults and calcite twins on the south-western margin of the Indochina Block. Tectonics. doi: 10.1002/2015TC003876

In-situ detrital zircon analyses within the south-western margin of the Indochina terrane, central Thailand: New insights on the Indosinian orogeny

Francesco Arboit [a]*, Alan S. Collins [a], Christopher Morley [b], Rosalind King [a] and Khalid Amrouch [c]

[a] Centre for Tectonics Resources and Exploration (TRaX), Department of Earth Sciences, The University of Adelaide, SA 5005, Australia.

[b] Chiang Mai University, 239 Huaykaew Road, Tumbol Suthep Amphur Muang, Chiang Mai, Thailand.

[c] The Australian School of Petroleum, The University of Adelaide, SA 5005, Australia.

Introduction

Southeast Asia is a composite region of continental crustal segments that originated along the northern (with respect to present-day Australia) Gondwana margin (Figure 1). These continental fragments rifted off Gondwana in the Palaeozoic and were accreted to the growing Asian continent from the Triassic to the Cenozoic. The terranes that make up mainland SE Asia, east of Myanmar, include Indochina, Sukhothai, Sibumasu, and Cathaysia. In previous studies, early Palaeozoic reconstructions of these terranes were primarily based on magnetic data, palaeo-biogeography, and stratigraphic correlations. The different approaches have resulted in significant ambiguity in the tectonic geography of the region throughout this time. This uncertainty in the origin of the SE Asian terranes is mirrored by controversy as to the timing and nature of the 'Indosinian orogeny'; the pan-East Asian orogeny that evolved during the Late Palaeozoic and Early Mesozoic and led to the formation of much of East Asia. These issues arise from the paucity of constraints on the palaeo-position of the SE Asia terranes, the lack of detailed structural studies regarding thrust transport direction and timing, and uncertainties regarding the dating, location, tectonic significance and even existence of suture zones and their closure. Samples used in this study were collected throughout the KKFTB. Eight hundred and thirty seven U-Pb zircon ages were analysed from six samples collected in the arenaceous rocks of the Saraburi Group. Considering the geographical distribution of the sandstones and their relative Maximum Depositional Ages, a differentiation of the samples in data from the south and the north of the KKFTB has been done to facilitate the understanding of the study.

Objectives

The siliciclastic units of the Permo-Triassic Saraburi Group within the Khao Khwang-thrust belt (KKFTB) (Figure 2) were examined in order to achieve a better understanding on the tectonic geography of this region through its evolving provenance record.

The Saraburi Group within the KKFTB comprises a number of formations that are either dominated by carbonate platform deposits (Khao Khad and Khao Khwang formations), or deeper water deposits comprising a mixture of interbedded shales, sandstones, cherts and limestones (Sap Bon, Pang Asok, and Nong Pong formations). Until now, very little has been known about the provenance ages of detrital zircons and the change of provenance through time of the basinal formations of the Saraburi Group.

Here, we discuss U-Pb and Hf-isotope data in detrital zircons from 6 samples collected in the Sap Bon, Pang Asok and Nong Pong formations. We, therefore, seek to provide a better constraint on the tectonostratigraphic evolution of the basin that lay in a marginal position on the Indochina terrane, and of the overall paleogeography of SE Asia during the Indosinian Orogeny.

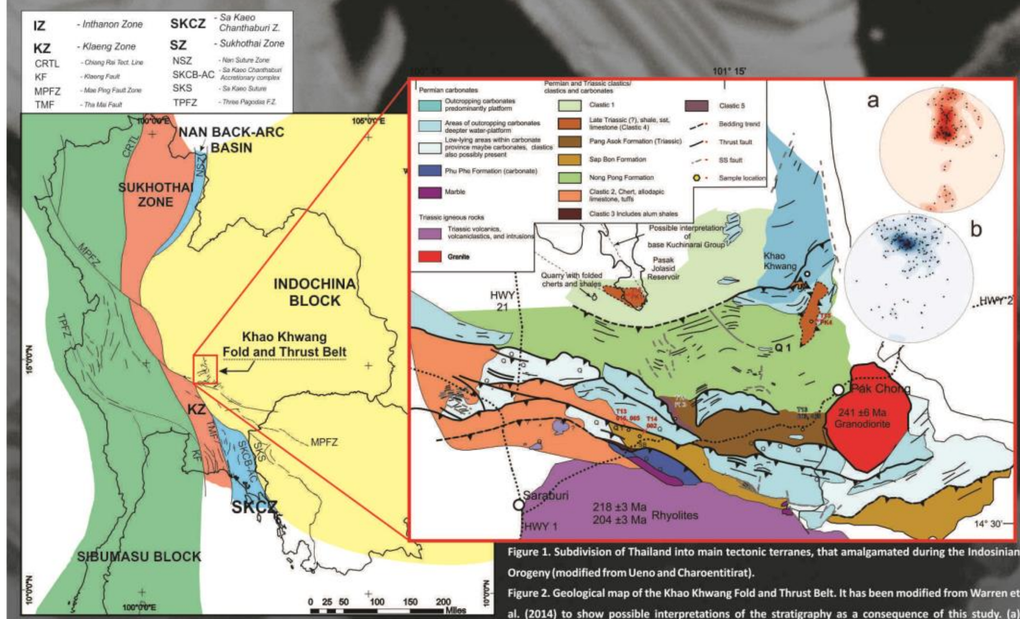

Figure 1. Subdivision of Thailand into main tectonic terranes, that amalgamated during the Indosinian Orogeny (modified from Ueno and Charoentitirat).

Figure 2. Geological map of the Khao Khwang Fold and Thrust Belt. It has been modified from Warren et al. (2014) to show possible interpretations of the stratigraphy as a consequence of this study. (a) Stereonet of poles to bedding for the region, (b) Stereonet of poles to main thrusts along Highway 21.

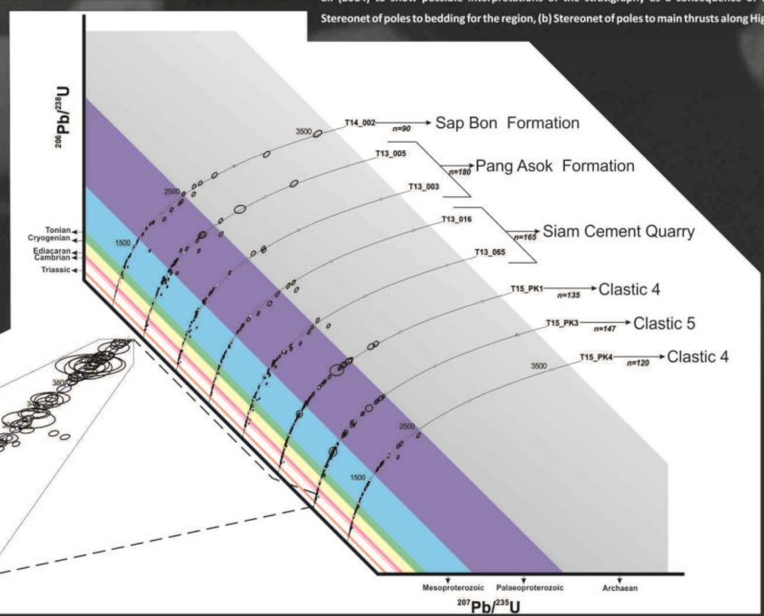

Figure 3. U-Pb concordia diagram of ages (in Ma) obtained from zircon grains in each sample by U/Pb detrital zircon laser-ablation–inductively coupled plasma–mass spectrometry (LA-ICP-MS). Inset showing T15_PK3 MDA with 2σ error of sample T15_PK3 from 100 to 450 Ma.

Figure 7. Schematic sequential evolution of the tectonic and depositional model within the KKFTB from Early to Late Triassic, based on the modified stratigraphy shown in Figure 2 and Figure 5.

a) Early Permian stages of the Indosinian Orogeny;

b) syn-tectonic emplacement of the Pak Chok granodiorite east of the KKFTB (foredeep);

c) transition from foredeep to foreland basin setting;

d) foreland deformation and post-tectonic emplacement of the Khao Yai rhyolite south of the KKFTB.

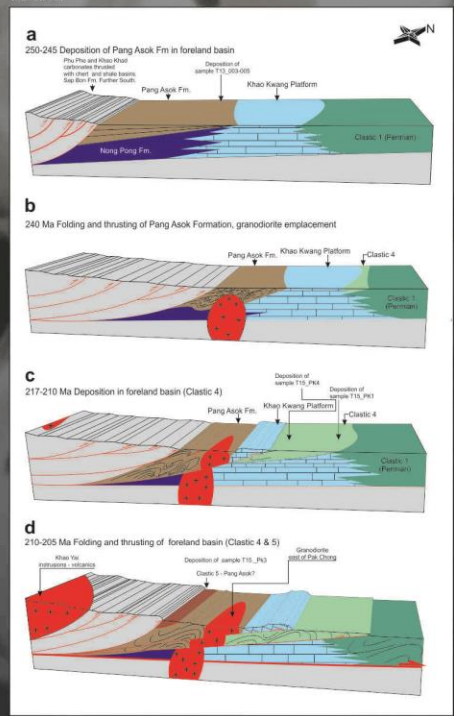

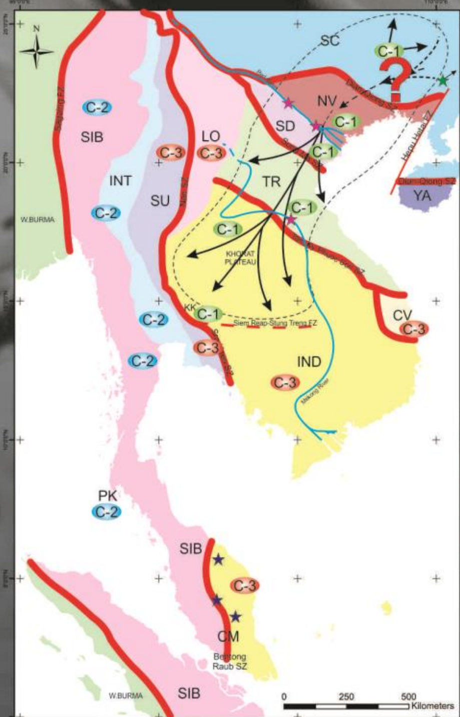

Figure 8. Schematic tectonic map of SE Asia representing a tentative reconstruction of the statistically most probable provenance sources and sedimentary pathways (black arrows) during Permian-Triassic ages. C-1,2,3 represent the provenance clusters obtained with MDS analysis. CM: Central Malaysia, CV: Central Vietnam, IND: Indochina, INT: Inthanon, LO: Loei, NV: Northeast Vietnam, SIB: Sibumasu, SC: South China, SD: Song Da, SU: Sukhothai, TR: Truong Son. Five-pointed stars= data from Sevastjanova et al. (2011); four-pointed stars= data from Bodet and Shärer (2000); six-pointed stars= data from Li et al., (2012).

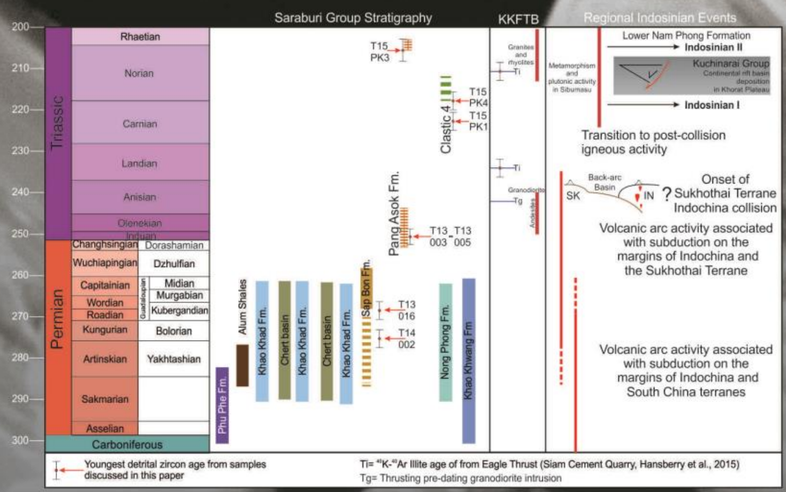

Figure 6. History of the Saraburi Group stratigraphy. Working stratigraphic model based on fieldwork and subsequently the working stratigraphic model has been modified on the basis of the detrital zircon from the siliciclastic formations of the Saraburi Group.

Major implications in provenance, stratigraphic and tectonic setting

1- A substantial revision to the stratigraphy of the Saraburi Group is indicated (Figure 6), with the Pang Asok Formation reassigned from the Permian to the Early Triassic. Instead of the Nong Pong Formation and Khao Kwang formations exclusively occupying the northern half of the area a new Late Triassic marine formation is identified, informally referred to as the Clastic 4 unit.

2- Interpretation of the Triassic basins as syn-tectonic foredeep or piggyback basins permits more precision about the timing of tectonic events (Figure 7). It is suggested that between ca. 250 Ma and 240 Ma the Pang Asok transitioned from deposition in a foredeep basin to being folded, thrusted, and intruded by a ca. 240 Ma granodiorite. Deformation slowly propagated northward with time, or experienced a hiatus. Deposition of the Clastic 4 unit during the Norian infers a possible gap >15 Ma between the end of known thrusting in the southern half of the area, and deformation in the northern area. The different ages probably reflect Early Triassic Sukhothai Terrane-Indochina collision, followed in the Late Triassic by the amalgamated Sukhothai Terrane/Indochina block-Sibumasu collision.

3- U-Pb detrital zircon ages revealed that deposition within the south-western margin of the Indochina terrane lasted until at least 205 ± 6 Ma (Figure 3). However, it is uncertain whether deposition was in a marine or lacustrine basin.

4- The age distributions yield dominant Ordovician to Devonian (~450-350 Ma) peaks (Figure 4a & 4b) with Neoproterozoic and Mesoproterozoic (~950, ~1200, ~1400 Ma) age groups, and individual zircons dating back to the Palaeoarchean. Hf-isotope data identify different magma sources (Figure 5a & 5b), indicating a complex history for the evolution of the Indosinian orogeny before and during the subduction of the palaeo-Tethys ocean.

5- Multidimensional scaling analysis on detrital zircon ages from throughout SE Asia collected in the last decades (Carter and Bristow, 2003; Li et al., 2012; Hara et al., 2013; Burrett et al., 2014), is interpreted to mean that the source of sediment feeding the western margin of the Indochina terrane during Permian and Triassic was coming from the NE (Figure 8), having high affinity with zircons from the Khorat Plateau, Truong Son and NE Vietnam terranes.

6- Further, the KS statistical analysis highlights the mismatch within Indochina, between the sediments from the Khorat Plateau in the north and Cambodia in the south strengthening the idea already advocated in the literature, of a possible provenance separation that may have been represented by a former E-W trending plate contacts within Indochina.

7- Late Triassic detritus from the KKFTB also preserved middle Mesoproterozoic and Triassic detritus that is interpreted as being sourced from the newly accreted Sibumasu Terrane.

8- The data indicate that the stratigraphy of the Saraburi Group needs more intensive study, particularly to understand the distribution of Triassic versus Permian sedimentary rocks.

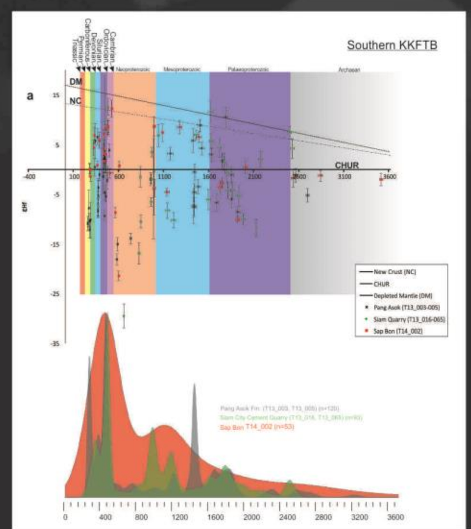

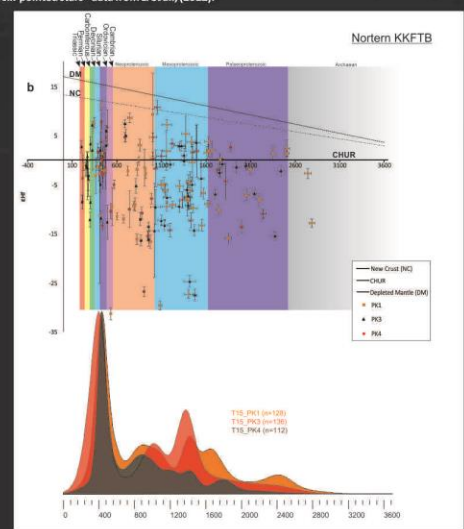

Figure 4a & 4b. U/Pb age versus εHf(t) plots of detrital zircon data from 8 samples throughout the KKFTB stratigraphy. a) Southern portion of the KKFTB, b) northern portion of the KKFTB. The kernel density estimate distribution for the samples are plotted below the U/Pb age versus epsilon Hf plots to provide a measure of the importance of each clastic unit.

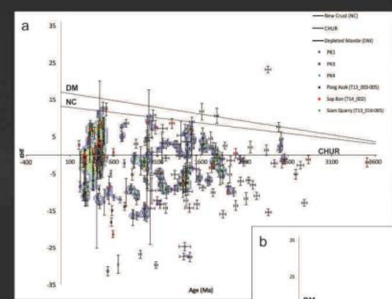

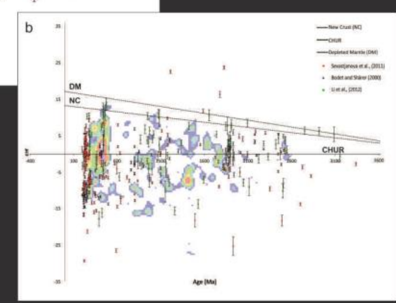

Figure 5. a) U/Pb age versus epsilon Hf plot of all the data from the KKFTB and relative density contour. b) U/Pb age versus epsilon Hf plot of published hafnium isotopic data from zircons from the Mekong River and Red River, from Permian sediments in southeast China, and the Malaya Peninsula river systems; compared with density contour of all the Hf isotopic data collected within the KKFTB.

REFERENCES

- Bodet, F., Schärer, U., 2000. Evolution of the SE-Asian continent from U–Pb and Hf isotopes in single grains of zircon and baddeleyite from large rivers. Geochimica et Cosmochimica Acta 64, 2067–2091
- Burrett, C., Zaw, K., Meffre, S., Lai, C. K., Khositanont, S., Chaodumrong, P., Udchachon, M., Ekins, S., Halpin, J., 2013. The configuration of Greater Gondwana—Evidence from LA ICPMS, U–Pb geochronology of detrital zircons from the Palaeozoic and Mesozoic of Southeast Asia and China. Gondwana Research. Vol. 26, pp. 31-51.
- Carter, A., & Bristow, C. S., 2003. Linking hinterland evolution and continental basin sedimentation by using detrital zircon thermochronology: a study of the Khorat Plateau Basin, eastern Thailand. Basin Research, 15(2), 271-285.
- Hara, H., Kon, Y., Usuki, T., Lan, C. Y., Kamata, Y., Hisada, K. I., ... & Charusiri, P., (2013). U–Pb ages of detrital zircons within the Inthanon Zone of the Paleo-Tethyan subduction zone, northern Thailand: New constraints on accretionary age and arc activity. Journal of Asian Earth Sciences, 74, 50-61.
- Li, G., Liu, X., Pullen, A., Wei, L., Liu X., Huang, F., Zhou, X., 2010, In-situ detrital zircon geochronology and Hf isotopic analyses from Upper Triassic Tethys sequence strata, Earth and Planetary Science Letters 297 (2010) 461–470
- Sevastjanova, I., Clements, B., Hall, R., Belousova, E.A., Griffin, W.L., Pearson, N., 2011. Granitic magmatism, basement ages, and provenance indicators in the Malay Peninsula: Insights from detrital zircon U-Pb and Hf-isotope data Gondwana Research, 19 (4), 1024-1039.